COLOR AND NANOMATERIALS IN OPTICAL SENSORS

PhD Thesis

Maria Ariza Avidad

Universidad de Granada
2014

UNIVERSITY OF GRANADA

FACULTY OF SCIENCES

Department of Analytical Chemistry

Research group FQM-118 "Espectrometría en Fase Sólida"

ECsens. Electronic and Chemical Sensing Solutions

PhD Thesis

COLOR AND NANOMATERIALS IN OPTICAL SENSORS

María Ariza Avidad

Granada, Julio 2014

Editor: Editorial de la Universidad de Granada
Autor: María Ariza Avidad
D.L.: GR 1968-2014
ISBN: 978-84-9083-168-7

Autor: María Ariza Avidad

UNIVERSITY OF GRANADA
FACULTY OF GRANADA
DEPARTMENT OF ANALYTICAL CHEMISTRY

COLOR AND NANOMATERIALS IN OPTICAL SENSORS:

The PhD dissertation presented encourage the recognition of doctoral dissertation at the national and international level in Chemistry

María Ariza Avidad

Luis Fermín Capitán Vallvey, Catedrático de Universidad y Alfonso Salinas Castillo, Profesor Contratado Doctor de Universidad, ambos del Departamento de Química Analítica de la Universidad de Granada.

CERTIFICAMOS:

Que el trabajo de investigación recogido en la presente memoria, titulada "Color and nanomaterials in optical sesors", y presentada por María Ariza Avidad para optar al grado de doctor por la Universidad de Granada, ha sido realizado en su totalidad bajo nuestra dirección en el Departamento de Química Analítica de la Universidad de Granada.

Granada, Julio de 2014

Dr. Luis Fermín Capitán Vallvey
Catedrático de Universidad

Dr. Alfonso Salinas Castillo
Profesor de Universidad

La doctoranda Maria Ariza Avidad y los directores de la tesis el Dr. Luis Fermin Capitán Vallvey y el Dr. Alfonso Salinas Castillo garantizamos, al firmar esta tesis doctoral, que el trabajo ha sido realizado por la doctoranda bajo la dirección de los directores de la tesis y hasta donde nuestro conocimiento alcanza, en la realización del trabajo, se han respetado los derechos de otros autores a ser citados, cuando se han utilizado sus resultados o publicaciones.

Granada, Julio de 2014

Director/es de la Tesis

Doctoranda

Fdo.: Luis F. Capitán Vallvey
Alfonso Salinas Castillo

Fdo.: María Ariza Avidad

A mamaita

AGRADECIMIENTOS

A mis abuelos y en particular a Mamaita, por todo lo que me has aportado con tu sabiduría y dedicación. Esta tesis esta dedicada a ti. Te llevaré siempre conmigo.

A mis padres, por acompañarme en la vida, apoyarme en mis decisiones y ayudarme a superar todos los obstáculos encontrados de la mejor forma posible. Gracias por soportar en ocasiones la carga que he supuesto para vosotros. Nada de lo que soy y por supuesto este libro no habría sido una realidad de no ser por vosotros, siempre os estaré agradecida.

A mi hermano Antonio por ayudarme siempre en todo lo que he necesitado tanto en el ámbito profesional como en el personal. Nunca me he encontrado desprotegida sabiendo que estas tú. A mi hermana Rosa, que siempre ha estado conmigo apoyándome en los momentos difíciles y acompañándome en los grandes. Siempre serás mi hermana y mi mejor amiga, por lo que me siento muy afortunada. Gracias, nunca me he sentido, ni me sentiré sola. A mi prima Elena por ser otra hermana más con la que contar siempre. Gracias por estar siempre ahí.

A mi cuñada Sonia, gracias por tus consejos y por estar siempre dispuesta a escuchar. A mi sobrina Elvira, desde que naciste me has hecho una persona mas feliz y completa. A mi cuñado Andrés, me alegro mucho de tenerte en la familia. A Ignacio, Luis, Ines y el niño que viene en camino que estoy deseando conocer.

A mis primos/as, tíos/as, en especial a Maria Jesús y Angel que son como unos padres y un ejemplo para mi.

A mi tío Ramiro, por tu ayuda desinteresada siempre que lo he necesitado.

A Fermin, por haberme inculcado valores tan importantes y necesarios en el ámbito personal y profesional. Gracias por tu dirección y gracias por tu templanza ante los problemas.

A Alfonso, además de ser una guía durante mi tesis, me has enseñado cosas más allá de la propia química, que considero muy importantes para triunfar en la vida.

A Dada, que un día me abrió una puerta y gracias a ella empecé el trabajo con el que comienzo este libro.

A Angel, por tu compañía, sabiduría y apoyo incondicional. Gracias por todos los momentos vividos juntos. A Rocio, que desde que empezamos la carrera siempre hemos estado juntas como compañeras y como amigas. A mis compañeras y amigas de carrera, en especial Chus y May, por los momentos vividos juntas. A Isabel, aunque en mi último tramo no estuviste personalmente acompañándome, siempre has estado ahí para lo que he necesitado. Me llevo muchos recuerdos que hemos vivido juntas. Gracias a todas las personas que han estado acompañándome en la mayor parte de mi tesis, especialmente a Miguel y a las "chicas del laboratorio de en frente", a Carmen, Paulina y Cristina, por todos los momentos que hemos pasado todos juntos.

A Manuel, gracias por haber estado siempre que lo he necesitado. Es una suerte poder contar contigo tanto en lo profesional como en lo personal.

A los nuevos y antiguos fichajes del laboratorio, especialmente, Antonio Inma y Agustín, espero poder tener la oportunidad de trabajar mas tiempo con vosotros en el futuro. Al grupo de electrónica, en especial a Antonio, Migue, Nuria, Almudena, Pepe, Sofía, Fernando y Diego con los que tantos momentos hemos vivido juntos.

A mis amigas y amigos y a sus parejas, en especial a Ana, , Fátima, Mare, Natalia y a Raquel, me alegro de tener amigas como vosotras, contagiándome vuestra alegría y ayudándome a superar los malos momentos. A chus y Juan, que aun no viéndonos como me gustaría nunca perdemos la amistad tan especial que tenemos.

I want to express my gratitude to my supervisor Mike. Thanks for all your support and your pacience. During my term in UCSD I felt very fortunate of being part of your group as a visiting scholar.

Thanks also to the peopple from the lab I was working with in UCSD, in especial to Joanna and Emily, I´m very glad of having known you. Our breaks,

conversations and dinners made my time there much better and funnier. I hope to see you girls again in some point of the future.

All the people I met in SD, specially Coral, with who I spent almost all my free time in SD and Handa, Victor F., Ryan, Christian. I will alway miss those lunchs in the UCSD and all the stuff we did together. Thank you for having done my stay in San Diego that special. To Jill, my flatmate for a long time in my stay in SD. Thank you for being such a good flatmate and friend.

The last but not the least Devon. Thank you for making my stay an unforgetable experience and having done the last part of my thesis such a special moment. I also will always be very grateful for all of your help.

TABLE OF CONTENTS

OBJETIVOS GENERALES

OBJETIVOS

El objetivo principal de esta Tesis Doctoral es el desarrollo y preparación de matrices de sensores colorimétricos de un solo uso para su empleo como lenguas ópticas para la identificación y determinación multianalito de iones metálicos de interés biológico en control ambiental, farmacéutico y alimentario; así como la preparación y caracterización de nanomateriales con finalidad sensora.

Para lograrlo, se plantean una serie de objetivos específicos:

- Desarrollar membranas sensoras para iones metálicos y aniones incluyendo químicas de reconocimiento de baja selectividad y suficiente sensibilidad. Así mismo se pretende la caracterización óptica de las membranas, modelizar la respuesta frente a posibles metales diana, evaluar el potencial de las membranas como sensores para iones metálicos, validando y aplicando los procedimientos que se establezcan.
- Diseñar e implementar una instrumentación portátil que permita la determinación in situ y simultánea de diversos analitos basado en los cambios de color que experimenten las membranas en presencia del analito o analitos.
- Extender la capacidad de discriminación del procedimiento aumentando, por una parte, el número de membranas sensoras con químicas de reconocimiento diferentes y, por otra, mejorando la reproducibilidad en la preparación de las membranas.
- Poner a punto la preparación de matrices de sensores mediante impresión por chorro de tinta, lo que exigirá la preparación de las tintas de impresión, elección de soportes y optimización de las condiciones de impresión.
- Establecer procedimientos tipo lengua óptica utilizando las matrices de sensores antes preparadas para identificar y determinar iones metálicos, basados en la

recogida de señal por técnicas de imagen y tratamiento de los datos de color mediante reconocimiento de patrones y/o análisis multivariado.

- Aplicar diversas rutas sintéticas y procedimientos de síntesis de nanopartículas tipo carbón dots; así mismo caracterizarlas y evaluar su potencial como sensores ópticos aplicados a muestras biológicas.
- Preparar y caracterizar silicio poroso nanoestructurado para estudiar su degradación en disoluciones acuosas a través de los cambios de color mediante las coordenadas RGB y HSV que experimentan, como son los cristales fotónicos. Comparar los resultados con los ofrecidos por la habitual técnica espectroscópica. Evaluar la posibilidad de utilizar instrumentación de bajo coste como puede ser la utilización de un Smartphone para aplicaciones en teledetección o suministro de medicamentos mediante liberación controlada.

THESIS ORGANIZATION

THESIS ORGANIZATION

This Thesis is presented under the system of a compilation of articles (agrupación de publicaciones) according to the Rules for development of the PhD dissertation at the University of Granada. The main results of the study conducted in this chapter have been presented as three articles in relevant journals.

This thesis is organized in the following manner:

* The Introduction is divided in two parts, Section I and Section II. Section I will include a review of the literature on sensors and mainly array-based sensors as well as concepts on color measurement and artificial intelligence techniques, the main tools used in chapters I and II. The Section II will consist on a review about nanotechnology and nanomaterials to introduce the topic described in chapters III and IV.

Chapter I addresses the design, development, characterization and validation of disposable sensors based on color change in response to metal ions as well as a first approximation to an optical tongue for the resolution of mixtures of metal ions. In a second stage we have designed and evaluated portable instrumentation for use in conjunction with the previously developed membranes. This work was done in collaboration with Department of Electronics and Computer Technology of the University of Granada.

The work presented in this chapter has resulted in the publication three articles already published. According to the system of compilation of articles, the first article "Characterization of disposable optical sensors for determination of heavy metals", and the second article, "Feasibility of using disposable optical tongue based on neural networks for identification and determination of heavy metals ", has been published in journals belonging to the first quartile of the field Analytical Chemistry, and are considered as Thesis papers. The third one, “Handheld colorimeter for

determination of heavy metal concentration", was carried out as an interdisciplinary collaboration with the group of Dr. Palma of the Department of Electronics and Computer Technology of the University of Granada.

Articles:

- J. Vukovik; M. Ariza-Avidad; L.F. Capitán Vallvey. Characterization of disposable optical sensors for heavy metal determination. Talanta, 94 (2012) 123.

- Ariza-Avidad, M.; Cuellar, M. P.; Salinas-Castillo, A.; Pegalajar, M. C.; Vukovic, J.; Capitán-Vallvey, L. F., Feasibility of the use of disposable optical tongue based on neural networks for heavy metal identification and determination. Anal. Chim. Acta (2013),783 (0), 56-64.

- López Ruiz, N.; Ariza-Avidad, M.; Martínez-Olmos, A.; Vukovic, J.; Palma, A. J.; Capitán-Vallvey, L. F. Handheld colorimeter for determination of heavy metal concentrations. J. Phys. : Conf. Ser.2011,307, 012037-1-012037/6.

Contributions to congresses:

- Congress: Reunión del Grupo Regional de la Sociedad Española de Química Analítica

  1.- Tittle: Evaluación de una cámara digital a color como dispositivo de medida en un sensor óptico multianalito

  Authors: Ariza-Avidad, María; Salinas-Castillo, Alfonso; Agudo-Acemel, Manuel; Capitán-Vallvey, Luis Fermín.

  Poster presentation. National. 2012. Málaga, España

  2.- Tittle: Desarrollo de un array óptico para screening de metales

Authors: Ariza-Avidad, María; Salinas-Castillo, Alfonso; Agudo-Acemel, Manuel; Capitán-Vallvey, Luis Fermín.

Poster presentation. National. 2012. Málaga, España

3.- Tittle: Análisis de sodio, potasio y dureza con sensores ópticos multianalito usando una cámara fotográfica digital.

Authors: Gómez-Sanchez, Joaquin; Ariza-Avidad, María; Salinas-Castillo, Alfonso; Capitán-Vallvey, Luis Fermín

Poster presentation. National. 2012. Málaga, España.

- Congress: I Simposium de Jóvenes Investigadores

  Tittle: Optical tongue for heavy metals based on colour measurement.

  Authors: Ariza-Avidad, María; Salinas-Castillo, Alfonso; Capitán-Vallvey, Luis Fermín.

  Oral communication. National. 2011. Torremolinos, Málaga, España.

- Congress: X European Conference on analytical chemistry, Euroanalysis XVI

  1.- Tittle: Disposable optical multisensor for heavy metals.

  Authors: M. Ariza Avidad, J. Vukovic, A. Salinas-Castillo, L.F. Capitán-Vallvey

  Poster presentation. Belgrade (Serbia).11-15 de Septiembre de 2011.

  2.- Tittle: Sensor array-based colorimetric portable instrument for pH determination in different matrices.

  Authors: S. Capel-Cuevas, M. Ariza Avidad, A. Martínez Olmos, N. López Ruiz, I. de Orbe-Payá, A.J. Palma, L.F. Capitán-Vallvey.

  Poster presentation. Belgrade (Serbia).11-15 de Septiembre de 2011.

- Congress: Sensors and their applications XVI

  Tittle: Handheld colorimeter for determination of heavy metal concentrations

  Authors: N. López Ruiz, M. Ariza, A. Martínez Olmos, J. Vukovic, A.J. Palma, L.F. Capitán-Vallvey.

Oral communication. Cork (Ireland). 12-14 de Septiembre de 2011.

- Congress: 13 Jornadas de Análisis Instrumental

  1.- Tittle: Disposable colorimetric sensor array for screening heavy metals

  Authors: Salinas-Castillo, Alfonso; Ariza-Avidad, María; Capitán-Vallvey, Luis Fermín

  Poster presentation. International. Barcelona.14-16/09/2011

  2.- Tittle: Handled CCD μcamera instrument for in-situ determination of heavy metals.

  Authors: Ariza-Avidad, María; López-Ruiz, Nuria; Martínez-Olmos, Antonio; Banqueri-Ozaez, Jesus; Capitán-Vallvey, Luis Fermín

  Poster presentation. International. Barcelona.14-16/09/2011

- Congress: I Simposio de jóvenes investigadores en espectroscopia aplicada

  Tittle: Mejora de la calibración multivariante de una lengua óptica para metales pesados por la técnica de bootstrapping

  Authors: M. Ariza Avidad, J. Vukovic, L.F. Capitán-Vallvey

  Poster presentation. National. Madrid. 6-9/07/2011.

- Congress: VII Colloquium Chemometricum Mediterraneum

  Tittle: Improving multivariate calibration of a disposable optical tongue for heavy metal analysis by Bootstrapping techniques

  Authors: Ariza-Avidad, María; Pegalajar-Cuéllar, Manuel; Pegalajar-Jiménez, Maria del Carmen; Capitán-Vallvey, Luis Fermín

  Poster presentation. National. 2010. Granada. España.

- Congress: European conference on optical chemical sensors and biosensors

  Tittle: Optical tongue for heavy metal determination based on disposable multisensor and colour measurement

  Authors: Ariza-Avidad, María; Pegalajar-Cuéllar, Manuel; Pegalajar-Jiménez,

Maria Del Carmen; Capitán-Vallvey, Luis Fermín

Poster presentation. International. 2010. Prague, Czech Republic.

- Congress: XII Reunión del Grupo Regional Andaluz de la Sociedad Española de Química Analítica.

  Tittle: Mejora de la calibración multivariante de una lengua óptica para metales pesados por la técnica de bootstrapping.

  Authors: Ariza-Avidad, María; Pegalajar-Cuéllar, Manuel; Pegalajar-Jiménez, Maria del Carmen; Capitán-Vallvey, Luis Fermín.

  Poster presentation. National. Córdoba, España. 2010.

Chapter II will be introduced and the printing inkjet system used to develop sensor arrays membranes with increased accuracy will be described as well as the development of the process of image gathering using a photographic camera, the selection of the region of interest and calculating the chromatic coordinate H of the HSV color space used as analytical signal. The composition and characteristics of the inks used and the working conditions of the printer will be of great importance for the development of arrays as well as the various treatments of neural networks developed to establish the presence and concentration of targeted metal ions. Two articles," Printed disposable colorimetric array for metal ion discrimination in water" and, "Inkjet-printed disposable metal complexing indicator-displacement assay for sulfide determination in water" support the work presented in this section. Both articles were sent to journals belonging to the first quartile of the area of Analytical Chemistry and are currently in the reviewing process.

Articles:

- M. Ariza-Avidad, A. Salinas-Castillo, M.P. Cuéllar, M. Agudo-Acemel, M.C. Pegalajar, and L.F. Capitán-Vallvey. Printed disposable colorimetric array for metal ion discrimination. Analytical Chemistry. 2014. In review.
- M. Ariza-Avidad, M. Agudo-Acemel, A. Salinas-Castillo and L.F. Capitán-Vallvey. Inkjet-printed disposable metal complexing indicator-displacement assay for sulphide determination in water. 2014. Analyst. Sent.

Contributions to congresses:

- Congress: XVIII Reunión SEQA

  1.- Tittle: Lengua electrónica impresa para clasificación y determinación de metales

  Authors: M. Ariza-Avidad, A. Salinas-Castillo, Manuel Agudo Acemel, M.P. Cuellar, M.C. Pegalajar, L.F. Capitán-Vallvey.

  Oral presentation. National. 2013. Hospital de Santiago. Úbeda (Jaén), España.

  2.- Tittle: Sensor óptico desechable para la detección colorimétrica de cobre (II) y sulfuro de hidrógeno en medios acuosos

  Authors: M. Ariza-Avidad, A. Salinas-Castillo, Manuel Agudo Acemel and L.F. Capitán-Vallvey.

  Poster presentation. National. 2013. Hospital de Santiago. Úbeda (Jaén), España.

Awards:

Award given by Sociedad Española de Química Analítica (SEQA) for the best comunication presented as a poster and defended as an oral flash communication to the XVIII Reunión de la Sociedad Española de Química Analítica conference, held in Úbeda, Jaén in 2013.

Chapter III will introduce and discuss the potential of detection of metal ions with biological applications with carbon nanoparticles. The possibility of using the Hue parameter, as an analytical parameter compared to the fluorimetric measurements will be discussed. Two articles already published in relevant journals guarantee the work developed and presented in this chapter. The first one, "Carbon dots for copper detection with down and upconversion fluorescent properties as excitation source", support the Thesis presented under the system of compilation of articles. The second paper, "Microsystem-assisted synthesis of carbon dots with fluorescent and colorimetric properties for pH detection" presented in this Thesis as Annex I is a work developed in collaboration with the Sensors and Biosensors Group headed by Professor J. Alonso Chamarro at the Department of Chemistry of the Autonomous University of Barcelona, Spain. The collaboration presented in this chapter deals with the development of a colorimetric chemical sensor for pH, using synthesized carbon dots and a camera to extract the analytical parameter, which was then compared with the results obtained by fluorescence measurements.

Articles:

- A. Salinas-Castillo; M. Ariza-Avidad; C. Pritz; M. Camprubí-Robles; B. Fernández; M.J. Rueda-Rama; A. Megía-Fernández; A. Lapresta-Fernández; F. Santoyo-González; A. Schrott-Fischer; L.F. Capitán-Vallvey. Carbon dots for copper detection with down and upconversion fluorescent properties as excitation source. Chem. Commun., (2013), 49, 1103.

- S. Gómez , A. Salinas-Castillo , M. Ariza-Avidad , A. Lapresta-Fernández , C. Sánchez-González , C. S. Martínez-Cisneros , M. Puyol , L. F. Capitán-Vallvey

and J. Alonso. Microsystem-assisted synthesis of carbon dots with fluorescent and colorimetric properties for pH detection. Nanoscale, (2014); 6(11):6018-24.

Contributions to congresses:

- Congress: XVIII Reunión de la SEQA 2013
  Tittle: Carbon dots for copper detection with visible and upconverting fluorescent properties as excitation source
  Authors: A. Salinas-Castillo, M. Ariza-Avidad, M. Camprubi-Robles, B. Fernández-López, A. Lapresta-Fernández, D. P. Morales, A. Palma, L.F. Capitán-Vallvey.
  Poster presentation. National. 2013. Hospital de Santiago. Úbeda (Jaén), España.
- Congress: 3rd International Conference on Bio-Sensing Technology
  Tittle: Evaluation of a reconfigurable portable instrument for copper determination based on luminescent carbon dots.
  Authors: Morales-Santos, Diego Pedro; Salinas-Castillo, Alfonso; Martínez-Olmos, Antonio; Ariza-Avidad, María; López-Ruiz, Nuria; Palma-López, Alberto J.; Capitán-Vallvey, Luis Fermín.
  Poster presentation. International. 2013. Barcelona, Sitges, España.

Chapter IV will introduce the synthesis and characterization of a novel nanostructured material called porous silicon. Different data processing of RGB and H parameters in order to monitor the porous silicon samples degradation will be discussed. A good correlation between both techniques will be demonstrated. One article, "Monitoring of degradation of porous silicon photonic crystals using digital photography", certify the work developed and presented in this last chapter. The work presented in this chapter was accomplish during the six months stay in the

group of Professor Michael Sailor at the University of California San Diego, UCSD, EEUU.

Article:

- M. Ariza-Avidad, A. Nieto, A. Salinas-Castillo, L.F. Capitán-Vallvey, G.M. Miskelly and M.J. Sailor. Monitoring of degradation of porous silicon photonic crystals using digital photography. Nanoscale Research Letters. In review.

Contributions to congresses:

- Congress: Porous Semiconductors - Science and technology 9th international conference
  Tittle: Monitoring of degradation of porous silicon photonic crystals using digital photography
  Authors: M. Ariza-Avidad, A. Nieto, A. Salinas-Castillo, L.F. Capitán-Vallvey, G.M. Miskelly and M.J. Sailor.
  Poster presentation. International. 2014. Benidorm, Alicante, Spain.

∗ The Conclusions section will summarize the results obtained in the Thesis and outline the potential future work.

Workshops:

- Summer school for Silicon nanotechnology, San Diego, California, EEUU, 2013.
- 3º workshop de Resolución estructural mediante difracción de rayos-x de monocristal, Granada, España, 2011.

- 8th Advanced study course on optical chemical sensors (ASCOS), Cork, Ireland, 2011.
- Workshop on Effective research writing and speaking. Zagreb, Croatia, 2009.

ACRONYMS

ACRONYMS

AAS	Atomic Absorption Spectroscopy
ACDA	(2- Aminocyclopentene-1- Dithiocarboxylic Acid)
AECID	Agencia Española de Cooperación Internacional para el Desarrollo
AFS	Atomic Fluorescence Spectroscopy
AMP	Adenosine monophosphate
ANNs	Artificial Neural Networks
ANOVA	Analysis of Variance
API	Atmospheric Pressure Ionization
ATP	Adenosine triphosphate
ATR-FTIR	Attenuated Total Reflectance-Fourier transform infrared
BFGS	Broyden-Fletcher-Goldfarb-Shanno
BODIPY	Boron-Dipyrromethene
Br-PADAP	2-(5-bromo-2-pyridylazo)-5-(diethylamino)phenol
BTC	Benzethonium chloride
CA	Cellulose acetate
CAD	Cadion. 1-(4-nitrophenyl)-3-(4-phenylazophenyl)triazene
CCD	Charge-coupled device
CMC	Carboxymethylcellulose sodium salt
CMYK	Cyan, magenta, yellow, and key (black)
CS	Chromazurol S. (Z)-5-((3-carboxy-5-methyl-4-oxocyclohexa-2,5-dien-1-ylidene)(2,6 -dichloro-3-sulfophenyl)methyl)-2-hydroxy-3-methylbenzoic acid ICP-MS In-ductively Coupled Plasma/Mass Spectrometry
DMEM	Dulbecco's Modified Eagle Medium
DMG	Dimethylglyoxime

DPC	Diphenylcarbazide
DTZ	Diphenylthiocarbazone. Dithizone
EDTA	Ethylenediaminetetraacetic acid
ELISA	Enzyme-linked immunosorbent assays
EMEA	European Medicine Agency
EOT	Effective Optical Thickness
EPA	Environmental Protection Agency
ERDF	European Regional Development Fund
FER	Ferrozine 3-(2-pyridyl)-5,6-diphenyl-1,2,4-triazine-4',4"-disulfonic acid sodium salt
FET	Field Effect Transistors
FFT	Fast Fourier Transform
fpSi	Freshly etched pSi
GTP	Guanosine-5'-triphosphate
HCA	Hierarchical Cluster Analysis
HDPE	High density polyethylene
HEK293 cells	Human Embryonic Kidney 293 cells
HSV	Hue Saturation Value
HTMAB	Hexadecyltrimethylammonium bromide
HVC	Hue-Value-Chroma
ICP-AES	Inductively Coupled Plasma/Atomic Emission Spectrometry
IR	Infrared
IRF	Instrument Response Function
ISE	Ion selective electrode
ISFET	Ion-Selective Field Effect Transistors
ISO	International Organization of Standardization
IUPAC	International Union of Pure and Applied Chemistry

LCD	Liquid Crystal Display
LD	Limit of the Detection
LED	Light-Emitting Diode
LTCC	Low Temperature Cofired Ceramic
MeSeMA	Metal-Sensor Multicomponent Analysis
MIP	Molecularly Imprinted Polymer
MLP	Multi-Layer Perceptron
MOSFET	Metal-Oxide-Semiconductor Field-Effect Transistor
MSE	Mean Square Error
MTT	3-(4,5-dimethylthiazol-2-yl)-2,5-diphenyltetrazolium bromide)
NIH-3T3 cells	Mouse embryonic fibroblast cells
NIR	Near Infrared Light
NN	1-nitroso-2-naphthol
NPOE	O-nitrophenyloctylether
NPs	Fluorescent nanoparticles
OLED	Organic Light-Emitting Diode
PAN	1-(2-pyridylazo)-2-naphthol
PAR	4-(2-pyridylazo)resorcinol
PCA	Principal Component Analysis
PDI	Polydispersity Index
PEG	Polyethylene glycol
PEI	Polyethylenimine
PET	Polyethylene terephthalate
PhCs	Photonic crystals
PID	Proportional-Integral-Derivative
PS	Polystyrene
pSi	Porous Silicon

pSi-ch	Freshly porous silicon coated with the polymer chitosan
pSi-o	Porous silicon oxidized
pSi-oC_8	pSi-o silanized with methoxyoctyldimethylsilane
PTFE	Polytetrafluorethylene
PTR	Proton Transfer Reaction
PVC	Polyvinyl Chloride
PVDF	Polyvinylidene difluoride
PID	Proportional-integral-derivative
SCENIHR	Scientific Committee on Emerging and Newly Identified Health Risks
SEM	Scanning Electron Microscope
SLIM	Spectroscopic Liquid Infiltration Method
SPIS	Spacecraft Plasma Interaction System
TAR	4-(2-thiazolyazo)-2-resorcinol
TBP	Tributyl Phosphate
TCBP	Potassium tetrakis(4-chlorophenyl)borate
TCSPC	Time Correlated Single Photon Counting
TEPA	Tetraethylenepentamine
TIFF	True Image File Format
USB	Universal Serial Bus
VOC	Volatile organic compounds
VP	Pyrocatechol Violet
XO	Xylenol Orange. 3,3'-bis[N,N-bis (carboxymethyl) aminomethyl]-o cresolsulfoneph-thalein disodium salt
XRD	X-ray diffraction
ZIN	Zincon.2-carboxy-2'-hydroxy-5'-sulfoformazyl-benzene monosodium salt

Section I

Colorimetric Sensor

STATE OF ART

INTRODUCTION TO SENSORS

There is an increasing demand to measure the chemical environment both inside the body and in the surrounding environment. The substitution of classical analytical methods with more robust and modular sensors can potentially solve this pressing demand. Sensors allow real-time *in-situ* information to be obtained using low cost devices and, in addition, provide sufficient sensitivity and specificity for the measurement of the concentration of different unique molecular species. The goal of sensors is to reduce the response time by simplifying the analytical procedure without compromising the accuracy of the results.

According to Janata [1], chemical sensing is part of an information-acquisition process in which an insight is obtained about the chemical composition of the system under study in real-time. In this process, an amplified electrical signal results from the interaction between some chemical species and the sensor.

Achieving an unanimously accepted definition of a sensor is controversial due to the many sensor variants that may arise. The most accurate definition of a sensor is the definition offered by the IUPAC [2], where a sensor is considered as a device capable of recording directly, continuously, and reversibly a physical parameter (physical sensor) or the presence or concentration of a chemical species (chemical sensor) [3].

The entire sensor system consists of a sensitive layer, a transducer, a data-acquisition process, and an evaluation [4]. In Figure 1 a general diagram block of an instrument is presented [5] where it can be seen that a signal conditioner is required prior to processing. The output must be presented to the user by presenting the result in a display or sent via wireless signal since a portable instrument should be self-contained [6].

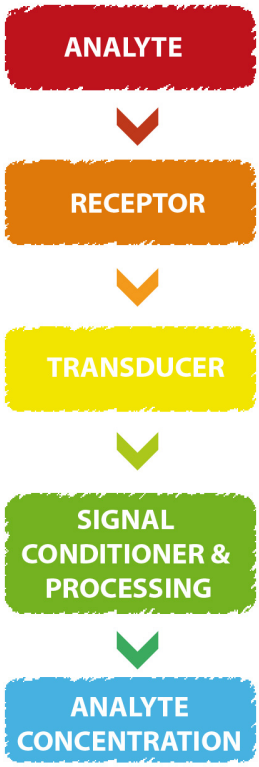

Figure 1. Diagram block of a sensor-based instrument.

A chemical sensor consists of a set of elements that can be grouped into three basic blocks (See Figure 2):

a) A recognition area where selective interaction occurs with the species or species of interest. The recognition element is the key component of any sensor. The interaction can either have optical, chemical, or biological origin. For example, electromagnetic radiation can be absorbed by an analyte, a chemical reaction can occur, or an interaction can occur between an analyte and an immobilized small-molecule or bio-molecule.

b) A transducer system able to convert chemical information into an electrical signal containing useful analytical information

c) An amplification system coupled to signal processing, whereby we obtain the results in units of interest.

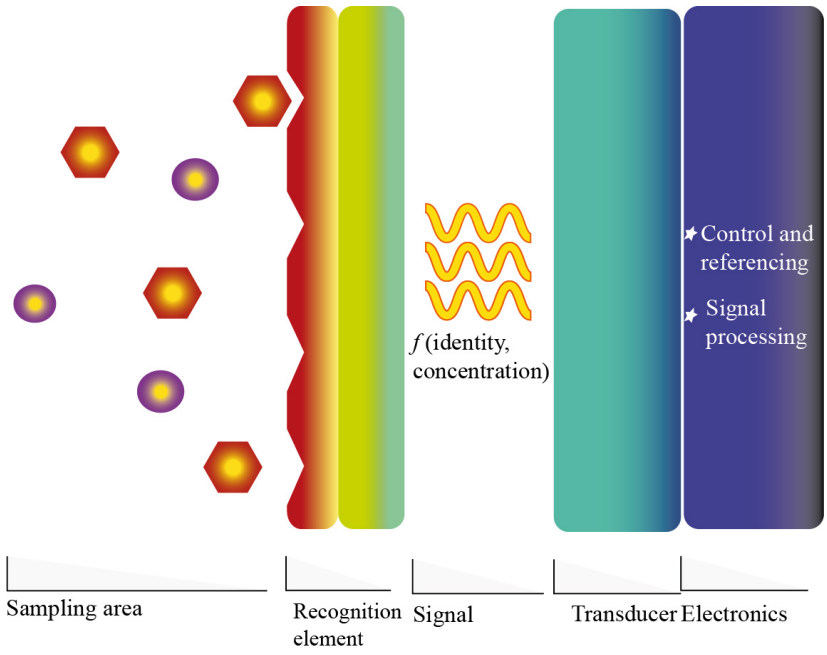

Figure 2. The main parts of a typical sensor

The general characteristics of a sensor can be grouped into four types: analytical, operational, temporal, and fabrication. The different components of each characteristic are: for analytical, precision, accuracy, selectivity and sensitivity; for operational, reversibility, reusability and an ability to simplify the analytical process; for temporal response, speed, real-time response, operational stability, and storage;

and finally, for fabrication, simplicity, cost, robustness, and integration capability, among others.

Jiří Janata [1] emphasizes two characteristics of a sensor which he considers fundamental: robustness and reversibility. The first, is defined as the ability of a device to maintain performance even under adverse operating conditions, such as conditions that can either be physical (shock, vibration, change of conditions) or chemical (changes in chemical ambient, which in turn is related to the selectivity). Alternatively, reversibility means that the response of the sensor is able to follow the changes in concentration of the analyte. The sensors can be thermodynamically reversible (ion selective electrode) or irreversible (enzymatic electrode).

The number of existing chemical sensors is huge and to give a general and schematic overview of the different types, we can classify them according to different criteria [7-9].

a) Type of process: passive, where the reaction between analyte and sensor is not directed but proceeds spontaneously, or active, where a reaction and/or separation of the analyte occurs in a specifically controlled recognition area.
b) Immobilized species in the recognition area: A species can be transiently or permanently immobilized by a chemical reaction.
c) The type of the recognition process: The recognition process can be based on different types of reactions and interactions such as complexation, redox, association, affinity, adsorption, catalysis or others leading to different types of interactions: host-guest, ligand-metal, carrier-ion, carrier-molecule, metal oxide-gas, enzyme-substrate, antigen-antibody, antigen-hapten or receptor-substrate, among others [9].
d) Sensing type layer: Active surface sensors whereby the immobilized reagents are located only at the surface, and thus the interaction of the analyte with the bulk membrane sensors only occurs at specified regions.

e) Separation process: separation may or may not occur in the recognition zone. This may be accomplished by adsorption, extraction, gas diffusion, dialysis or other mechanisms.

f) Type of generated signal: One can measure a very large number of different properties but in practice the most common [2] are optical, electrochemical, electrical, mass, magnetic or thermometric.

g) Relationship between receptor and transducer: Both elements may be different but connected, optical or electrically, or integrated into one device.

h) Mode of operation: A reversible sensor is the ideal sensor as these sensors respond like a physical sensor without consuming reagents to interact with the analyte. In contrast, irreversible sensors cause a response as a result of an irreversible reaction but may be reusable through a regeneration step if desired.

i) Arrangement of the sensor and the contact method with the sample: There are three different arrangements for the sensor. First, probe type, where a rod which is inserted into the solution in which the sensing phase is supported, i.e. in a waveguide in optical sensors [10;11]. Second, flow type, where the sample is injected or aspirated along with reagents to a flow cell connected or integrated with the measurement system, which can be a FIA [12;13] or microchip [14]. Third, flat drop type, where the receptor is a flat area where a small volume of problem is deposited. These types include single use sensors such as the conventional test strip [15] or the immunochromatographic lateral flow strip tests [16].

j) Form of operation: continuous or discontinuous.

k) Number of species monitored: one (monoparameter sensor) or more (multi-parameter sensor).

Numerous chemical sensors exist, however, the work presented is confined to optical sensors, whose principle consists of the interaction of electromagnetic radiation with a sample after a recognition event that modifies various optical parameters that may be recorded. Optical chemical sensors present some advantages as well as drawbacks with respect to alternative sensors. Among the pros we can mention: a) facility of use; b) no electrical interferences; c) no need of contact between the sensor and the sample; d) good sensitivity and reversibility; e) the information concerning the analyte can be encoded in varied forms; namely amplitude, phase, polarization or spectral information, which opens up the possibility of multiplexing; f) no consumption of analyte during measurement; g) can support, in some cases, extreme environmental conditions of temperature and humidity; and finally, h) their size can be reduced if necessary. Among the disadvantages are a) the influence of undesired variables on the measurement; b) the crossed sensitivity results in output signals with errors; c) the influence of a light source in the measurement; d) reduction in the ability of recognition by immobilization of reagents; e) problem of photodecomposition of immobilized reagents; f) large response times, in some cases; and g) calibration functions with short analytical range [17-20].

ARRAY-BASED SENSORS

Simultaneous analysis of complex mixtures is one of the most complex challenges that can be addressed by analytical chemistry. From the several approaches used for multianalyte systems, sensors are one of the most promising. One type of sensors of great interest are single-use sensors, also known as disposable sensors or one-shot sensors, by the advantages they offer of short analysis time, ease of use, low price, in situ results, no need for a skilled user, easy storage, preservation and transport of samples and absence of waste, and finally a representative green methodology. These

types of sensors are defined as self-contained analytical devices, as all necessary reagents are incorporated in and respond to the analyte by a (bio)chemical reaction [15].

One of the more interesting applications for the field of sensors is multi-analyte systems. The conventional approach involves having a different sensor for each analyte. This requires preparing a set of specific receptors for each of the target analytes through the design and synthesis of specific receptors using lock and key principles [21]. The disadvantage of this approach is due to the difficulty of achieving good selectivity for similar analytes and the multiple sensors required.

An alternative sensing paradigm has evolved which was inspired by mimicking the structure and properties of biological systems, namely the receptors involved in taste and smell. Thus, the nose and electronic tongue concepts have emerged, which have been shown very effective for identification and discrimination, opening the door to artificial multi-analyte systems that parallel the sensitivity and selectivity of the human senses [22].

In the case of smell, discrimination (> 10,000 substances) is attributed to a large number of low selective receptors, with high cross-reactivity, which is coupled to signal processing in the central and peripheral nervous systems.

Taste also involves a number of receptors, but discrimination is much less than smell, at least in humans, and there are only five existing types (sweet, salty, sour, bitter and umami) such that manifestation of taste is very qualitative [23]. The overall impression of foods is thus a superposition of both taste and smell, and the identification of foods is accomplished by both of these senses [24].

The initial idea for an electronic nose came in 1982 with the work of Persaud and Dodd in Nature [25] and was extended a few years later to allow for the identification of various gases and liquid. An electronic nose involves the use of a set, which will be called a matrix, of non-specific or low selective sensors to produce analytically useful signals for the analysis of multi-component samples that are then treated with

advanced mathematical procedures of signal processing by recognition patterns and/or multivariate analysis (neural networks, principal component analysis or others) [26]. Using these procedures, it is possible to identify chemicals using nonselective sensors and also to detect a large number of species with a small set of sensors.

Although the name of such analytical devices can be different, either referred to as an artificial nose, mechanical nose, odor sensor, taste sensor, taste system and taste chip [27], names which are often subject to controversy and used according to geographical areas; however, we prefer to keep the electronic tongue designation interchangeably with electronic sensing array within this Thesis.

One of the most interesting features of these devices is that they have helped to address irresolvable analytical problems with traditional approaches, such as qualitative descriptions of natural products (good coffee, wine or tea), which is not easily traceable to simple inspection of the constituents.

The efficiency of these systems can be achieved by increasing the amount of orthogonal chemical information generated by the set. This objective can be achieved in several ways: 1) increasing the number of sensors in the array with different sensitivity and materials that use the same principle of transduction; 2) by measuring various physical properties of each individual sensor using different principles of transduction; or 3) modulating the operating conditions of each individual sensor [28].

In any of these ways, the sensor array that constitutes both noses and electronic tongues produces signals that are not necessarily specific to any particular species but where the signal pattern correlates with certain features or qualities of the sample. Highlighting the utility of electronic noses, the use of electronic noses in industrial settings continues to increase as part of the monitoring of industrial processes, especially in agribusiness [22;29] (Figure 3).

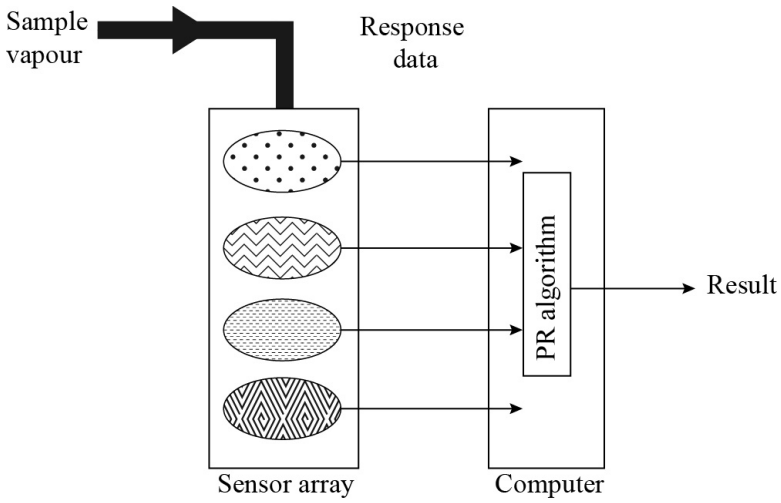

Figure 3. A generic electronic nose [22].

A second use of these devices is for quantitative analysis, since some analytes that cause interference or overlapping signals can be quantified directly using a set of sensors that characterize the cross-response together with appropriate multivariate calibration [25]. This possibility is particularly important for the detection of harmful or dangerous substances and for analysis in the biomedical field. Thus, the main objectives of these devices is in the qualitative discrimination, classification and identification of analytes and these devices can be expanded into the quantitative analysis of these analytes making them highly desirable in multicomponent determination.

An electronic nose includes three major elements: a sample delivery system, a detection system, and a computing system. The sample delivery system enables the generation of the volatile compounds of a sample. The volatile compounds are then injected into the detection system, which consists of a sensor array that reacts to these compounds, modifying some properties. Typically, each sensor is sensitive to

all volatile molecules but in different way. The computing system combines the responses of all of the sensors, uses these responses as input for the data treatment, and finally provides results [30].

Different principles have been used for the preparation of sensor arrays for both noses and electronic tongues. For electronic noses the systems more commonly used are: tin oxide catalytic sensors, conducting polymer sensors, acoustic wave sensors, quartz crystal microbalance sensors, sensors based on MOSFET technology, systems based on ion mobility spectrometry as well as in mass spectrometric techniques such as API or PTR and, finally, optical techniques, mainly fluorescence, in conjunction with fiber optics [22;31].

In the case of electronic tongues, electrochemical sensors are the most common, thus potentiometric, amperometric and voltammetric, but there are also optical sensors and biosensors [27;32]. However, most of these systems are based on potentiometric sensors, in particular ion selective electrodes (ISE). The main disadvantage of the potentiometric measurements is the influence of temperature, which must be minimized by control of the same or with previous tempering.

Many commercial instruments are electronic noses. A growing number of companies are involved in the development of instruments and these include, but are not limited to [27;30;32;33], Agilent Technologies (https://www.home.agilent.com, USA), Alpha MOS (www.alpha-mos.com, Francia), Atsugi (Japón) Bloodhound Sensors (www.bloodhoundssc.com, England), Cyrano Sciences Inc. (http://spinoff.nasa.gov/spinoff2001/ps4.html, USA), eNose (http://www.enose.nl, Holland), E-Nose Pty Ltd (www.enose.info, Australia), Food Valley Netherlands http://www.foodvalley.nl, Holland), Illumina Inc. (www.illumina.com, USA), Insents (http://www.insent.co.jp/en/, Japan), Marconi Applied Technologies (www.marconitech.com, England), McScience (http://www.mcscience.com, South Korea); Osmetech PLC (acquired in 2003 by Roche Diagnostic), Sensobi Sensoren

GmbH http://www.sensobi.com/index.htm, Germany), and TNO Food & Nutrition Research (https://www.tno.nl, Holanda).

The types of sensors mostly used in commercial instruments are potentiometric electrodes, ISFET and ISE, respectively, with a number of sensors ranging from 7 to 8. Taste Sensing System from Insents (Intelligent Sensor Technology Co.; Anritsu / Atsugi, Japan) is built like a multi-channel electrode in a robotic arm. It moves from a sample container to a cleaning solution and then re-samples. Recalibration is needed after a few cycles of measurement. Another commercial system - ASTREE (Alpha MOS, France) - uses chemical field effect transistor technology and is mainly dedicated to the pharmaceutical industry for estimating the acidity of biological substances, investigating the masking effects of various flavoring additives and the stability of the developed formulas (see Figure 4).

Figure 4. ASTREE electronic tongue from Alpha MOS (www.alpha-mos.com).

The eNose Company focuses on three product-lines containing e-nose technology for different fields:

i) Exhaled-breath detection (Aeonose™) with a diagnostic unit for exhaled-breath analysis. This unit can be used for screening of tuberculosis, asthma, throat cancer, and other diseases. The patient has to breathe into the diagnostic unit, and within minutes a proper indication is given whether additional patient examination is required.

ii) Detecting and identifying pathogenic bacteria (Aetholab™) with a diagnostic unit analyzing gases produced in the metabolic process of pathogenic bacteria in blood and other body fluids.

iii) Exploring new applications (Aerekaprobe™) with a laboratory type, compact electronic nose containing a set of sensors for developing new applications that could be transformed to dedicated electronic-nose products in larger volumes.

Finally, Multiarray Chemical Sensor (McScience, Inc. South Korea) is based on PVC membranes and polyurethane that detects $H^{+,}$ Na(I), K(I), Ca(II), NH^{4+}, NO^{3-} and Cl^{-}; and is dedicated to the quantitative analysis of different flavors and recognition of beer and tea. In all these devices the procedure for obtaining results is based on principal component analysis (PCA). The equipment is relatively complex in both use and maintenance and may be used only under controlled laboratory conditions. As examples we can cite some interest in the food industry, where they were used for the identification of spirits, olive oils, cheeses, meat products or water or agriculture to develop irrigation strategies 34 for assessment of fruit maturity 35 or for evaluating the freshness of fish 36 .

In short, the main advantage of the electronic tongue systems is the ability to adjust the operating mode to the desired application (Figure 5).

This means that, after a proper calibration, such devices can perform functions such as: 1) multi-analyte quantitative analysis (detailed analysis of a wine); 2) discrimination; 3) classification (type of wine); 4) recognition (fruit ripening) and 5) simulation of human tasting panels.

Figure 5. Electronic tongue Cyranose 320 by Cyrano Sciences, California, USA.

OPTICAL ELECTRONIC NOSES

For electronic noses, the number of laboratory and commercial devices is much higher than in the case of tongues. The most interesting experimental approaches based on optical sensors that have been described are:

1) Based on a set of optical fibers, with the sensing phase located at the distal end, gathering the image by a CCD camera, which is then treated with various mathematical techniques. The use of fiber optic arrays is a powerful alternative, especially for fluorescent sensors. In order to increase the dimensionality of the data usually fluorescence is measured (intensity, lifetime, wavelength and shape of the

spectrum) and even the evolution of signal over time is measured. As a sensing phase it has been used a solvatochromic indicator –usually Nile Red- usually adsorbed on different polymers of varied polarity causing different temporal patterns by changes in microenvironmental polarity and swelling of the polymer when exposed to volatile organic compounds (VOC).

Including these sensing phases in the set of optical fibers (array) different procedures have been used: a) by simple coating [37], b) by photopolymerization [38;39], and c) by chemically etching a set of microwells at the end of the fiber where the sensing phases are randomly placed incorporated into microspheres [40-42]. In order to ameliorate the loss of physical position as a useful measurable property, these beads are functionalized with optical encoding elements so as to identify themselves during the analysis. To achieve simultaneous, multi-analyte, high-density, and high-throughput sensing analysis, the arrays were prepared using optical fiber bundles that comprise thousands of individual single-core fibers which are individually modified with a diverse sensing chemistry using a random assembly method [43] (see Figure 6).

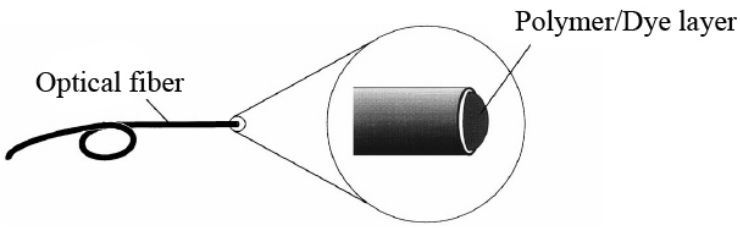

Figure 6. A fiber optic chemical sensor, in which a fluorescent dye is immobilized at the distal tip of the fiber [42].

The main problem of arrays with a sensing phase deposited is its inability to

transfer training from one array to another due to the lack of reproducibility in the preparation of the arrays[44]. With the incorporation of alumina particles a considerable increase in sensitivity is achieved [45], the increased sensitivity arising from the use of chromatographic microspheres of different composition thereby improving both accuracy and temporal stability (Figure 7). This is due both to the high homogeneity of the material and the use of a large number of redundant sensors to average signals [46].

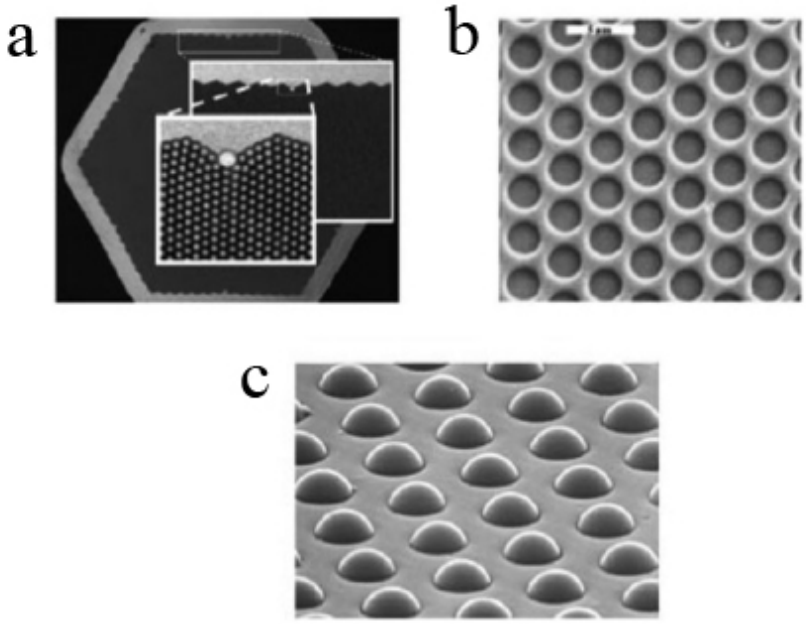

Figure 7. SEM images of etched fiber-optic bundles. a) Optical fiber-based array with hexagonal pits contains 50000–60000 fibers; inset shows magnified views of the individual fibers; b) microwells etched into the individual fibers and surrounded by cladding; darker gray circles correspond to the ends of the optical fibers defining the bottom of each well; c) beads loaded into wells [51].

This technology has been used in situations where it is necessary to quickly discriminate the presence of certain compounds at very low levels, for example, nitroaromatic compounds produced from the decomposition of explosives in buried

landmines [47-49]. Detection has been improved in the case of 2,4-dinitrotoluene vapors by combining nonspecific sensors with semi-selective sensors, such as a pentiptycene-derived fluorescent polymer that acts as a molecular switch [50].

This type of recognition along with pattern recognition techniques has allowed for the development of portable instrumentation for field use [52] (Figure 8).

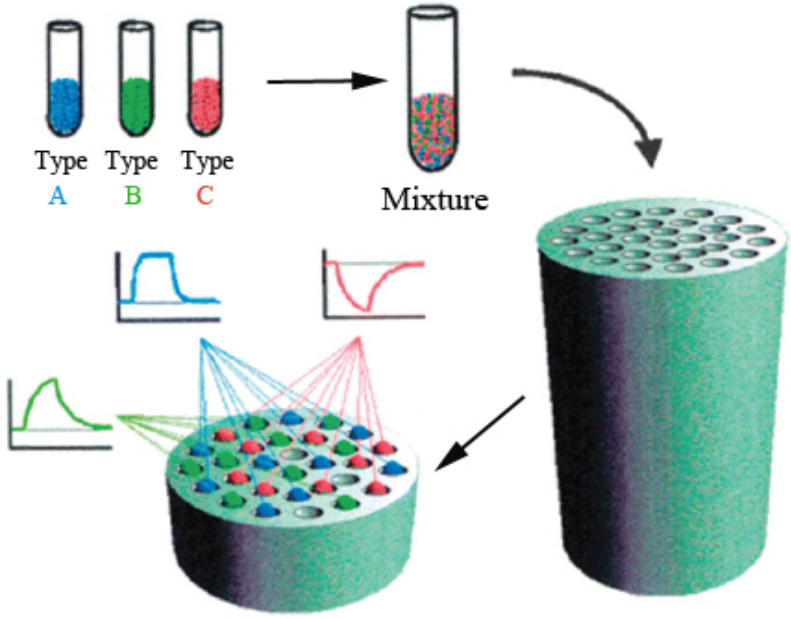

Figure 8. General strategy used for creating bead microarrays using etched fiber optic bundles. Types A, B, and C indicate the types of self-encoded beads, while the insets represent a typical time-based sensor response to an exposed analyte [41]

2) These devices are based on a set of different membranes (matrix), for example 25 or 36, arranged on a support, which change color upon exposure to the gas or vapor and whose image is collected with a conventional scanner. The signals generated, usually the RGB coordinates of each membrane, are processed with

pattern recognition and / or multivariate analysis (HCA, PCA) [53;54]. In this strategy, unlike the previous one, a greater variety of reagents is used which try to explore differences in charge, polarity, acid-base character and donor-acceptor character of analytes [55].

Based on the intermolecular interactions responsible for optical changes, one may divide chemoresponsive reagents into five separate classes: a) Lewis acid–base dyes (i.e., metallic complexes); b) Brønsted acid or basic dyes (i.e., pH indicators); c) dyes with large permanent dipoles (i.e., zwitterionic, solvatochromic, or vapochromic dyes) for detection of local polarity and hydrogen bonding; d) redox dyes; and e) chromogenic aggregative colorants (including simple ionic sulfides and plasmonic nanoparticle precursors) [51].

For gas phase sensing, the colorimetric sensor array is digitally imaged before and during exposure to mixtures of odorants, usually by means of a flatbed scanner, digital camera, portable handheld readers, or even smart phones with a camera (See Figure 9).

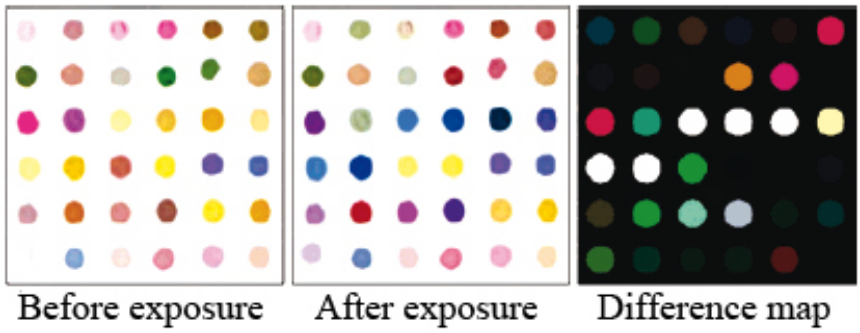

Figure 9. Image of the 36-dye colorimetric sensor array before exposure (left) and after exposure to decylamine (middle) after equilibration at full vapor pressure at 295 K [53].

Each analyte generates a characteristic pattern of colors which allows its identification, as several properties are analyzed simultaneously [56].

In general, the substrates used are hydrophobic, thus hydrophobic silica gel chromatoplates, polymers like nylon or PVDF, however, paper has also been used [57]. The potential solution of analytes is larger than in the first approach described (optical fiber) (amines, alcohols, arenes, ethers, phosphines, thioethers, thiols, ketones, halocarbons) [55], although inorganic gases such as CO, PH_3, H_2S or NH_3 can also be detected. In regards to gases, many can be identified and even quantified, with groups up to two or four gases and/or vapors [58].

The main applications although not unique to optical sensor arrays can be classified into three groups: 1) Discrimination of volatile organic compounds; 2) Toxic industrial chemicals and 3) Explosives detection [51].

One application of interest is the discrimination of amines, as they have been studied 12 different ways utilizing metallic complex sensing phases that discriminate by size/shape, analyte acidity/basicity, and polarity [45]. Additionally, this concept has been applied to the discrimination of food products such as beers by analyzing headspace volatiles [59;60], coffee by analyzing the aroma of coffees both in whole bean and ground form [61] or commercially available soft drinks [62]. The research group of Dr. Suslick at the University of Illinois (USA) has developed this type of electronic nose, that has been marketed through the company ChemSensing, Inc. (http://www.chemsensing.com/ ChemSensing , Inc./).

A similar system have been proposed by Huang et al. for monitoring fish freshness based on volatile compounds produced during spoilage of fish and a colorimetric sensor array by printing the nine chemoresponsive dyes on a reverse phase silica gel plate [63]. The incorporation of different dyes into inorganic solids then placed in a ELISA microplate was used by Salinas et al. for monitoring chicken meat freshness [64]. Using the same concept, Carey et al. identified different species and

specific strains of human pathogenic bacteria, 10 strains of bacteria including *Enterococcus faecalis* and *Staphylococcus aureus*, based on volatile compounds produced during bacterial growth [65]. A disposable colorimetric paper sensor array for the detection and discrimination of five explosives –triacetone triperoxide, hexamethylene triperoxide diamine, 4-amino-2-nitrophenol, nitrobenzene, and picric acid- has been presented based on the chemical interactions between the explosive species and the chemical reagents, extracting the colorimetric pattern using a smartphone [66] (See Figure 10).

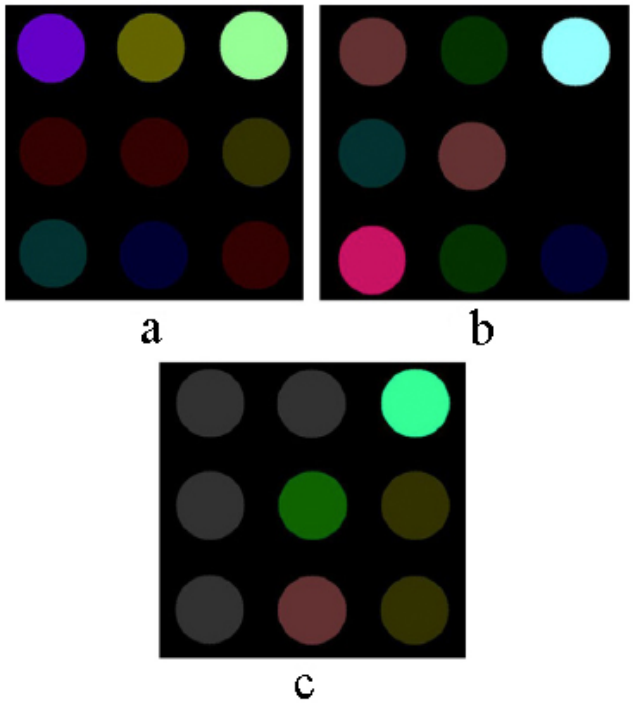

Figure 10. Difference images of the sensor array containing metalloporphyrins, pH indicators and solvatochromic dyes, before and after exposure to volatiles for a fish sample at day 1 (a), day 4 (b) and day 7 (c)[63].

3) There are other approaches, although with less interest and limited utility. Akrajas et al. [55] proposed using Langmuir-Blodgett type membranes, containing four

types of metalloporphyrins, placed in a flow system by measuring the reflected radiation after reacting with the VOC solution (two alcohols and two ketones) when illuminated successively with four LED of different color. Tanaka et al. [67], for their part, proposed the use of well known gas indicators tubes to monitor "bad smells" in the living environment by measuring with a scanner when the gas passes through the tube.

OPTICAL ELECTRONIC TONGUES

As previously indicated, most of the electronic tongues are based on electrochemical measurements, and to a much lesser extent on optical type measurements. If we consider the optical type electronic tongues [51;68;69], the focus in this Thesis, various approaches have been described:

1) Use of optical fiber with a set of fluorescent reagents, thus reagents for pH, O_2 and CO_2, covalently bonded or entrapped at the distal end of the same fiber so that the signal transmitted by the same generate a characteristic fingerprint [59]. The reagents may also be deposited in different optical fibers [70] or incorporated into microspheres placed in microwells engraved at the end of the fiber and which signals are later deconvoluted using multivariate algorithms. The immobilized fluorescent bead strategy that the Walt group developed for use with microwelled optical fiber bundles has also been applied as optical tongue too for detection of three strains of *E. coli* [71].

2) Use of matrices of polymeric microspheres with the surface chemically modified to allow covalent binding of receptors (conventional reagents, enzymes, antibodies). These microspheres, which somehow resemble the taste buds, are placed in micromachined wells made in silicon structures. Various methods have been used for contacting the sample with the device. In a first design the 3x3 matrix is contacted with the solution via a set of pipes and after equilibration the image is

collected by a CCD camera [52]. A further refinement placed the microspheres within pyramidal wells dug into silicon wafers, where there can be over 100 of such microspheres, which serve as microreactors and analysis chambers, improving the contact with the sample through a flow cell, in addition, a video card was included to measure the evolution of the signal with time [72]. This experimental design was used with various types of recognition systems addressing different problems: a) reagents covalently bonded to PEG-PS beads, thus fluorescein (pH), or o-cresolphthalein complexone (Ca(II), pH), alizarin complexone (Ce(III), Ca(II), pH) and boronic esters (fructose, pH) [73]; b) differential receptors fixed on microspheres, thus guanidinium type on Tentagel microspheres with optical transduction based on indicator-displacement assay for recognition of ATP, AMP and GTP nucleotides using principal component analysis (PCA), [74] or receptors with peptide and boronic acid groups and transduction with bromopyrogallol red forming a reversible cyclic ester with boronic groups, or receptors for recognition of proteins and glycoproteins by PCA [75]; c) multilayer microspheres with a reagent that changes color in the interior and linking groups uncolored at the surface (called microspheres with chromatographic and detection layers integrated), thus alizarin complex on the inside and EDTA and acetate units on the surface to recognize Zn(II), Ni(II) and Pb(II) using the RGB signals varying with time and pattern recognition algorithms [76]; d) use of polymeric membrane arrays including quantum dots suspended over cavities in silicon wafers, with bound reagents which change color by the interaction with the analytes, which are measured by conventional spectrophotometry or fluorimetry [73] (see Figure 11).

3) Molecularly imprinted polymers (MIPs) to discriminate among aromatic amines using the change in absorbance of the analytes themselves retained in the MIP upon interaction with linear discriminant analysis [77]. The restriction that the

analytes themselves generate the signal was later resolved in a study using the dye displacement technique [78].

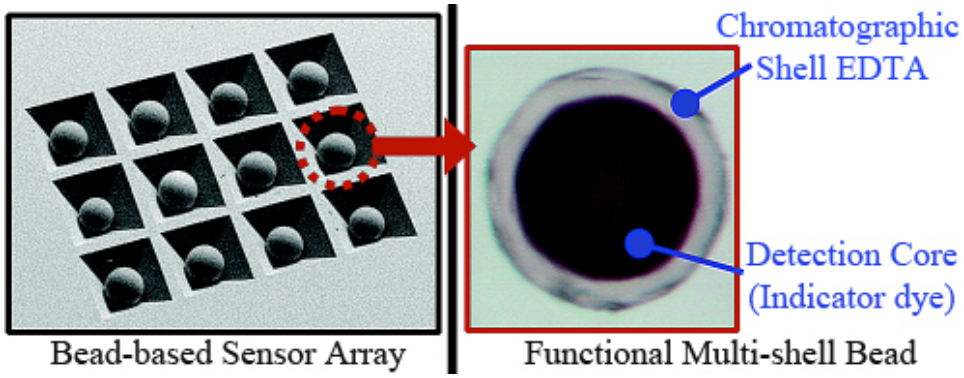

Figure 11. Array Sensors with multishell microspheres with integrated chromatographic and detection layers [76].

4) Different approximations have been described for an optical tongue using a set of receptors, although measuring the optical response in solution, usually by providing the reagents in microwells and routinely measuring the absorbance at one or more wavelengths. An example is the proposal by Rangin et al. [79] and later modified by West et al. [80] to identify Gram negative bacteria based on the specific glycolipids sequence they possess. For this, they use a set of liposomes prepared from different polydiacetylenes derivatized with amino acids. The color changes from blue to purple with the set of different liposomes for a given bacterium providing a discernible fingerprint. Another example is the proposal of Lee et al. [81] for discriminating 23 carbohydrates based on their reaction with a boronic acid. The different stability constant of resulting cyclic esters causes the pH of the solution to vary depending on the carbohydrate present, which is highlighted by using a set of pH indicators. Chang et al. have developed a spectrophotometric microplate assay for the evaluation of tap and bottled water using 45 dyes of different types, that classify water samples in terms of their place of origin, metal ion content, and

carbohydrate content [82]. On other occasions, the optical information from microplate wells was obtained by a CCD camera. Thus, it has been described an array for the detection of proteins using tetraphenylporphyrins derivatized in the periphery with amino acids and peptides resulting in receptors of differing in charge, size, hydrophobicity and symmetry, allowing the fluorescent transduction through variation in fluorescence intensity or quenching [83].

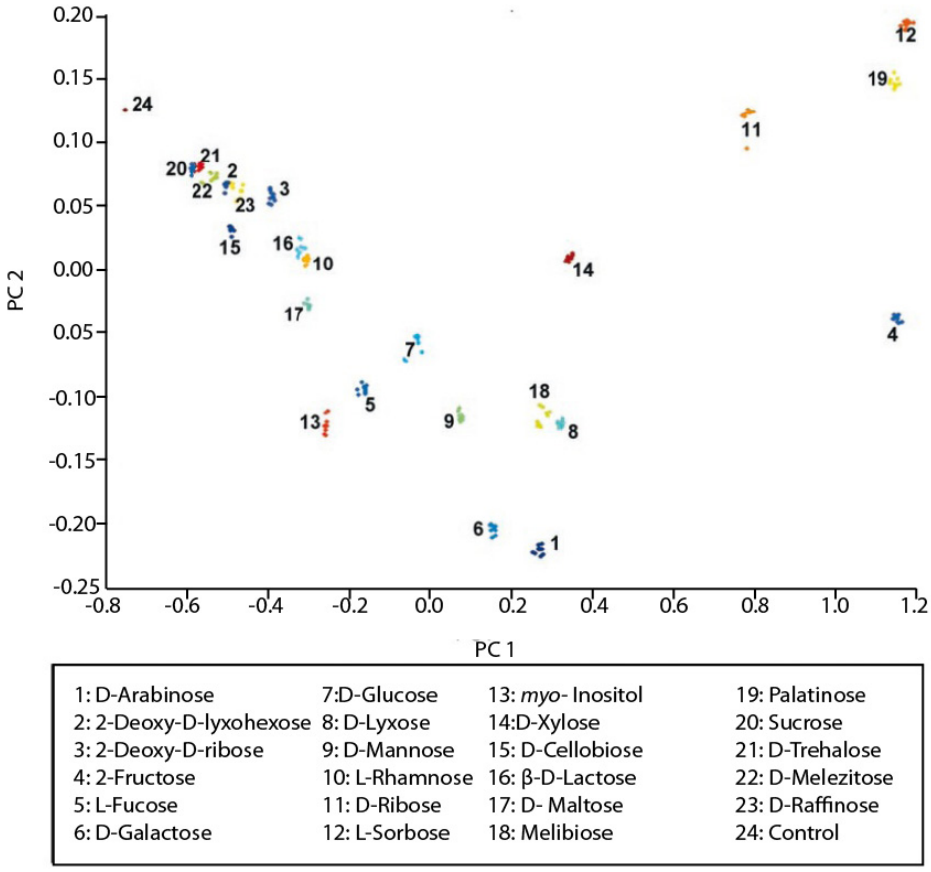

Figure 12. Principal component analysis (PCA) plot for the identification of 23 carbohydrates using six probe pairs based on their different binding constants to boronic acid, that generate diverse changes in pH [81].

Another example is the use of an array of different oligonucleotides with recognition sites based on three-way junctions functionalized with a fluorophore, capable of interacting with different molecules and used for discriminating cocaine and various steroids [84] (Figure 12).

Unlike these previous examples, recognition reagents can be set on the chip itself.

Thus, various fluorescent dyes immobilized in PEG for the detection of Ca(II), Na(I), Mg(II), Hg(II), SO_4^{2-} and Cl^- using a Dual Lifetime Referencing technique with CCD camera although working in grayscale [85]. In further work, the procedure for determination of mixtures of Ca(II), Cu(II), Ni(II), Cd(II) and Zn(II) was refined improving the instrumental system for measuring the fluorescence with the CCD camera and using neural networks and support vector machines for data processing [86].

5) Systems based on arrays of different colorimetric membranes bidimensionally arranged on a flat support of hydrophobic silica. They change color after the reaction, picking up the image with a scanner. The RGB coordinates of each membrane are used for classification by HCA, having been proposed for recognition of organic compounds in water [87]. Musto, Lim, and Suslick have developed a colorimetric sensor array for detection and quantification of sugars and artificial sweeteners using arrays of chemoresponsive chromophores based on boronic acids interaction with diols [88]. Others systems of this type have been suggested, thus for metals [89] and specific cases, such as Fe(II)/Fe(III) speciation with the reagents arranged on filter paper [90].

In the ECsens research group in which has been carried out this Thesis work disposable optical tongues have been developed for the detection of alkaline ions based on transparent supports containing membranes that operate by ionophore-chromoionophore chemistry, each membrane bearing different nonselective ionophores for alkaline ions. The image of the sensing device after reaction with the

solution is obtained by a scanner using as an analytical signal the chromatic coordinate hue (H) of the HSV color space. Two different approaches for calculating alkaline ion concentrations have been used. In the first approach, the response of each sensing membrane is modeled and the concentrations predicted using the K-nearest neighbor classification method [91], while in the second approach, signals are processed by multilayer artificial neural networks [92].

Another line of research developed in ECsens group refers to a color-based disposable sensor array for operation in the full pH range (0-14). The pH sensing elements were a set of different pH indicators immobilized in plasticized polymeric membranes working by ion-exchange or co-extraction. The color changes of the 11 elements of the optical array were obtained from a commercial scanner using the hue or H component of the hue, saturation, value (HSV) color space, which provides a robust and precise parameter, as the analytical parameter. Different approaches for pH prediction from the hue H of the array of the sensing elements previously equilibrated with an unknown solution were used: linear model, a sigmoidal competition model and sigmoidal surface model [93], as well as neural networks [94]. To reduce the size of the sensing array a multicriteria optimization task with the dual objectives of error minimization between the network pH prediction and the reference pH in the calibration data, and of minimizing the network complexity and the number of network inputs was used. After the analysis, it can be concluded that the use of a sensor array made up of 4 sensing elements offers a good pH prediction over the full-range working with 4 hidden neurons [95] (Figure 13).

The previous approaches show certain limitations; thus, multivariate regression methods require higher amounts of computer memory or speed so therefore they are not suitable for implementation in portable electronic devices with low resources, while the neural networks method is a "black box" whose operation cannot be easily modeled and explained for industrial development validation.

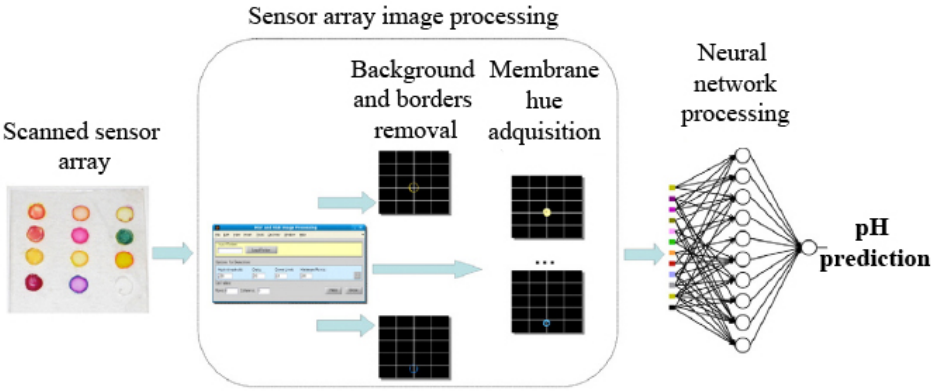

Figure 13. Optical tongue for full-range pH determination based on color measurement [94].

To overcome these problems a system has been developed that makes an accurate pH prediction, and it comprises a balance between memory and microprocessor speed for its integration within embedded systems with low memory and chip resources, providing in addition, a suitable explanation of why such predictions are made [96].

Various portable optical instruments based on a pH array previously described has been developed. The first uses only four membranes containing acid–base indicators to cover the full range of pH using the H coordinate. The membranes were directly cast onto a plastic support to form a two-dimensional array, located between an OLED display as the programmable light source and a set of digital color detectors. The microcontroller-based instrument permits pH determination using a simple programmed algorithm [97]. Also, the previously characterized portable instrumentation has been improved by implementing a neural network programming method optimized for the prediction of the pH in the full range [98] (See Figure 14).

6) A very different strategy is used by Edelman et al. [99] for estimating astringency in wine based on the interaction of polyphenols with immobilized proline-rich proteins in the cell a flow system monitored by IR spectroscopy.

In summary, there are a number of approaches to multi-analyte analysis using both electronic tongues and noses, of which few are of the optical type, as seen by the summary above. Almost without exception, the different optical devices have only been studied to demonstrate the usability, however their utility in practical applications has not been pursued [26].

Most of the different optical approaches used for both tongues and noses are based on the measurement of color using different color spaces obtained from the image generated by imaging devices, scanners and CCD cameras mainly. By far the most used space is RGB, and these coordinates are processed by the system of pattern recognition and/or multivariate analysis.

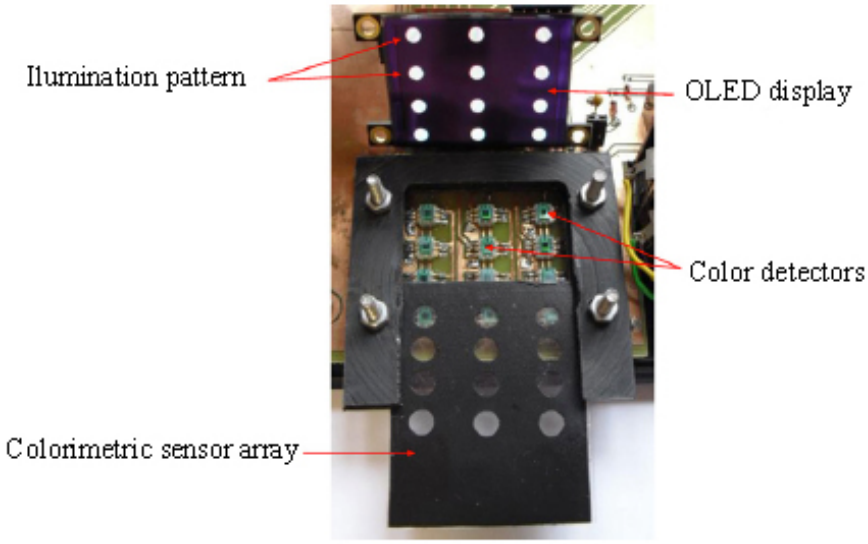

Figure 14. Sensor array-based optical portable instrument for determination of pH. Detail of sensing module showing the OLED display, the colorimetric sensor array support and the digital color detector array [97].

The basic requirements for optical tongue type systems referring to the sensor array, that is the system key, are that sensors present low selectivity, or what is the same, high cross-sensitivity and reproducibility [26]. At a certain sensitivity and selectivity threshold a sensor becomes less robust [55]. One solution is the use of disposable sensors and therefore not integrated into the device such that the sensor can subsequently be re-used. The sensor however must remain cheap and portable.

Sensor arrays explore chemical properties of analytes, rather than physical properties. The primary limitation is that it gives a composite response to complex mixtures which in turn is an advantage, since it can respond to different analytical goals. Is a mixture similar to another? How many components have changed? Is the mixture genuine or counterfeit? Was this material processed correctly or not? In that way the composite response generated can fingerprint complex mixtures, answering complex questions that have a difficult solution. A significant characteristic of sensor arrays is that there is no uniform intrinsic response to different analytes. This is interesting in some cases as for highly reactive analytes, e.g., toxic gases, easily detected at very low concentrations. In other cases, with less reactive gases, the sensitivity decreases dramatically. A specific problem for optical tongues is the need for the analytes to easily access the immobilized reagents while the reagents must not dissolve or leach into the solution. The right selection of the polymer membrane, the correct methods of chemical immobilization, and recognition are key to ensuring the success of the sensing array.

One of the problems with many of the systems described is the lack of precision of the measurements, which increases the error of the predictions. The lack of precision is due to the variability in the preparation of the array as well as the batch to batch variability. Some of the alternatives proposed include the use of microspheres placed on a micromecanized silicon chip [77], which leads to systems with good performance, although suffering from being experimentally complex and

possessing a high price. The second most used alternative is marketed by the company ChemSensing, although more for noses than for optical tongues. The usual way of preparing these matrices occurs by depositing small volumes of a solution containing reagents on a cromatoplate, however this shows some variability which results in difficulties for the quantification of analytes.

COLOR MEASUREMENT

Color is a visual perception that is generated in the brain when synapses are received after light reaches the retina. Thus, the color is not an intrinsic feature of the matter, but depends on how light is reflected by an object and how it is perceived by each person [100]. While color can be described accurately by measuring the spectral power distribution of the light originating (energy per unit area and wavelength of a given lighting), this entails a high degree of redundancy because the retina is sensitive to color in three broad areas of wavelengths, corresponding approximately to red (L, large wavelengths), green (M, medium wavelengths) and blue (S, short wavelengths) regions of the spectra. The electrical signals of these retinal cells (cones) together with the intensity sensitive cells (rods) are combined in the brain leading to the different sensations of color clarity, hue, saturation, shape, size, texture, location or other, and are called color psychological attributes.

Despite the subjectivity of color, as it depends on how it is perceived by the observer, the color can be specified numerically from the resulting experimental laws of empirical generalization known as trichromatic generalization [101]. From physical measurements of radiant power and using various types of sensors, it is possible to define numerically a color. The most common are thermal and photonic devices, the latter being based on the external photoelectric effect (photoemission) or the internal photoelectric effect (photovoltaic and photoconductivity), where the devices that are

frequently used are either charge-coupled devices (CCD) and complementary-metal-oxide-superconductor (CMOS) devices.

In all the applications related to color, the light source is an important feature to take into account. The International Commission on Illumination (CIE) has defined several standard illuminants identified by a letter or a number. In this way, illuminant A represents incandescent light, B direct sunlight, C an average of the daylight, D represents the phases of daylight, E is the equal-energy illuminant, and F the fluorescent light sources. The D65 illuminant is the most common used in colorimetric applications which represents a phase of natural daylight with a color temperature of 6504 K approximately [102].

The way to specify, create and visualize colors is through so-called color spaces. A color space is a combination of an abstract mathematical model and an appropriate graphical representation of this model. The color space describes different colors as a sequence of numbers, which depends on the used model. Commonly, a color is defined as a linear combination of the main color components used in a color space. It is possible to classify the color spaces in four different types: linear-light tristimulus (XYZ, RGB, CMYK), xy chromaticity, perceptually uniform (CIELAB) and hue oriented (HSV, HVC) [102]. In this Thesis the color spaces mostly used are the RGB and HSV (see Figure 15).

To understand the measurement of color it is necessary to define several concepts related to the colorimetry. Although using a three-dimensional diagram, the colors visible by the human eye can be represented, the concept of color can be also separated in two different sides: luminance and chromaticity. Luminance, which is related with the perception of brightness of the human visual system, is defined as the luminous intensity of light per unit area, which is the amount of light that is emitted from a particular area.

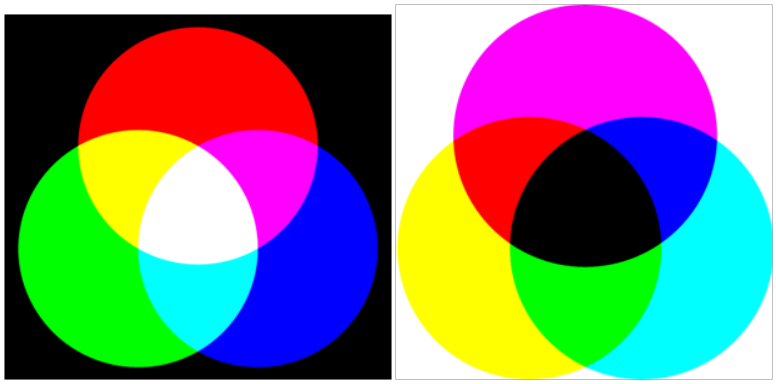

Figure 15. Comparison between the RGB color space (additive color mixing) and CMYK (substractive color mixing).

Chromaticity is denoted as the proportion between the three colour stimuli that are needed to describe a colour. It provides an objective definition of the quality of color independently of the luminance, and is usually determined by the hue and the saturation values. Hue denotes the appearance of the color and it is associated with the dominant wavelength. Saturation is defined as the colorfulness in proportion to the brightness of the object itself or indicative of which channel dominates [103] (see Figure 16).

The RGB color space is an additive color space where any specific color can be defined by the combination of the three chromaticities of red, green and blue [103]. In Figure 16a it can be seen the representation of the color gamut for this space where the values of each coordinate vary from 0 to 255.

The number of colors available inside the gamut depends on the number of bits used for the system to extract the color information, which is called the bit depth. Therefore, if 8 bits are used for each component, there are 256 levels of color for each coordinate.

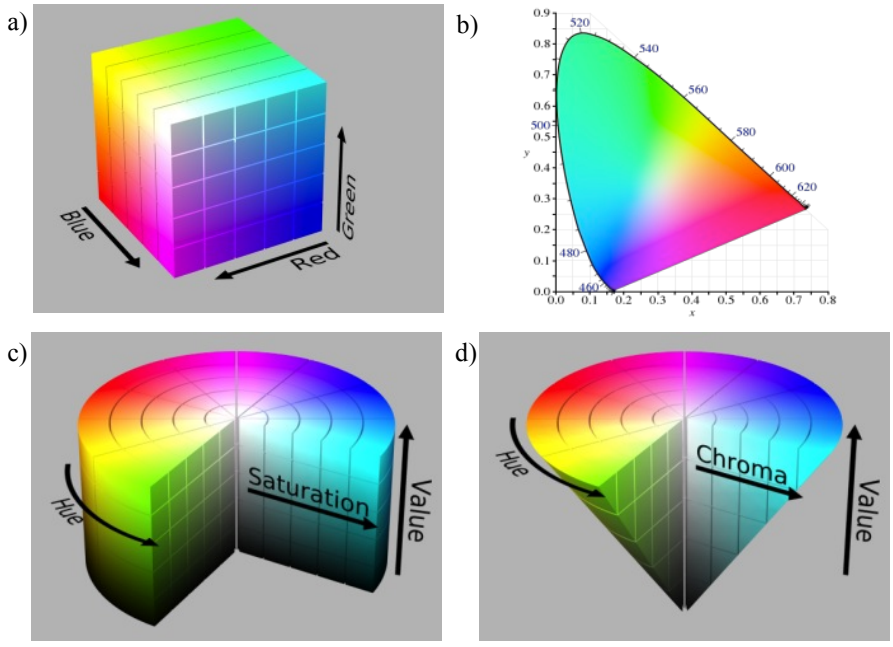

http://en.wikipedia.org/

Figure 16. Graphic representation of the different color spaces: (a) RGB, (b) XYZ, (c) HSV and (d) HVC.

The RGB color space is device-dependent since different devices detect and reproduce a given RGB color in a different way. The response to the red, green and blue wavelengths depends on each manufacturer. RGB is the most used color space in capture devices since the human visual system works in a similar way, and, for this reason is used as the initial color space from where other coordinates of other spaces are obtained. However, the combination of the three primary colors used in this case is not enough to obtain all the colors.

The XYZ is a space derived from the RGB color space. The X and Z coordinates are defined with zero luminance, therefore, just the Y coordinate contributes to the luminance component. For a given value of luminance, X and Z describe all the possible chromaticities. To represent this space, as shown in the chromaticity

diagram of Figure 16b, only two coordinates are needed: x and y. To calculate the XYZ components from the RGB coordinates provided by a device, there are some standard equations.

In the CIELAB color space, the L coordinate represents the luminance in a range from 0 to 100, while the a* and b* coordinates represents the change of color from magenta to green and yellow to cyan respectively. The range for the two components varies from -60 to 60, although it can vary with the application. It is not possible to transform directly to CIELAB from RGB coordinates, so it is necessary to use a intermediate step by transforming RGB into XYZ coordinates and using some transformation get the La*b* coordinates [101]. The XYZ and the CIELAB color spaces were designed to comprise all the colors that human visual system is able to see, but CIELAB is more perceptually uniform than XYZ, which means that a change in a color value produce the same visual change.

The HSV color space is an alternative representation derived from the RGB color space. HSV stands for hue, saturation and value respectively. The value coordinate denotes the brightness, which determines the extent to which an area appears to exhibit light. The hue value varies from 0 to 360º while saturation and value coordinates vary from 0 to 1. Since most of the capture devices provide RGB information, it is needed to define the transformations between the RGB and HSV color spaces [104].

$$\mathrm{M} = \max(\mathrm{R}, \mathrm{G}, \mathrm{B}) \qquad \text{(Eq. 1)}$$

$$m = \min(R, G, B) \qquad \text{(Eq. 2)}$$

$$C = M - m \quad \text{(Eq. 3)}$$

$$H = 60º \times \begin{cases} \text{undefined, if } C = 0 \\ \left(\frac{G-B}{C}\right)/6, \text{if } M = R \\ \left(\frac{B-R}{C} + 2\right)/6, \text{if } M = G \\ \left(\frac{R-G}{C} + 4\right)/6, \text{if } M = R \end{cases} \quad \text{(Eq. 4)}$$

$$S = \begin{cases} 0 \text{ if } C = 0 \\ \frac{C}{V}, \text{otherwise} \end{cases} \quad \text{(Eq. 5)}$$

$$V = \max(R, G, B) \quad \text{(Eq. 6)}$$

The main feature of this HSV color space is the possibility of representation of the color in a single parameter, the hue component. In this way, previous studies of this group have shown the relevance of the hue component as a quantitative parameter [105]. Since the H value determines the color information by using just one single coordinate, it offers a good alternative to the RGB color space where three coordinates are needed to extract and define completely the color information. Besides, it has been demonstrated that the hue component is more robust to slight variations of light that could affect the measurements. Therefore, the hue value is obtained from the RGB coordinates provided by different devices, such as digital sensors, cameras or scanners, and the statistical mode of the hue components of an image is used as analytical parameter [105].

Analytical chemistry uses information coming from different imaging devices with quantitative purposes, thus, manual or desktop scanners working both by reflection and transmission, CCD devices, video cameras, digital cameras and digital color analyzers. From all color spaces above mentioned, the most commonly used from the point of view of the chemical analysis are the tristimulus space (RGB) and the x-y chromaticity. The problem with these spaces is that the colors are defined as a mixture of basic colors and often a single channel of the three is used, with the consequent loss of information that entails, or several of them at once, especially as coordinate ratio. Therefore, we must face the decision to either use a procedure in which the three colorimetric coordinates are necessary in order to properly define the color of analytical system, which makes the process more complex, or use a single channel with the information loss that entails, although the procedure is easier. This loss of information is reflected in turn in a reduction in signal robustness.

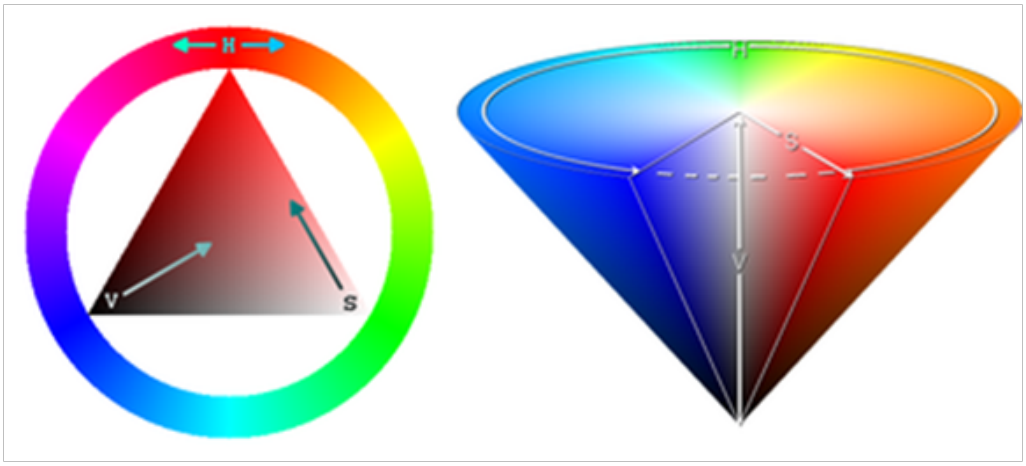

Figure 17. HSV color space representation.

To resolve these issues it has been proposed by this research group to use the HSV color space previously defined [105]. Equations 1-6 allow the calculation of H, S and V, respectively. Based on the RGB values of each pixel of the imager, the H coordinate is calculated and, from all the pixels that exist in the image of each sensing element, the mode of the set of data H obtained, which is used as representative value. Due to the circular nature of H, is often represented as a circle whose possible values are between 0 and 360, where 0 and 360 represent the same tone (Figure 17). In order to simplify the calculation using all H, the angle values are normalized between 0 and 1.

ARTIFICIAL INTELLIGENCE TECHNIQUES

There is no unanimously accepted definition of the term Artificial Intelligence, despite wide dissemination of the definition given by Munakata [106] in 1998. Traditional definitions that refer to the ability of computer programs to operate in the same way human thoughts perform learning and recognition processes. Another definition focuses on the simulation of human intelligence in a machine; in this way, the machine would be able to identify and use pieces of knowledge needed to solve a problem.

There are two main approaches within the broad spectrum of Artificial Intelligence (AI). One is symbolic AI, which is characterized by a high level of abstraction at the macroscopic view. This category includes classical psychology, knowledge-based systems, the symbolic machine learning, search techniques and natural language processing. The second approach is characterized by a low level of abstraction and microscopic biological models, such as neurons in artificial neural networks and chromosomes in genetic algorithms.

Currently, AI is being applied to many activities of humans, highlighting among others the following lines of scientific research: robotics, computer vision, learning techniques and knowledge management.

Next, the use of Artificial Neural Networks (ANN) are shortly described, the AI technique is used in this Thesis for the processing of the sensing arrays studied.

The brain is an information processor with very striking features: it is able to process at high speed large amounts of information from the senses, combine or compare the information to the stored information and then develop appropriate responses, even in new situations. But most notably, in the development of such skills, it has the ability to obtain and learn information without having explicit instructions to do so. Although much is still unknown about how the brain learns to process information, models have been developed that attempt to mimic such abilities, called RNA or connectionist models of computation (other names are neural computation and parallel distributed processing).

Building these models involves, first, the deduction of the features or essential features of neurons and their connections; and second, the implementation of the model on a computer, in such a way that they can be simulated.

In short, the ANN is a simplified model of an artificial human brain, which is the best model for a system that is capable of acquiring knowledge through experience. An ANN is a new system for data processing, whose basic processing unit is inspired by the fundamental unit, the cell of the human nervous system, or the neuron.

Basic structure of a neural network and analogy between biological and artificial neural networks

a) Biological Neural Networks (BNN)

Broadly speaking, the human brain is composed of tens of billions of interconnected neurons that form circuits or networks that perform specific

functions. A typical neuron collects signals from other neurons via a set of delicate structures called dendrites. The neuron emits electrical pulses along a long thin fiber called an axon, which split into many branches. The ends of these branches contact with the dendrites from other neurons and establish connections called synapses, in which a transformation of the electrical pulse is produced in a neurochemical message via the release of neurotransmitters (Figure 18).

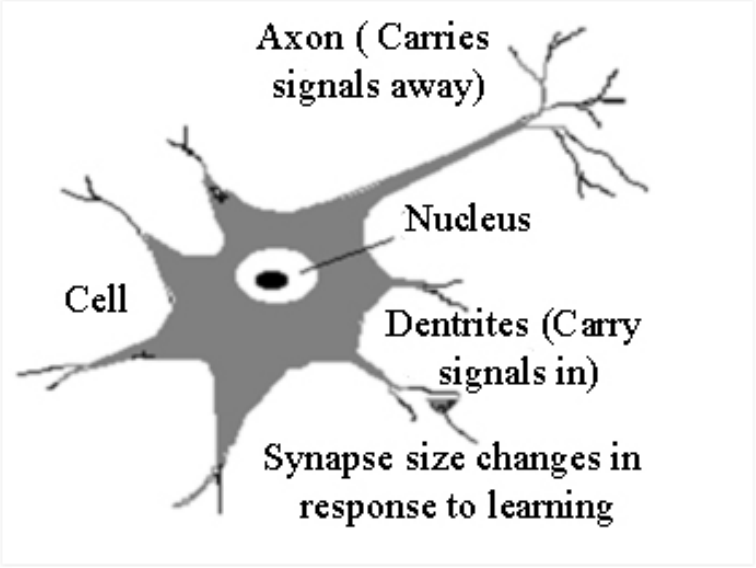

Figure 18. BNN processing unit.

The effect of neurotransmitters on the receiving neuron may be excitatory or inhibitory, and this effect is variable depending on the intensity of many factors. The excitatory and inhibitory signals received by a neuron are combined, and based on the total stimulation received, the neuron attains a degree of activation, which results in the generation of nerve impulses with a given frequency and propagation along the axon to the neuron with which it is bound.

Thus, the information is transmitted from a neuron to another neuron and is processed through the synaptic connections and neurons themselves. The BNN

learning occurs by varying the effectiveness of the synapse, thereby changing the influence of some neurons on others. It follows that architecture, the type and effectiveness of connections in a given time represent, in a sense, memory, or the state of knowledge of BNN. It is estimated that the human brain contains over 10^{11} neurons and 10^{14} synapses.

b) Artificial Neural Networks

ANNs are a technique of parallel and mass processing of information that emulates the essential characteristics of the neuronal structure of the biological brain. It comprises a number of processing units, also called artificial neurons, linked by weighted connections. Each unit receives signals through a number of input channels, and responds to the stimulus by signaling, which may be binary (0.1) or real within a continuous range, to all those with which have an output connection. Therefore the network consists of core calculations, with a vector of input connections and output connection (Figure 19).

- Propagation function. Compute the base usually as a simple weighted sum of all entries received, i.e., the inputs multiplied by the weight or value of connections. Equivalent to the combination of excitatory and inhibitory signals of biological neurons.
- Activation function. Is the principal characteristic of neurons, and defines the behavior of the same. Different types of functions are used, from simple threshold functions to nonlinear functions. It is responsible for calculating the level or activation state of the neuron as a function of the total input.
- Weighted connections. Perform the role of synaptic connections, so that the weight of the connection is equal to the effectivity of the synapse. The existence of a connection determines whether a unit may influence over another; the value of the weights and the sign thereof define the type (excitatory / inhibitory) and intensity of the influence.

- Output. Calculate the output of the neuron as a function of their activation, but normally it is not applied more than the identity function and the output is taken as the trigger value. The output value would serve as the firing rate in biological neurons.

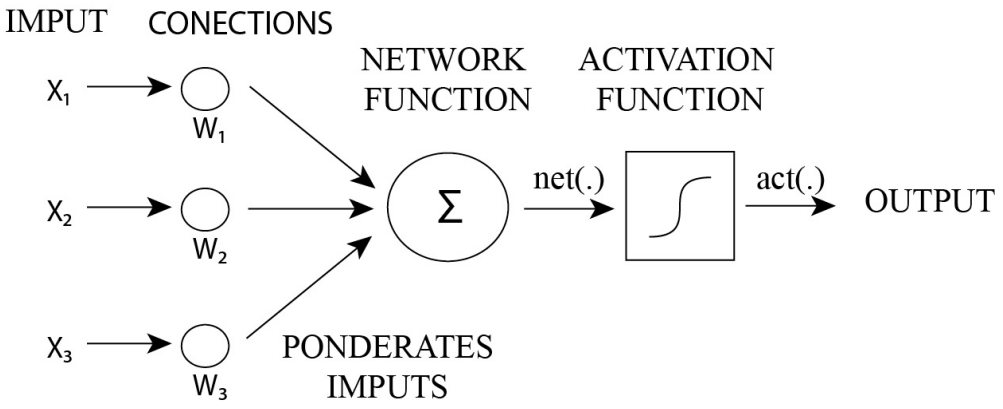

Figure 19. ANN processing unit.

Therefore, an ANN is formed by a collection of interconnected neurons arranged in layers, which are in turn made up of a number of neurons individually. Although initially developed as a single layer ANN, it is usual to have three or more layers (multilayer systems) [107]. Thus, the basic parameters of the ANN are: the number of layers and the number of neurons per layer, the degree of connectivity and the type of connections between neurons.

There are several architectures of ANN; the most common are:

• Layered neural networks (feed -forward). They are composed of layers and each neuron layer receives signals from the previous layer (Figure 20), the most

common layer known as the multilayer perceptron. This type of network is characterized in that the neurons are grouped into different levels (input layer, hidden layers and output layers). Neurons are responsible for receiving raw data from outside, where they store or perform simple pre-processing operations and transmit the processed information to the next layers. The intermediate layers or hidden layers are mainly responsible for extracting, processing and storing information, while the latter acts as the output layer of the network, providing the answer to each of the input patterns. Usually this type of network is used in problems of recognition or pattern classification.

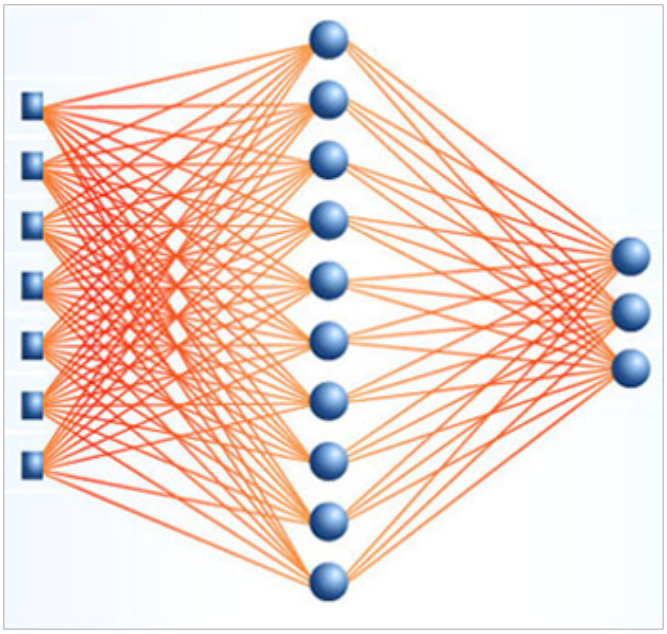

Figure 20. Three-layered Artificial Neural

The connections between each layer may be total or partial, in which case only one unit is connected with some of the layers of the next unit, usually following some random pattern or pseudo-random (e.g. using genetic algorithms).

• Recurrent neural networks (feed-back). Each neuron is connected to all neurons in the network, even with itself, which means that the information can return to places they had passed, forming loops. This type of network is characterized by its dynamic nature, because it evolves from one state to another. The network is stable when its state remains unchanged after several iterations; Hopfield networks illustrate this classification, which are typically used in tasks related to self-association.

• Laterally connected neural networks. Neurons are arranged at the nodes of a grid of about 1 or 2 dimensions. The most common is the Kohonen network.

• Networks with supervised or unsupervised learning. The fundamental difference between the two types lies in the existence of an external agent (supervisor) that controls the learning network, determining the response that should generate the network from a particular input. In networks with supervised learning, the supervisor checks the output of the network, and in the case that it does not coincide with the desired output, proceeds to modify the weights of the connections, in order to ensure that the output approximates to desired. Networks with unsupervised learning require no external influence to adjust the weights of the connections between neurons. The network does not receive any information from the environment to indicate whether the generated output is correct or not, so there are several possibilities to interpret the output of these networks. Additionally, there are hybrid neural networks and supervised learning involving unsupervised. The weights are adjusted by supervised learning and the rest is obtained by an unsupervised learning.

• Self-organizing maps of Kohonen (Self-Organizing Map, SOM). Correspond to a variation of the feed-forward ANN and are based on the principle of formation of topological maps to establish commonalities between information input and output characteristics. They thus present connections forward (feed-

forward) and lateral inhibition connections are implied, as each of the output neurons have influence on its neighbors. This allows for network development; only one of the output neurons will be activated given a vector p of attributes in the input layer.

PRINTING TECHNIQUES

The fabrication of lab devices for different application in chemical, biochemical and immunological analysis requires the use of film-forming techniques. It is noticeable that there are many known, well-developed and currently explored film-forming techniques, and yet so few of them have been used in this field. This is because many techniques require large amounts of material, the reproducibility is sometimes difficult, and many techniques are unsuited for the small scales used in laboratory studies [108].

The techniques well suited for individual processing of small substrates are spin coating, doctor blading, casting, gravure and inkjet printing. Film-forming techniques developed for high volume processing of paper, plastic and textile materials where the substrate is in the form of a continuous roll of material including roll-to-roll coating or reel-to-reel coating.

1. Casting technique

Casting is the simplest film-forming technique. The procedure is to simply cast a solution onto a substrate, which is then followed by drying. With this technique it is possible to prepare thick films of good quality, however this technique suffers from a lack of control over the film thickness and often picture framing effects are observed near the edges of the film, or there is precipitation during drying [108].

2. Spin coating technique

Spin coating is a film-forming technique based on the process of applying a solution to a horizontal rotating disc, resulting in ejection and evaporation of the solvent and leaving a liquid or solid film [109]. It has the advantage of preparation of a highly uniform film on a planar substrate over a large area (Ø 30 cm) with a highly controllable and reproducible film thickness.

The different stages of processing that define the spin coating technique are: 1) Deposition of the coating material onto the support´s surface. Spraying or dripping the solution onto the support offers different options to deposit the material; 2) Routing of substrate at high speed in order to spread the liquid across the surface by a centrifugal force. The rotation time depends on the film thickness desired; 3) Spinning of the wafer at a constant rate to achieve homogeneity and reproducibility of the spin coated layers; and 4) Removing the edge beaded material using a backside wash cycle.

Depositing a viscous fluid on a horizontal rotating disc produces a uniform liquid film. During deposition the disc should either be static or be rotating at a low angular velocity, where after the disc is rapidly accelerated to a high angular velocity (spin speed). The adhesive forces at the liquid/substrate interface and the centrifugal forces acting on the rotating liquid result in strong sheering of the liquid which causes a radial flow in which most of the polymer solution is rapidly ejected from the disc (Figure 21). This process combined with subsequent evaporation of the liquid causes the thickness of the remaining liquid film to decrease. For a solution, e.g. a polymer solution containing recognition chemistry, the evaporation process causes the polymer concentration to increase (and thus the viscosity) at the liquid/vapor interface, i.e. a concentration gradient is formed through the liquid film, which, after evaporation of most of the remaining solvent, consequently results in the formation of a uniform, practically solid, polymer film [109].

To control the thickness of the film, the rotational speed and other parameters like the nature of the polymer (viscosity, drying rate, percent of solids, surface tension, etc.) have to be considered. The solvents used are usually volatile to accelerate the evaporation during the process. Some additional factors that must be considered in order to achieve uniform films are concentration of the solution, solution viscosity, evaporation rate of the solvent, spin time and angular velocity.

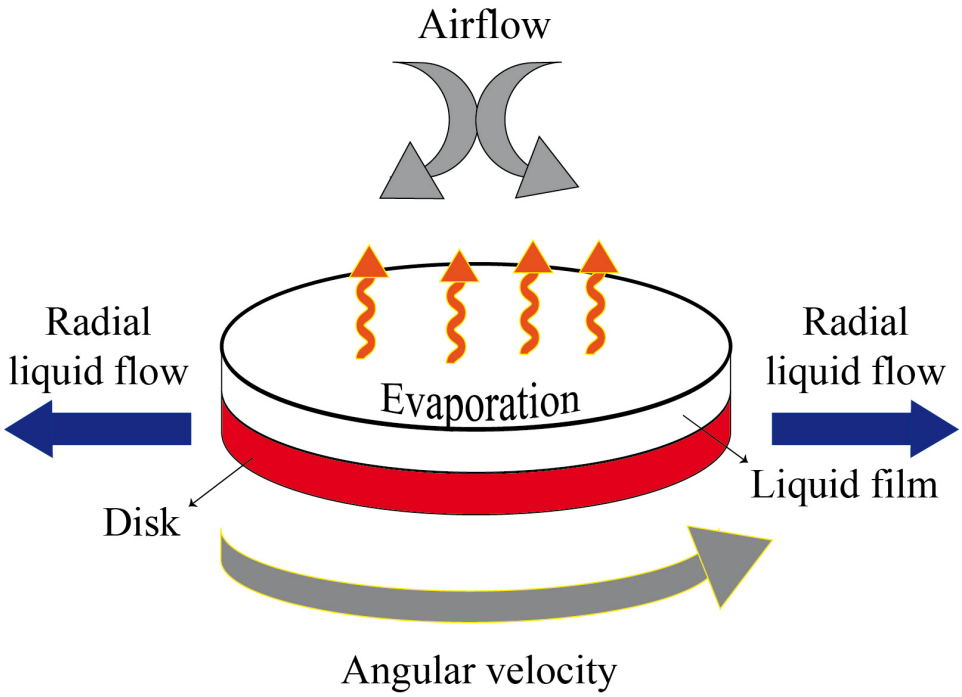

Figure 21. Schematic illustration of spin coating technique [109].

3. Doctor blading technique.

Doctor blading is a technique that allow for the formation of films with a well-defined thickness. In contrast to spin coating the technique is quite parsimonious and

with some practice the loss of the coating solution can be minimized such that less than 5% is lost. The technique works by placing a sharp blade at a fixed distance from the substrate surface that is to be coated (typically 10–500 mm). The coating solution is then placed in front of the blade that is then moved linearly across the substrate leaving a thin wet film after the blade. The final wet thickness of the film is ideally half the gap width but may vary due to the surface energy of the substrate, the surface tension of the coating solution and the viscosity of the coating solution. It also depends on the meniscus formed between the blade and the wet film on the trailing edge of the blade, which is related to the shear field (proportional to the speed of the blade/knife) (See Figure 22).

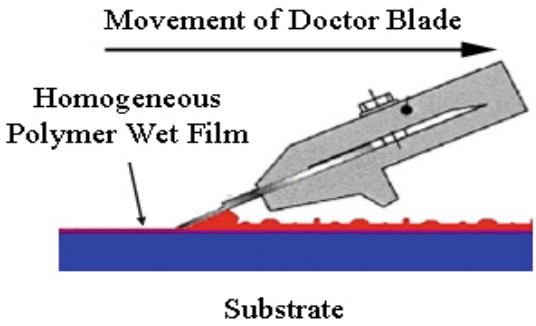

Figure 22. Principle of the film formation for films deposited by doctor blading [110].

4. Gravure technique.

Gravure printing is a promising technology for high resolution printing. It is used in industry for high quality, high speed, large-run printing such as currency printing. In gravure printing, a cylinder patterned with cavities is uniformly coated as it turns through an ink reservoir. A blade then removes ink that is not within the cavities. The filled cavities then turn with the gravure cylinder and are pressed onto a target

substrate. The ink wets the substrate and the pattern is transferred as the patterned role moves away (Figure 23). The high resolution and high throughput of gravure printing make it suited for low-cost device fabrication, as is the case of the impedance based electrochemical biosensor proposed by Redy at al. [111], or the demonstrated gravure-printed intelligent packaging for monitoring kimchi fermentation [112].

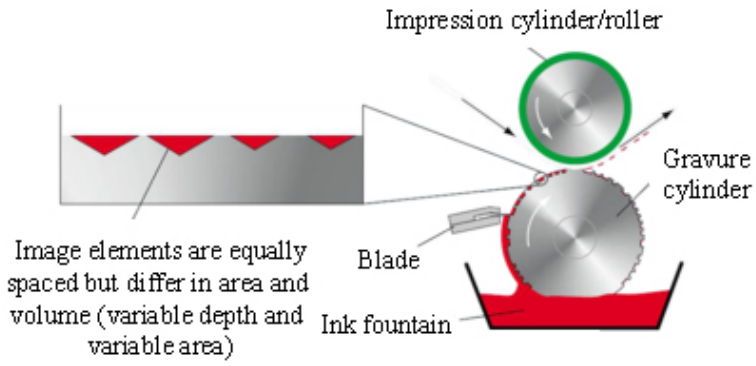

Figure 23. Gravure printing schematic with close-up of inked wells to left [113].

5. Screen printing technique.

Screen printing is a very versatile printing technique that allows for full 2-dimensional patterning of the printed layer. It is an economical system and there is essentially no loss of coating solution during printing. The main distinction from all other printing and coating techniques is a large wet film thickness and a requirement for a relatively high viscosity and a low volatility of the coating solution. The process involves a screen of woven material (i.e. synthetic fiber or steel mesh) that has been glued to a frame under tension (Figure 24). The pattern is obtained by coating the screen with an emulsion that is impervious to the coating solution in the areas where

no print should appear. The area of the printed pattern is kept open (without emulsion). The screen is then filled with coating solution and brought into proximity of the substrate

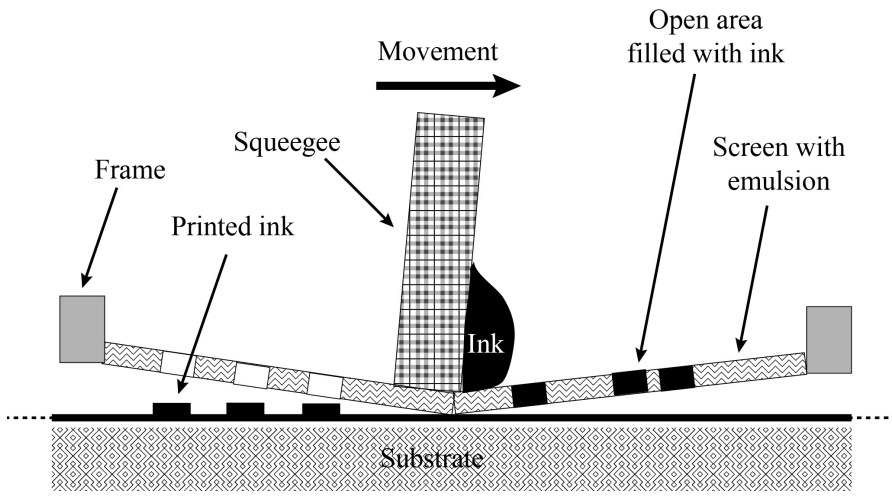

Figure 24. Schematics of the screen-printing process [108].

A so-called squeegee is forced into to screen bringing it into contact with the substrate and then drawn linearly across the screen thus forcing coating solution through the open areas onto the substrate, reproducing in that manner the pattern. The wet thickness of the coated film is in principle given by the theoretical paste volume of the screen, i.e. the volume between the threads of the mask and the thickness of the emulsion; measured in the volume of ink per area of open screen.

Some factors, however, are influential on this such that not all the material in the screen is deposited. This varies with the force with which the squeegee is pushed into the screen, the snap-off distance, the speed of the squeegee and the viscosity of the solution. The limiting factors of the technique are the large wet thickness, the requirement for a high viscosity and low volatility.

Screen printing is inherently batch operated but highly roll-to-roll (R2R) compatible as exemplified on a roll-to-roll Klemm line where rectangular screens are used and the material is passed through the machine at constant speed. The screen and support follow the web at constant speed while printing is in progress. After each print the screen and support reverses back and the printing cycle is repeated. It can also be fully adapted to a R2R process in rotary screen printing where the screen is shaped as a cylinder with a squeegee on the inside and the substrate fed past the outside of the rotary screen and supported by a roller (Figure 25).

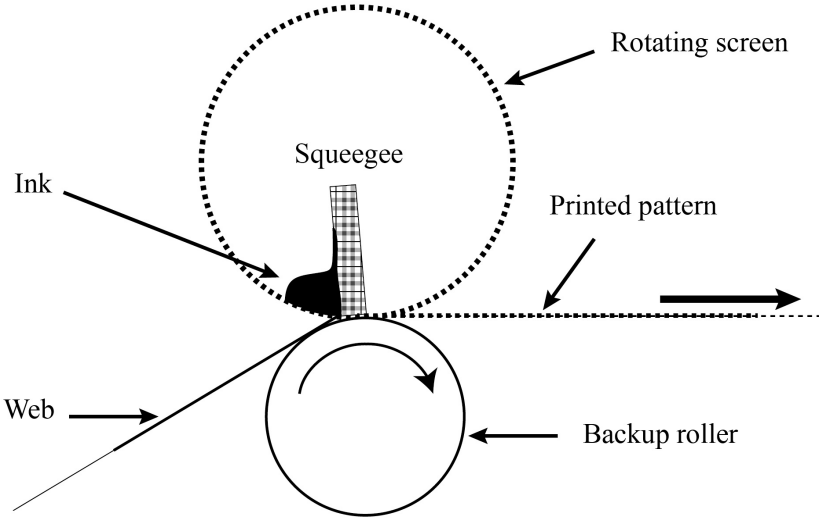

Figure 25. Schematic drawing of a rotary screen printer [109].

6. Ink jetting technique.

Inkjet technology in addition to office printing technology, has gradually become a versatile tool for various industrial fabrication processes for accurately depositing

very small quantities of materials at defined spots on the surface of a wide variety of substrates [114]. It does not rely on the use of a specific mask, and cleanroom facilities are not a prerequisite. This technology has been mostly applied in plastic electronics as is the case of the manufacture of flexible graphene patterns [115] or organic light-emitting diodes [116]. Inkjet printing has become an alternative arraying technique for biological sample arrays, which, in contrast to contact-based methods such as pin spotting systems, has the advantages of reduced contamination and no risk of substrate damage [117;118]. Taking into account its advantages in its flexibility, low cost, and ease of highly parallel mass production, the potential of inkjet printing is begin to use in the field of analytical chemistry. The ammonia gas sensor uses conducting films assembled on interdigitated electrode arrays and inkjet-printed with polyaniline nanoparticles [119], the moisture [120] or hydrogen sulfide sensors [121] for smart packaging applications, or the prototyping of paper-based microfluidic devices [122-124].

Inkjet printing is a relatively novel process from the point-of-view of industrial printing and coating and the technology has been driven forward by the typical low-cost inkjet printer for the home office. Its minimal demand on materials and the lack of waste during processing are one of the attractive characteristics of this technique. There are no limitations for the substrates because inkjet printing is an additive technique, which permits the accurate positional placement of picoliter volumes of fluid on an arbitrary substrate. It can be used for materials like metal inks, functional and conductive polymers between others. Flexible substrates can be used in conjunction with rigid, planar surfaces. The method shows high versatility and can be applied to a disparate group of topics.

The low cost, high quality of output, and fast production times represent some of the advantages of the inkjet printing technique. While having many benefits, inkjet printing also has disadvantages, for example, the ink from inkjet printing exhibits a

complex drying behavior, which makes the prediction of final film properties difficult.

The physical operations that include inkjet printing are: a) generation of droplets, b) positioning of and interaction of the droplets on a substrate, and c) drying or other solidification mechanisms to produce a solid deposit.

The two mechanisms by which inkjet printers generate droplets are continuous inkjet (CIJ) printing and drop-on-demand (DOD) inkjet printing. Both methods of drop generation can produce fluid drops with diameters in the range of 10 to 150 μm [125].

In continuous inkjet printing a stream of drops is formed by the Rayleigh instability of a liquid column that is ejected under pressure through a small nozzle. To direct and position these drops, the nozzle is held at a potential relative to ground, which imparts a small charge on each drop as it is formed. Individual drops in the stream are steered by applying a further potential to the deflector plates (Figure 26). CIJ printing, by definition, produces a continuous stream of liquid drops, even when no printing is required. Unwanted drops are deflected by the electric field to a gutter, and for many applications in product marking and graphics, the unused ink is recycled

Drop-on-demand inkjet printers generate individual drops when required and are thus more economical with ink delivery than are CIJ systems. Drop positioning is achieved by manually locating the printer nozzle above the desired location on the substrate before drop ejection. Drops are formed by propagating a pressure pulse in the fluid held in a chamber behind the printing nozzle.

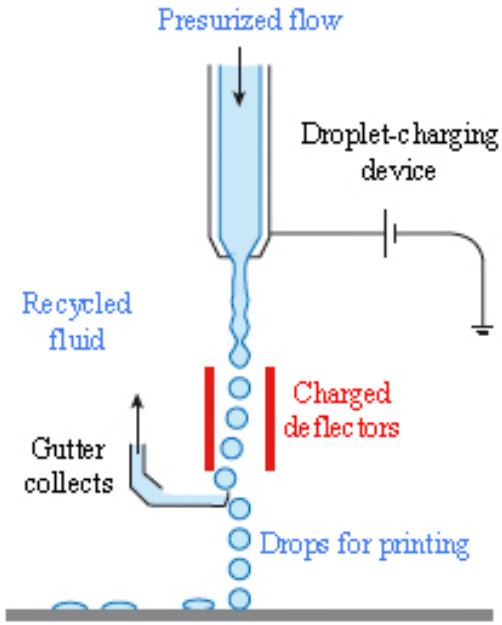

Figure 26. Principles of operation of a CIJ printer [125].

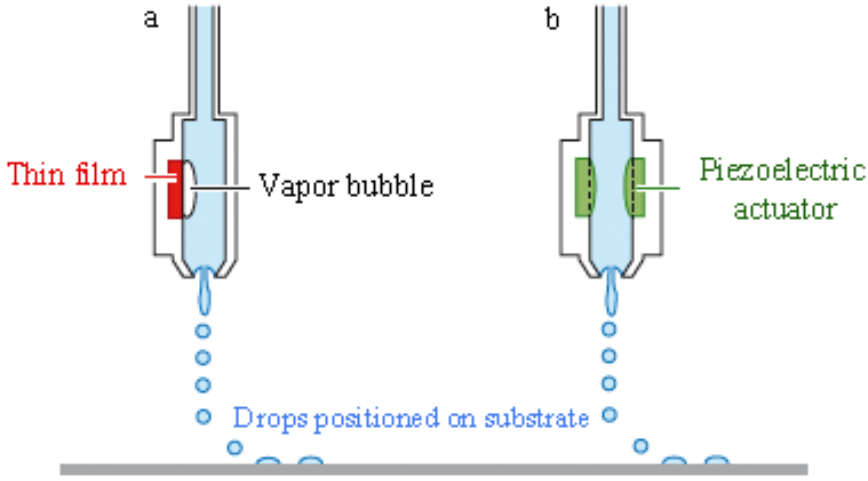

Figure 27. Schematic of a DOD inkjet printing system. a) thermal inkjet; b) piezoelectric inkjet [125].

If the pulse exceeds some threshold at the nozzle, a drop is ejected. In the absence of a pressure pulse, liquid is held in place by the surface tension at the nozzle. Drop size is approximately equal to the nozzle size, but it is possible to control both the drop size and ejection velocity (within a defined range) by management of the pressure pulse used to form the drops.

On passing a current through this heater, the fluid in immediate contact is heated to above its boiling temperature to form a small vapor pocket or bubble (Figure 27a). After the current is removed, heat transfer leads to rapid bubble collapse.

The rapid expansion and collapse of the bubble generates the required pressure pulse. In piezoelectric DOD printing (Figure 27b), the pressure pulse is generated by direct mechanical actuation using a piezoelectric transducer.

In DOD printing the mechanical deformation of a piezoceramic element takes place generating a pressure wave in the fluid (See Figure 28). Fluid ejection, droplet formation and droplet impact with the support are the steps that take place in piezoelectric DOD printers. Four kinds of deformations modes are described in the literature: bend, shear, push and squeeze mode.

These printers can use tubular or planar transducers. They also have a system that controls factors like the temperature in order to fix the viscosity and high frequency vibration purge settings that fill the nozzle with the ink. A waveform editor and drop-watch camera system can be integrated in these printers in order to manipulate the electronic pulses to the piezo-jetting device.

The generation of droplets in a DOD printer is a complex process, and the precise physics and fluid mechanics of the process description of liquid drops can be characterized by a number of dimensionless groupings of physical constants, the most useful of which are the Reynolds (Re) (Eq. 7), Weber (We) (eq. 8), and Ohnesorge (Oh) (eq. 9) numbers that consider density (ρ), dynamic viscosity (η), and surface tension (γ) of the fluid, being v the velocity and a is a characteristic length[125].

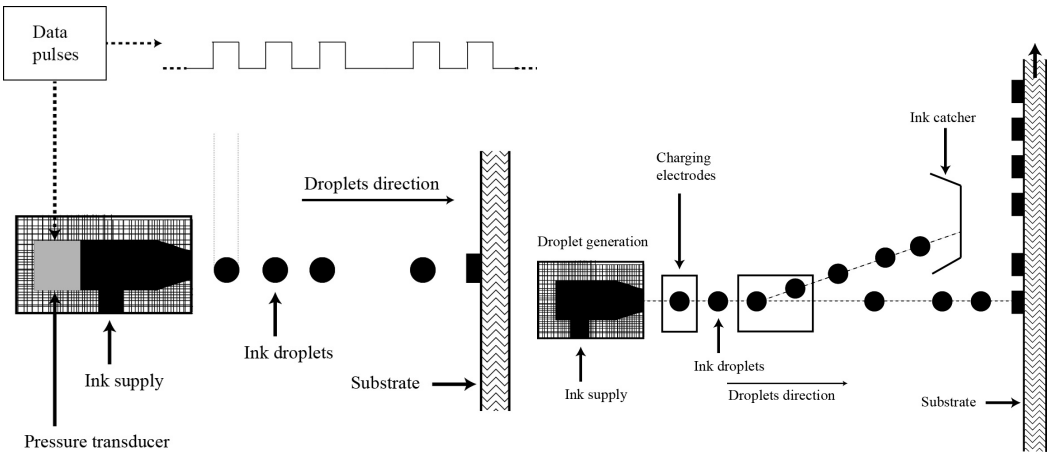

Figure 28. Schematic of the inkjet printing process using a data pulse train to generate droplets on demand via a pressure transducer (left) and a system where droplets are generated continuously and the pattern created by deflecting the unwanted droplets away from the substrate (right) [108].

$$\mathrm{Re} = \frac{v\rho a}{\eta} \qquad \text{(Eq. 7)}$$

$$\mathrm{We} = \frac{v^2\rho a}{\gamma} \qquad \text{(Eq. 8)}$$

$$\mathrm{Oh} = \frac{\sqrt{\mathrm{We}}}{\mathrm{Re}} = \frac{\eta}{\sqrt{\gamma\rho a}} \qquad \text{(Eq. 9)}$$

The Ohnesorge number, Oh, is considered as the appropriate grouping of physical constants to characterize drop formation, but as Z = 1/Oh, being the range, $10 > Z > 1$, for stable drop formation [126].

At low values of Z, viscous dissipation prevents drop ejection, whereas at high values the primary drop is accompanied by a large number of satellite droplets.

A limiting factor for drop generation is the influence of the fluid/air surface tension at the nozzle. The minimum velocity for drop ejection is given by eq. 10 [127] where d_n is the nozzle diameter

$$v_{min} = \left(\frac{4\gamma}{\rho d_n}\right)^{1/2} \quad \text{(Eq. 10)}$$

This equation 10 can be reformulated in terms of the Weber number to give a minimum value for printing,

$$We = v_{min}\left(\frac{\rho d_n}{\lambda}\right)^{1/2} > 4 \quad \text{(Eq. 11)}$$

A last factor to consider is the impact of the ejected drop on a substrate. The drop must impact so as to leave a single isolated spread drop. The appropriate threshold for the onset of splashing is given by Stow and Hadfield equation [128] (equation 12) that groups critical dimensionless variables where f(R) is a function of surface roughness which for flat and smooth surfaces f(R) ≈ 50:

$$We^{1/2}Re^{1/2} > f(R) \quad \text{(Eq. 12)}$$

Figure 29 shows a map with coordinates Re and We that can be used to define the fluid properties that are usable in DOD inkjet systems.

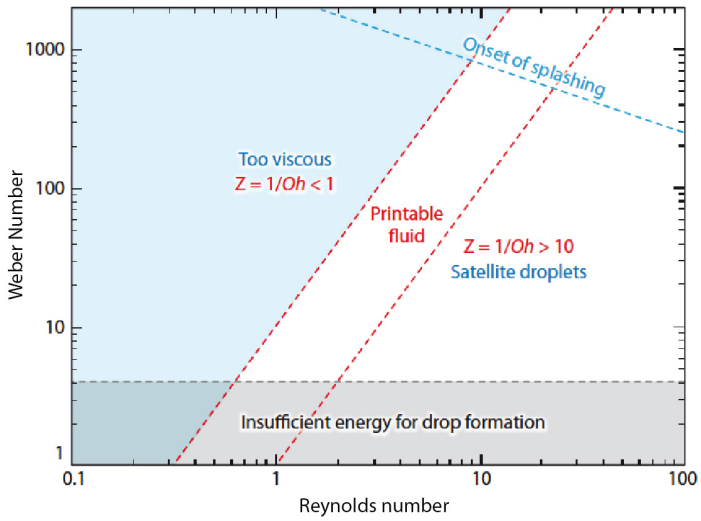

Figure 29. Regime of fluid properties where DOD inkjet printing is possible [125].

REFERENCES

1. J. Janata in *Principles of Chemical Sensors,* 2 ed., Springer, 2009.

2. A. Hulanicki, S. Geab and F. Ingman, *Pure Appl.Chem.* 1991, 63, 1247-1250.

3. K. Cammann, G.G. Guilbault, H. Hal, R. Kellner O.S. Wolfbeis in *The Cambridge Definition of Chemical Sensors, Cambridge Workshop on Chemical Sensors and Biosensors,* Cambridge University Press, New York, 1996.

4. G. Gauglitz, *Anal.Bioanal.Chem.* 2005, 381, 141-155.

5. H. Eren in *Electronic Portable Instruments: Design and Applications,* CRC Press, 2005.

6. L.F. Capitán-Vallvey, A.J. Palma, *Anal.Chim.Acta* 2011, 696, 27-46.

7. M. Valcarcel, M.D. Luque de Castro in *Flow-Through (Bio)Chemical Sensors,* Elsevier Science B.V., Amsterdam, 1994.

8. C. Perez Conde in *Sensores ópticos,* 1 ed., Servicio de Publicaciones Universidad de Valencia, Valencia, 1996.

9. U.E. Spichiger-Keller in *Chemical Sensors and Biosensors for Medical and Biological Applications,* 1 ed., Wiley-VCH, Weinheim, 1998.

10. F. Baldini, A. Giannetti, A.A. Mencaglia and C. Trono, *Curr.Anal.Chem.* 2008, 4, 378-390.

11. M.D. Marazuela, M. Cruz Moreno-Bondi, *Anal.Bioanal.Chem.* 2002, 372, 664-682.

12. C. Bosch Ojeda, F. Sánchez Rojas, *Sensors* 2006, 6, 1245-1307.

13. M. Miro, W. Frenzel, *TrAC, Trends Anal.Chem.* 2004, 23, 11-20.

14. J. Wang, *Anal.Chim.Acta* 2004, 507, 3-10.

15. L.F. Capitán-Vallvey in *Encyclopedia of Sensors*, Grimes, C. A.; Dickey, E. C.Pishko, M. V., Eds. ed. , 1 ed., The Pennsylvania State University, Pennsylvania, USA, 2005, 55-93.

16. K. Faulstich, R. Gruler, M. Eberhard, D. Lentzsch K. Haberstroh in *Lateral Flow Immunoassay*, Wong, R. C.; Tse, H. Y., Eds. ed. , Humana Press, New York, 2009, 157-184.

17. F. Baldini, A.N. Chester J. Homola in *Optical Chemical Sensors,* Springer, 2006.

18. C. McDonagh, C.S. Burke and B.D. MacCraith, *Chem.Rev.* 2008, 108, 400-422.

19. Orellana, G. and Moreno-Bondi, M. C. Frontiers in Chemical Sensors: Novel Principles and Techniques. Wolfbeis, O. S. [3]. 2005. Springer. Springer Series on Chemical Sensors and Biosensors.

20. X.D. Wang, H.X. Chen, Y. Zhao, X. Chen, X.R. Wang and X. Chen, *TrAC, Trends Anal.Chem.* 2010, 29, 319-338.

21. J.J. Lavigne, E.V. Anslyn, *Angew.Chem.Int.Ed.* 2001, 40, 3118-3130.

22. A.K. Deisingh, D.C. Stone and M. Thompson, *Intern.J.Food Sci.Tech.* 2004, 39, 587-604.

23. Y.G. Vlasov, A.V. Legin and A.M. Rudnitskaya, *Rus.Chem.Rev.* 2006, 75, 125-132.

24. F. Winquist, C. Krantz-Rulcker and I. Lundstrom, *Sensors Update* 2003, 11, 279-306.

25. K. Persaud, G. Dodd, *Nature* 1982, 299, 352-355.

26. Y. Vlasov, A. Legin, A. Rudnitskaya, C. Di Natale and A. D'Amico, *Pure Appl.Chem.* 2005, 77, 1965-1983.

27. P. Ciosek, W. Wroblewski, *Analyst* 2007, 132, 963-978.

28. J. Mitrovics, H. Ulmer, U. Weimar and W. Goepel, *Acc.Chem.Res.* 1998, 31, 307-315.

29. K. Yoshida, *Reito* 2010, 85, 918-922.

30. H.V. Ramamoorthy, S.N. Mohamed and D.S. Devi, *J.Nanosci.Nanotechnol.* 2014, 2, 370-376.

31. T.C. Pearce, S.S. Schiffman, H.T. Nagle J.W. Gardner in *Handbook of Machine Olfaction - Electronic Nose Technology,* John Wiley & Sons, 2003.

32. A. Legin, A. Rudnitskaya and Y. Vlasov, *Comprehensive Analytical Chemistry* 2003, 39, 437-486.

33. A.K. Deisingh in *Sensors for Chemical and Biological Applications*, Ram, M. K.; hethanabotla, V. R., Eds. ed. , CRC Press, 2010, 173-192.

34. M. Gutierrez, S. Alegret, R. Caceres, J. Casades ·s, O. Marfa and M. Del Valle, *Comp.Elec.Agr.* 2007, 57, 12-22.

35. M.Y.M. Sim, M.N. Ahmad, A.Y.M. Shakaff, C.P. Jul and C.C. Cheen, *Sensors* 2003, 3, 555-564.

36. C. Di Natale, G. Olafsdottir in *Fishery Products: Quality, safety and authenticity*, John Wiley & Sons Ltd., 2009, 105-126.

37. T.A. Dickinson, J. White, J.S. Kauer and D.R. Walt, *Nature* 1996, 382, 697-700.

38. S.R. Johnson, J.M. Sutter, H.L. Engelhardt, P.C. Jurs, J. White, J.S. Kauer, T.A. Dickinson and D.R. Walt, *Anal.Chem.* 1997, 69, 4641-4648.

39. J. White, J.S. Kauer, T.A. Dickinson and D.R. Walt, *Anal.Chem.* 1996, 68, 2191-2202.

40. K.J. Albert, D.R. Walt, D.S. Gill and T.C. Pearce, *Anal.Chem.* 2001, 73, 2501-2508.

41. T.A. Dickinson, K.L. Michael, J.S. Kauer and D.R. Walt, *Anal.Chem.* 1999, 71, 2192-2198.

42. D.R. Walt, T. Dickinson, J. White, J. Kauer, S. Johnson, H. Engelhardt, J. Sutter and P. Jurs, *Biosens Bioelectron* 1998, 13, 697-699.

43. P. Pantano, D.R. Walt, *Chem.Mater.* 1996, 8, 2832-2835.

44. D.R. Walt, *Current opinion in chemical biology* 2002, 6, 689-695.

45. N.A. Rakow, A. Sen, M.C. Janzen, J.B. Ponder and K.S. Suslick, *Angew.Chem.Int.Ed.* 2005, 44, 4528-4532.

46. S.E. Stitzel, L.J. Cowen, K.J. Albert and D.R. Walt, *Anal.Chem.* 2001, 73, 5266-5271.

47. K.J. Albert, D.R. Walt, *Anal.Chem.* 2000, 72, 1947-1955.

48. G.A. Bakken, G.W. Kauffman, P.C. Jurs, K.J. Albert and S.S. Stitzel, *Sens.Actuators B* 2001, 79, 1-10.

49. J.M. Phelan, S.W. Webb in *Mine Detection Dogs: Training, Operations and Odour Detection*, McLea, I. G., Ed. ed. , Geneva International Centre for Humanitarian Demining(GICHD), 2003.

50. K.J. Albert, M.L. Myrick, S.B. Brown, D.L. James, F.P. Milanovich and D.R. Walt, *Environ Sci Technol* 2001, 35, 3193-3200.

51. J.R. Askim, M. Mahmoudi and K.S. Suslick, *Chem.Soc.Rev.* 2013, 42, 8649-8682.

52. J.J. Lavigne, S. Savoy, M.B. Clevenger, J.E. Ritchie, B. McDoniel, S.J. Yoo, E.V. Anslyn, J.T. McDevitt, J.B. Shear and D. Neikirk, *J.Am.Chem.Soc.* 1998, 120, 6429-6430.

53. M.C. Janzen, J.B. Ponder, D.P. Bailey, C.K. Ingison and K.S. Suslick, *Anal.Chem.* 2006, 78, 3591-3600.

54. N.A. Rakow, K.S. Suslick, *Nature* 2000, 406, 710-713.

55. Akrajas, M. Mat Salleh and M. Yahaya, *Sens.Actuators B* 2002, 85, 191-196.

56. M.K. LaGasse, J.M. Rankin, J.R. Askim and K.S. Suslick, *Sens.Actuators B* 2014, 197, 116-122.

57. K.S. Suslick, N.A. Rakow and A. Sen, *Tetrahedron* 2004, 60, 11133-11138.

58. C. Potera, *Environmental Health Perspectives* 2001, 109, A129-A131.

59. B.G. Healey, D.R. Walt, *Anal.Chem.* 1997, 69, 2213-2216.

60. C. Zhang, D.P. Bailey and K.S. Suslick, *J.Agric.Food Chem.* 2006, 54, 4925-4931.

61. B.A. Suslick, L. Feng and K.S. Suslick, *Anal.Chem.* 2010, 82, 2067-2073.

62. C. Zhang, K.S. Suslick, *J.Agric.Food Chem.* 2007, 55, 237-242.

63. X. Huang, J. Xin and J. Zhao, *J.Food Eng.* 2011, 105, 632-637.

64. Y. Salinas, J.V. Ros-Lis, J.L. Vivancos, R. Martinez-Mañez, M.D. Marcos, S. Aucejo, N. Herranz and I. Lorente, *Analyst* 2012, 137, 3635-3643.

65. J.R. Carey, K.S. Suslick, K.I. Hulkower, J.A. Imlay, K.R.C. Imlay, C.K. Ingison, J.B. Ponder, A. Sen and A.E. Wittrig, *J.Am.Chem.Soc.* 2011, 133, 7571-7576.

66. M.O. Salles, G.N. Meloni, W.R. de Araujo and T.R.L.C. Paixao, *Anal.Methods* 2014, 6, 2047-2052.

67. Y. Tanaka, T. Nakamoto and T. Moriizumi, *Sens.Actuators B* 2006, B119, 84-88.

68. M.y. Jia, L. Feng, *Fenxi Huaxue* 2013, 41, 795-802.

69. R. Pal, S. Dahal and A. Gurung, *Asian J.Biochem.Pharm.Res.* 2013, 3, 92-99, 8.

70. K.L. Michael, L.C. Taylor, S.L. Schultz, F. Szurdoki and D.R. Walt, *Proc.SPIE* 1998, 3270, 34-41.

71. M. Manesse, A.F. Phillips, C.N. LaFratta, M.A. Palacios, R.B. Hayman and D.R. Walt, *Lab Chip* 2013, 13, 2153-2160.

72. A.P. Goodey, J.J. Lavigne, S.M. Savoy, M.D. Rodriguez, T. Curey, A. Tsao, G. Simmons, J. Wright, S.J. Yoo, Y. Sohn, E.V. Anslyn, J.B. Shear, D.P. Neikirk and J.T. McDevitt, *J.Am.Chem.Soc.* 2001, 123, 2559-2570.

73. H. Hogan, *Photon.Spectra* 2007, 11, 98.

74. S.C. McCleskey, M.J. Griffin, S.E. Schneider, J.T. McDevitt and E.V. Anslyn, *J.Am.Chem.Soc.* 2003, 125, 1114-1115.

75. A.T. Wright, M.J. Griffin, Z. Zhong, S.C. McCleskey, E.V. Anslyn and J.T. McDevitt, *Angew.Chem.Int.Ed.* 2005, 44, 6375-6378.

76. A.P. Goodey, J.T. McDevitt, *J.Am.Chem.Soc.* 2003, 125, 2870-2871.

77. N.T. Greene, S.L. Morgan and K.D. Shimizu, *Chem.Comm.* 2004, 1172-1173.

78. N.T. Greene, K.D. Shimizu, *J.Am.Chem.Soc.* 2005, 127, 5695-5700.

79. M. Rangin, A. Basu, *J.Am.Chem.Soc.* 2004, 126, 5038-5039.

80. M.R. West, T.W. Hanks and R.T. Watson, *J.Chem.Educ.* 2009, 86, 373-375.

81. J.W. Lee, J.S. Lee and Y.T. Chang, *Angew.Chem.Int.Ed.* 2006, 45, 6485-6487.

82. S.A. Chan, J. Lee and Y. Chang, *Australian Journal of Chemistry* 2009, 62, 1040-1046.

83. L. Baldini, A.J. Wilson, J. Hong and A.D. Hamilton, *J.Am.Chem.Soc.* 2004, 126, 5656-5657.

84. M.N. Stojanovic, E.G. Green, S. Semova, D.B. Nikic and D.W. Landry, *J.Am.Chem.Soc.* 2003, 125, 6085-6089.

85. T. Mayr, G. Liebsch, I. Klimant and O.S. Wolfbeis, *Analyst* 2002, 127, 201-203.

86. T. Mayr, C. Igel, G. Liebsch, I. Klimant and O.S. Wolfbeis, *Anal.Chem.* 2003, 75, 4389-4396.

87. C. Zhang, K.S. Suslick, *J.Am.Chem.Soc.* 2005, 127, 11548-11549.

88. C.J. Musto, K.S. Suslick, *Curr.Opin.Chem.Biol.* 2010, 14, 758-766.

89. D. Sareen, P. Kaur and K. Singh, *Coord.Chem.Rev.* 2014, 265, 125-154.

90. A. Abbaspour, M.A. Mehrgardi, A. Noori, M.A. Kamyabi, A. Khalafi-Nezhad and M.N. Soltani Rad, *Sens.Actuators B* 2006, 113, 857-865.

91. M.M. Erenas, O. Piñeiro, M.C. Pegalajar, M.P. Cuellar, I. de Orbe Paya and L.F. Capitan-Vallvey, *Anal.Chim.Acta* 2011, 694, 128-135.

92. M.M. Erenas, M.C. Pegalajar, M.P. Cuellar, I. de Orbe Paya and L.F. Capitan-Vallvey, *Sens.Actuators B* 2011, 156, 976-982.

93. S. Capel-Cuevas, M.P. Cuellar, I. De Orbé Payá, M.C. Pegalajar and L.F. Capitán-Vallvey, *Anal.Chim.Acta* 2010, 681, 71-81.

94. S. Capel-Cuevas, M.P. Cuellar, I. de Orbe-Paya, M.C. Pegalajar and L.F. Capitán-Vallvey, *Microchem.J.* 2011, 97, 225-233.

95. M.P. Cuellar, S. Capel-Cuevas, M.C. Pegalajar, I. de Orbe-Paya and L.F. Capitán-Vallvey, *New J.Chem.* 2011, 35, 1042-1053.

96. S. Capel-Cuevas, M.P. Cuellar, M.C. Pegalajar, I. de Orbe-Paya and L.F. Capitan-Vallvey, *Sensors Journal, IEEE* 2012, 12, 1197-1206.

97. A. Martinez-Olmos, S. Capel-Cuevas, N. Lopez-Ruiz, A.J. Palma, I. de Orbe and L.F. Capitán-Vallvey, *Sens.Actuators B* 2011, 156, 840-848.

98. S. Capel-Cuevas, N. Lopez-Ruiz, A. Martinez-Olmos, M.P. Cuellar, M. del Carmen Pegalajar, A.J. Palma, I. de Orbe-Paya and L.F. Capitan-Vallvey, *Sensors* 2012, 12, 6746-6763.

99. A. Edelmann, B. Lendl, *J.Am.Chem.Soc.* 2002, 124, 14741-14747.

100. M.B. Denton, H.A. Lewis and G.R. Sims, *ACS Symp.Ser.* 1983, 236, 133-154.

101. G. Wyszecki, W.S.Stiles in *Color Science: Concepts and Methods, Quantitative Data and Formulae,* 2nd Edition ed., John Wiley & Sons, New York, 1982.

102. G. Wyszecki, W.S. Stiles in *Color Science: Concepts and Methods, Quantitative Data and Formulae,* Wiley Classics Library, Denver, USA, 2000.

103. R.W.G. Hunt in *The Reproduction of Colour,* John Wiley and Sons, 2004.

104. A.R. Smith, *Proceedings of the 5th Annual Conference on Computer Graphics and Interactive Techniques* 1978, 12-19.

105. K. Cantrell, M.M. Erenas, I. Orbe-Paya and L.F. Capitán-Vallvey, *Anal.Chem.* 2010, 82, 531-542.

106. T. Munakata in *Fundamentals of the New Artificial Intelligence: beyond Traditional Paradigms,* Springer, 2008.

107. P.D. Wassermann in *Neural computing: Theory and Practice,* VNR, New York, 1989.

108. F.C. Krebs, *Sol.Energ.Mat.Sol.Cells* 2009, 93, 394-412.

109. K. Norrman, A. Ghanbari-Siahkali and N.B. Larsen, *Annu.Rep.Prog.Chem., Sect.C: Phys.Chem.* 2005, 101, 174-201.

110. E. Cantatore in *Applications of Organic and Printed Electronics: A Technology-Enabled Revolution,* Springer, 2013.

111. A.S.G. Reddy, B.B. Narakathu, M.Z. Atashbar, M. Rebros, E. Rebrosova and M.K. Joyce, *Procedia Eng.* 2011, 25, 956-959.

112. S.I. Hong, *Packag.Technol.Sci.* 2002, 15, 155-160.

113. H. Kipphan in *Handbook of print media : technologies and production methods,* Spinger, Berlin New York, 2001.

114. K. Abe, K. Suzuki and D. Citterio, *Anal.Chem.* 2008, 80, 6928-6934.

115. E.B. Secor, P.L. Prabhumirashi, K. Puntambekar, M.L. Geier and M.C. Hersam, *J.Phys.Chem.Lett.* 2013, 4, 1347-1351.

116. F. Villani, P. Vacca, G. Nenna, O. Valentino, G. Burrasca, T. Fasolino, C. Minarini and D. della Sala, *J.Phys.Chem.C* 2009, 113, 13398-13402.

117. G. Arrabito, B. Pignataro, *Anal.Chem.* 2010, 82, 3104-3107.

118. Pierik, Anke. Ink jet printing of bio-molecules. Printing of microarrays. 2006.

119. K. Crowley, A. Morrin, A. Hernandez, E. O'Malley, P.G. Whitten, G.G. Wallace, M.R. Smyth and A.J. Killard, *Talanta* 2008, 77, 710-717.

120. T. Unander, H.E. Nilsson, *Sensors Journal, IEEE* 2009, 9, 922-928.

121. J. Sarfraz, P. Ihalainen, A. Maattanen, T. Gulin, J. Koskela, C.E. Wilen, A. Kilpela and J. Peltonen, *Sens.Actuators B* 2014, 191, 821-827.

122. X. Li, J. Tian, G. Garnier and W. Shen, *Colloids Surf., B* 2010, 76, 564-570.

123. A.W. Martinez, S.T. Phillips, B.J. Wiley, M. Gupta and G.M. Whitesides, *Lab Chip* 2008, 8, 2146-2150.

124. S.M.Z. Hossain, J.D. Brennan, *Anal.Chem.* 2011, 83, 8772-8778.

125. B. Derby, *Annu.Rev.Mater.Res.* 2010, 40, 395-414.

126. N. Reis, B. Derby, *Mater.Res.Soc.Symp.Proc.* 2001, 624, 65-70.

127. P.C. Duineveld, E. Haskal, M.M. de Kok, M. Buechel, A. Sempel, K.A.H. Mutsaers, P. van de Weijer, I.G.J. Camps, T. van de Biggelaar and J.E. Rubingh, *Proc.SPIE-Int.Soc.Opt.Eng.* 2002, 4464, 59-67.

128. C.D. Stow, M.G. Hadfield, *Proc.R.Soc.Lond.A.* 1981, 373, 419-441.

Chapter I

Towards a disposable optical tongue for metal ions

CHAPTER I: TOWARDS A DISPOSABLE OPTICAL TONGUE FOR METAL IONS

OBJECTIVES

The overall objective of the work presented in this chapter is the preparation, characterization and validation of disposable membranes containing conventional chromogenic reagents for the determination of metal ions based on absorption and color measurement.

The specific objectives to achieve are:

- Selection of chromogenic and additional reagents and preparation of sensing membranes by a spin coating technique.
- Characterization and modeling of optical sensing membranes.
- Implementation of various strategies to correlate the experimental optical data with metal ion concentration.
- Validation of the proposed methodology for metal ion sensing.
- Design of a portable optical instrument for use with the metal ion sensing membranes developed.

CHARACTERIZATION OF DISPOSABLE OPTICAL SENSORS FOR HEAVY METAL DETERMINATION

ABSTRACT

This paper presents the development, characterization and quality control of analytical methods based on the use of disposable optical sensors for determination of heavy metals. Chromogenic reagents such as 1-(2-pyridylazo)-2-naphthol, (2-pyridylazo) resorcinol, Zincon, Ferrozine, and Chromazurol S were used to develop optical sensors of heavy metal ions found as contaminants in pharmaceutical substances and products, such as Zn(II), Cu(II), Ni(II), Fe(II), and Fe(III). The chromogenic reagents were immobilized in polymeric membranes by spin-coating from cocktails containing all reagents needed. The methods were prevalidated using a comprehensive quality control strategy based on a system of mathematical/statistical testing and diagnosis of each prevalidation step. This system involved characterization of analytical groups; checking of two limiting groups; testing of data homogeneity; recognition of outliers; and determination of analytical functions, limiting values, precision and accuracy. The prevalidation strategy demonstrated the reliability of the proposed method and pointed out some limitations. Combining the optical sensors with multicomponent linear regression allowed simultaneous determination of multiple metals in synthetic mixtures with different compositions. Good agreement between experimental and theoretical amounts of heavy metals in the mixtures was obtained for the majority of sensors and metals. Even better agreement was obtained between the experimental and theoretical total amounts of metals in the mixtures. The proposed analytical methods were successfully applied to the determination of Zn(II) in pharmaceutical preparations of insulin and the determination of metal mixtures in a commercial nasal spray of isotonic sea water. The reliable and sensitive individual optical sensors developed in this study may be

useful for designing a multi-membrane optical tongue that with appropriate further optimization can be used for screening heavy metals in various matrices.

INTRODUCTION

Heavy metals are ubiquitous and monitoring them is important in various fields because of their effects on ecosystems and living organisms [1-5]. For example, an important part of drug quality control is detecting and determining heavy metals. Bulk drug substances and their intermediates can be contaminated by metals in many ways, such as from raw materials, reagents, and solvents; from electrodes, reaction vessels, storage containers, plumbing and other equipment used in synthesis; or from exposure to air-borne particles. Metal catalysts and metal reagents, are substances used in the synthesis of the drug substance or are used as excipients used in a medicinal products, and, therefore, can also introduce various metals into drug preparations [6, 7]. Although evaluated for their potential risk to human health and placed into one of three classes (metals of significant, low, and minimal safety concern), some of them, such as Fe(II) and (III), Zn(II), and Cu(II) are also important in human nutrition.

For over a century [7], drug quality control departments have relied on the heavy metal limit test recommended by most pharmacopoeias [8-11]. Besides the heavy metal limit test, European Pharmacopoeia [8] prescribes determination of specific metals in drug substances, such as Cu(II) in ascorbic acid, Zn(II) in insulin, Ni(II) in polyols, and others. The heavy metal limit test is based on sulfide precipitation in a weakly acidic medium and comparison with a lead solution. The test can be easily transferred from one laboratory to another and does not require expensive instrumentation or highly trained laboratory personnel. However, it suffers from several disadvantages. It requires subjective visual interpretation, large amounts of sample, and usually a

heating step that causes losses of volatile elements. In addition, it does not provide any qualitative or element-specific information. Several attempts have been made to overcome these limitations [12, 13], but no major improvements have been achieved. Thus, this standard method remains suitable for only a few elements, and it cannot specify the content of any particular metal ion but only the overall content of ions [12].

Recently, as another alternative to the pharmacopoeial heavy metal limit test, a simple and sensitive methodology was proposed for simultaneous determination of metals in mixtures using solid-phase spectrophotometry [14]. This methodology was successfully applied to the determination of several heavy metals as impurities in pharmaceutical substances.

Several investigators have suggested replacing the heavy metal limit test with more sophisticated analytical methods such as ICP-MS to test drug substances, intermediates, and raw materials [15-18]. ICP-MS allows sensitive, rapid and automated multi-elemental analysis with a minimum of sample size and elemental interferences. In spite of the promise offered by this technique, the heavy metal limit test remains in use, mainly due to the lack of an alternative that provides the required information with comparable ease and simplicity.

In the past several years, the use of optical sensors for heavy metal analysis has increased because they are simple and inexpensive, and they allow remote and continuous monitoring [2, 19]. These so-called optodes for metal ion determination can be fabricated by employing different types of reagents, such as chromogenic, fluorescent, and ionophoric compounds and enzymes. Numerous optical sensors based on chromogenic reagents have been described, such as Xylenol orange [20], Dithizone [21], Chromazurol S [22], PAN [23-25], PAR [25, 26], TAR [27], Br-PADAP [28-30], ACDA [31], NN [25], and Pyrocatechol violet [32]. Although some of these reagents are selective for certain metals under specific conditions, most of them show low selectivity.

Electronic tongues are a special case of optical sensors consisting of an array of sensors exhibiting different selectivities; pattern recognition systems analyze their responses to determine the profile of analytes present in the sample [33]. These tongues have been prepared using sensors based on a variety of principles, including tin oxide catalysis, conducting polymers, acoustic waves, quartz crystal microbalance, ion-selective field effect transistors (FET), ion mobility spectrometry, and mass spectrometry techniques like atomic pressure ionization (API) and proton transfer reaction (PTR). Tongues have also been prepared using sensors based on optical techniques, principally fiber optics and fluorescence [34]. In optical tongue systems, the sensors should present low selectivity or high cross-sensitivity, and they should have reproducible analytical characteristics. In addition, the systems should be relatively inexpensive and portable. Ideally the sensors should be more sensitive and more robust, which is contradictory to a certain degree, since the more sensitive a sensor is, the less robust it becomes [35]. One solution is to use disposable sensors that are not integrated into the device.

We are developing an approach to analyze heavy metals which are important in pharmaceutical practice (such as Zn(II), Cu(II), Ni(II), Fe (III), and Fe(II)) using an optical tongue that consists of an array of membranes containing conventional chromogenic reagents immobilized on a transparent support. At present, metals are selected according to EMEA [6] classification for metallic residues in drug substances and excipients, where besides platinoids, Ni (Class 1) Cu (Class 2), Zn and Fe (Class 3) are metals with potential toxic effect. It may even be possible to extend the use of optical tongue to the analysis of other metals, such as Pb, Cd, Hg, Co, As, and Mn. As a first step, we present here the development and characterization of individual, disposable optical sensors that could be assembled into a disposable multi-membrane sensor for simultaneous determination of heavy metals. The analytical quality of the individual membranes was assessed using a comprehensive prevalidation strategy [36].

In addition, the sensors were tested using synthetic metal mixtures and real pharmaceutical preparations; optical response was processed using powerful multicomponent analysis [37]. This analytical system may be a valuable alternative to the present pharmacopoeial heavy metal limit test, and it may prove useful for the determination of heavy metals in different matrices.

EXPERIMENTAL

Reagents and materials

Working standard solutions of Zn(II), Cu(II), Ni(II), and Fe(III) (100 μg mL^{-1}) were prepared by appropriate dilution of the standard stock solution of each metal (1000 μg mL^{-1}) (Sigma-Aldrich Química S.A., Madrid, Spain) acidified with conc. HNO3 (Sigma). Fe(II) stock solution (100 μg mL^{-1}) was prepared by dissolving ammonium Fe(II) sulfate hexahydrate (Panreac, Barcelona, Spain) in water acidified with conc. HNO3. Solutions of lower concentrations were prepared by dilution with water.

Sensor films were prepared using polyurethane hydrogel D4 (Tyndale Plains-Hunter, Lawrenceville, NJ, USA) and the following reagents, all purchased from Sigma-Aldrich (Madrid, Spain): high molecular weight polyvinyl chloride (PVC), o-nitrophenyloctylether (NPOE), tributyl phosphate (TBP), potassium tetrakis (4-chlorophenyl) borate (TCPB), hexadecyltrimethylammonium bromide (HTMAB), benzethonium chloride (BTC), cellulose acetate (CA), and tetrahydrofuran (THF). Sheets of Mylar-type polyester (Goodfellow, Cambridge, UK) were used as a support.

The following chromogenic reagents were purchased from Sigma: 1-(2-pyridylazo)-2-naphthol (PAN), 1-10-phenanthroline, 4,7-diphenyl-1, 10-phenanthroline, 3-(2-pyridyl)-5,6-diphenyl-1,2,4-triazine-4',4"-disulfonic acid sodium

salt (Ferrozine, FER), (Z)-5-((3-carboxy-5-methyl-4-oxocyclohexa-2,5-dien-1-ylidene) (2,6-dichloro-3-sulfophenyl) methyl)-2-hydroxy-3-methylbenzoic acid (Chromazurol, CS), 2-carboxy-2'-hydroxy-5'-sulfoformazyl-benzene monosodium salt (Zincon),3,3'-bis[N,N-bis(carboxymethyl)aminomethyl]-o-cresolsulfonephthalein disodium salt (Xylenol orange, XO), 8-hydroxyquinoline, Tetraphenylporphyrin, 1,8-dihydroxynaphthalene-3,6-disulfonic acid disodium salt (Chromothropic acid disodium salt), Salicylhydroxamic acid, and Dimethylglyoxime. In addition, the chromogenic reagents 1,2,4-trihydroxy-9,10-anthracenedione (Purpurin) and 4-(2-pyridylazo)resorcinol (PAR) from Fluka (Madrid, Spain), and 1,2-dihydroxy-9,10-anthracenedione (Alizarine) from TCI (Zwijndrecht, Belgium) were used. All chemicals were of analytical-reagent grade, and reverse osmosis-purified water (Milli-RO 12 plus Milli-Q station, Millipore) was used throughout.

Preparation of disposable membranes and measurement set-up

The following cocktails were prepared in order to make heavy metal-sensing membranes: (a) PAN cocktail (133.7 mmol of PAN kg^{-1} of PVC), containing 30.0 mg PVC, 60.0 mg NPOE, and 1.0 mg PAN dissolved in 1 mL of freshly distilled THF; (b) PAR cocktail (38.7 mmol of PAR kg^{-1} of D4), containing 240.0 mg D4 polyurethane hydrogel, 2.0 mg PAR, and 10.3 mg TCPB dissolved in a mixture of 3.6 mL of ethanol and 0.4 mL of water; (c) Zincon cocktail (43.3 mmol of Zincon kg^{-1} of D4), containing 100.0 mg D4 polyurethane hydrogel, 2.0 mg Zincon, and 10.0 mg BTC dissolved in a mixture of 3.0 mL of ethanol and 0.2 mL of water; (d) FER cocktail (38.9 mmol of FER kg^{-1} of D4), containing 100.0 mg D4 polyurethane hydrogel, 2.0 mg FER, and 2.0 mg TCPB dissolved in a mixture of 3.0 mL of ethanol and 0.2 mL of water; and (e) CS cocktail (35.5 mmol of CS kg^{-1} of D4), containing 100.0 mg D4 polyurethane hydrogel, 2.0 mg CS, and 10.0 mg HTMAB dissolved a mixture of 3.0 mL of ethanol and 0.2 mL of water.

To prepare membranes, the different cocktails (20 μL) were placed individually on polyester sheets (14 mm × 4 cm × 0.5 mm thick) and subjected to spin coating. The sensing zone on each membrane was a circle 7 mm in diameter. The membranes were stored in a closed container at room temperature to enable slow solvent evaporation and then kept in a dark place until use to avoid photodegradation.

The response of PAN and Zincon membranes was evaluated using 8 mL of test solution together with 2 mL of 2 M ammonia buffer solution (pH 9.5); the response of PAR, FER and CS membranes was evaluated using 2 mL of 2 M acetic acid buffer (pH 4.0). Test solutions were prepared either of individual metals at concentrations ranging from 1.0-10.0 μg mL^{-1}, or of mixtures of 2-5 metals at individual concentrations of 1.0-5.0 μg mL^{-1}. The mixtures of test and buffer solutions were placed in polyethylene tubes (10 cm × 1.5 cm), a disposable sensor was inserted, and the tube was capped. The samples were shaken for 10 min on a vibrating agitator at 800 oscillations per minute at room temperature. The sensors were then removed from the tubes, residual solution was dried from the membrane surface, and membrane absorbance was measured using a Hewlett-Packard diode array UV/Vis spectrophotometer (Model 8453; Norwalk, CT, US) equipped with a custom-made membrane holder. The holder was an Fe block painted matte black and measuring 44 mm high and 12 mm wide [38]. This cell holder enables measurements of a zone of constant diameter that is smaller than the diameter of the sensor's active zone, which avoids noise due to variation in the surface area of the membrane active zone. All sample and blank measurements were carried out against a clear Mylar polyester strip, at room temperature (20±3 °C). The membranes were not conditioned before use.

Absorbance measurements were collected using Chemstation software (Hewlett-Packard). Data were analyzed using the Statgraphics software package (version 6.0; Statpoint Technologies, Warrenton, Virginia, US).

Prevalidation study

A comprehensive prevalidation strategy [36] was carried out to diagnose the accuracy and reliability of the procedures using the PAN, PAR, Zincon, FER, and CS membranes (Me-sensor systems). Prevalidation experiments were based on 24 measurements divided into six analytical groups (6 standard solutions of metal j). Each analytical group comprised 4 replicate experiments (i). For each measurement of the standard, the corresponding blank solution was also measured (24 blank measurements). Working solutions of heavy metals were prepared by appropriate dilution of the standard stock solution of each heavy metal(1.0xU = x_1=10.0 μg mL^{-1}, upper end of analyte range; 0.8xU = x_2 = 8.0 μg mL^{-1}, 0.6xU = x_3 = 6.0 μg mL^{-1}; 0.4xU = x_4 = 4.0 μg mL^{-1}; 0.2xU = x_5 = 2.0 μg mL^{-1};and 0.1xU = x_6 = xL = μg mL^{-1}, lower end of analyte working range), and measurements were carried out according to the procedure described in section Preparation of disposable membranes and measurement set-up. Blank solutions were prepared and absorbance measured in the same way, but without analyte. The data were analyzed using descriptive and prognostic statistics to assess measurement quality at the lower end of the analytical working range, assess data homogeneity, determine calibration and analytical evaluation functions, detect outliers, and estimate limiting values, precision and accuracy.

Method for multicomponent analysis of heavy metals

A combination of sensors (PAN, PAR, Zincon, FER, and CS sensors) and a chemometric algorithm of multicomponent analysis by multiple linear regression (Metal-Sensor Multicomponent Analysis, MeSeMA) were used as a valid methodological approach for the simultaneous determination of heavy metals in a synthetic mixture without previous concentration or separation.

Establishment of the molar absorptivity matrix k

The first step in the multicomponent analysis is the establishment of the absorptivity matrix K, the elements of which are the absorptivities of m components (metals) at n wavelengths. These elements can be obtained from the spectra of the pure components. Therefore, a concentration-normalized spectrum of each system containing 10 μg mL^{-1} of a particular metal was recorded in the corresponding wavelength range (Table 1).

Table 1. Characteristic wavelengths of sensing systems

Sensor	Characteristic wavelengths, λ (nm)						K-matrix
	Zn(II)	Cu(II)	Ni(II)	Fe(II)	Fe(III)	Range	
PAN	560	563	573	-	-	520-600	3×10
PAR	520	530	540/580	-	720	490-720	4×12
Zincon	-	624	675	-	-	580-740	2×11
FER	-	-	-	560	-	560-610	1×6
CS	-	-	-	-	680	600-710	1×4

The elements of the K matrix were treated as the independent variables, and the number of wavelengths was equal to or greater than the number of components. Matrix elements were apparent molar absorptivities ε obtained at 4, 7, 9, 10 and 11 wavelengths from recorded spectra of each metal for CS, FER, Zincon, PAN, and PAR membranes. The order of the matrix (m×n) used for multicomponent analysis depended on the number of metals in the mixture and ranged from 1×4 (CS sensor) to 4×12 (PAR sensor).

Determination of metals in synthetic mixtures

The MeSeMA methodology was used to determine total and specific amounts of

metals in synthetic mixtures with different compositions and metal amounts. The following systems were investigated: (a) PAN sensor with a mixture of Zn(II), Cu(II), and Ni(II); (b) PAR sensor with a mixture of Zn(II), Cu(II), Ni(II), and Fe(III); (c) Zincon sensor with a mixture of Cu(II) and Ni(II); (d) FER sensor with a mixture of Zn(II), Cu(II), Ni(II), and Fe(II); and (e) CS sensor with a mixture of Zn(II), Cu(II), Ni(II), and Fe(III). The concentrations of individual metals in the mixtures varied from 1.0 to 5.0 μg mL^{-1}. Calculations were performed using the appropriate absorptivity matrix K and a set of equations for multiple linear regression [37, 39]. To perform faster calculations, SPIS software for multicomponent analysis of mixtures by multiple linear regression was used [14].

Determination of Zn in pharmaceutical preparations of insulin

Insulin preparations were obtained from the Croatian Agency for Medicines and Medical Products, which had received them from various pharmaceutical manufacturers for mandatory routine testing. The following preparations were obtained: Humalog®, Humalog Mix25®, Humalog Mix50®, and Humulin M3® (Eli Lilly, USA); Insulatard® Penfill® (Novo Nordisk, Denmark); and Lantus® Solostar® (Sanofi Aventis, France). Each preparation was shaken gently, and a volume containing 200 IU of insulin was diluted to 25 mL with 0.01 M hydrochloric acid. A series of samples was prepared by adding known amounts of Zn(II) to 1 mL of the insulin dilutions prepared in the previous step. The procedure described in the section Preparation of disposable membranes and measurement set-up was applied and Zn(II) content was determined in spiked samples according to the MeSeMA methodology.

Determination of metals in isotonic sea water

A series of samples were prepared by adding known amounts of metals (Zn(II),

Cu(II), Ni(II), and Fe(III)) to 8 mL of a commercial nasal spray of isotonic sea water (Sterimar®, Sodibel-Laboratoires, Fumouze, France). The procedure described in the section Preparation of disposable membranes and measurement set-up was applied to spiked samples and metal content was determined according to the MeSeMA methodology.

RESULTS AND DISCUSSION

Selection of the reagents

The goal of this study was to prepare a set of heavy metal-sensing membranes for the analysis of mixtures of Zn(II), Cu(II), Ni(II), Fe(II), and Fe(III) ions based on absorbance measurement. Fifteen different chromogenic reagents were studied (see section Reagents and materials) in different cocktails containing different types and amounts of membrane polymer, plasticizer, and lipophilic salt. Membranes were prepared from selective and non-selective chromogenic reagents in order to achieve different selectivity patterns for the heavy metals with no leaching over the entire concentration range studied.

Five membranes satisfying these criteria were selected: PAN, PAR, Zincon, FER, and CS (Table 1). These membranes gave a fast reaction, leaching of the reagents or reaction product was not observed, and they were easily immobilized onto the appropriate support (PVC or D4). PAN, PAR and Zincon showed non-selective behavior, reacting with several metal ions. In contrast, FER and CS were selective for Fe(II) and Fe(III), respectively. These five reagents yielded membranes that gave the greatest color change in the presence of analyte.

The composition of five selected membranes was optimized to (1) minimize leaching by varying the lipophilic salt, plasticizer, and membrane polymer; (2) maximize color intensity by varying the concentration of chromogenic reagent; and

(3) minimize response time by varying plasticizer, membrane polymer, and the volume of cocktail used to prepare the membrane. The optimum compositions are indicated in section Preparation of disposable membranes and measurement set-up. The optimal lipophilic salt/reagent ratio varied widely from 1:1 to 8:1.

Optimization of experimental parameters

The effect of pH on product formation and sorption on membranes was investigated in the range pH 3 to 12. Maximal response was obtained at pH 9.5 for PAN and Zincon membranes and at pH 4.0 for PAR, FER, and CS membranes. At pH values above 7.0, leaching of PAR into the solution was observed. The Zincon sensor was sensitive to Cu(II) and Ni(II) at basic pH, but it did not detect Ni(II) at acidic pH. Longer reaction time (over 30 min) increased optical response, especially for the PAN sensor, but leaching from the PAR membrane was observed for reaction times longer than 15 min. Therefore, a reaction time of 10 min was used for all sensing membranes.

Color change of sensing membranes

All of the sensing membranes gave different color changes in the presence of different metals (Figure 1).

The PAN membrane gave a positive reaction in the presence of Zn(II), Cu(II), and Ni(II); the PAR membrane, in the presence of Zn(II), Cu(II), Ni(II), and Fe(III); and the Zincon membrane, in the presence of Cu(II) and Ni(II). The FER and CS sensing membranes showed a highly selective response than the other three membranes; they gave color changes for Fe(II) and Fe(III), respectively.

In order to describe the sensing mechanism of our membranes, we studied the complexation between PAN in the membrane and Cu(II) in solution at pH 9.5.

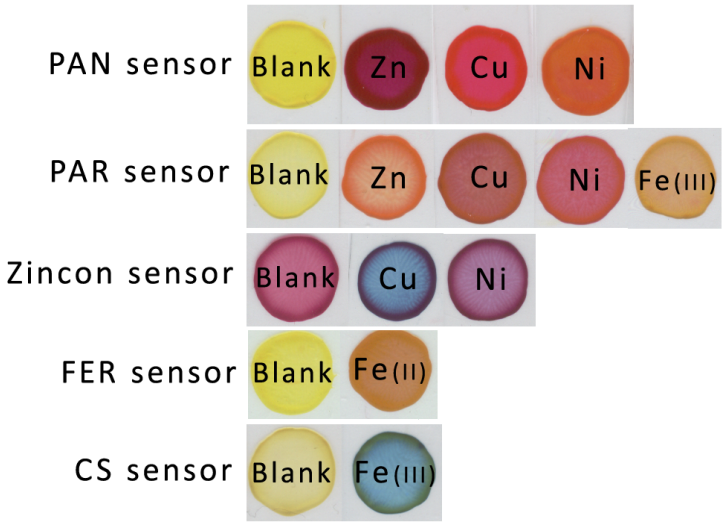

Figure 1. Optical sensor before (blank) and after the reaction with metal.

We assumed a 1:1 stoichiometry [40], which is usually observed when PAN is used as chromogenic reagent for different metals in ion-exchange materials [41-44], lipophilic salts [45] and adsorbents [46-48]. We therefore described the complexation with eq. 1:

$$Cu^{2+} + X^{-} + \overline{HL} \leftrightarrow \overline{CuLX} + H^{+} \qquad \text{(Eq. 1)}$$

This co-extraction equilibrium is characterized by a constant Ke that includes, for the ion pair involved, a stability constant, dissociation constant, distribution constant between aqueous and membrane phases of different species, and dissociation constant. The activity of the Cu(II) ion in the aqueous phase is related to the equilibrium constant Ke through a sigmoidal response function that includes the experimental degree of uncomplexed chromogenic reagent α (eq. 2).

$$K_e = \frac{(1-\alpha)\cdot a_{H^+}}{\alpha \cdot a_{Cu^{2+}} \cdot a_{X^-}} \qquad \text{(Eq. 2)}$$

The good fit of experimental data to eq. 2 (R^2 = 0.9999) supports the 1:1 stoichiometry, with a K_e of $1.2 \cdot 10^{10}$.

Spectral characterization of sensing membranes

The spectral characteristics of all complexes investigated are shown in Figure 2. Substantial overlap of the spectra was observed, due to the low selectivity of PAN, PAR, and Zincon sensors. The complexes Zn(II)-PAN, Cu(II)-PAN, and Ni(II)-PAN showed absorption maxima in the range 520-580 nm. The absorption maxima of nearly all products on the PAR sensor were in the range 470-600 nm.

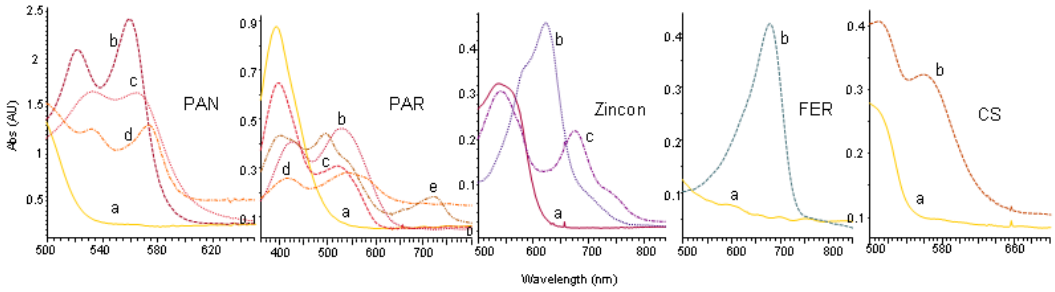

Figure 2. Absorption spectra of sensors for heavy metals. PAN sensor at pH 9.5: (a) PAN (blank); (b) Zn(II)-PAN product (10 mg mL^{-1} of Zn(II)); (c) Cu(II)-PAN product (10 mg mL^{-1} of Cu(II)); (d) Ni(II)-PAN product (10 mg mL^{-1} of Ni(II)). PAR sensor at pH 4.0: (a) PAR (blank); (b) Zn(II)-PAR product (10 mg mL^{-1} Zn(II)); (c) Cu(II)-PAR product (10 mg mL^{-1} Cu(II)) (d) Ni(II)-PAR product (10 mg mL^{-1} Ni(II)); (e) Fe(III)-PAR product (10 mg mL^{-1} Fe(III)). Zincon sensor at pH 9.5: (a) Zincon (blank); (b) Cu(II)-Zincon (10 mg mL^{-1} Cu(II)); (c) Ni(II)-Zincon (10 mg mL^{-1} Ni(II)). FER sensor at pH 4.0: (a) FER (blank); (b) Fe(II)-FER product (10 mg mL^{-1} Fe(II)). CS sensor at pH 4.0: (a) CS (blank); (b) Fe(III)-CS product (10 mg mL^{-1} Fe(III)).

The absorption spectrum of Fe(III)-PAR differed significantly from that of the others, with a maximum at 730 nm. In the case of the Zincon sensor, the overlap between the spectra of Cu(II)-Zincon and Ni(II)-Zincon was less extensive. Of all the sensing membranes investigated, the FER and CS membranes showed the highest selectivity; they were selective for Fe(II) and Fe(III), respectively. Absorbance

of the reagent blanks for nearly all sensors was negligible in the wavelength range where the reagent-metal complexes had their absorption maxima.

Prevalidation of sensor results

A comprehensive prevalidation strategy was carried out to diagnose the quality of Me-sensor systems and identify any limitations. Initial prevalidation data were as follows: amounts of metal ion (x) were within the working range from 1.0 to 10.0 μg mL^{-1}, absorbances were obtained from measurements of the blank (B) and the sample (y), and the corrected absorbance (S) was calculated as the difference y − B. The following membrane-metal systems were analyzed in the prevalidation: Zn(II)-PAN, Cu(II)-PAN, and Ni(II)-PAN; Zn(II)-PAR, Ni(II)-PAR; Cu(II)-Zincon, Ni(II)-Zincon; Fe(II)-FER; and Fe(III)-CS.

The first step in calculating descriptive statistics of the prevalidation process was to characterize six analytical groups of all investigated systems by calculating average values and standard and relative standard deviations. These values were used to evaluate repeatability of the measurements as a part of precision (Table 2). Relative standard deviations of blank absorbances showed low precision of blank measurements in most systems. These fluctuations of the blank values may reflect variability in sensor quality or method's performance characteristics.

Nevertheless, even in the worst cases, the fluctuations in blank values could be ignored because they were so small compared to the analyte signal. In contrast, relative deviations of sample measurements and corrected absorbances showed high precision for nearly all systems. The Me-PAN system showed the highest precision; deviations (s_{ry} from ±0.80% to ±5.40%, s_{rs} from ±0.87% to ±5.82%) satisfied the strict prevalidation criterion of s_r <±5% [36]. In most systems for which s_{ry} and s_{rs} were somewhat higher than ±5%, the offending deviations occurred with the smallest quantity of analyte (x6).

Table 2. Precision of the measurements of *Me-sensor* systems

	s_r (%)								
	Zn-PAN	Cu-PAN	Ni-PAN	Zn-PAR	Ni-PAR	Cu-Zincon	Ni-Zincon	Fe(II)-FER	Fe(III)-CS
B	25.8-140.8	21.8-81.0	10.1-95.4	2.8-12.4	2.5-24.8	22.9-50.0	21.6-42.5	6.7-27.7	7.9-24.2
y	0.8-5.4	1.6-3.5	4.1-7.7	1.3-8.8	0.6-7.0	1.7-14.7	2.0-12.5	2.5-9.6	0.4-11.1
S	0.9-5.8	1.5-3.8	4.2-8.0	1.7-13.5	0.7-9.0	1.9-23.6	2.0-16.3	2.4-9.8	0.7-12.7
A	0.9-5.8	1.5-3.8	4.2-8.0	1.7-13.5	0.7-9.0	1.9-23.6	2.0-16.3	2.4-9.8	0.7-12.7

A preliminary check of analytical groups 1 and 6, which limit the working range of the proposed method, indicated good quality of measurements and unambiguous distinction between analyte and blank signals in the group with x_6. The analyte signal in the Me-PAR and Me-Zincon systems was slightly different from blank signal, while the blank signal was significantly lower than analyte signal in the group with x_6 in the case of Me-PAN (AC=158.7 for Zn(II), AC=122.6 for Cu(II), and AC=12.6 for Ni(II)), Fe(II)-FER (AC=21.4), and Fe(III)-CS (AC=11.8). Additional checking of how well the systems resolved analyte and blank signals at x_6 showed excellent resolution in the case of Zn(II)-PAN, Cu(II)-PAN, and Fe(II)-FER; very good resolution in the case of Ni(II)-PAN, Zn(II)-PAR, and Fe(III)-CS; and good resolution in the case of Ni(II)-PAR, Cu(II)-Zincon, and Ni(II)-Zincon.

These criteria were satisfied in the case of Zn(II)-PAN and Cu(II)-PAN, and nearly so in the case of Ni(II)-PAN and Fe(II)-FER, and each y value was corrected with a grand blank mean. In contrast, although ANOVA of blank values showed homogeneity in the case of Zn(II)-PAR, Ni(II)-PAR, Cu(II)-Zincon, and Fe(III)-CS, the inhomogeneity was not small in relation to the corresponding analyte values, so the influence of the blanks on the results could not be neglected.

Bartlett's test was used to test the homogeneity of s and s_r values for y, S, A, and apparent mass ($\hat{x}$) values for the different analytical groups.

The test indicated that most values of s and s_r in all systems were almost homogeneous, homogeneous, or strongly homogeneous. Inhomogeneous s_r values were obtained only for gross (y) and corrected (S) values in the Zn(II)-PAN system.

The relationship between analytical signal (absorbance) and analyte content (heavy metal quantity) was determined using three methods: preliminary linearity check, method of least squares, and systematic t-testing of the reality of constants (Table 3).

A preliminary linearity check, applied to A values (measure of particular sensitivity, $A_n = S_n/x_n$) of limiting groups 1 and 6, showed that linear calibration functions were expected for Ni(II)-PAN, Zn(II)-PAR, Cu-(II)Zincon, and Ni(II)-Zincon. The method of least squares showed that correlation existed in all systems, with Cu(II)-PAN, Zn(II)-PAR, and Ni(II)-PAR showing the highest correlation coefficients. Through systematic evaluation of analytical functions, constants were determined for the calibration and analytical evaluation functions over the entire analyte working range, and ideal analytical functions were found for most systems, except Ni(II)-Zincon, Fe(II)-FER, and Fe(III)-CS, which were characterized by linear functions with an intercept (Table 3). These analytical functions were used to test for outliers, determine limiting values, and evaluate apparent signal values $(\hat{S})$ and apparent quantities of heavy metals $(\hat{x})$.

Outlier testing was performed to check whether any measurement differed significantly from the others in the set of signals used to carry out calibration (S) and in the set of heavy metal quantities (x) used to generate the analytical evaluation function. The presence of regression outliers was checked by comparing $|S^*|$ and $|x^*|$ values with the t-values of the 95% and 99% confidence intervals. Only one outlier was obtained in each of the following systems: Zn(II)-PAN ($2.807 > |S_6^*| > 2.069$), Ni(II)-PAN ($2.807 > |S_{13}^*| > 2.069$, $2.807 > |x_{13}^*| > 2.069$), Cu(II)-Zincon ($2.807 > |S_{20}^*| > 2.069$, $2.80 > |x_{20}^*| < 2.069$), and Fe(II)-FER ($2.807 > |S_{13}^*| > 2.069$, $2.80 > |x_{13}^*| < 2.069$).

According to the prevalidation criteria [36], the data remain homogeneous despite these outliers. No outlier values were found in the other systems. Limiting values, such as limiting signal value, limit of detection and limit of quantification were estimated using the analytical evaluation function and recommended concepts of limiting values [49, 50].

Table 3. The relationship between analyte and signal in *Me-sensor* systems

System	Least square method	Calibration function	Analytical evaluation function
Zn(II)-PAN	y = 0.1888x + 0.0559 r^2 = 0.9911	$\hat{S}$= 0.20x s_M = ± 0.088	$\hat{x}$= 5.06S s_M = ± 0.44
Cu(II)-PAN	y = 0.1430x + 0.0262 r^2 = 0.9983	$\hat{S}$ = 0.15x s_M = ± 0.031	$\hat{x}$= = 6.81S s_M = 0.21
Ni(II)-PAN	y =0.0575 + 0.0229 r^2 = 9916	$\hat{S}$ = 0.06x s_M = ± 0.027	$\hat{x}$= = 16.38S s_M = 0.44
Zn(II)-PAR	y = 0.0463x + 0.0069 r^2 =0.9985	$\hat{S}$= 0.047x s_M = ± 0.0092	$\hat{x}$= = 21.1S s_M = ± 0.194
Ni(II)-PAR	y = 0.0464x – 0.0086 r^2 = 0.9982	$\hat{S}$= 0.045x s_M = ± 0.0103	$\hat{x}$= = 22.1S s_M = 0.227
Cu(II)-Zincon	y = 0.0311x + 0.0136 r^2 = 0.9925	$\hat{S}$= 0.03x s_M = ± 0.014	$\hat{x}$= = 30.2S s_M = ± 0.44
Ni(II)-Zincon	y = 0.013x + 0.0061 r^2 = 0.9967	$\hat{S}$= 0.013x +0.006 s_M = ± 0.0035	$\hat{x}$= = 77.0S – 0.43 s_M = 0.270
Fe(II)-FER	y = 0.020x + 0.0134 r^2 = 0.9973	$\hat{S}$= 0.02x + 0.0134 s_M = ± 0.0049	$\hat{x}$= = 49.7S – 0.639 s_M = ± 0.244
Fe(III)-CS	y = 0.039x + 0.046 r^2 = 0.9904	$\hat{S}$= 0.039x +0.046 s_M = ± 0.018	$\hat{x}$= = 25.5S – 1.07S s_M = 0.459

For nearly all systems, estimated limiting values were significantly lower than the amount of metal at the lowest level of analyte (<1μg mL^{-1}), with Me-PAN and Fe(II)-FER showing the lowest limiting values (Table 4). In the Me-Zincon system, the LQ was slightly higher than 1 μg mL^{-1}; this could be due to the high fluctuation of blank values observed in the homogeneity testing.

The final calibration and analytical evaluation functions were used to determine apparent signal values $(\hat{S})$ and apparent masses of analyte $(\hat{x})$, respectively. The

analytical evaluation function was also used to evaluate the precision and accuracy of the systems. Information on accuracy was further obtained by comparing actual (x) and observed ($\hat{x}$) amounts of heavy metal. The data structure for the systems is given in Table 4. The systematic deviations, a measure of accuracy, ranged from -29.7% to +40.8%. As could be expected, the lowest degree of accuracy in all systems was in the analytical group with the smallest amount of heavy metal (1 μg mL^{-1}), while in the other groups favorable accuracy was obtained.

It is likely that large deviations between blank values and analyte values were the main cause of large systematic errors and therefore lower accuracy. The highest level of accuracy was obtained for Ni(II)-Zincon (from -3.6% to +4.2%) and Fe(III)-FER (from -3.4% to +3.3%). Random deviations, a measure of precision of analytical systems, ranged from ±0.7% to ±32.2%. Most systems showed high precision, with Me-PAN showing the highest, based on the prevalidation criterion of $s_r \leq \pm 5\%$.

In systems showing lower precision, such as Me-Zincon and Fe(III)-CS, unfavourable precision was obtained only in the analytical group with the smallest amount of heavy metal (x6).

In summary, evaluation of repeatability of the measurements, homogeneity testing, reality of the linear analytical evaluation function, agreement of actual and found amounts of heavy metals, as well as random and systematic deviations showed good measurement quality.

Very low limiting values indicated that the procedures were sensitive and could be successfully applied to the determination of heavy metal traces. A significant influence of blank dispersion was found to be a possible disadvantage in some systems. Me-Zincon was the only system where reliable measurement could not be made at the lowest level of the working range, because LQ was somewhat higher than the analyte amount in x_6.

Table 4. Metrological characteristics of *Me-sensor* systems

	Analyte amount (μgmL^{-1})						Random deviations		Systematic deviations		L_D (μg mL^{-1})	L_Q (μg mL^{-1})
Actual (μgmL^{-1})	10.0	8.0	6.0	4.0	2.0	1.0	$S_{\hat{x}}$ (μg mL^{-1})	$S_{r\hat{x}}$ (%)	$\Delta\bar{x}$ (μg mL^{-1})	$\Delta\bar{x}$ (%)		
	Found (μg mL^{-1})											
Zn(II)-PAN	9.6	8.6	5.5	4.1	2.1	1.4	(±0.022) – (±0.489)	(±0.9) – (±5.8)	(-0.46) – (+0.57)	(-7.5) – (+40.8)	0.014	0.082
Cu(II)-PAN	10.0	8.0	5.8	4.2	2.1	1.2	(±0.046) – (±0.264)	(±1.5) – (±3.7)	(-0.23) – (+0.23)	(-3.8) – (+22.7)	0.008	0.049
Ni(II)-PAN	9.7	8.0	5.8	4.5	2.4	1.0	(±0.067) – (±0.624)	(±4.3) – (±8.0)	(-0.34) – (+0.50)	(-3.4) – (+18.2)	0.050	0.302
Zn(II)-PAR	9.9	8.0	6.1	4.2	2.0	1.1	(±0.103) – (±0.220)	(±1.7) – (±13.5)	(-0.12) – (+0.20)	(-1.2) – (+19.8)	0.080	0.460
Ni(II)-PAR	9.9	8.2	6.1	3.8	1.9	0.8	(±0.059) – (±0.291)	(±0.7) – (±9.0)	(-0.21) – (+0.18)	(-21.0) – (+2.2)	0.147	0.891
Cu(II)-Zincon	9.6	8.2	6.1	3.9	2.4	1.3	(±0.187) – (±0.490)	(±1.9) – (±23.6)	(-0.38) – (+0.43)	(-3.8) – (+31.0)	0.592	3.601
Ni(II)-Zincon	10.0	8.0	6.0	3.9	2.1	1.1	(±0.211) – (±0.354)	(±2.1) – (±23.0)	(-0.15) – (+0.09)	(-3.6) – (+4.2)	0.296	1.802
Fe(II)-FER	10.0	8.0	6.0	4.1	1.9	1.0	(±0.053) – (±0.467)	(±2.6 – (±11.3)	(-0.08) – (+0.02)	(-3.4) – (+3.3)	0.019	0.118
Fe(III)-CS	10.2	7.5	5.7	4.3	2.5	0.7	(±0.061) – (±0.413)	(±0.8) – (±32.2)	(-0.49) – (+0.45)	(-29.7) – (+22.6)	0.043	0.261

For this system, the working range should be changed and the prevalidation procedure repeated.

Applicability of the MeSeMa procedure

* **Synthetic mixtures**

New analytical procedures based on the use of disposable optical sensors were used to develop a sensitive, fast, and simple procedure for determination of heavy metals in mixtures without previous concentration or separation of analytes. The combination of sensitive sensors and the chemometric algorithm of multicomponent analysis by multiple linear regression (MeSeMA procedure) enabled determination of specific metals in synthetic mixtures, despite similarity in the spectral characteristics of the various analytes present. The results of the heavy metal screening are presented in the Tables 5 and 6.

Due to the low selectivity of the PAN, PAR, and Zincon reagents, metal complexes retained onto the corresponding sensing membranes showed similar absorption spectra, with some differences in spectral characteristics and sensitivity. These small differences in absorption spectra were exploited by powerful multicomponent analysis to simultaneously determine the content of specific metals in metal mixtures. Metal mixtures for PAN and Zincon sensors contained Zn(II), Cu(II), and Ni(II) in different ratios. The mixtures for the PAR sensor contained the same metals, as well as Fe(III). In contrast to the other reagents, FER and CS were selective for Fe(II) and Fe(III), even in the presence of the other metals.

Table 5. Content of specific metal in the mixture

Sensor	Metal	Added (µg mL^{-1})	Found (µg mL^{-1})	SD[a] (µg mL^{-1})	RSD (%)	Recovery (%)	Matrix
PAN	Zn(II)	3.00	3.20	0.071	2.21	106.7	Cu(II), Ni(II)
		0.00	0.0	0.000	0.00	0.0	Cu(II), Ni(II)
		1.00	1.06	0.058	5.41	106.7	Cu(II), Ni(II)
	Cu(II)	3.00	2.75	0.071	2.57	91.7	Zn(II), Ni(II)
		4.00	4.33	0.141	3.26	108.3	Zn(II), Ni(II)
		1.00	0.95	0.071	7.44	95.0	Zn(II), Ni(II)
	Ni(II)	3.00	2.85	0.212	7.44	95.0	Zn(II), Cu(II)
		4.00	3.90	0.000	0.00	97.5	Zn(II), Cu(II)
		5.00	5.05	0.354	7.00	101.0	Zn(II), Cu(II)
PAR	Fe(III)	3.00	2.85	0.071	2.48	95.0	Zn(II), Cu(II), Ni(II)
		2.00	1.80	0.566	31.43	90.0	Zn(II), Cu(II), Ni(II)
		3.00	2.50	0.000	0.00	83.3	Zn(II), Cu(II), Ni(II)
Zincon	Cu(II)	3.00	3.10	0.000	0.00	103.3	Zn(II), Ni(II)
		5.00	5.75	0.212	3.69	115.0	Zn(II), Ni(II)
		1.00	1.00	0.000	0.00	100.0	Zn(II), Ni(II)
	Ni(II)	2.00	2.05	0.212	10.35	102.5	Zn(II), Cu(II)
		4.00	3.40	0.212	6.24	85.0	Zn(II), Cu(II)
		4.00	4.25	0.071	1.66	106.2	Zn(II), Cu(II)
FER	Fe(II)	5.00	4.45	0.212	4.77	89.0	Zn(II), Cu(II), Ni(II)
		2.00	1.75	0.212	12.12	87.5	Zn(II), Cu(II), Ni(II)
		2.00	2.00	0.00	0.00	100.0	Zn(II), Cu(II), Ni
CS	Fe(III)	5.00	5.55	0.212	3.82	111.0	Zn(II), Cu(II), Ni(II)
		3.00	3.40	0.00	0.00	113.3	Zn(II), Cu(II), Ni(II)
		2.00	1.65	0.354	21.43	95.0	Zn(II), Cu(II), Ni(II)

[a] Mean of three determinations

An absorptivity matrix K was calculated for each metal mixture using the procedure described in section Establishment of the molar absorptivity matrix K. Then the procedure described in section Determination of metals in synthetic mixtures was used to determine the content of particular metals in the mixture, as well as the total amount of metals. The good agreement obtained between experimental and theoretical amounts of individual metals and total metals in the mixtures confirmed the validity of the proposed method.

Table 6. Content of total metals in mixtures

Analytical system	Composition (µg mL^{-1})	Total amount (µg mL^{-1})		SD[a] (µg mL^{-1})	RSD (%)	Recovery (%)
		Added	Found			
PAN (Zn(II), Cu(II), Ni(II))	(3:3:3)	9.00	8.75	0.071	0.81	97.2
	(0:4:4)	8.00	8.20	0.212	2.59	102.5
	(1:1:5)	7.00	7.00	0.141	2.02	100.0
PAR (Zn(II), Cu(II), Ni(II), Fe(III))	(3:3:3:3)	12.00	13.4	2.263	16.89	111.7
	(0:5:5:2)	12.00	11.2	0.656	5.85	93.3
	(1:1:5:3)	10.00	13.7	0.990	7.23	137.0
Zincon (Zn(II), Cu(II), Ni(II))	(3:3:2)	5.00	5.15	0.071	1.37	103.0
	(0:5:5)	10.00	9.65	0.071	0.73	96.5
	(1:1:5)	6.00	5.80	0.141	2.44	96.7
FER (Zn(II), Cu(II), Ni(II), Fe(II))	(3:0:3:5)	5.00	4.45	0.212	4.77	89.0
	(0:3:3:2)	2.00	1.75	0.212	12.12	87.5
	(1:1:3:2)	2.00	2.00	0.000	0.00	100.0
CS (Zn(II), Cu(II), Ni(II), Fe(III))	(3:0:3:5)	5.00	5.55	0.212	3.82	111.0
	(0:3:3:3)	3.00	3.40	0.000	0.00	113.3
	(1:1:3:2)	2.00	1.65	0.356	21.43	95.0

[a] Mean of three determinations

The only case where the MeSeMA procedure could not determine the amount of particular metal in the mixture was the PAR system. Although the total amount of metals was predicted with acceptable precision, the prediction of specific metal amounts using PAR sensor was unsuccessful. Only the amount of Fe(III)

could be predicted, since its spectrum differed greatly from that of the other metals in the mixture.

* **Pharmaceutical samples**

The PAN sensor was used to determine Zn(II) in pharmaceutical preparations of insulin, and the PAN, Zincon, and CS sensors were used to determine three metals in nasal spray of isotonic sea water (Tables 7 and 8). The European Pharmacopoeia [8] recommends that Zn(II) be determined in pharmaceutical preparations of insulin, and that no more than 40.0 μg per 100 IU of insulin should be present. In all pharmaceutical samples of insulin, the amounts of Zn(II) determined ranged from 0.15 to 0.29 μg mL^{-1} (Table 7), all of which were above the limit of quantitation determined in the prevalidation procedure (0.082 μg mL^{-1}, Table 4). In the analysis of isotonic sea water, the amounts of Zn(II), Cu(II), Ni(II) or Fe(III) were either below the limits of quantitation determined during prevalidation of the PAN, Zincon and CS sensors (Table 4), or they could not be determined.

In order to check the accuracy of the proposed method, recovery experiments for different amounts of metals were carried out. Highly satisfactory recoveries were obtained, ranging from 98.9% to 109.8% for insulin preparations (Table 7).

Recoveries ranged from 94.0 % to 105.7% for commercial nasal spray, showing that the PAN, Zincon, and CS disposable optical sensors could be successfully applied to the determination of metals (Table 8).

Table 7. Zn(II) in pharmaceutical preparations of insulin

Sample	Amount of Zn(II) (µg mL^{-1})		SD[a] (µg mL^{-1})	RSD (%)	Recovery (%)
	Added	Found			
Humalog®	0.00	0.20	0.002	1.42	-
	0.50	0.74	0.020	2.52	107.1
	2.00	2.30	0.020	0.89	104.7
	4.00	4.24	0.166	3.91	101.0
Humalog Mix25®	0.00	0.15	0.002	1.53	-
	0.50	0.66	0.093	1.40	101.5
	2.00	2.13	0.035	1.72	99.0
	4.00	4.17	0.240	5.37	100.3
Humalog Mix50®	0.00	0.16	0.005	4.92	-
	0.50	0.67	0.001	1.37	103.2
	2.00	2.21	0.093	4.45	102.8
	4.00	4.12	0.227	5.31	99.2
Humulin M3®	0.00	0.29	0.014	5.23	-
	0.50	0.84	0.029	4.05	109.8
	2.00	2.21	0.119	5.17	100.2
	4.00	4.12	0.013	0.32	99.8
Insulatard®Penfill®	0.00	0.27	0.004	1.43	-
	0.50	0.77	0.036	4.68	101.0
	2.00	2.28	0.024	1.08	100.3
	4.00	4.26	0.000	0.00	99.6
Lantus®Solostar®	0.00	0.28	0.005	1.67	-
	0.50	0.77	0.005	0.66	103.7
	2.00	2.28	0.028	1.17	103.5
	4.00	4.26	0.245	5.79	98.9

[a] Mean of three determinations

Table 8. Metals in isotonic sea water

Sensor	Metal	Added (µg mL^{-1})	Found (µg mL^{-1})	SD[a] (µg mL^{-1})	RSD (%)	Recovery (%)	Matrix
PAN	Zn(II)	1.00	0.94	0.095	10.1	94.0	Cu(II), Ni(II)
		1.00	1.07	0.042	4.08	104.0	Cu(II), Ni(II)
	Cu(II)	1.00	1.06	0.064	6.08	105.7	Zn, (II) Ni(II)
		2.00	2.10	0.085	4.16	102.0	Zn(II), Ni(II)
	Ni(II)	4.00	3.78	0.257	6.84	94.5	Zn(II), Cu(II)
		1.00	0.98	0.021	2.20	96.5	Zn(II), Cu(II)
	Total	6.00	5.78	0.336	5.82	96.3	
		4.00	4.05	0.106	2.62	101.1	
Zincon	Cu(II)	1.00	1.02	0.010	0.98	102.0	Zn(II), Ni(II)
		2.00	2.00	0.049	2.48	99.8	Zn(II), Ni(II)
	Ni(II)	5.00	5.05	0.028	0.56	101.0	Zn(II), Cu(II)
		3.00	2.90	0.007	0.24	96.5	Zn(II), Cu(II)
	Total	6.00	6.07	0.042	0.70	101.2	
		5.00	4.89	0.042	0.87	97.8	
CS	Fe(III)	2.00	2.04	0.042	2.04	102.2	Zn(II), Cu(II), Ni(II)
		3.00	3.04	0.035	1.16	101.2	Zn(II), Cu(II), Ni(II)

[a]Mean of three determinations

Multicomponent analysis based on the MeSeMA method for determination of total and specific heavy metals in mixtures may prove to be an important advance in the development of pharmacopoeial methodology. In contrast to official general methods for analysis of heavy metals, the proposed MeSeMA method enables identification of particular metal ions with a limit of determination lower than 5 mg L^{-1}, without the need to compare with lead solution. The proposed optical sensors are especially sensitive for Zn(II), Cu(II), Ni(II), Fe(II) and Fe(III).

With the proposed procedures, it is not possible to determine all heavy metals with the same success. However, by adjusting experimental conditions, it may be

possible to determine a greater number of important heavy metals such as lead, cadmium, cobalt, and, with less sensitivity, manganese and mercury [14]. Furthermore, it may be possible to apply these procedures to the determination of other heavy metals important in pharmaceutical analysis, such as Ru, Rh, Pd, Pt, Ir, Au, Ag, As, Sb, and Bi.

CONCLUSIONS

We have designed five disposable optical sensors using nonselective (PAN, PAR, and Zincon) and selective (FER and CS) reagents for determination of Zn(II), Cu(II), Ni(II), Fe(II), and Fe(III). By combining these sensors with powerful chemometric multicomponent analysis (MeSeMA), the levels of these individual metals can be determined simply and rapidly, without previous concentration or separation of analytes. A comprehensive prevalidation procedure confirmed that most sensors showed a linear relationship between analyte and signal, acceptable accuracy and precision and low limits of detection. At the same time, the prevalidation revealed some limitations of the proposed procedure, such as non-negligible influence of blank signals on measurements under certain conditions, and lower sensitivity of the Zincon sensor. The proposed sensors were used to determine the total and individual amounts of metals in various synthetic mixtures. Good agreement was obtained between experimental and theoretical amounts of heavy metals, showing that most of the optical sensors could be used for simultaneous determination of heavy metals. The agreement was slightly better for total amounts of metals in the mixtures, indicating that there is room for improvement in the proposed procedure. In the case of the PAR sensor, it was not possible to resolve the mixture of metal ions, which suggests the need for further optimization of the sensor and experimental conditions. When the method was applied to the determination of

Zn in insulin preparations and determination of metals in isotonic sea water, recoveries ranged from 98.9% to 109.8% and from 94.0% to 105.7%, respectively. These results confirm the accuracy of the proposed procedures obtained during prevalidation.

This work describes the first step in our efforts to develop disposable multi-membrane tongues for simultaneous testing of multiple metals in complex matrices. Our results suggest that the disposable optical sensors described here can be integrated into such tongues, though further optimization will almost certainly be necessary in order for all sensors to work well under identical experimental conditions. These sensors may prove to be an efficient and inexpensive alternative to the present pharmacopoeial heavy metal limit test. It may also be possible to integrate them into a portable device for in situ analysis of heavy metals in different matrices.

REFERENCES

1. I. Palchetti, M. Mascini, M. Minunni, A. R. Bilia, F. F. Vincieri, J. Pharm. Biomed. Anal. 32 (2003) 251-256.

2. I. M. Raimundo, R. Narayanaswamy, Sens. Actuators B 90 (2003) 189-197.

3. D. W. O'Connell, C. Birkinshaw, T. F. O'Dwyer, Bioresour. Technol. 99 (2008) 6709-6724.

4. E. E. Kostenko, M. I. Shtokalo, J. Anal. Chem. 59 (2004) 1158-1164.

5. S. K. Yadav, S. Afr. J. Bot. 76 (2010) 167-179.

6. European Medicine Agency, Committee for human medicinal products, Guideline on the specification limits for residues of metal catalysts, London, 2007.

7. R. Ciciarelli, D. Jäkel, E. König, R. Müller-Käfer, M. Röck, M. Thevenin, H. Ludwig, Pharmacopoeial Forum 21 (1995) 1638-1640.

8. E. D. f. t. Q. o. M. Council of Europe, European Pharmacopoeia, Strasbourg, 2006.

9. British Pharmacopoeia Commission, British Pharmacopoeia, The Stationery Office, Norwich (UK), 2009.

10. United States Pharmacopeial Convention, The United States Pharmacopeia, Rockville (USA), 2002.

11. The Society of Japanese Pharmacopoeia, The Japanese Pharmacopoeia, Tokyo, 2001.

12. K. Brozovic-Pohl, H. Altorfer, X. Perlia, Fresenius' J. Anal. Chem. 343 (1992) 348-351.

13. G. E. Veeman, A. Bult, J. P. Franke, J. S. Faber, Psharm. Weekbl. 117 (1982) 8-13.

14. J. Vukovic, S. Matsuoka, K. Yoshimura, V. Grdinic, R. J. Grubesic, O. Zupanic, Talanta 71 (2007) 2085-2091.

15. J. Huang, X. Hu, J. Zhang, K. Li, Y. Yan, X. Xu, J. Pharm. Biomed. Anal. 40 (2006) 227-234.

16. J. F. Kauffman, B. J. Westenberger, J. D. Robertson, J. Guthrie, A. Jacobs, S. K. Cummins, Regul. Toxicol. Pharmacol. 48 (2007) 128-134.

17. A. S. R. K. Murty, U. C. Kulshresta, T. N. Rao, M. V. N. K. Talluri, Indian J. Chem. Technol. 12 (2005) 229-231.

18. N. Lewen, J. Pharm. Biomed. Anal. 55 (2011) 653-661.

19. I. Oehme, O. S. Wolfbeis, Mikrochim. Acta 126 (1997) 177-192.

20. I. Klimant, M. Otto, Mikrochim. Acta 108 (1992) 11-17.

21. Oliveira W.A., R. Narayanaswamy, Talanta 39 (1992) 1499-1503.

22. M. Ahmad, R. Narayanaswamy, Talanta 42 (1995) 1337-1344.

23. M. J. Ayora Cañada, M. I. Pascual-Reguera, A. Molina-Diaz, Anal. Chim. Acta 375 (1998) 71-80.

24. M. Ahmad, R. Narayanaswamy, Anal. Chim. Acta 291 (1994) 255-260.

25. N. Malcik, O. Oktar, M. E. Ozser, P. Caglar, L. Bushby, A. Vaughan, B. Kuswandi, R. Narayanaswamy, Sens. Actuators, B B53 (1998) 211-221.

26. A. A. Ensafi, M. Fouladgar, Sens. Actuators B B113 (2006) 88-93.

27. B. Kuswandi, M. N. Taib, R. Narayanaswamy, Sens. Actuators A 76 (1999) 183-190.

28. Z. T. Jiang, Anal. Chim. Acta 392 (1999) 247-253.

29. A. A. Vaughan, R. Narayanaswamy, Sens. Actuators B 51 (1998) 368-376.

30. M. K. Amini, T. Momeni-Isfahani, J. H. Khorasani, M. Pourhossein, Talanta 63 (2004) 713-720.

31. A. A. Ensafi, Z. N. Isfahani, IEEE Sens. J. 7 (2007) 1112-1117.

32. I. M. Steinberg, A. Lobnik, O. S. Wolfbeis, Sens. Actuators B 90 (2003) 230-235.

33. P. Ciosek, W. Wroblewski, Analyst 132 (2007) 963-978.

34. A. K. Deisingh, D. C. Stone, M. Thompson, Intern. J. Food Sci. Tech. 39 (2004) 587-604.

35. M. C. Janzen, J. B. Ponder, D. P. Bailey, C. K. Ingison, K. S. Suslick, Anal. Chem. 78 (2006) 3591-3600.

36. V. Grdinić, J. Vuković, J. Pharm. Biomed. Anal. 35 (2004) 489-512.

37. D. L. Massart, B. G. M. Vanderginste, L. C. M. Buydens, S. de Jong, P. J. Lewi, J. Smeyers-Verbeke, Handbook of Chemometrics and Qualimetrics: Part A, Elsevier Science, Amsterdam, 1997.

38. L. F. Capitan-Vallvey, M. D. Fernandez-Ramos, P. Alvarez de Cienfuegos, F. Santoyo-Gonzalez, Anal. Chim. Acta 481 (2003) 139-148.

39. J.N. Miller, J.C. Miller, Statistics, Chemometrics for Analytical Chemistry, Pearson Education Limited, Essex, 2000.

40. J. R. Paddock, A. T. Maghasi, W. R. Heineman, C. J. Seliskar, J. Chem. Ed. 82 (2005) 1370-1371.

41. S. D. Kolev, T. J. Cardwell, R. W. Cattrall, L. d. Coo, Talanta 82 (2010) 1156-1163.

42. F. Lazaro, M. D. L. de Castro, M. Valcarcel, Anal. Chim. Acta 214 (1988) 217-227.

43. J. E. Madden, T. J. Cardwell, R. W. Cattrall, L. W. Deady, Anal. Chim. Acta 319 (1996) 129-134.

44. S. B. Savvin, L. M. Trutneva, O. P. Shvoeva, V. K. Belyaeva, I. N. Marov, Zhurnal Neorganicheskoi Khimii 36 (1991) 393-399.

45. N. Alizadeh, A. Moemeni, M. Shamsipur, Anal. Chim. Acta 464 (2003) 187-196.

46. I. M. Maksimova, E. I. Morosanova, A. A. Kukhto, N. M. Kuz'min, Y. Zolotov, Zh. Anal. Khim. 49 (1994) 1210-1214.

47. E. Morosanova, A. Velikorodnyi, Yu. Zolotov, Fresenius J. Anal. Chem. 361 (1998) 305-308.

48. S. A. Morozko, V. M. Ivanov, J. Anal. Chem. 50 (1995) 572-578.

49. ICH Harmonized Tripartite Guideline prepared within the International Conference on the Harmonization of Technical Requirements for the Registration of Pharmaceuticals or Human Use (ICH) Q2B. Validation of Analytical Procedures: Methodology, 1996. URL: http://www.ich.org/ich5q.html.

50. M. Thompson, S. L. R. Ellison, R. Wood, Pure Appl. Chem. 74 (2002) 835-855.

Talanta 94 (2012) 123–132

Contents lists available at SciVerse ScienceDirect

Talanta

journal homepage: www.elsevier.com/locate/talanta

Characterization of disposable optical sensors for heavy metal determination

Jadranka Vuković [a,*], María Ariza Avidad [b], Luis Fermín Capitán-Vallvey [b]

[a] Department of Analytics and Control of Medicines, Faculty of Pharmacy and Biochemistry, University of Zagreb, A. Kovačića 1, HR-10000 Zagreb, Croatia
[b] ECsens, Department of Analytical Chemistry, Campus Fuentenueva, Faculty of Sciences, University of Granada, E-18071 Granada, Spain

ARTICLE INFO

Article history:
Received 16 November 2011
Received in revised form 27 February 2012
Accepted 5 March 2012
Available online 8 March 2012

Keywords:
Optical membranes
Heavy metal determination
Disposable sensors
Prevalidation strategy
Multicomponent analysis

ABSTRACT

This paper presents the development, characterization and quality control of analytical methods based on the use of disposable optical sensors for determination of heavy metals. Chromogenic reagents such as 1-(2-pyridylazo)-2-naphthol, (2-pyridylazo)resorcinol, Zincon, Ferrozine, and Chromazurol S were used to develop optical sensors of heavy metal ions found as contaminants in pharmaceutical substances and products, such as Zn(II), Cu(II), Ni(II), Fe(II), and Fe(III). The chromogenic reagents were immobilized in polymeric membranes by spin-coating from cocktails containing all reagents needed. The methods were prevalidated using a comprehensive quality control strategy based on a system of mathematical/statistical testing and diagnosis of each prevalidation step. This system involved characterization of analytical groups; checking of two limiting groups; testing of data homogeneity; recognition of outliers; and determination of analytical functions, limiting values, precision and accuracy. The prevalidation strategy demonstrated the reliability of the proposed method and pointed out some limitations. Combining the optical sensors with multicomponent linear regression allowed simultaneous determination of multiple metals in synthetic mixtures with different compositions. Good agreement between experimental and theoretical amounts of heavy metals in the mixtures was obtained for the majority of sensors and metals. Even better agreement was obtained between the experimental and theoretical total amounts of metals in the mixtures. The proposed analytical methods were successfully applied to the determination of zinc in pharmaceutical preparations of insulin and the determination of metal mixtures in a commercial nasal spray of isotonic seawater. The reliable and sensitive individual optical sensors developed in this study may be useful for designing a multimembrane optical tongue that with appropriate further optimization can be used for screening heavy metals in various matrices.

© 2012 Elsevier B.V. All rights reserved.

1. Introduction

Heavy metals are ubiquitous and monitoring them is important in various fields because of their effects on ecosystems and living organisms [1–5]. For example, an important part of drug quality control is detecting and determining heavy metals. Bulk drug substances and their intermediates can be contaminated by metals in many ways, such as from raw materials, reagents, and solvents; from electrodes, reaction vessels, storage containers, plumbing and other equipments used in synthesis; or from exposure to air-borne particles. Metal catalysts and metal reagents, are substances used in the synthesis of the drug substance or an excipient used in a medicinal product, and, therefore, can also introduce metals into drug preparations [6,7]. Although evaluated for their potential risk to human health and placed into one of three classes (metals of significant, low, and minimal safety concern), some of them, such as Fe, Zn, and Cu are also important in human nutrition.

For over a century [7], drug quality control departments have relied on the heavy metal limit test recommended by most pharmacopoeias [8–11]. Besides the heavy metal limit test, European Pharmacopoeia [8] prescribes determination of specific metals in drug substances, such as copper in ascorbic acid, zinc in insulin, and nickel in polyols. The heavy metal limit test is based on sulfide precipitation in a weakly acidic medium and comparison with a lead solution. The test can be easily transferred from one laboratory to another and does not require expensive instrumentation or highly trained laboratory personnel. However, it suffers from several disadvantages. It requires subjective visual interpretation, large amounts of sample, and usually a heating or ashing step that causes losses of volatile elements. In addition, it does not provide any qualitative or element-specific information. Several attempts have been made to overcome these limitations [12,13], but no major improvements have been achieved. Thus, this standard method remains suitable for only a few elements, and it cannot specify the content of any particular metal ion but only the overall content of ions [12].

* Corresponding author. Tel.: +385 1 4920089; fax: +385 1 4920089.
E-mail addresses: jadranka@pharma.hr (J. Vuković), mariavidad@hotmail.com (M.A. Avidad), lcapitan@ugr.es (L.F. Capitán-Vallvey).

0039-9140/$ – see front matter © 2012 Elsevier B.V. All rights reserved.
doi:10.1016/j.talanta.2012.03.006

DOI: 10.1016/j.talanta.2012.03.006

FEASIBILITY OF THE USE OF DISPOSABLE OPTICAL TONGUE BASED ON NEURAL NETWORKS FOR HEAVY METAL CLASSIFICATION AND DETERMINATION

ABSTRACT

This study presents the development and characterization of a disposable optical tongue for the simultaneous identification and determination of the heavy metals Zn(II), Cu(II) and Ni(II). The immobilization of two chromogenic reagents, 1-(2-pyridylazo)-2-naphthol and Zincon, and their arrangement forms an array of membranes that work by complexation through a co-extraction equilibrium, producing distinct changes in color in the presence of heavy metals. The color is measured from the image of the tongue acquired by a scanner working in transmission mode using the H parameter (hue) of the HSV color space, which affords robust and precise measurements. The use of artificial neural networks (ANNs) in a two-stage approach based on color parameters, the H feature of the array, makes it possible to identify and determine the analytes. In the first stage, the metals present above a threshold of 10^{-7} M are identified with 96% success, regardless of the number of metals present, using the H feature of the two membranes. The second stage reuses the H features in combination with the results of the classification procedure to estimate the concentration of each analyte in the solution with acceptable error. Statistical tests were applied to validate the model over real data, showing a high correlation between the reference and predicted heavy metal ion concentration.

INTRODUCTION

The disadvantages of conventional approaches for multi-analyte sensors based on specific receptors are largely related to problems with selectivity and the number of sensors needed, which increases proportionally with the number of analytes. The alternative concept based on differential receptors[1] proposes making use of arrays of non-specific or low selective sensors (electronic tongues) that produce analytical signals encoded in the overlapping measurements that are useful for the analysis of multi-component samples. These are later treated through advanced mathematical procedures for signal processing by pattern recognition and/or multivariate analysis to extract both qualitative and quantitative information.[2-4] The characteristics of cross sensitivity and reproducibility make it possible to extract the analytical information without any separation of interfering species or eliminating the matrix effect.

Different approaches based on chemical sensor arrays have been reported, most of which are based on electrochemical sensors (voltammetric, potentiometric) and to a much lesser extent, on optical sensors[4-7] mainly for food and beverage, environmental, clinical and pharmaceutical analysis[3].

Heavy metals are ubiquitous and monitoring them is important in different fields because of their effects on ecosystems and living organisms. The determination of trace metal ions in water samples has long been an important issue in environmental analysis. Thirteen transition metal ions are listed as priority pollutants by the Environmental Protection Agency (EPA)[8]. Although the determination of trace metal ions, mainly by atomic techniques, is a well-resolved issue, the screening and determination of metal ions in water and other matrices using fast and low-cost procedures remains a challenge.

Most different optical approaches used for tongues are based on the measurement of color from the image captured by imaging devices, mainly CCD cameras or

scanners using different color spaces. By far, the most commonly used color space is RGB, whose coordinates are used for processing with multivariate techniques. However, in this work, we used the HSV color space, whose main characteristic is that it represents the useful information about the color in one single parameter, the H coordinate (hue). Previous studies from our group have shown that the use of the H coordinate in bitonal sensors that produce a change in color by reaction yields a substantial improvement in resolution and repeatability[9].

The analysis of the data acquired by sensor arrays is performed by various numeric procedures from the data acquired to build the chemometric procedure.[4;10] One of the mathematical procedures used is the artificial neural network (ANN), which performs well with tasks such as classification, automatic control, pattern recognition, learning and non-linear regression.[11-13]

In this paper we present the use artificial neural networks (ANNs) for the classification of the presence/absence of heavy metals in a solution along with an estimation of the corresponding metal concentration from an optical tongue comprising two sensing membranes that use the tonal characteristics as an analytical parameter to build the chemometric tool.

EXPERIMENTAL

Reagents, materials and solutions

The chemicals used to prepare the heavy metal sensitive films were high molecular weight polyvinyl chloride (PVC), o-nitrophenyloctylether (NPOE), benzethonium chloride (BTC), 1-(2-pyridylazo)-2-naphthol (PAN), 2-carboxy-2′-hydroxy-5′-sulfoformazyl-benzene monosodium salt (Zincon) and tetrahydrofuran (THF), all purchased from Sigma (Sigma-Aldrich Química S.A., Madrid, Spain) as well as polyurethane hydrogel D4 (Tyndale Plains-Hunter, Lawrenceville, NJ, USA). Sheets

of Mylar-type polyester (Goodfellow, Cambridge, UK) were used as support. Working standard solutions of Zn(II), Cu(II) and Ni(II) (100 μg mL^{-1}) were prepared by appropriate dilution of the standard stock solution of each metal (1,000 μg mL^{-1}) (Sigma-Aldrich) acidified with conc. HNO_3 (Sigma). Solutions of lower concentrations were prepared by dilution with water. All chemicals were of analytical-reagent grade, and reverse osmosis-purified water (Milli-RO 12 plus Milli-Q station, Millipore) was used throughout.

Apparatus and software

A Microtek ScanMaker I700 scanner (Microtek, CA, USA) managed by the proprietary software Silver Fast Aiwas was used to acquire images of the heavy metal sensor array. The scanner was calibrated using an IT8 calibration target. The images were processed with a set of scripts and functions developed by us in Matlab r2007b (The MathWorks Inc, Natick, MA, USA). Statistical calculations were performed with Microsoft Excel (Microsoft Corp., Redmond, WA, USA), which was used for general calculations. A Crison pH-meter (Crison Instruments, Barcelona, Spain, model Basic 20) with a combined double junction glass electrode, calibrated against two standard buffer solutions (pH 4.0 and 7.0), was used for pH measurements.

Heavy metal sensor array preparation

The sensor array was prepared on a 5 cm x 4 cm transparent Mylar polyester support covered with an adhesive black film of PVC with 12 holes (3 columns and 4 rows), 5 mm in diameter each. The sensing films were cast by carefully placing 8 μL of the corresponding cocktail in each hole, whose surface tension and quick evaporation make it possible to prepare the sensing membrane. The array containing 6 membranes of each type were stored in a closed container at room temperature to enable slow solvent evaporation and then kept in a dark place until use to avoid

photodegradation. The cocktails for the heavy metal membranes were prepared by dissolving the different chemicals needed in 1 mL of distilled THF according to the following composition: a) PAN cocktail (133.7 mmol of PAN kg^{-1} of PVC), containing 30.0 mg PVC, 60.0 mg NPOE, and 1.0 mg PAN; b) Zincon cocktail (43.3 mmol of Zincon kg^{-1} of D4), containing 100.0 mg D4 polyurethane hydrogel, 2.0 mg Zincon, and 10.0 mg BTC dissolved in a mixture of 3.0 mL of ethanol and 0.2 mL of water.

Response evaluation

The response of the sensor array was evaluated using standard solutions of Zn(II), Cu(II) and Ni(II)at pH 9.5 with ammonia buffer. Standard solutions were prepared either of individual metals at concentrations ranging from $1.0x10^{-7}$ to $1.0x10^{-3}$ M or with mixtures of 2 or 3 of the metals under study at individual concentrations from $4.0x10^{-6}$ to $4.0x10^{-5}$ M. The prepared solutions placed in 100 mL glass beakers with the sensor array dipped by hanging it from a support were magnetically stirred for 15 min at room temperature. After equilibration, the arrays were pulled out of the solution and imaged using a scanner.

Image acquisition and treatment

The acquisition of the images with the scanner was performed working in transmission mode lighting the membranes placed on the glass surface of the scanner with cold cathode fluorescent (2.72 Klx). The obtained images were stored in TIFF (True Image File Format) file format to prevent any loss of information since this does not compress the image. To extract the hue parameter from each sensing element in the scanned image, software developed by us in Matlab was used. To recognize the sensing membranes digitalized in the image, the software detects pixels in each normalized R, G and B channel, coming from the non-colored area of the

image (background) by comparing each pixel with the maximum observed difference in the entire image multiplied by a predefined threshold value [9].

After slicing the image of each membrane from the whole image, which typically contains 1,000 pixels, the R, G and B channels of each membrane were scaled and the H coordinate calculated from the R, G and B coordinates of each pixel using eq. 1. The H value calculated for each sensing element was the mode of the hues calculated for all the pixels in the same membrane, since this parameter provides a low error rate during the image processing. This procedure provided us with the data sets necessary for the experimental calibration and validation as described in the following sections.

$$H = \frac{\left(\frac{G-B}{max_{channel}-min_{channel}}+0\right)}{6} \quad \text{If max= R*}$$

$$H = \frac{\left(\frac{B-R}{max_{channel}-min_{channel}}+2\right)}{6} \quad \text{If max= G} \qquad \text{(Eq. 1)}$$

$$H = \frac{\left(\frac{R-G}{max_{channel}-min_{channel}}+4\right)}{6} \quad \text{If max= B}$$

* if H is less than 0 then add 1 to H

Because of the circular nature of H, which is defined as an angle that varies between 0 and 360° and represented as a color wheel where 0° is located at the top of the wheel, the values are bounded between 0 and 1, with both 0 and 1 representing the same hue. However, this work allows H to be from -360º to 360º,

with the values therefore between -1 and 1, to avoid discontinuities in H evolution with the pH if it passes through the origin.

Two-stage artificial neural network approach for heavy metal classification and concentration estimation

Artificial neural networks (ANNs)[11] are used in this paper to both classify the presence/absence of heavy metals in solution and to estimate the corresponding metal concentration from two hue color parameters from the disposable sensor array. Thus, we propose a two-stage classification and estimation approach based on the response of the network models and color parameters. In a first stage, two parameter values (H_{PAN}, H_{ZIN}) corresponding to the H feature of the HSV color space obtained from the color change of the array are inputs to an ANN-based classification module. This module returns the metals (Zn(II), Cu(II) and/or Ni(II)) that caused the array color change. After that, in the second stage we reuse the H features (H_{PAN}, H_{ZIN}) in combination with the results of the classification procedure to estimate the concentration of each metal in the solution with better performance. Figure 1 illustrates this approach and provides further details about the system input/output and the data transfer between stages.

With respect to the classification module, it has two inputs corresponding to the values of the parameters (H_{PAN}, H_{ZIN}) from the sensors, which are normalized to the range [0, 1]. The module is made up of 3 artificial neural networks and each one is in charge of classifying the presence/absence of a specific metal in the solution. Each network must return a single output with value 1 if its corresponding metal is detected from the input (H_{PAN}, H_{ZIN}) values, and value 0 otherwise. Thus, the output of the classification module is a 0/1-valued vector (M_1, M_2, M_3) indicating the presence/absence of each metal (Zn(II), Cu(II), Ni(II)) from the hue input values.

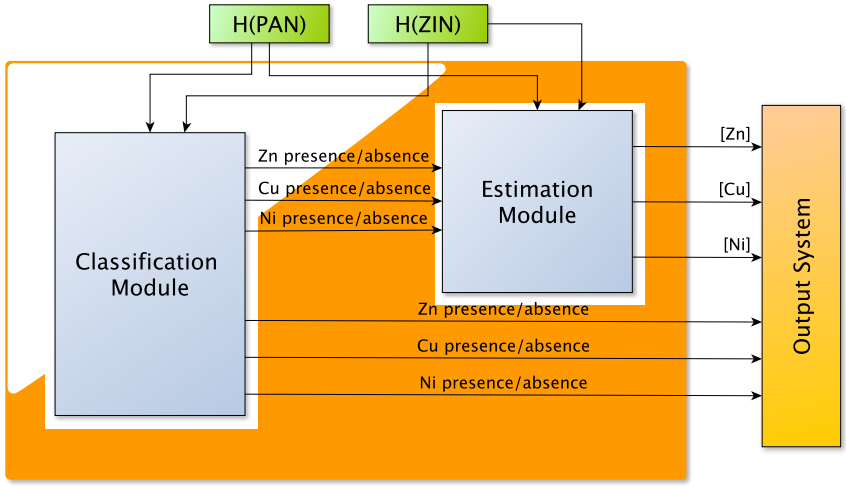

Figure 1. Two-stage system for heavy metals classification and concentration estimation.

Figure 2 details the outline of the module. To achieve this module structure, we tested different network models such as Radial Basis Function networks and Multi-Layer Perceptron networks[11] in a preliminary experiment. Also the network internal topology was optimized experimentally, considering in addition the use of a single network with 2 inputs and 3 binary 0/1 outputs, one for each metal classification. The best results from the preliminary experiments were used to design this module's internal organization, composed of a network for the isolated classification of each heavy metal.

For the second stage, the input data are built as the combination of the hue values with the results provided by the classification module, i.e. the input vector (H_{PAN}, H_{ZIN}, M_1, M_2, M_3). The module contains three neural networks with 5 inputs and 1 output, and each network is in charge of estimating a metal concentration (Zn(II), Cu(II) and/or Ni(II)) according to the input vector. Finally, the outputs of both classification and estimation values are returned as the system output. Figure 3 summarizes the internal organization of the estimation module.

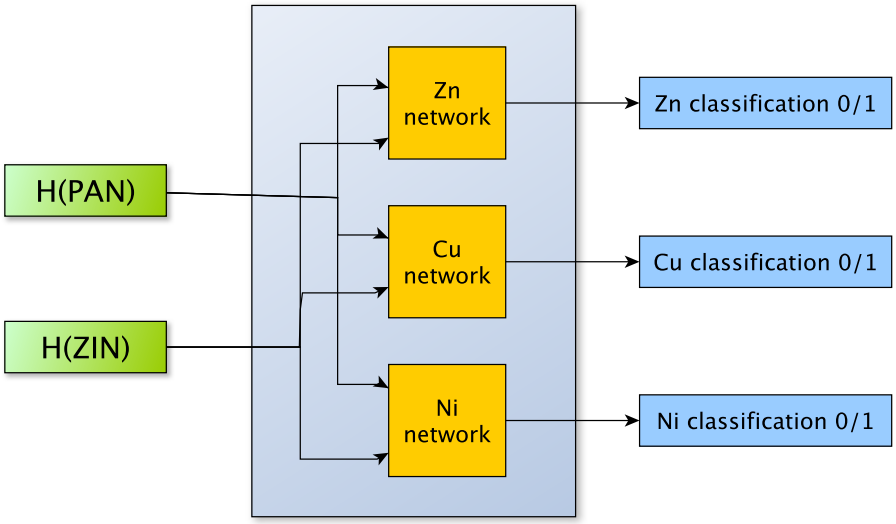

Figure 2. The classification module.

The structure of this module was also designed after the analysis of a preliminary experiment, as in the classification module, and we selected Multi-Layer Perceptron networks as estimation models since they provided us with promising results as in other prior developments regarding parameter value estimation[14;15].

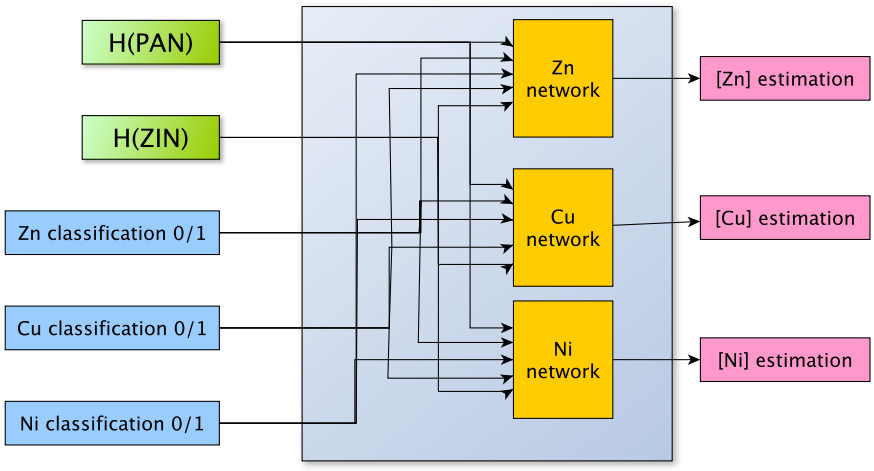

Figure 3. The estimation module.

In both the classification and estimation modules, the Multi-Layer Perceptron neural network operation follows a similar procedure[11]: The output value $f_i^l(x_i^l)$ of the neuron i at an intermediate network layer l is computed as in equation (eq. 2). The value x_i^l is the weighted sum of the network response from all the neurons at the previous network layer l-1, if neuron i belongs to an intermediate layer, or the weighted sum of the network input values if it belongs to the first layer as equation (eq. 3) shows. Here, the value w_{ij}^l is the weight for the connection between the neuron j located at layer l-1 and neuron i located at layer l; the value b_i^l is a bias value for neuron i at layer l, and I_j^p is the j-th component of the input vector to the network of the sample pattern p.

$$f_i^l\left(x_i^l\right) = \frac{1}{1+e^{x_i^l}}; 1 \leq l < L \qquad \text{(Eq. 2)}$$

$$x_i^l = \begin{cases} \sum_{j=1}^{N^{l-1}}\left(W_{ij}^l I_j^{l-1}\right) + b_i^l & l = 1 \\ \sum_{j=1}^{N^{l-1}}(W_{ij}^l I_j^{l-1}(x_j^{l-1}) + b_i^l & 1 < l < L \end{cases} \qquad \text{(Eq. 3)}$$

The differences for the application of the Multi-Layer Perceptron models to both classification and estimation tasks are found at the output layer L. For the first problem, the networks provide a value in the range [0, 1], which is computed using the sigmoid transfer function in the output neurons (eq. 4). Positive output patterns must return value 1, while negative samples return value 0. To achieve this goal, we round the network output value to 1 if the network output value is over 0.5 and round to 0 otherwise, as eq. 5 shows.

$$f_i^L\left(x_i^L\right) = \frac{1}{1+e^{x_i^L}}; \text{(classification problem)} \qquad \text{(Eq. 4)}$$

$$O\left(x_i^L\right) = \begin{cases} 1 & f_i^L\left(x_i^L\right) > 0.5 \\ 0 & f_i^L(x_i^L) \geq 0.5 \end{cases} \quad \text{(Eq. 5)}$$

On the other hand, for the estimation problem, the network output is a pure linear function (eq. 6), with the aim of allowing the network to provide output values in the real line corresponding to the heavy metal concentration.

$$O\left(x_i^L\right) = f\left(x_i^L\right) = x_i^L; \text{(estimation problem)} \quad \text{(Eq. 6)}$$

Neural network training is an optimization procedure to find the best values in the set of real numbers for the network weights w^l_{ij} and biases b^l_i, which minimizes an error measure between the network outputs and the sample patterns. The most used error measure for this purpose is the Mean Square Error (MSE) (eq. 7), which is derivative, meaning that gradient-based optimization techniques can be used for the optimization. In eq. 7, P is the number of sample patterns used for the optimization, N^L is the number of network outputs, and D^p_i is the desired value for network output i at sample pattern p. With respect to training algorithms, Back Propagation is the most popular[11]. However, during the last decade other algorithms have been proposed based on second-order derivative estimation, such as BFGS and Levenberg-Marquardt[16]. In this paper, we use this latter method due to its high performance in previous works with respect to the classic methods[16-18], and the minimization of the MSE as error criterion.

$$MSE = \frac{1}{P}\sum_{p=1}^{P}\sum_{i=1}^{N^L}\left(D_i^P - f_i^L(x_i^L)\right)^2 \quad \text{(Eq. 7)}$$

RESULTS AND DISCUSSION

In this work we explore the possibility of performing multi-analyte analysis with easily available and widely distributed imaging devices such as standard flatbed scanners. Previously, we studied disposable optical sensors based on chromogenic reagents for heavy metals that, through a prevalidation procedure, confirmed that the individual sensors showed a linear relationship between heavy metal concentration and absorbance, acceptable accuracy and precision and low limits of detection[19]. In this paper we study an array consisting of two types of membranes containing non-selective chromogenic reagents, namely PAN and Zincon, as a disposable optical tongue for the identification and quantification of mixtures of Zn(II), Cu(II) and Ni(II). The sensing polymeric membranes work by complexation with the immobilized chromogenic reagents through a co-extraction equilibrium that produces intense changes in color[19]. The change in color of the array obtained by means of imaging techniques is used as the input for a neural network. Instead of utilizing the captured RGB data from the scanned sensing areas of the array, they are transformed to the HSV (Hue, Saturation, and Value) color space that represents the dominant color in one single parameter, the coordinate H (hue). Previous studies have shown that the use of this tonal coordinate, a qualitative signal, in bitonal sensors that change the color by reaction yields a substantial improvement in precision and are better suited for quantification[9]. The H value is stable, simple to calculate, and easily obtained from commercial devices, maintaining a superior precision with variations in indicator concentration, sensor thickness, detector spectral responsivity and illumination. In contrast to other approaches that use the RGB color space to achieve the pH prediction[20;21], this approach provides the additional advantage of the degression of the parameter space from three dependent variables to only one.

The composition of the two membranes that compose the array was optimized to: a) minimize the leaching by varying the lipophilic salt, plasticizer and membrane polymer; b) maximize the color intensity by varying the concentration of the chromogenic reagent; and c) minimize the response time by varying the plasticizer, membrane polymer, and the volume of cocktail used to prepare the membrane.

The pH dependence on the reaction and retention of ion metals on membranes was studied in the pH range 3 to 12. The highest response was obtained at pH 9.5 for PAN and Zincon membranes. The Zincon sensor was sensitive to Cu(II) and Ni(II) at basic pH, but it did not detect Ni(II) at acidic pH. A longer reaction time (over 30 min) increased, as usual, the optical response, but some leaching could be observed for reaction times longer than 15 min. Therefore, a reaction time of 10 min was used for all the sensing membranes.

Artificial neural networks calibration for heavy metal classification

A data set of 273 samples covering the concentration range from 1.0 10^{-7} to 1.0 10^{-3} M, including control measurements without metals, of three heavy metals Zn(II), Cu(II) and Ni(II) was used for the calibration of the classification module in Figure 1. Each sample is a vector of 5 components (H_{PAN}, H_{ZIN}, C_{Zn}, C_{Cu}, C_{Ni}). From these data, 175 samples (including 3 replicates) were obtained from solutions containing different amounts of a single metal, distributed uniformly for all metals and concentration ranges. 60 samples of the data set were obtained from solutions containing two metals, with different concentrations, including 6 replicates (Zn(II) and Cu(II), Zn(II) and Ni(II), Cu(II) and Ni(II)), and the experimentation also considered uniform distribution of the data. Finally, the remaining 54 samples were obtained from solutions containing all the heavy metals in different concentrations, with 6 replicates.

Figure 4 shows by way of example the evolution of the H coordinate with the logarithm of Cu(II) concentration and the change in color for the two membranes studied.

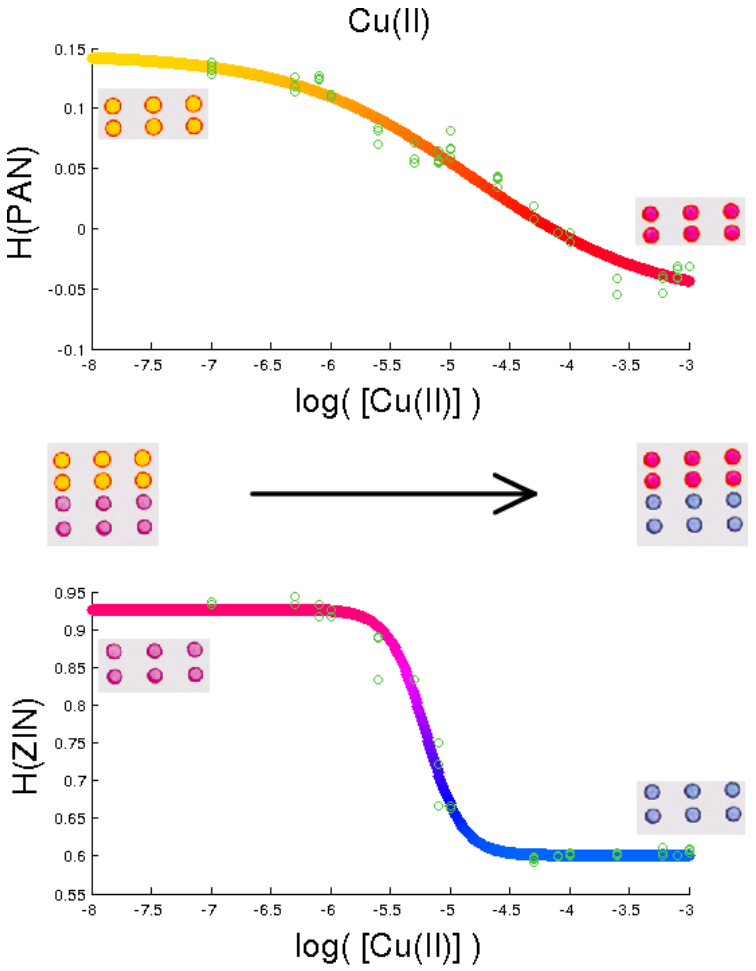

Figure 4. Evolution of H coordinate of the array with Cu(II) concentration (PAN up, Zincon down; green circles: experimental data). In the middle the type of array used containing 12 membranes of two types is shown.

Before training the network, preprocessing over the initial data set was required to transform the concentration of the metals in all the samples into 0/1 values. To achieve this, we needed to find a threshold τ for which concentration values equal to or over τ are considered a metal presence in the solution, and values under τ are assumed to indicate the absence of metal. Preliminary experimentation suggested that the threshold value should be $\tau=10^{-7}$ M, since greater values reduced the number of positive samples substantially and made the network learning difficult, and lower values did not improve the network performance.

Thus, we built the 3 data sets for calibration of the classification networks for Zn(II), Cu(II) and Ni(II), each one containing the samples (H_{PAN}, H_{ZIN}, B_{Zn}), (H_{PAN}, H_{ZIN}, B_{Cu}) and (H_{PAN}, H_{ZIN}, B_{Ni}), where B_x is calculated as eq. 8 shows. The first two values of the sample were used as network inputs, and the last one as the network desired output.

$$B_x = \begin{cases} 1 & [x] \geq \tau \\ 0 & [x] < \tau \end{cases} \qquad \text{(Eq. 8)}$$

The data set built for each network was split into sets for training (70%), testing (15%) and validation (15%). The best neural network for each metal classification was obtained with a trial-and-error procedure by testing the number of hidden layers ranging from 1 to 2 and the number of hidden neurons from 3 to 10. The cross validation method was used to shuffle the training and test data 500 times. Each network was trained using the Matlab R2011a Neural Networks Toolbox with the Levenberg-Marquardt optimization algorithm. The training parameters used 1000 iterations of the algorithm as the primary stopping criterion, or to reach an MSE of 0.01 in training data as a secondary stopping criterion. The best results were provided by a network with 1 hidden layer and 9 neurons for the classification of Zn(II), 1

hidden layer and 10 neurons for the classification of Cu(II), and 1 hidden layer and 8 neurons for the classification of Ni(II).

Table 1 summarizes the performance of these networks, where PP stands for samples that contain the corresponding metal and the network hits, NN is used for samples that do not contain the corresponding metal and the network hits, PN encompasses the samples that contain the metal but the network fails in its classification, and NP is for the samples than do not contain the metal but the network recognizes its presence.

Table 1. Summary of network performance for heavy metal classification.

Metal		Zn(II) classification success		Cu(II) classification success		Ni(II) classification success	
		samples	%	samples	%	samples	%
Training	PP	106	99.07 %	120	98.36 %	77	97.47 %
	PN	1	0.93 %	2	1.64 %	2	2.53 %
	NN	82	97.62 %	69	100 %	109	97.32 %
	NP	2	2.38 %	0	0 %	3	2.68 %
Average hits		188	98.43 %	189	98.95 %	186	97.38 %
Test	PP	27	100 %	22	100 %	19	95 %
	PN	0	0 %	0	0 %	1	5 %
	NN	14	100 %	19	100 %	20	95.24 %
	NP	0	0 %	0	0 %	1	4.76 %
Average hits		41	100 %	41	100 %	39	95.12 %
Validation	PP	21	87.50 %	23	100 %	16	94.12 %
	PN	3	12.50 %	0	0 %	1	5.88 %
	NN	17	100 %	16	88.89 %	22	91.67 %
	NP	0	0 %	2	11.11 %	2	8.33 %
Average hits		38	92.68 %	39	95.12 %	38	92.68 %
Total Average Success		267	97.80 %	269	98.53 %	263	96.34 %

The table includes the results for all the training, test and validation data sets.

As shown in Table 1, the average performance in all the networks exceeds 96% success in the classification of the presence/absence of heavy metal in a solution.

In order to support these data, Figure 5 illustrates the presence/absence of each metal combined with the discrimination curve after network learning. The symbol "+" stands for a positive sample that is correctly classified; the symbol " · " is for samples that do not contain the metal and are correctly classified; the symbol "o" represents positive samples that are not correctly classified by the network; and a square "□" is for those negative samples that are recognized as positive. Finally, the curve is the function learnt by the network to discriminate between positive and negative data. With respect to the color legend, red plots represent samples with a single metal in the solution; green ones are for samples containing two metals, and blue plots are for samples with the presence of all metals.

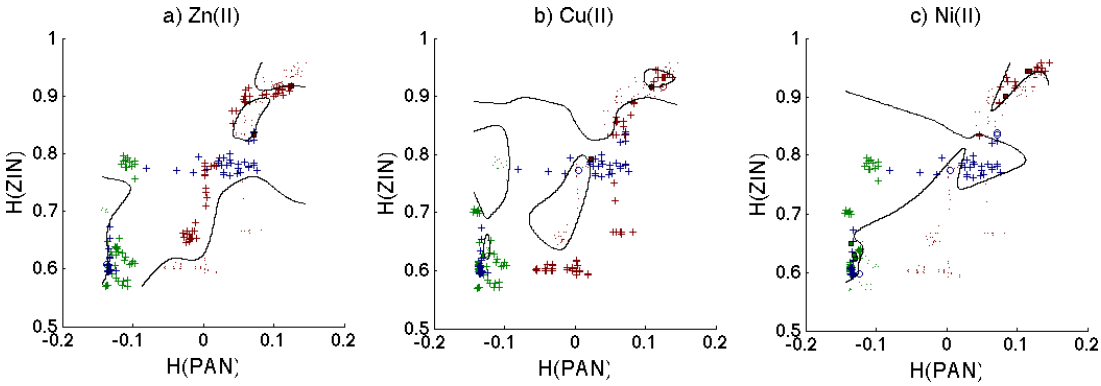

Figure 5. Classification space for the metals) Zn(II); b) Cu(II); c) Ni(II). "+" = positive sample correctly classified; " · "= negative samples correctly classified; "o"= positive samples classified as negative; "□ "=negative samples classified as positive. Red= samples with a single metal; Green= samples with two metals; Blue= samples with three metals.

Artificial neural networks calibration for the estimation of heavy metal concentration

This section begins with an explanation about why it is suitable to use the output of the classification module as the input for estimating heavy metal concentration. According to the above, our approach is able to discriminate a heavy metal

presence/absence with an average success over 96%. This leads to questions regarding whether the same parameters (H_{PAN}, H_{ZIN}) are sufficient to predict the metal concentrations. The same data set of 273 samples described in the previous section was also used in preliminary experiments for the calibration of 3 networks, each one associated with a heavy metal, whose input is the hue feature from the 2 sensors and they provide a single output with the concentration of their corresponding metal. The internal structure of these networks is also the same as the one previously described, with the difference in the number of network inputs described here.

We designed the 3 data sets for calibration of the corresponding estimation networks, each one containing samples composed of vectors of 3 components (H_{PAN}, H_{ZIN}, C_{Zn}) for training the Zn(II) estimation network, (H_{PAN}, H_{ZIN}, C_{Cu}) for the Cu(II) estimation network, and (H_{PAN}, H_{ZIN}, C_{Ni}) for the Ni(II) one. These data were split into training with 70% of the samples, 15% for testing, and the remaining 15% for validation. Once these data sets were obtained, the output value of each data set underwent a logarithmic transformation in order to escalate the network error equally and improve the calibration performance. We also applied a trial-and-error procedure to obtain the network topology that best approximates the metal concentrations. Experiments were carried out ranging from 1 to 3 hidden layers and 3 to 10 hidden neurons per layer. For each network topology, we applied the cross validation method 500 times, training with the Levenberg-Marquardt algorithm and using 1000 iterations as the primary stopping criterion, or when an MSE of 0.001 was obtained.

Table 2 describes the average error, maximum error and its standard deviation in training, testing and validation. These data are also shown in log scale to improve legibility and illustrate the behavior of the approach without data escalation limitations.

Table 2. Summary of calibration results for heavy metal estimation using (H_{PAN}, H_{ZIN})

Metal	Data set	Mean error Log [metal]	Maximum error Log [metal]	S.D. of error Log [metal])
Zn(II)	Training	0.50	3.33	0.66
	Test	0.58	3.59	0.78
	Validation	0.51	2.95	0.65
	Total	0.5148	3.59	0.67
Cu(II)	Training	0.45	3.02	0.50
	Test	0.49	1.65	0.46
	Validation	0.56	2.70	0.62
	Total	0.47	3.02	0.51
Ni(II)	Training	0.41	3.07	0.55
	Test	0.57	3.64	0.72
	Validation	0.52	2.32	0.58
	Total	0.45	3.64	0.58

In addition, Figure 6 illustrates the regression line between the real and estimated data for Zn(II), Cu(II) and Ni(II) concentrations. Although a positive correlation exists between the real and estimated data (correlation coefficient R=0.93 for Zn(II), R=0.95 for Cu(II), R=0.95 for Ni(II)), the dispersion is high and therefore the average error increases.

To improve these results, we decided to provide the networks with further information about which metals are present in the samples.

This new information could help to reduce the network error and it would come from the previous data processing stage carried out in the classification module. To achieve this goal, we designed the 3 data sets for calibration of the corresponding estimation networks, each one containing samples made up of vectors of 6 components (H_{PAN}, H_{ZIN}, B_{Zn}, B_{Cu}, B_{Ni}, C_{Zn}) to train the Zn(II) estimation network, (H_{PAN}, H_{ZIN}, B_{Zn}, B_{Cu}, B_{Ni}, C_{Cu}) for the Cu estimation network, and (H_{PAN}, H_{ZIN}, B_{Zn}, B_{Cu}, B_{Ni}, C_{Ni}) for the Ni one. The Bx values are computed according to eq. 8. The

first 5 values of the sample were used as network inputs and the 6th as the network desired output.

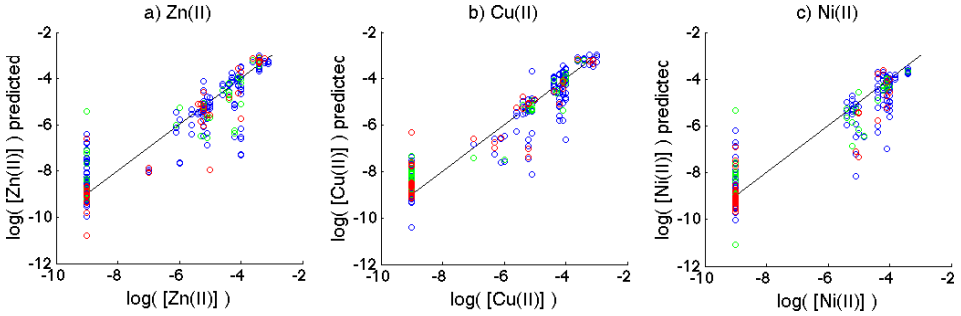

Figure 6. Estimation performance using (H_{PAN}, H_{ZIN}) for a) Zn(II); b) Cu(II); c) Ni(II).

The networks were trained using the same experimental settings as the previous estimation ones. After this experiment, the best results for Zn(II) concentration estimation were obtained by a network with 2 hidden layers and 8 neurons per layer. In the case of Cu(II) concentration estimation, the best network had 3 hidden layers and 9 neurons per layer. Finally, the network with the best performance for Ni(II) concentration estimation had 2 hidden layers and 7 neurons per layer. Table 3 summarizes the results of all the networks in training, testing and validation.

According to Table 3, the proposed model is able to provide an estimation of Zn(II) concentration with an average error of 0.06±0.10, an average error of 0.05±0.07 for Cu(II) concentration, and an average error of 0.02±0.03 for Ni(II) concentration. In terms of molar concentration, these results suggest that our approach estimates the metal concentration with a decimal unit lower than the real molar concentration on average. For instance, if a sample contains a Cu concentration of 1.0 10^{-4} M, then the system error is 1.0 10^{-5} M on average.

Table 3. Summary of calibration results for heavy metal estimation using (H_{PAN}, H_{ZIN}, B_{Zn}, B_{Cu}, B_{Ni}).

Metal	Data set	Mean error Log [metal]	Maximum error Log [metal]	S.D. of error Log [metal]
Zn(II)	Training	0.06	0.68	0.10
	Test	0.08	0.29	0.08
	Validation	0.05	0.20	0.06
	Total	0.06	0.68	0.10
Cu(II)	Training	0.05	0.48	0.07
	Test	0.04	0.16	0.05
	Validation	0.04	0.15	0.05
	Total	0.05	0.48	0.07
Ni(II)	Training	0.02	0.10	0.02
	Test	0.02	0.11	0.02
	Validation	0.02	0.16	0.04
	Total	0.02	0.16	0.03

The maximum mean error occurs with Zn(II), and the lowest with Ni(II). Finally, the mean error of Cu(II) has an intermediate value between Zn(II) and Ni(II). Despite these differences, all the networks provide an average error below 0.1 in log scale, which suggests that our approach is able to provide suitable heavy metal concentration estimations with a decimal unit lower than the real molar concentration in average. Table 3 also describes the maximum error found in the concentration estimation of metals. This study provides knowledge about how the system would react under extreme conditions due to noisy data acquisition from sensors or other external experimental events. The maximum error is produced in almost all the cases in the training data set, which suggests that the network has been able to generalize the training sample patterns in both test and validation data and has high noise tolerance.

To support this experimentation, we applied a correlation test between the real metal concentrations and their corresponding predicted network values. Figure 7

illustrates the regression line between the real and estimated data. The results for the tests provided a correlation coefficient of R=0.99 for Zn(II) concentration estimation, R=0.99 for Cu(II) concentration estimation and R=0.99 for Ni(II) concentration estimation. This analysis concludes that there is a significant positive correlation between the real and predicted data and, in combination with the results in Table 3, our approach is able to provide the estimation of error concentration with suitable error. In contrast to the results shown in Table 2, the inclusion about which metals are present in the solution as additional information for the estimation system may contribute to improving the accuracy of the estimation.

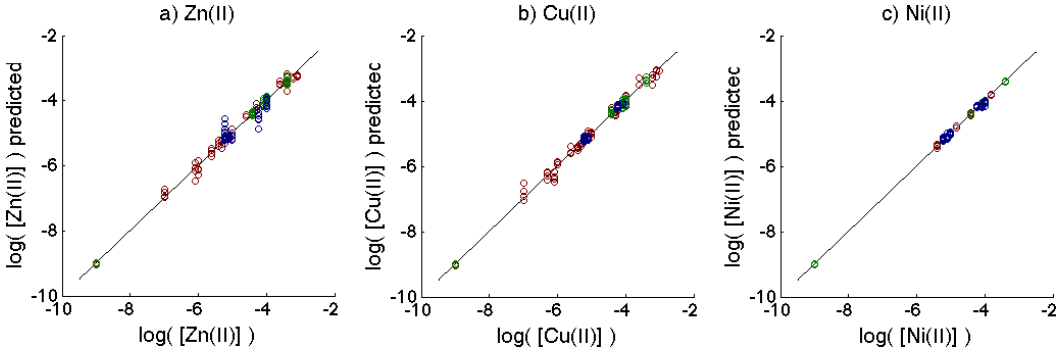

Figure 7. Estimation performance for the metals using the estimation module: a) Zn(II); b) Cu(II); c) Ni(II).

Two-stage approach for the determination of heavy metal concentration

In this section, we assume that the system has been calibrated and provide the results of the behavior of the entire system. First, classification information on the presence/absence of heavy metal is provided in Table 4 where the training, testing and validation data are organized into sets of samples containing 1, 2 or 3 metals. We did this reorganization to verify that the network is able to learn the metal classification in all situations, regardless of the number of metals in the solutions. This is the case and the networks have learnt to generalize the relationships between

the H parameter of the input sensors and the presence/absence of metals in the solutions.

Table 4. Summary of heavy metal classification by number of metals in sample.

Metal		Zn(II) classification success		Cu(II) classification success		Cu(II) classification success	
		samples	%	samples	%	samples	%
1-metal samples	PP	60	96.77 %	70	98.59 %	26	100 %
	PN	2	3.23 %	1	1.41%	0	0 %
	NN	95	97.94 %	86	97.73 %	130	97.74 %
	NP	2	2.06 %	2	2.27 %	3	2.25 %
Average hits		155	97.48 %	156	98.11 %	156	98.11 %
2-metal samples	PP	42	100 %	42	100 %	36	100 %
	PN	0	0 %	0	0 %	0	0 %
	NN	18	100 %	18	100 %	21	87.50 %
	NP	0	0 %	0	0 %	3	12.50 %
Average hits		60	100 %	60	100 %	57	95 %
3-metal samples	PP	52	96.30 %	53	98.15 %	50	92.59 %
	PN	2	3.70 %	1	1.85 %	4	7.41 %
	NN	-	-	-	-	-	-
	NP	-	-	-	-	-	-
Average hits		52	96.30 %	53	98.15 %	50	92.59 %
Total Average Success		267	97.80 %	269	98.53 %	263	96.34 %

Additionally, the discrimination is similar regardless of the metal to be classified, which suggests that the method developed in this work is robust whether the metal ions are Zn(II), Cu(II) or Ni(II).The success of the classification module in our system is key to achieving a suitable estimation of metal concentration, since the output of this module is also used as the input for the second stage in Figure 1.

Indeed, our approach is able to provide an accurate estimation of metal concentration, but this estimation is limited to the suitable metal discrimination in the classification stage. Figure 8 helps to support this conclusion, where a high error

rate is observed for those solutions that were not correctly classified and high accuracy for the ones where the metals were identified successfully. As a final conclusion, our system is able to provide accurate metal concentration estimation in 97.80% of the cases for Zn(II), 98.53% of the cases for Cu(II), and 96.33% of the cases for Ni(II). In these situations, the expected error is 0.06±0.10 for Zn(II) (log scale of molar concentration), 0.05±0.05 for Cu(II) and 0.02±0.03 for Ni(II). This error is below a decimal unit with respect to the real metal concentration in the solution, which is a promising result to the best of our knowledge.

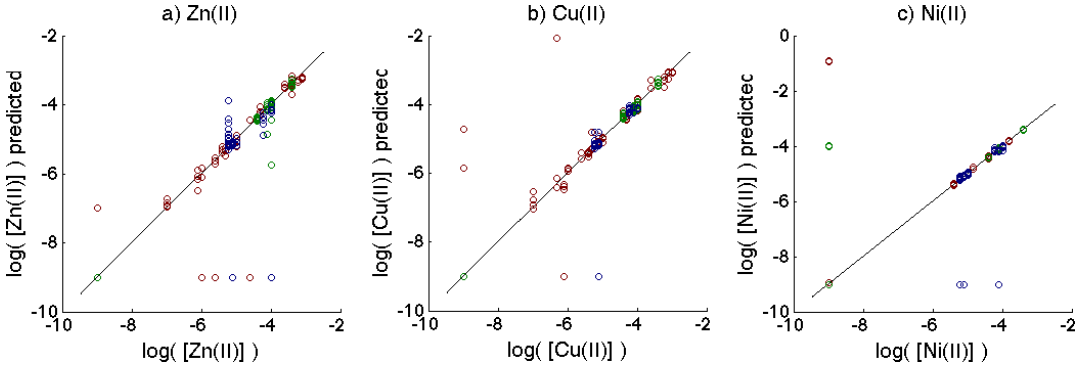

Figure 8. Estimation performance using the two-stage approach: a) Zn(II); b) Cu(II); c) Ni(II).

CONCLUSIONS

An optical tongue for the simultaneous identification and determination of the heavy metals Zn(II), Cu(II) and Ni(II) has been developed and characterized. The tongue consists of an array of two polymeric membranes that work by complexation with chromogenic reagents through a co-extraction equilibrium producing distinct changes in color. The color that the two-membrane optical tongue shows in the presence of the sample solution is used as the analytical signal. The color is measured from the image of the tongue in a scanner working in transmission mode, using the

H parameter (hue) of the HSV color space, which affords robust and precise measurements. The prediction of the analyte concentration, based on the hues obtained from the multi-membrane, was carried out using a neural network approach.

A two-stage approach based on the response of the network models and color parameters is presented and validated. In the first stage, the metals present are classified, with 96% success over a threshold of 10^{-7} M regardless of the number of metals present, using the H feature of the two membranes. In the second stage we reuse the H features in combination with the results of the classification procedure to estimate the concentration of each metal in the solution with acceptable error. Statistical tests were applied to validate the model over real data, showing a high correlation between the reference and predicted analyte concentration.

At this time, the use of inkjet printing techniques for array preparation and the development of small, hand-held, battery operated instruments that will include developed algorithms to work with captured imaging data is being studied.

REFERENCES

1. J.J. Lavigne, E.V. Anslyn, Angew.Chem.Int.Ed. 2001, 40, 3118-3130.

2. Y. Vlasov, A. Legin, A. Rudnitskaya, C. Di Natale and A. D'Amico, Pure Appl.Chem. 2005, 77, 1965-1983.

3. A.K. Deisingh in Sensors for Chemical and Biological Applications, Ram, M. K.; hethanabotla, V. R., Eds. ed. , CRC Press, 2010, 173-192.

4. P. Ciosek, W. Wroblewski, Analyst 2007, 132, 963-978.

5. A.K. Deisingh, D.C. Stone and M. Thompson, Intern.J.Food Sci.Tech. 2004, 39, 587-604.

6. Y. Vlasov, A. Legin and A. Rudnitskaya, Anal.Bioanal.Chem. 2002, 373, 136-146.

7. M.M. Erenas, O. Pineiro, M.C. Pegalajar, M.P. Cuellar, I. de Orbe Paya and L.F. Capitan-Vallvey, Anal.Chim.Acta 2011, 694, 128-135.

8. EPA, Clean Water Act ,1972.

9. K. Cantrell, M.M. Erenas, I. Orbe-Paya and L.F. Capitán-Vallvey, Anal.Chem. 2010, 82, 531-542.

10. F. Winquist, C. Krantz-Rulcker and I. Lundstrom, Sensors Update 2003, 11, 279-306.

11. S. Haykin in Neural Networks: A comprehensive foundation, Prentice Hall, Upper Saddle River, NJ, USA, 1999.

12. R. Linggard, D.J. Myers C. Nightingale in Neural Networks for Vision, Speech and Natural Language, Ed. Chapman & Hall, London, UK, 1992.

13. W. Thomas-Miller, R.S. Sutton R.J. Werbos in Neural Networks for control, 2nd ed., The MIT Press, Cambridge, MA, USA, 1991.

14. M.P. Cuellar, S. Capel-Cuevas, M.C. Pegalajar, I. de Orbe-Paya and L.F. Capitán-Vallvey, New J.Chem. 2011, 35, 1042-1053.

15. M.M. Erenas, M.C. Pegalajar, M.P. Cuellar, I. de Orbe Paya and L.F. Capitan-Vallvey, Sens.Actuators, B 2011, 156, 976-982.

16. Cuellar, M. P.; Delgado, M.; Pegalajar, M. C. 2005 24-5-2005; Proc.International Conference on Enterprise and Information Systems; 35-42.

17. M.P. Cuellar, M. Delgado and M.C. Pegalajar, Expert Systems 2006, 23, 99-117.

18. M.P. Cuellar, M. Delgado and M.C. Pegalajar, IEEE Transactions on Systems, Man and Cybernetics B 2008, 38, 1-25.

19. J. Vukovic, M. Ariza-Avidad and L.F. Capitan-Vallvey, Talanta 2012, 94, 123-132.

20. A. Abbaspour, M.A. Mehrgardi, A. Noori, M.A. Kamyabi, A. Khalafi-Nezhad and M.N. Soltani Rad, Sens.Actuators B 2006, 113, 857-865.

21. C. Zhang, K.S. Suslick, J.Agric.Food Chem. 2007, 55, 237-242.

Analytica Chimica Acta 783 (2013) 56–64

Contents lists available at SciVerse ScienceDirect

Analytica Chimica Acta

journal homepage: www.elsevier.com/locate/aca

Feasibility of the use of disposable optical tongue based on neural networks for heavy metal identification and determination

M. Ariza-Avidad[a], M.P. Cuellar[b], A. Salinas-Castillo[a], M.C. Pegalajar[b], J. Vuković[c], L.F. Capitán-Vallvey[a,*]

[a] Department of Analytical Chemistry, University of Granada, Faculty of Sciences, Avda. Fuentenueva s/n, E-18071, Granada, Spain
[b] Department of Computer Science and Artificial Intelligence, E.T.S. Ingeniería Informática y de Telecomunicación, University of Granada, C/Periodista Daniel Saucedo Aranda s/n, E-18071, Granada, Spain
[c] Department of Analytics and Control of Medicines, Faculty of Pharmacy and Biochemistry, University of Zagreb, A. Kovačića 1, HR-10000 Zagreb, Croatia

HIGHLIGHTS

- Identification and determination of heavy metals by means of a disposable optical tongue.
- Use of the color features of the two-membrane array in a chemometric tool based on ANNs.
- Two-stage ANN approach based on a classification step followed by a second for quantification.

GRAPHICAL ABSTRACT

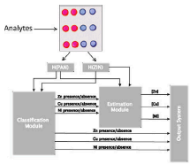

ARTICLE INFO

Article history:
Received 30 January 2013
Received in revised form 15 April 2013
Accepted 17 April 2013
Available online 26 April 2013

Keywords:
Heavy metals classification
Heavy metals determination
Artificial neural networks
Disposable optical array

ABSTRACT

This study presents the development and characterization of a disposable optical tongue for the simultaneous identification and determination of the heavy metals Zn(II), Cu(II) and Ni(II). The immobilization of two chromogenic reagents, 1-(2-pyridylazo)-2-naphthol and Zincon, and their arrangement forms an array of membranes that work by complexation through a co-extraction equilibrium, producing distinct changes in color in the presence of heavy metals. The color is measured from the image of the tongue acquired by a scanner working in transmission mode using the H parameter (hue) of the HSV color space, which affords robust and precise measurements. The use of artificial neural networks (ANNs) in a two-stage approach based on color parameters, the H feature of the array, makes it possible to identify and determine the analytes. In the first stage, the metals present above a threshold of 10^{-7} M are identified with 96% success, regardless of the number of metals present, using the H feature of the two membranes. The second stage reuses the H features in combination with the results of the classification procedure to estimate the concentration of each analyte in the solution with acceptable error. Statistical tests were applied to validate the model over real data, showing a high correlation between the reference and predicted heavy metal ion concentration.

© 2013 Elsevier B.V. All rights reserved.

1. Introduction

The disadvantages of conventional approaches for multi-analyte sensors based on specific receptors are largely related to problems with selectivity and the number of sensors needed, which increases proportionally with the number of analytes. The alternative concept based on differential receptors [1] proposes making use of arrays of non-specific or low selective sensors (electronic

* Corresponding author. Tel.: +34 958 248436; fax: +34 958 243328.
E-mail addresses: mariavidad@ugr.es (M. Ariza-Avidad), manupc@decsai.ugr.es (M.P. Cuellar), alfonsos@ugr.es (A. Salinas-Castillo), mcarmen@decsai.ugr.es (M.C. Pegalajar), jadranka@pharma.hr (J. Vuković), lcapitan@ugr.e (L.F. Capitán-Vallvey).

0003-2670/$ – see front matter © 2013 Elsevier B.V. All rights reserved.
http://dx.doi.org/10.1016/j.aca.2013.04.035

DOI: http://dx.doi.org/doi:10.1016/j.aca.2013.04.035

HANDHELD COLORIMETER FOR DETERMINATION OF HEAVY METAL CONCENTRATIONS

ABSTRACT

A portable instrument that measures heavy metal concentration from a colorimetric sensor array is presented. The use of eight sensing membranes, placed on a plastic support, allows to obtain the hue component of the HSV color space of each one in order to determinate the concentration of metals present in a solution. The developed microcontroller-based system captures, in an ambient light environment, an image of the sensor array using an integrated micro-camera and shows the picture in a touch micro-LCD screen, which acts as user interface. After image processing of the regions of interest selected by the user, color and concentration information are displayed on the screen.

INTRODUCTION

The detection and determination of heavy metals in the area of analytics and drug control are important and demanding tasks, and, therefore, drug analysis and quality control require increasingly better analytical methods and procedures to solve specific problems in pharmaceuticals and in the industrial production of medicines [1]. A recent trend to obviate the difficulties of obtaining single analyte sensors based on specific receptors – problems of selectivity – is to combine non-specific sensors in an array that produce a set of analytical signals (electronic tongue for gaseous species/electronic nose for species in solution). This information with higher dimensionality, encoded in the overlapping measurements, can be processed to extract qualitative and quantitative information through advanced mathematical procedures of pattern recognition and/or multivariate analysis [2,3], improving in this way the performance of the sensors [4].

Different principles have been used for the preparation of sensor arrays for electronic tongues, with the most widely used being: tin oxide catalytic sensors, conducting polymer sensors, acoustic wave sensors, quartz crystal microbalance sensors, sensors based on MOSFET technology, systems based on ion mobility spectrometry as well as mass spectrometry techniques like API and PTR, and lastly, optical techniques, principally fiber optics and fluorescence [5].

The basic requirements for the optical tongue systems, in reference to the sensing array, which is the key of the system, is that sensors should present low selectivity or high cross-sensitivity, and that they have reproducible analytical characteristics. Moreover, it is necessary to look for sensors to be more sensitive and more robust, which is contradictory to a certain degree, since usually the more sensitive a sensor is, the less robust it becomes [6]. One solution is to use disposable sensors, which are, therefore, not integrated into the device. Additional requirements refer to cost and portability.

Most different optical approaches used for tongues are based on the measurement of color using different color spaces obtained from the image captured principally by imaging devices, mainly CCD cameras or scanners. By far, the most commonly used space is RGB, whose coordinates are used for processing with multivariate techniques. However, in this work, we used the HSV color space, whose main characteristic is that it represents the useful information of the color in one single parameter, the coordinate H (hue). Previous studies from our group have shown that the use of the H coordinate in bitonal sensors that produce a change in color by reaction yields a substantial improvement in resolution and repeatability [7].

We approached the analysis of heavy metals using the concept of an optical tongue using an array of membranes placed on a transparent support that contains immobilized conventional chromogenic reagents [8]. Their usual drawback, i.e. their

lack of selectivity, is used here as the source of non-selective information about the metals present, considering their usual good sensitivity.

EXPERIMENTAL

Preparation of the sensing array

Different chromogenic reagents for heavy metals were tested for immobilization using different strategies such as ion exchange, adsorption, and entrapment using as criteria for selection the conditions of no leaching, change in tonal color coordinate by reaction and non-selective behavior.

As chromogenic reagents for this proof of concept study, 1-(2-pyridylazol)-2-naphtol (PAN) and Zincon (ZIN) were used and the needed amounts of polymers, reagents, plasticizers and lipophilic salts were optimized. For characterization of sensing films, individual membranes were prepared by using a spin-coating technique from the cocktails containing all the reagents in THF or in ethanol: water mixture on the sheets of Mylar-type polyester. In addition sensing arrays were prepared on a Mylar support covered by an adhesive and transparent PVC layer with 12 holes, 5 mm in diameter each. The array was produced by placing 8 μL of the corresponding cocktail in each hole.

Description of the instrument

The portable instrument here developed is a microcontroller-based system that allows to calculate the H component of the HSV color space from an image of a colorimetric sensor array obtained with a micro-camera. The color information is used to determinate the concentration of metals in a solution. The block diagram of the prototype described is in Figure 1.

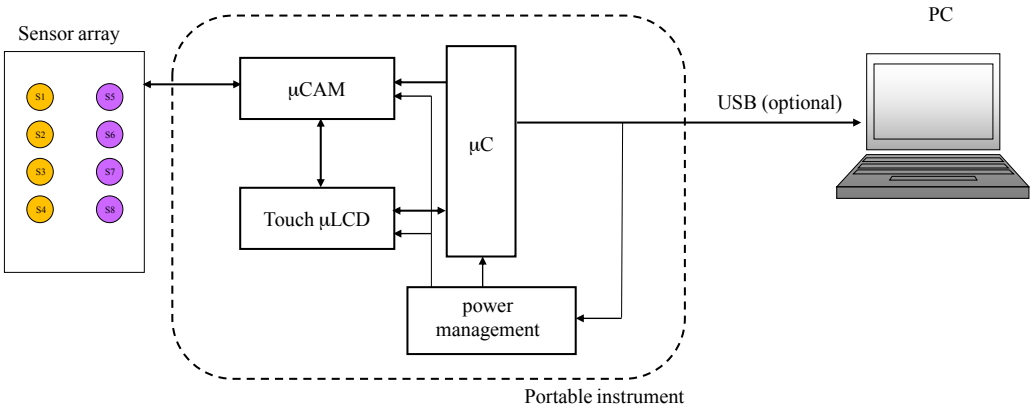

Figure 1: Block diagram of the instrument.

The model of microcontroller used in this instrument is the PIC18F2550 (Microchip Technology Inc., USA), which is a low cost device with an integrated USB module that has been used for developing and calibration purposes. The user can interact with the instrument through a touch micro-LCD screen model μLCD-32PT-SGC (4DSystems, Australia) included in the prototype, which also shows the color information obtained from the sensors. Therefore, there is no need of external elements to handle the instrument. The touch micro-LCD screen integrates a 4-wire resistive touch panel, which has a 240x320 QVGA resolution and 65K colors. The dimensions of the screen are 56 x 77.6 x 3.7 mm and 3.2'diagonal, which are high enough to present an easy and clear interface to the user. Moreover, the screen integrates an on-board micro-SD memory card adaptor for multimedia storage and data logging purposes.

The instrument makes use of a micro-camera model TTL-μCAM (4DSystems, Australia) to capture an image from the sensor array, which is shown in the micro-LCD screen. The micro-camera is a module with serial output that allows acquiring images in JPEG or RAW format in different sizes and color or gray-scale resolutions.

Both the micro-camera and the touch-screen provide a set of embedded commands for an easy communication and programming. The main reasons for choosing this model of LCD-screen are the touch function to avoid external elements for user interaction and the high color resolution, which is enough for the explained purpose, achieving a handheld colorimeter.

For this work, a 16-bit color RGB and RAW format was chosen because of the simplicity in the structure of this format, which does not use any compression algorithm. Thanks to the compatibility between the micro-camera and the micro-LCD screen the RAW format permits direct communication between them with no action of the microcontroller or any external memory. However, since RAW is an uncompressed format, the received data from the micro-camera are heavier than JPEG format which increases the time required to obtain the image, but it makes possible a direct treatment of the pixel information with no need for prior processing.

In Figure 2, a photo of the prototype described is presented. The micro-LCD screen shows an image of the sensor array in which are presented different membranes. The user can select, by touching the screen, the individual sensors to calculate the H coordinate and metal concentration, so that a defective sensor can be ignored. The sensor array is placed at the bottom of the instrument, in a hole built facing the micro-camera, covered by a transparent Mylar polyester sheet, to allow visualization of the membranes, where the visualization is subsequently processed.

The prototype has multiple ways to obtain the power supply: from a PP3 battery of 9V through a voltage regulator to generate 5 V, from an AC/DC external adaptor or via the USB port.

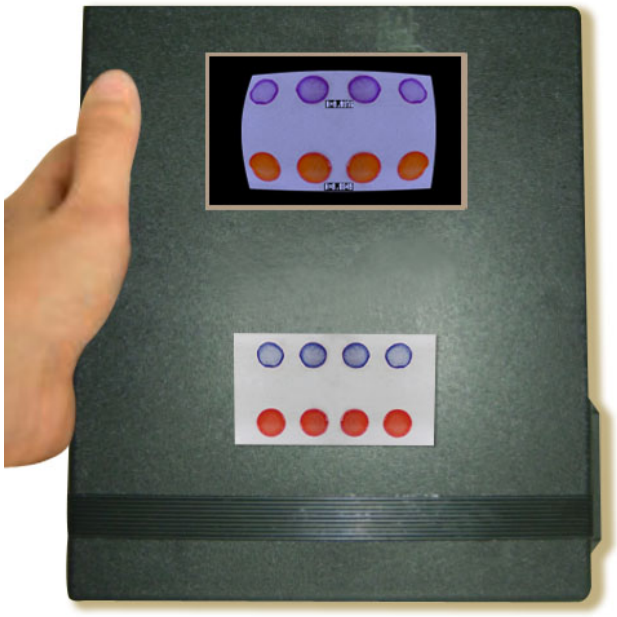

Figure 2: Photography of the instrument.

* **Measurement procedure**

The concentration of metals through color determination of the sensor array is carried out after image processing from the picture of the membranes captured with the micro-camera. The image is taken in an ambient light environment; therefore the prototype has no need of a specific light source to obtain a fine image. To avoid overexposure in the image, a thin white film of PVC is positioned between the sensor array and the light source to act as an intensity attenuator of the ambient light. The sensor array is placed by the user in a holder situated facing the micro-camera. The aperture has a piece of transparent Mylar to situate the sensor array for taking the image. After the sensor array is positioned in the instrument, the user starts the capture of the picture by touching the micro-LCD screen, which was in a sleep mode.

Once the image is presented on the micro-LCD screen, the user can select a particular sensor to obtain its H component and the correspondent metal concentration, as it can be seen in Figure 3. The touch option offers the user the possibility of discarding defective membranes of the image and only takes into account good quality membranes to calculate the concentration of metals. On the other hand it is possible to determine the H component of every membrane at the same time. As the user can select a specific sensor by touching the micro-LCD screen, the position of the sensor array respect to the micro-camera is not critical since the H parameter is determined using the area selected by the user.

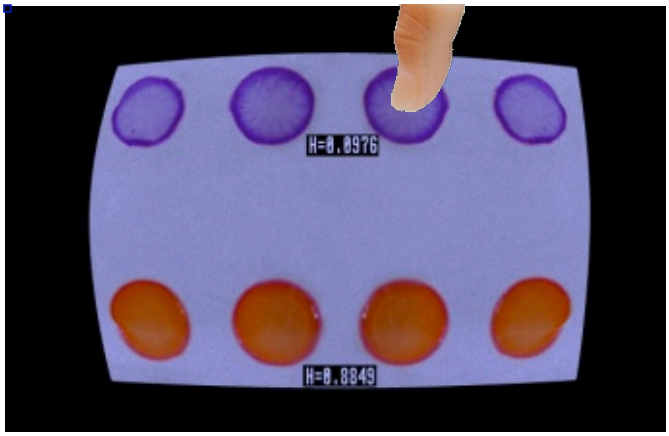

Figure 3: Micro-LCD screen showing obtained H components for two membranes.

The algorithm used to obtain the H value consist of a pixel-by-pixel treatment of the image in which the RGB coordinates are loaded and processed to generate the hue component for the regions of the image corresponding to the metal sensitive membranes. A statistic of these pixels is carried out to determine the mode of the H data, which is taken as the value for the whole membrane. After image processing to estimate the hue component, the concentration of Cu and Zn can be calculated and shown in the micro-LCD screen.

RESULTS

The characterization of the sensor array was performed using four replicates for each kind of membrane, PAN or Zincon, using solutions containing the metals ions in a range from 0.06 to 65 mg L^{-1} for each metal. The reaction conditions (equilibration time, pH) were studied and optimized using single membranes against each metal ion. A comparison between the response of the prototype and a commercial scanner ScanMaker i900 (Microteck, Taiwan) is shown in Figure 4. The used scanner has a 6400 x 3200 dpi resolution and a maximum optical density of 4.2 and 24 to 48 bits of color. The H parameter is calculated from the scanned image using the software Matlab r2007b (The MathWorks, Inc, Natick, MA, USA) [7].

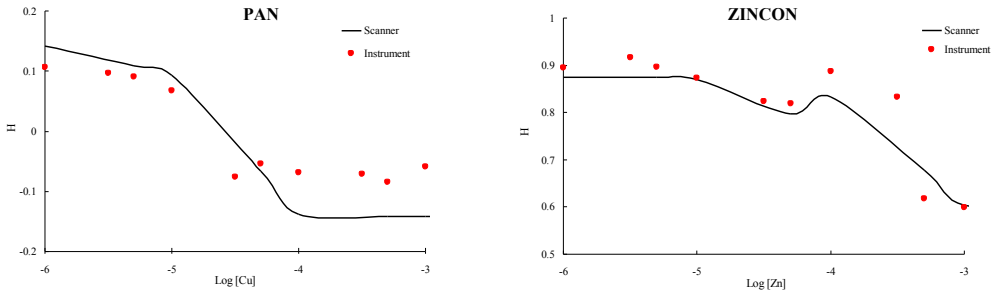

Figure 4: Response of the sensor array for Cu and Zn.

As depicted in Figure 4, the response curves obtained with the scanner and the prototype for Cu and Zn concentrations present the same behavior and in both cases are obtained through image processing of the captured image. Nevertheless, there are some discrepancies on the responses, caused by the different light sources and the lower resolution of color in the micro-camera. The experimental curves for Cu and Zn were modeled by splitting them into linear sections in order to obtain the metal concentration from the H parameter previously determined [9].

CONCLUSIONS

A handheld colorimeter which uses the hue component of HSV color space for a colorimetric sensor array to calculate the concentration of metals in solutions such as Zn and Cu is presented. The analytical procedure consists of determining the color changes in two different kind of sensing membranes, PAN or Zincon, and relating them with variations of the metal concentration.

The H component of the colorimetric sensor is obtained from an image captured with an integrated micro-camera and displayed in a touch-micro LCD screen. The main advantage of the direct communication between the micro-camera and the LCD screen is to avoid the necessity of using an external memory to save the image, since the color information of each pixel can be directly read from the screen. The prototype works in an ambient light environment; therefore there is no need for a specific light source integrated on the prototype. Because of this, the result is a simple electronic design with a reduced number of electronic components.

A study of the membranes response in solutions with different metal concentrations was carried out to obtain a complete characterization of the instrument. The obtained curves show good agreement with the acquired models using a reference instrument, in this case, a commercial scanner. Although in this work the membranes response have been modeled only for a unique specific metal in a solution, future work will be focused in determine metals concentration in mixtures.

REFERENCES

1. J. Vuković, S. Matsuoka, K. Yoshimura, V. Grdinić, R. Jurišić Grubešić, O. Županić, 2007 Simultaneous determination of traces of heavy metals by solid-phase spectrophotometry, Talanta, vol 71 pp 2085-2091

2. Yu. Vlasov, A. Legin, A. Rudnitskaya, C. Di Natale, A. D'Amico, 2005 Non-specific sensor arrays («electronic tongue») for chemical analysis of liquids, Pure and Applied Chemistry, Vol.77 pp 1965-1983

3. P. Ciosek, W. Wróblewski, 2007 Sensor arrays for liquid sensing - electronic tongue systems, Analyst, vol 132 pp 963 - 978

4. J. Gallardo, S. Alegret, R. Muñoz, M. De Roman, L. Leija, P.R. Hernandez, M. Del Valle, 2003 An electronic tongue using potentiometric all-solid-state PVC-membrane sensors for the simultaneous quantification of ammonium and potassium ions in water, Analytical and Bioanalytical Chemistry, vol 377 pp 248-256

5. A.K. Deisingh, D.C. Stone and M. Thompson, 2004 Applications of electronic noses and tongues in food analysis, Int. J. Food Sci. Technol. Vol 39 pp 587–604.

6. M. C. Janzen, J. B. Ponder, D. P. Bailey, C. K. Ingison, and K. S. Suslick, 2006 Colorimetric sensor arrays for volatile organic compounds, Anal. Chem. Vol 78 pp 3591–3600.

7. K. Cantrell, M.M. Erenas, I. Orbe-Paya, L.F. Capitan-Vallvey, 2010 Use of the Hue Parameter of the Hue, Saturation, Value Color Space As a Quantitative Analytical Parameter for Bitonal Optical Sensors, Anal.Chem. vol 82 p 531.

8. T. Mayr, C. Igel, G. Liebsch, I. Klimant, O.S. Wolfbeis, 2003 Cross-Reactive Metal Ion Sensor Array in a Micro Titer Plate Format, Anal.Chem. vol 75 p 4389.

9. A. Martínez-Olmos, S. Capel-Cuevas, N. López-Ruiz, A.J. Palma, I. de Orbe and L.F. Capitán-Vallvey, Sensor Array-Based Optical Portable Instrument For Determination Of Ph, Sensors And Actuators B, 2011 doi:10.1016/j.snb.2011.02.052

Sensors & their Applications XVI IOP Publishing
Journal of Physics: Conference Series **307** (2011) 012037 doi:10.1088/1742-6596/307/1/012037

Handheld colorimeter for determination of heavy metal concentrations

N. López Ruiz*[1], M. Ariza[2], A. Martínez Olmos[1], J. Vukovic[3], A.J. Palma[1], L.F. Capitan-Vallvey[2]

ECSens [1]ETSIIT, Departamento de Electrónica, Universidad de Granada. C\ Periodista Daniel Saucedo s/n 18071 Granada, Spain. [2]Department of Analytical Chemistry. Faculty of Sciences. University of Granada, E-18071 Granada, Spain. [3]Department of Analytics and Control of Medicines, Faculty of Pharmacy and Biochemistry, University of Zagreb, A. Kovačića 1,HR-10000 Zagreb, Croatia.

* e-mail: nurilr@ugr.es

Abstract. A portable instrument that measures heavy metal concentration from a colorimetric sensor array is presented. The use of eight sensing membranes, placed on a plastic support, allows to obtain the hue component of the HSV colour space of each one in order to determinate the concentration of metals present in a solution. The developed microcontroller-based system captures, in an ambient light environment, an image of the sensor array using an integrated micro-camera and shows the picture in a touch micro-LCD screen which acts as user interface. After image-processing of the regions of interest selected by the user, colour and concentration information are displayed on the screen.

1. Introduction

The detection and determination of heavy metals in the area of analytics and drug control are important and demanding tasks, and, therefore, drug analysis and quality control require increasingly better analytical methods and procedures to solve specific problems in pharmaceuticals and in the industrial production of medicines [1]. A recent trend to obviate the difficulties of obtaining single analyte sensors based on specific receptors – problems of selectivity – is to combine non-specific sensors in an array that produce a set of analytical signals (electronic tongue for gaseous species/electronic nose for species in solution). This information with higher dimensionality, encoded in the overlapping measurements, can be processed to extract qualitative and quantitative information through advanced mathematical procedures of pattern recognition and/or multivariate analysis [2,3], improving in this way the performance of the sensors [4].

Different principles have been used for the preparation of sensor arrays for electronic tongues, with the most widely used being: tin oxide catalytic sensors, conducting polymer sensors, acoustic wave sensors, quartz crystal microbalance sensors, sensors based on MOSFET technology, systems based on ion mobility spectrometry as well as mass spectrometry techniques like API and PTR, and lastly, optical techniques, principally fibre optics and fluorescence [5].

The basic requirements for the optical tongue systems, in reference to the sensing array, which is the key of the system, is that sensors should present low selectivity or high cross-sensitivity, and that they have reproducible analytical characteristics. Moreover, it is necessary to look for sensors to be more sensitive and more robust, which is contradictory to a certain degree, since usually the more

Published under licence by IOP Publishing Ltd

Doi: 10.1088/1742-6596/307/1/012037
Website: http://iopscience.iop.org/1742-6596/307/1/012037

CONCLUSIONS

The aim of the work presented in this chapter has been the development and characterization of disposable optical sensors for metal ions from absorption and color measurements. After applying various estimation strategies to correlate the experimental data with metal ion concentration, we have found that is possible to use sensing membranes prepared on transparent supports for classification and determination of selected metal ions by using different models to fit data.

The main conclusions we can highlight are the following:

- We have prepared, using a spin coating technique, five types of sensing membranes containing different immobilized chromogenic reagents demonstrating the characteristics of minimal leaching, short reaction times, a wide change in color by reaction, and high adherence to the support.
- The combination of prepared absorbance-based sensors and the chemometric algorithm of multicomponent analysis by multiple linear regressions enabled the determination of five selected metal ions in mixtures, despite similarity in their spectral characteristics. A pre-validation study confirmed that most sensors showed a linear relationship between analyte and signal, acceptable accuracy and precision and low limits of detection, as well as, the limitations of the procedure.
- We have developed a sensing array comprising two sensing membranes that use the tonal coordinate H of the HSV color space as analytical parameter obtained from a conventional scanner working in a transmission mode.
- The classification or the determination of presence/absence of metal ions was achieved by using artificial neural networks (ANNs) methods operating

on color parameters in a two-stage approach, which allowed the estimation of the corresponding metal concentration. The first stage, the classification, presents an average success of 96% in the identification of metals present above a threshold of 10^{-7} M, regardless of the number of metals present, using the H feature of the two membranes. In the second stage, a combination of the results obtained in the classification procedure and the H feature were used for the estimation of the concentration of each analyte in the solution with acceptable error. A high correlation between the reference and predicted metal ion concentration were shown for the real data with the statistical test applied to validate the model over real data.

- A handheld colorimeter which uses the hue component of HSV color space obtained from the colorimetric sensing array to calculate the concentration of metals in solutions such as Zn and Cu is developed and characterized. The analytical procedure consists of determining the color changes in two different kind of sensing membranes, PAN or Zincon, and relating them with variations of the metal concentration.
- A CMOS micro-camera module has been tested to develop the colorimeter working with the H coordinate of the array above described and calculated from the image captured. The microcontroller included in the prototype carried out the processing of the image captured with the micro-camera and the direct communication between the camera and the touch-micro LCD screen included avoiding the need of using an external memory to save the image, since the color information of each pixel can be directly read from the screen. The prototype was applied to the determination of metal ions in solution using the prepared sensing membranes.

Chapter II

Sensing membrane fabrication by inkjet printing process

CHAPTER II. SENSING MEMBRANE FABRICATION BY INKJET PRINTING PROCESS

OBJECTIVES

The main objective of the work presented in this Chapter II consists of the preparation of sensing membranes with increased reproducibility using advanced printing techniques. These sensing membranes demonstrate increased discriminating power for colorimetric sensors both in an optical tongue format for metal ions or in a displacement assay for anions.

The specific proposed objectives are the following:

- Prepare a disposable array composed of membranes containing chromogenic reagents with increased homogeneity and reduce the size by using an ink-jet printing technique in order to avoid the limitations imposed by previously used spin coating techniques.
- Optimize ink-jet printer variables and the preparation and characterization of water-based chemical inks making the membranes preparation more ecological and environmentally friendly.
- Use of an easy and rapid system to extract the analytical information from the array using an imaging technique a conventional digital camera.
- Use of a color coordinate obtained from array images as the robust analytical parameter containing all useful information.
- Develop a procedure for the identification and determination of the target metal ions selected by using artificial neural networks as the technique for data processing using only as input the color coordinates obtained from array images.

- Develop a procedure for anion sensing based on a colorimetric metal complexing indicator–displacement assay prepared by an ink-jet printing technique.

PRINTED DISPOSABLE COLORIMETRIC ARRAY FOR METAL ION DISCRIMINATION

ABSTRACT

An increase in the discriminatory power of a colorimetric array is achieved by increasing the reproducibility of the preparation controlling the inkjet printing conditions of the array, which makes it possible to identify 13 metal ions using a 19x31 mm Nylon array containing 35 sensing membranes. The color is measured from the image of the array acquired by a digital camera using the H coordinate of the HSV color space as the analytical parameter, which produces robust and precise measurements. Both the detection and concentration estimation of the metal ions was readily achieved using a two-stage neural network approach with higher accuracy than with previous approaches. The described disposable colorimetric array can be used for the resolution of different mixtures, selecting convenient recognition chemistries.

INTRODUCTION

The identification and determination of metallic ions, mainly multivalent transition metals, with potential toxicity or ecotoxicity[1] in the lab is a well-established subject that uses an ample variety of analytical techniques, including inductively coupled plasma/atomic emission spectrometry (ICP-AES), inductively coupled plasma/mass spectrometry (ICP-MS), atomic absorption spectroscopy (AAS) and atomic fluorescence spectroscopy (AFS).

However, the persistence of these metals in both natural and contaminated environments and their involvement in the development of human cancer and neurodegenerative diseases, encourages the development of fast, cheap procedures that can be performed in situ by untrained personnel, able to manage a large number

of samples that provide qualitative and quantitative information on metal ions, particularly in drinking and natural waters and wastewaters.[2]

One of the most interesting approaches for rapid multianalyte analysis is a sensor array design –not those based on specific receptors because of selectivity problems, but rather those based on non-specific sensors producing a set of high dimensional analytical signals. The processing of signals through advanced mathematical procedures of pattern recognition and/or multivariate analysis[3,4] makes it possible to obtain qualitative and quantitative information.

From the existing sensing array schemes, optical arrays (also known as optical electronic tongues) offer a reasonable combination of discriminatory power, sensitivity and simplicity to convey the requirements of these analytical devices. These are mainly combined with imaging devices for simultaneous signal acquisition, such as scanners and digital cameras and more recently, with digital cameras integrated into portable devices such as tablets and smartphones, because the built-in microprocessors can be programmed to carry out the image processing and mathematical data treatment.

Different approaches have been described for optical electronic tongues,[5] but with regard to metal ion discrimination alone, three different formats have been devised: membranes,[6,7]microtiter plates[6,8-13] and paper-based sensing devices.[14-16]

The microtiter plate format arranges the reagents in the wells either immobilized as a membrane at the bottom[8,9,13] or as a solution placed in vials that are arranged in an array before acquiring the analytical signal.[10] That format needs only a small volume of sample, even at submicroliter level,[12] although in the usual application for water analysis is not the main problem.

Membrane and paper-based devices offer the additional advantage of preconcentration, lowering the detection limit. For instance, the arrangement of metal ion reagents in ormosils coated on a cellulose acetate/nitrate membrane has

been proposed for the discrimination of eight metal ions with detection limits of 50 nM.[7] Different types of paper-based devices have been described: Hossain and Brennan[14] use a flower design with wax-printed hydrophobic channels and ink-jet printed detection areas in which the stem is the sampling area. Feng et al.[15] describe an eight detection area wheel design paper device with a sampling area in the middle that improves the pre-concentration, including a water absorbent cell on each detection area and a water absorbent resin placed at the end of each hydrophilic channel. In this way it is possible to filter through a sample volume as high as 800 μL. A different design presented by Feng et al.[16] uses a 3x3 membrane array prepared as above with a wax-printing technique for the pattern and by drop coating the reagents. The location of a piece of filter paper under the array makes it possible for analytes (600 μL) to pass through the spots enriched with the metals.

Different chemistries, both colorimetric and luminescent, have been employed for the described devices. Conventional colorimetric reagents both alone[7] or in combination with an enzymatic test like the β-galactosidase-based test,[14] have been used for the discrimination of 7-8 metal ions. Additionally, some luminescent reagents have been employed based on the combination of different coordination chemistries and signal transduction schemes, such as turn-on, turn-off and ratiometric schemes to generate discriminatory data for metal classification.[9,11,12] In other cases, the array is composed of a family of reagents that combine receptor and fluorophore in the molecule to introduce subtle differences to increase the discriminatory power. Examples include reagents based on di-2-picolyamine derivatives as receptors and Bodipy as the fluorophore[10] or 8-hydroxyquinoline as the receptor and different oligofluorenes as the fluorophore.[13]

In general, different imaging techniques have been used to obtain analytical signals ranging from a conventional scanner[14] to a fluorescence scanner,[11-13] a CCD camera for lifetime measurements[8,9] and a digital camera.[10,16]

One of the weak points of these devices is the reproducibility of the preparation since the most common way to deposit the reagents in the detection area is by drop coating, which increases the inhomogeneity of the recognition area, reducing the reliability of the device and the precision in quantitative determinations.

In this paper we study the preparation of colorimetric arrays for metal ions based on conventional metal-ion reagents emphasizing the reproducibility of the preparation by printing techniques and the use of the H coordinate from HSV color space as the analytical signal[17] in order to increase the discriminatory power of the array and the precision of the determinations. The membrane array was prepared with a drop-on-demand printing method based on piezoelectric inkjet technology, a reliable system for membrane production taking into account the low volume of chemical ink required, the disposable piezo inkjet used and the low cost of the array.

In this case, the colorimetric response of any membrane in the sensor array is a sigmoid-shape non-linear function of the color coordinate with respect to the metal concentration.[18] Thus, we need to use a multivariate non-linear mathematical technique able to provide a calibration model for the whole array. In this work, we use artificial neural networks (ANN),[19] due to their multivariate and non-linear nature and their features such as noise tolerance and generalization properties for the calibration data. These types of techniques have been widely and successfully used in similar tasks.[20,21] More specifically, ANNs are used in our approach to identify up to 13 metal ion mixtures in solution and to estimate the corresponding metal concentration from a sensing array composed of seven sensing membranes that use the hue color feature as an analytical parameter.

EXPERIMENTAL SECTION

Materials

Dilution of the standard stock solution of the metals (1000 μg mL^{-1} as chloride in HCl 5M for Sb(III); Zn(II), Cu(II), Fe(III), Al(III), Cr(III), Co(II), and Cd(II) as nitrate in 0.5 M HNO_3; Mn(II) as nitrate in 1M HNO_3; Ni(II), Pb(II) and Hg(II) as nitrate in H_2O) (Sigma–Aldrich Química S.A., Madrid, Spain). Fe(II) stock solution (100 μg mL^{-1}) was prepared from ammonium iron(II) sulphate hexahydrate (Panreac, Barcelona, Spain) in water acidified with concentrated HNO_3. Working standard solutions of all the metals (100 μ g mL^{-1}) and (10 μ g mL^{-1}) were prepared by appropriate dilution in water. The chromogenic reagents used to prepare the metal ion sensitive films were: 4-(2-pyridylazo)resorcinol (PAR) and 5-[(3-carboxy-5-methyl-4-oxo-2,5-cyclohexadien-1-ylidene)(2,6-dichloro-3-sulfophenyl) methyl]-2-hydroxy-3-methylbenzoic acid trisodium salt (Chromazurol S, CS) from Merk; 3-(2-pyridyl)-5,6-diphenyl-1,2,4-triazine-4',4"-disulfonic acid sodium salt (Ferrozine, FER) and 1-(2-hydroxy-1-naphthylazo)-2-naphthol-4-sulfonic acid sodium salt (Calcon, CAL) from Fluka; 1-(2-pyridylazo)-2-naphthol (PAN); 2-carboxy-2'-hydroxy-5'-sulfoformazyl-benzene monosodium salt (Zincon, ZIN), Pyrocatecholsulfonphthalein (Pyrocatechol Violet, VP), 1-(4-nitrophenyl)-3-(4-phenylazophenyl)triazene (Cadion, CAD); Diphenylcarbazide (DPC), Dimethylglyoxime (DMG) and Diphenylthiocarbazone (Dithizone, DTZ) from Sigma- Aldrich.

The rest of the reagents used were: ethylene glycol, potassium tetrakis(4-chlorophenyl)borate (TCPB), Brilliant blue G, thiourea, sodium carbonate, ethanol, tetrahydrofuran (THF), isopropanol and low viscosity carboxymethylcellulose sodium salt (CMC), all purchased from Sigma–Aldrich. All reagents were of analytical reagent grade and were used without any further purification. All aqueous solutions

required were prepared in reverse-osmosis type quality water (Milli-RO 12 plus Milli-Q station (Millipore, Bedford, MA, USA), conductivity 18.2 mS).

Supports for the membrane and array printing were plastic supports like polyethylene terephthalate (PET), polystyrene, polyvinyl chloride (PVC), Mylar-type polyester (Goodfellow, Cambridge, UK); cellulosic support like nitrocellulose membranes and Whatman papers (Sigma-Aldrich) and nylon transfer membranes Biodyne A, Biodyne B, Biodyne C, Biodyne Plus and Nytran SPC all purchased from Pall (Pall Life Sciences, Ann Arbor, MI, USA).

Ink preparation and disposable array printing

The chemical inks were prepared from solutions in hydroalcoholic media of the above cited chromogenic reagents with viscosity, surface tension and pH adjusted to printer requirements (10-12 cPs viscosity; 28-33 dynes/cm surface tension; <100 ºC boiling point; >1 g cm^{-3} density; <0.2 μm particle size; 4-9 pH) (Table 1) with appropriate reagents according to Table 2. Viscometer Visco Basic Plus (Fungilab, Barcelona, Spain) and surface tensiometer Theta Lite Attension (Biolin Scientific AB, Stockholm, Sweden) were used to characterize the inks. The prepared inks were degassed after preparation by means of an ultrasonic bath to prevent dissolved gas, which inhibits jetting. The inks were filtered through a 0.2 μm filter before filling the cartridge and then maintained in vacuum for almost two hours after use for optimal jetting.

To prepare the array, the different prepared sensing inks were printed on the supports using a Fujifilm Dimatix DMP-2831 printer (Fujifilm Dimatix, Inc., Santa Clara, CA, USA). After printing, the array of sensing membranes was stored in a closed container at room temperature to enable low solvent evaporation and then kept in a dark place until use to avoid photo degradation.

Table 1. Physical properties of the sensing inks.

Sensing inks	Viscosity (cPs, 33°C)	Surface tension (dynes cm^{-1})	Density (g cm^{-3})
ZIN	7.9	37.48	1.010
VP/PAR	9.3	33.68	1.011
CS/CAL/PAN	12.7	32.88	1.015
FER	10.9	31.05	1.013

Image capture and processing

The change in color of the printed array was measured with a digital camera using the H coordinate of the HSV color space as the analytical parameter. To keep all the image-gathering conditions the same, a Cube Light Box was used (Figure 1).

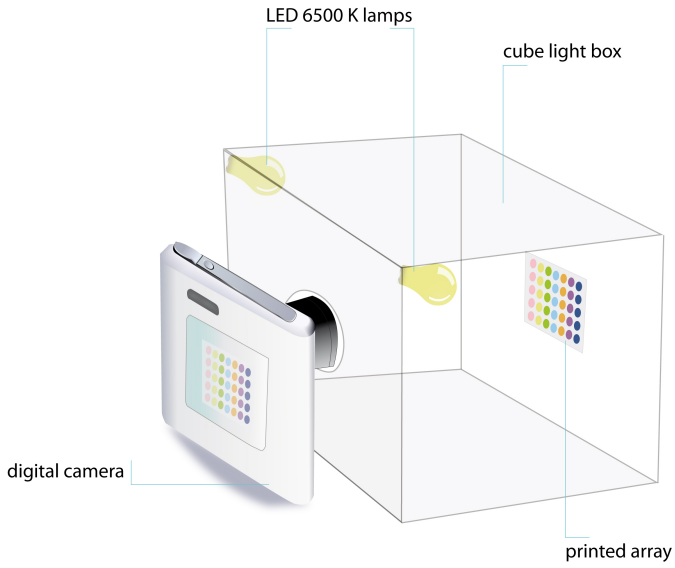

Figure 1. Cube light box.

The camera was placed in the front of a homemade white wooden box with two LED 6500 K lamps (placed at 45º with respect to the digital camera) with the array in a fixed position inside the box to be isolated from external light, a position that was maintained constant for all the experiments. For the image acquisitions and digitalization, a Canon PowerShot G12 camera (Canon Inc., Tokio, Japan) was used. All parameters of the camera were set and optimized. The setting conditions used to photograph the array were: macro, ISO 100, shutter speed 1/500s, aperture value f/4 and focal length of 6.1 mm.

To evaluate the color change of the printed array both before and after reacting with metal ion solution, a photograph of each array was taken in JPEG format. Then, the images were treated with Adobe Photoshop CS5 software to remove the areas containing no relevant information, using a negative image of the printed array, which plays the role of a mask. The images were processed with a set of scripts and functions developed by us in Matlab r2010b (MathWorks Inc., Natick, MA, USA). Each channel was normalized independently to calculate the RGB values, the H parameter of the HSV color space and their corresponding standard deviations.

Response array evaluation

The response of the arrays was evaluated using test solutions with pH adjusted with a 2 M ammonia buffer solution (pH 9.5). Test solutions were prepared either of individual metals at six concentrations ranging from 10^{-3} to 10^{-7} mol L^{-1} or of mixtures of 2–5 metals at individual concentration of 10^{-5} mol L^{-1}. The test mixtures with the adjusted pH were placed in 30 mL wide neck polyethylene containers (HDPE) along with a disposable array. After the containers were capped, they were shaken for 10 min on a vibrating agitator at 500 oscillations per minute at room temperature. Next, the arrays were pulled out of the solution, wiped to remove any

solution droplets and placed in the Cube Light Box for image acquisition. The sensing arrays were not conditioned before use.

Artificial neural network processing

Artificial neural networks (ANNs)[19] are composed of the interconnection of smaller information and processing units called neurons. They are powerful tools to solve tasks such as non-linear regression or classification.[20,21] The Multi-Layer Perceptron (MLP) neural network is the most known neural network model due to properties such as universal approximation, noise tolerance and generalization,[19] and it is the model we selected to develop our approach due to its good experimental results. In an MLP, the neurons are organized in layer sets. The output value of the i-th neuron at the l-th layer, $f_i^l(x_i^l)$, is computed as in equation (eq. 1), where x_i^l stands for the weighted sum of the neuron output values at the previous layer l-1 when l is an intermediate layer. On the other hand, x_i^l is the weighted sum of the network input values if l is the first layer, as equation (eq. 2) shows. In eq. 2, the value w_{ij}^l stands for the weight of the connection between the neuron j located at layer l-1 and neuron i located at layer l; the value b_i^l is a bias value for neuron i at layer l, and I_j^p is the j-th component of the input vector to the network of the sample pattern p. Finally N^l is the number of neurons at layer l.

$$f_i^l\left(x_i^l\right) = \frac{1}{1+e^{x_i^l}}; 1 \leq l < L \qquad \text{(Eq. 1)}$$

$$x_i^l = \begin{cases} \sum_{j=1}^{N^{l-1}} \left(W_{ij}^l I_j^{l-1}\right) + b_i^l & l = 1 \\ \sum_{j=1}^{N^{l-1}} \left(W_{ij}^l I_j^{l-1}(x_j^{l-1})\right) + b_i^l & 1 < l < L \end{cases} \qquad \text{(Eq. 2)}$$

The output neurons, located in the last network layer L, are in charge of providing the expected response to the input data vector. The function calculated by these neurons depends highly on the problem to be solved. For a classification problem with two classes 0/1 to be distinguished, eq. 2 may be used to calculate the network output, where an output value over the cut-off threshold 0.5 means that the network recognized the input data as class 1, and an output value under the cut-off threshold means that the network assigned the input data to class 0. Eq. 3 describes this example, where O (x_i^L) stands for the network output provided by network output neuron i.

$$O\left(x_i^L\right) = \begin{cases} 1 & f_i^L\left(x_i^L\right) > 0.5 \\ 0 & f_i^L\left(x_i^L\right) \geq 0.5 \end{cases} \quad \text{(Eq. 3)}$$

In addition, to solve other problems such as non-linear regression, the network output is usually a linear weighted aggregation of the neuron output values at the previous layer, plus a bias value. Eq.4 illustrates this idea.

$$O\left(x_i^L\right) = x_i^L \quad \text{(Eq. 4)}$$

The training of neural networks is a numerical optimization procedure of network weights w_{ij}^l and biases b_i^l, to minimize the error between network outputs and the training/calibration samples. The most used error measure for this purpose is the Mean Square Error (MSE) (eq. 5), where P is the number of calibration samples, N^L is the number of network outputs, and $D^p{}_i$ is the desired value for network output i at sample p. In the last decade, second order optimization methods and quasi-Newton algorithms have provided high accuracy in the training of neural networks.[22]

For this reason, in this paper we use the Levenberg-Marquardt method due to its high performance in previous works with respect to the classic methods.[22]

$$MSE = \frac{1}{P}\sum_{p=1}^{P}\sum_{i=1}^{N^L}(D_i^P - f_i^L(x_i^L))^2 \quad \text{(Eq. 5)}$$

ANNs are used in this approach to determine the presence or absence of 13 metal ions in solution and also to estimate the concentration of the detected metals. We use the color hue from 7 membranes $H=(h_1, h_2, ..., h_7)$ in a sensor array as analytical parameters. These parameters are input data for the classification of MLP neural networks, which return the presence or absence of the metals in a binary vector with 13 components $M=(m_i)$, $1\leq i\leq 13$. Each value m_i is 1 if the solution contains metal i, otherwise m_i is 0. Stage 1 in Figure 1 illustrates this idea. The Stage 1module is composed of 13 classification MLP neural networks, each one in charge of determining the value m_i for the concrete i-th metal ion. Thus, the calibration data for an MLP for the classification of metal i is composed of a set of samples ($h_1, h_2, ..., h_7, m_i$), where ($h_1, h_2, ..., h_7$) are the input analytical parameters and (m_i) is a 0/1 value to describe whether the sample contains the metal i (value 1) or not (value 0).

After determining the presence/absence of the 13 metal ions in the solution, a second stage is in charge of estimating the concentration of each detected metal in the solution. Stage 2 in Figure 2 illustrates this idea: The hue vectors H together with the vector M of the detected metals are the inputs for the non-linear regression MLP neural networks. As in stage 1, there are 13 MLPs, each one in charge of the concentration estimation of the i-th metal ion.

The whole system output $S=(s_i)$, $1\leq i\leq 13$, is a vector with the concentration of the 13 metals that are estimated by our approach. In this stage, the calibration data for an MLP for the concentration estimation of the metal i is composed of a set of samples ($h_1, h_2, ..., h_7, c_i$), where ($h_1, h_2, ..., h_7$) are the input analytical parameters and

(c_i) is a real value with the concentration of the metal i in the solution. In our approach, (c_i) is the concentration of the metal i in a log scale of molar concentration, since this preliminary data pre-processing provided us with the best results after experimental calibration.

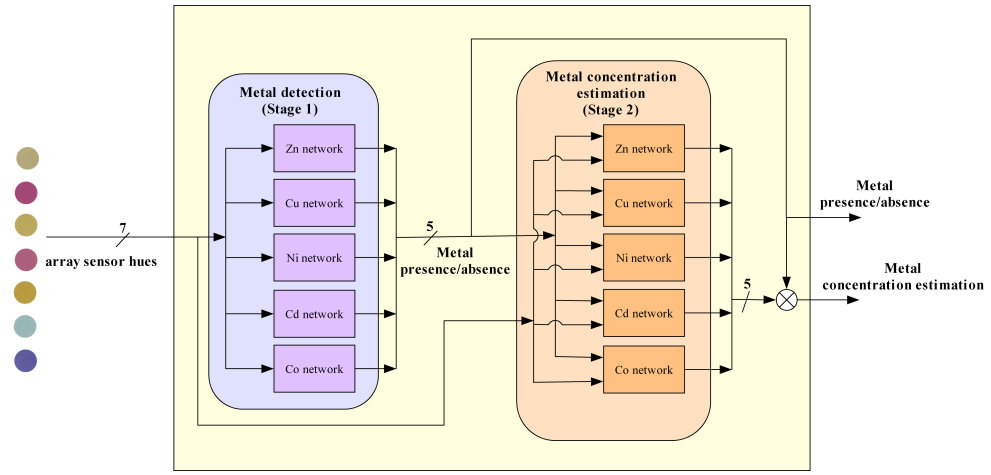

Figure 1. General design of approach for heavy metal detection and concentration estimation: Stage 1 detects metal concentration and Stage 2 computes the concentration estimation for the detected metals.

RESULTS AND DISCUSSION

Different types of optical arrays based on different chemistries have been proposed by our group for the quantitative analysis of common ions in water (K(I), Mg(II), hardness),[23] alkaline ions (Na(I), K(I)),[5,21] metal ions (Zn(II), Cu(II), Ni(II))[24] and pH in full range[25] using different imaging techniques: 1) CCD camera,[23] 2) reflection and transmission flatbed scanner,[5,21] 3) digital photographic camera[26] and 4) portable microcontroller-based system based on an OLED display and digital color

detectors,[27] to extract the color coordinates (RGB, HSV) used as the analytical parameter. One of the main limiting factors we found in previous studies in our group was the reproducibility of the optical array preparation, typically by spin coating and drop casting techniques, which produce membranes that are not fully homogeneous. In this paper we improve the ability of optical arrays to perform multianalyte analysis, preparing the optical arrays using an inkjet printing technique.

Inkjet printing is a maskless, drop-on-demand technique which deposits ink layers on flexible or rigid substrates with the advantages of short production times, a low cost and material savings, high spatial resolution, and good reproducibility, which are very interesting characteristics for the development of low-cost sensors.[28,29]

Chemical ink preparation

Chemical inks containing chromogenic reagents typically soluble in water were developed in this work for array preparation. Water-based printing is a desirable technology for industries and consumers who care about the environment and their impact. At the same time, they have advantages; they do not require additional dry and/or curing processes and therefore reduce manufacturing costs. In order to prepare chemical inks for array printing with high water content, their rheological properties at jetting temperature had to be controlled according to printer specifications.

As the inkjet inks developed in this work have a high proportion of water, the low viscosity (1.002 cP) and high surface tension of the water (72.75 dynes cm^{-1} at 20ºC), used as a solvent for chromogenic reagents was a problem in terms of correctly printing the sensing membranes. To solve this problem, isopropanol(21.7 dynes cm^{-1}) was added so that the pendent drop would have a suitable surface tension for appropriate inkjet printing.

Carboxymethylcellulose (CMC) was used not only to raise the viscosity to printer technical specifications but also to improve the adherence of the ink to the support. The use of this viscosity-increasing water-miscible agent stabilizes the mixture and facilitates the incorporation of chromogenic reagents to the sensing membrane. A low proportion of CMC (<1%) is used to raise the viscosity in order to prevent the obstruction of the nozzles. Additionally, its dispersing properties stabilize the ink composition, preventing particle aggregation processes, which can obstruct the nozzles. To completely achieve the required ink viscosity, we included ethylene glycol in the formulation, which also provides a high boiling point, preventing precipitation in the nozzles. To remove the possible undissolved >0.2 μm particles in the ink, which would block the nozzles, a filtration was carried out.

Selection of chromogenic reagents

The criteria used for the metal ion sensing elements containing colorimetric reagents include conditions of: a) no leaching or blooming; b) inclusion of commercially available metal-reagents with significant cross-reactivity; c) tonal color coordinate change by reaction; d) non-redundant information from different sensing elements; and e) printability and good adherence to the support.

The goal of this study was to prepare a set of sensing membranes for the analysis of metal ions based on color measurements. Eleven different conventional chromogenic reagents (PAN, PAR, FER, ZIN, CS, CAL, CAD, VP, DTZ, DPC, and DMG) were selected at first and a set of cocktails were prepared and tested containing different types and amounts of polymers, plasticizers, lipophilic salts, dispersing agents, humectants, water and solvents, if necessary. The membranes were prepared from selective and non-selective chromogenic reagents in order to achieve different selectivity patterns for the metal ions with no leaching over the entire concentration range studied, preventing secondary products and achieving strong

adherence to the support. In the case of the colorless Ferrozine membrane, Brilliant blue G dye is included to achieve a bitonal change by reaction (typically from blue to violet).

The composition of these sensor cocktails was optimized and only seven cocktails satisfied the rheological conditions for subsequent inkjet printing: ZIN, FER, PAN, PAR, CAL, VP and CS (Table 2).

The chromogenic reagents eliminated were DTZ, because of its photosensitivity and its sensitivity, which makes it reacts with the nozzle metal before it is put into contact with the problem solution. The reagents CAD, DPC and DMG were dismissed because the reactivity with different metal ions was not very informative with respect to the other reagents.

These seven reagents yielded membranes that gave the greatest color change in the presence of the selective analytes, providing enough discriminatory power for the purpose of this study. The final concentrations (moles Kg^{-1} polymer CMC) of the chromogenic reagents in the sensing membranes included in the array were: PAN (0.80), PAR (0.87), ZIN (0.28), CS (0.21), CAL (0.31), VP (0.52) and FER (0.25).

Selection of support

As mentioned above, the cocktails were prepared in hydro-alcoholic media. Different types of supports were tested for array printing. Initially, plastic substrates such as PET and PVC were used to prepare stable arrays; however they present problems like improper wettability, which requires the need for a pretreatment process such as plasma or corona to activate the surface. Absorbent supports, mainly cellulosic ones like nitrocellulose membranes, Whatman papers, offset papers or coated papers, show good drying by evaporation but little mechanical resistance to water or reaction with coatings, which precludes their use.

Table 2. Composition of the metal ion sensing inks.

Sensor membrane	Chromogenic reagent (%)	Membrane polymer (CMC%)	Humectant EG (%)	Lipophilic salt TCBP(%)	Brilliant Blue G (%)	Isopropanol (%)	EtOH (%)	THF (%)	H_2O (%)
1	PAR (0.10)	0.50	27.61	-	-	6.52	15.53	-	49.74
2	PAN (0.12)	0.59	33.10	-	-	7.81	18.62	-	39.75
3	ZIN (0.10)	0.49	27.14	-	-	-	15.27	-	57.04
4	CS (0.12)	0.60	33.11	-	-	7.81	18.63	-	39.77
5	CAL (0.12)	0.60	33.11	-	-	7.81	18.63	-	39.77
6	VP (0,10)	0.50	27.61	-	-	6.52	15.53	-	49.74
7	FER (0.13)	0.64	23.66	0.08	0.30	8.38	19.96	4.26	42.63

An alternative was the use of aliphatic polyamide synthetic fibers such as nylon, which can absorb hydro alcoholic solvents, does not present difficulties in drying and also offers suitable dimensional stability when submerged in water. Another advantage is that they have an excellent whiteness and smoothness, which allows for suitable colorimetric measurements.

Four commercial membranes, typically used as transfer membranes, were tested for printing (Biodyne A, Biodyne B, Biodyne C and Biodyne Plus), with Biodyne A presenting the best behavior not only for sensor membrane printing but also when reacting with aqueous metal ion solutions at different pH conditions. This membrane, made with amphoteric Nylon 6.6, is resistant to the ink solvents used in this work and has high versatility due to the presence of both negatively and positively charged groups, enabling it to bind both reagents and metallic complexes without leaching.

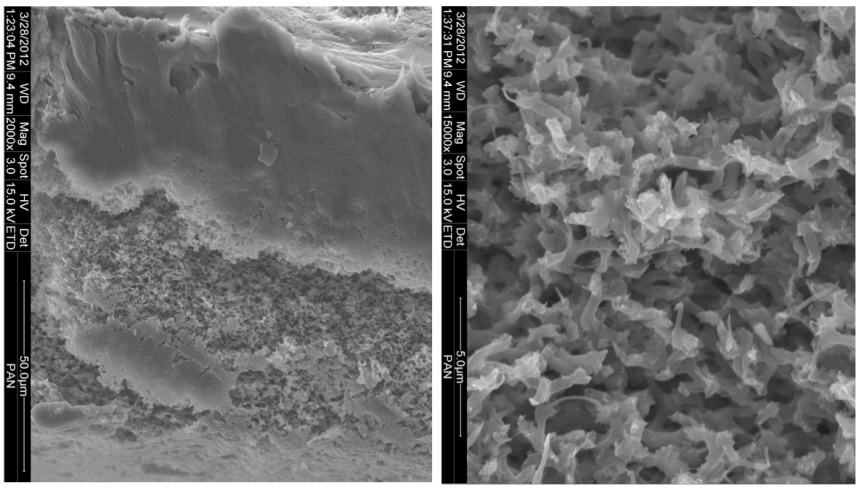

Figure 3. a) Cross section of ZIN membrane on the support. b) Biodyne A support.

The good adherence and structure of the sensing membrane prepared on nylon was evaluated by SEM techniques. As an example, Figure 3 shows a transversal cut

of the membrane containing Zincon.

Design of the array

The conditions to select the optimum sensor membrane size were: 1) colorimetric changes can be easily distinguished by the naked eye; and 2) it frames and focuses the array with the camera. To select the best size, a set of circular geometric shapes on the bit map screen was generated with size Ø 1-5 mm and printed with prepared inks.

Three different images of membranes using different resolutions were captured with the camera under the same conditions and treated with Photoshop to select the regions of interest.

The relation between the membrane size and the pixel number of the membrane image is presented in Table 3.

Table 3. Pixel number based on both image resolution and membrane size.

Resolution/size	1 mm	2 mm	3 mm	4 mm	5 mm
640 x 480	37	156	316	540	853
2816 x 2112	706	2842	6638	11930	18780
3648 x 2736	1086	4880	10.550	20.100	31.460

Membranes of Ø 3 mm were selected for their good perceptibility. Additionally and in order to maintain a balance between the color information required and to limit the size of the data storage, a resolution of 3648 x 2736 pixels was used to capture the images. The size selected as the sensor array diameter provided 10,550 pixels of color information.

Once the size was optimized, the final design of the array consists of 7 different sensing membranes printed in rows (1 (VP), 2 (ZIN), 3 (PAN), 4 (CAL), 5 (PAR), 6

(FER), and 7 (CS)) with 5 replicates each one printed in columns, producing a 35 membrane matrix, with the array size being 31 mm wide and 19 mm high and proportional to the image dimension.

To optimize the chemical ink and the substrate used, a 28 arrays matrix was printed on a 20 x 20 cm nylon sheet (Figure 4).

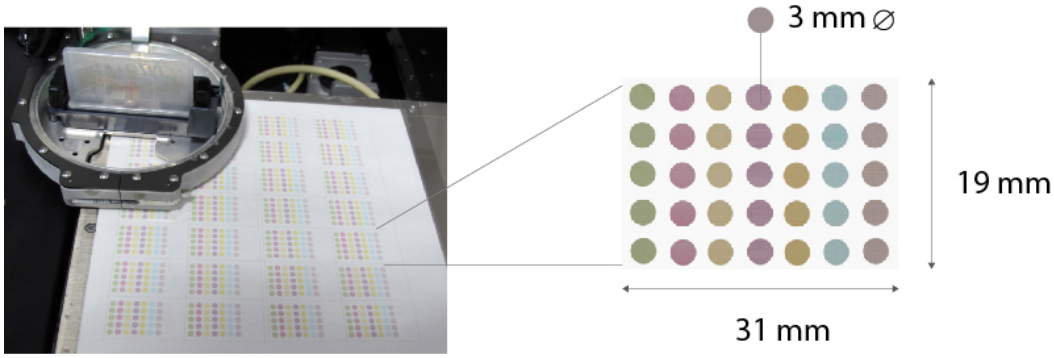

Figure 4. Sensor array design

Printed layer study

To find out the optimum amount of the sensing chemistry deposited on the substrate, the ink volume was studied. As the choice of the spacing between the centers of the drops is determined by the drop diameter deposited by the nozzles on the support, appropriate spacing prevents phenomena such as drop overlap or non-printed areas. In our case, the drop volume is 10 pL, so the volume of ink deposited in a 3 mm Ø circle was 0.35 µL per printing layer, calculated from the drop spacing on the surface and the drop number per surface (drops mm^{-2}).

To obtain a suitable colorimetric change by reaction without any leaching of the reagent on the substrate, a study to optimize the printing layers was required. To

select the optimum number of layers, six columns with 4 replicates of different numbers of layers (1-6 layers) of PV ink were printed on the support and reacted with 10^{-3} M Al (III) solution at pH 9.5 (Figure 5).

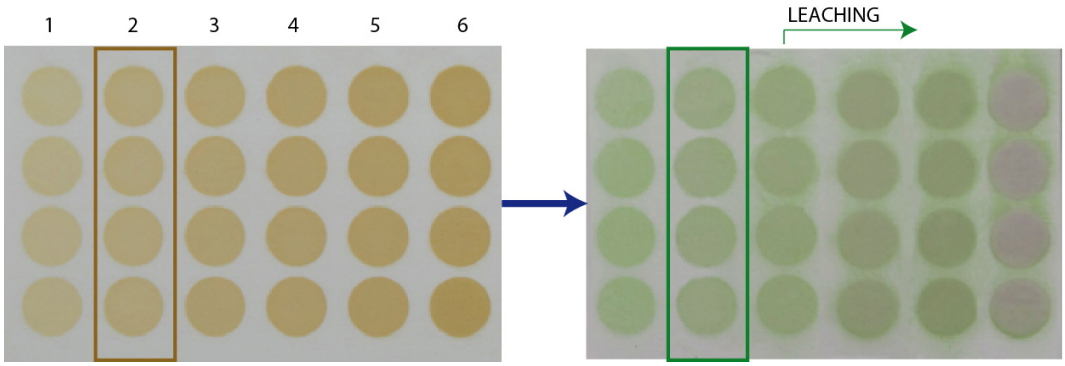

Figure 5. Printed layers study

Table 4 shows the evolution in the tonal coordinate H with printed layers. One layer is not enough to cover the surface of the support, producing a color mixed with the background.

A constant value was obtained from the second print layer. In addition, leaching was observed from the third layer and so the optimum volume was two printing layers.

Table 4. Evolution in tonal coordinate H of VP membrane with printed layers before and after reaction with Al (III).

Number of layers	Volume (µL)	H average blank	H average after reaction
1	0.35	0.137 ± 0.001	0.251 ± 0.003
2	0.70	0.126 ± 0.001	0.232 ± 0.003
3	1.05	0.127 ± 0.001	0.232 ± 0.005
4	1.40	0.122 ± 0.001	0.214 ± 0.004
5	1.75	0.122 ± 0.002	0.221 ± 0.007
6	2.10	0.120 ± 0.002	0.14 ± 0.02

Manufacturing array reproducibility

A crucial aspect in the design of a sensing array, mainly in colorimetric arrays that use a color coordinate as analytical parameter, is the reproducibility in the array fabrication, understood both as the reproducibility between different arrays and the homogeneity of each membrane that makes up the array.

This is the basis for increasing the discrimination ability of this analytical device along with the variation in the tonal coordinate between different reagents and reaction products.

The reproducibility of the array manufacturing process and reliability of each sensor was studied separately. Also, we compared the array preparation process by ink jetting with previous techniques.

Table 5. H parameter mode values of five replicates of the sensor membrane printed on three different sheets of nylon on three different printing days. Day 1.

Sensor membrane	Array 1	Array 2	Array 3	Array 4
VP	0.181±0.003	0.181±0.003	0.181±0.003	0.181±0.003
ZIN	0.913±0.001	0.913±0.001	0.913±0.001	0.913±0.001
PAN	0.146±0.001	0.146±0.001	0.146±0.001	0.146±0.001
CAL	0.94±0.01	0.937±0.001	0.94±0.01	0.94±0.01
PAR	0.143±0.003	0.143±0.004	0.143±0.004	0.143±0.004
FER	0.496±0.006	0.496±0.006	0.496±0.006	0.496±0.006
CS	0.842±0.006	0.842±0.006	0.842±0.006	0.842±0.006

To test the manufacturing reproducibility, 4 different arrays were printed, each one with the 7 sensing areas indicated and 5 replicates (Table 5-7).

Two of them were printed on the same sheet using the same ink (arrays A1 and A2), a third one on another sheet with the same ink (array A3), and a last one on

another different sheet with a different ink prepared separately from the first ink (array A4).

Table 6. H parameter mode values of five replicates of the sensor membrane printed on three different sheets of nylon on three different printing days. Day 2.

Array 5	Array 6	Array 7	Array 8
0.177±0.002	0.177±0.002	0.176±0.002	0.177±0.002
0.904±0.004	0.909±0.003	0.910±0.003	0.909±0.003
0.143±0.001	0.143±0.001	0.143±0.001	0.143±0.001
0.930±0.006	0.143±0.001	0.143±0.001	0.143±0.001
0.1373±0.0006	0.1372±0.0006	0.1372±0.0006	0.1374±0.0006
0.495±0.004	0.494±0.004	0.491±0.004	0.494±0.004
0.853±0.009	0.853±0.008	0.852±0.008	0.853±0.008

Table 7. H parameter mode values of five replicates of the sensor membrane printed on three different sheets of nylon on three different printing days. Day 3.

Array 9	Array 10	Array 11	Array 12
0.170±0.002	0.167±0.002	0.170±0.002	0.169±0.002
0.911±0.002	0.912±0.002	0.910±0.002	0.911±0.002
0.1409±0.0002	0.1410±0.0002	0.1412±0.00002	0.1411±0.0002
0.9349±0	0.9349±0	0.9349±0	0.9348±0
0.1371±0.0005	0.1372±0.0005	0.1373±0.0005	0.1372±0.0005
0.492±0.003	0.492±0.003	0.493±0.003	0.4923±0.003
0.847±0.003	0.847±0.003	0.847±0.003	0.846±0.003

Then they were imaged and the mode of the H of all the replicates of all the sensors were acquired and serialized into data arrays $A_i=(H^i_{11}, H^i_{12},\ldots, H^i_{15}, H^i_{21}, H^i_{22},\ldots, H^i_{25},\ldots, H^i_{sr},\ldots, H^i_{75})$, where H^i_{sr} is the H from array i, sensor s, replicate r. These 4 data distributions were compared using a paired t-test, to check if there were significant differences between each pair of arrays $\{A_i, A_j\}$ with the null hypothesis

that the data distribution A_i-A_j is mean 0 and with the same, but unknown, standard deviation.

Since none of the probability values at a 95% confidence level were under 0.05 ($p(A_1, A_2)=0.07$, $p(A_1, A_3)=0.15$, $p(A_1, A_4)=0.65$, $p(A_2, A_3)=0.15$, $p(A_2, A_4)=0.65$, $p(A_3, A_4)=0.30$), the null hypothesis was accepted and there are no significant differences between any pair of data distributions and thus, the ink preparation and substrate manufacturing process do not significantly influence the color response of the array.

To study the variability with respect to the color homogeneity inside each sensing area of the array, the previous H data was grouped into 7 distributions, $S_i= (H^1_{i1}, H^1_{i2},..., H^1_{i5}, H^2_{i1},..., H^2_{i5},..., H^a_{ir},..., H^4_{i5})$, $1\leq i\leq 7$, i.e. the H response of all the replicates and arrays of the same membrane, assuming that two values H^a_{ir} and H^b_{ir} belong to the same probability distribution resulting from the previous test. The variability between the two different sensors of the array, S_i and S_j, is compared by means of the H variability in the first sensor S_i with respect to the H variability of S_j. The homogeneity of each sensor response due to the fabrication is measured by the standard deviation of the H of the sensor with respect to the possible range for H ($std(S_j)/H_{range}$) (Table 5-7).

The Bertnett test at a 95% confidence level was used to check for significant differences between the variability of the H in two sensors with null hypothesis meaning that all the data distributions $\{S_1, S_2, ..., S_7\}$ have the same variance, casting a p-value lower than 10^{-16}, which means that some sensors are more sensitive than others. Sorting the sensors by precision and comparing the variability of the groups by pairs using a Bertnett test, 4 different groups of sensors were found: PAN and ZIN with the lowest variability (see Table 8, column 2); VP, FER and CAL with medium variability and PAR and CS with the highest variance in the response of the H value.

According to the results in Table 8, the average internal H variability of the array is 0.81% considering all sensors.

Finally, we validated the inkjet-printing array fabrication process with respect to previous approaches of drop casting that were used to build a full range optical pH sensing array.[25] The internal variability is compared in terms of standard deviation of the H values acquired from all the pixels in a sensor image for the array prepared by ink-printing (M1) and by drop casting (M2).

An unpaired t-test with a 95%confidence level for the two distributions M1 and M2 shows significant differences between H variation within a sensor using the methods M1 and M2 (p-value $<10^{-16}$).

The average standard deviation of H in a sensor using M1 is 0.004 and 0.12 for M2.

Thus, the ink-printing method provides more robust sensors considering the H response in comparison to conventional drop casting procedures.

Table 8. Bertnett test results and sensor sorting according to internal H variability; (+) refers to statistical differences found between the variability of the sensors and (-) if there were none.

Sensor	Internal H variability (%)	Compared to	Bertnett test (p-value)	Statistical Significance
PAN	0.23	PAN	1	(-)
ZIN	0.28	PAN	0.36	(-)
VP	0.41	PAN	0.01	(+)
FER	0.50	VP	0.41	(-)
CAL	0.53	VP	0.28	(-)
PAR	0.86	VP	0.002	(+)
CS	2.88	PAR	$2.28\ 10^{-6}$	(+)

Response array evaluation

The pH dependence on the reaction and retention of ion metals on the array was studied in the pH range from 3 to 12. The highest response and discrimination against the target metal ions was obtained at pH 9.5. A longer reaction time (over 30 min) increased, as usual, the optical response, but some leaching from the membrane was observed for reaction times longer than 10 min. Therefore, a reaction time of 10 min was used for all sensing membranes.

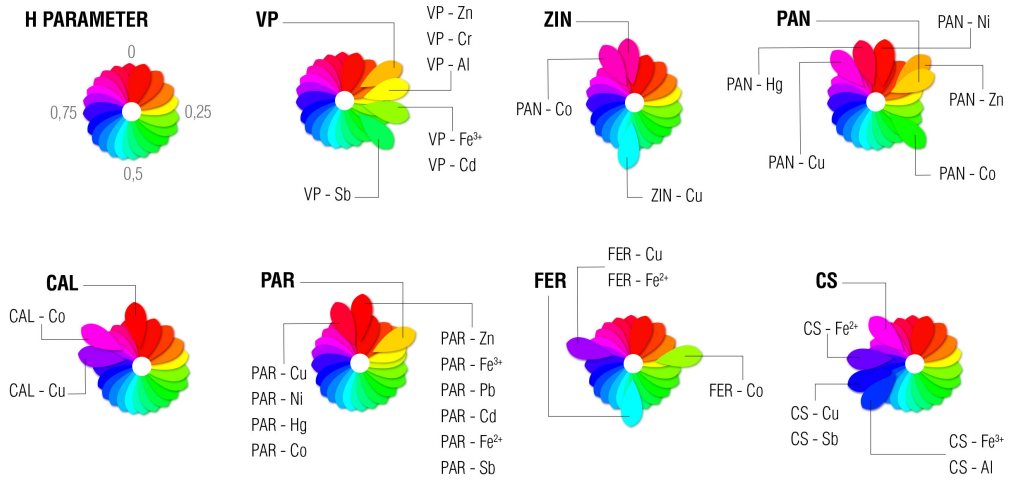

Figure 5. Infographics of sensing array reactivity against target metal ions.

In order to study the evolution of the color coordinate H with the metal ion for each sensing membrane and the dependence of the color coordinate H with the concentration of different metal ions for the different reagents included in the array, working solutions from 10^{-3} to 10^{-7} M of different metal ions were prepared by appropriate dilution of each standard stock solution. Corresponding blank solutions containing no analyte were prepared in the same way. After equilibration with the array, imaging and H measurements were carried out according to the procedure

described above. The change in the tonal coordinate H by reaction with the metal ions is shown in Figure 5 for each membrane and each cation studied and the data is presented in Table 9.

In a second step, a set of solutions was prepared containing Zn(II), Cu(II), Ni(II), Cd(II) and Co(II) in different ratios, namely 5 solutions containing only one metal, 8 mixtures of two metals, 9 mixtures with three metals, 5 mixtures with four metals and 1 mixture with all of the metals. Each metal concentration was fixed at 10^{-5} M. The criterion followed the response of each sensor for each metal. The concentration value was selected at 20% of the sigmoid curve.

ANN calibration for metal ion classification (stage 1)

A data set composed of 65 arrays (7 sensors in each array) was used to calibrate (70%), test (15%) and validate (15%) the classification of the MLP neural networks for the detection of the presence/absence of 13 metal ions. The experimental samples contain only one metal in each case and cover the concentration range 10^{-3} to 10^{-7} M, as well as control measurements without metals. There are 5 replicates for each experimental setting (455 data). The 65 arrays were serialized to have the structure (h_1, h_2, ..., h_7, m_{Zn}, m_{Cu}, m_{Ni}, m_{Fe3+}, m_{Pb}, m_{Cd}, m_{Cr}, m_{Hg}, m_{Al}, m_{Fe2+}, m_{Co}, m_{Mn}, m_{Sb}), which are the H parameters provided by the array, and the presence value (1) or absence value (0) of each metal in the sample, used as inputs/outputs for the neural network.

The values m_i are calculated using a concentration cut-off value τ, as shown in eq. 6. Samples that contain a concentration of metal I greater or equal to τ are assumed to contain metal i (m_i= 1), and those samples where the concentration of metal i is under τ are not assumed to contain any i-th metal concentration (m_i= 0).

Table 9. Change in H value of sensing array by reaction with metals

Sensor	H_0	H_{Zn}	H_{Cu}	H_{Ni}	H_{Fe3+}	H_{Pb}	H_{Cd}	H_{Cr}	H_{Hg}	H_{Al}	H_{Fe2+}	H_{Co}	H_{Mn}	H_{Sb}
VP	0.181	0.225	0.192	0.174	0.240	0.191	0.240	0.212	0.189	0.228	0.172	0.197	0.204	0.392
ZIN	0.913	0.905	0.547	0.908	0.927	0.907	0.905	0.906	0.911	0.907	0.905	0.883	0.908	0.903
PAN	0.146	0.112	0.856	0.011	0.120	0.139	0.138	0.143	0.961	0.141	0.106	0.324	0.138	0.128
CAL	0.940	0.937	0.766	0.925	0.967	0.928	0.925	0.928	0.925	0.926	0.933	0.848	0.928	0.929
PAR	0.143	0.017	0.970	0.954	0.086	0.096	0.094	0.131	0.976	0.128	0.060	0.995	0.119	0.065
FER	0.496	0.440	0.748	0.5	0.417	0.492	0.424	0.471	0.497	0.477	0.722	0.229	0.441	0.493
CS	0.842	0.867	0.689	0.838	0.606	0.837	0.851	0.847	0.861	0.647	0.739	0.860	0.850	0.676

Thus, the value τ may be considered as the detection limit of our system. We experimentally calculated the value of $\tau = 10^{-5}$ M as the minimum concentration value that provided us with suitable results for the detection of all of the metals for almost all the metal ions considered, except for Pb(II) ($\tau = 10^{-3}$ M), Cr(III) and Mn(II) ($\tau = 10^{-4}$ M).

$$B_x = \begin{cases} 1 & [x] \geq \tau \\ 0 & [x] < \tau \end{cases} \quad \text{(Eq. 6)}$$

We trained 13 different classification neural networks, one for each metal i, with data patterns (h_1, h_2, ..., h_7, m_i) coming from the calibration data. The first 7 values were used as inputs and the remaining one as the desired output. Each network was trained using the Levenberg-Marquardt optimization algorithm, using cross-validation 100 times. The training parameters used 1000 iterations of the algorithm as the primary stopping criterion or reaching an MSE of 0.01 in training data as a secondary stopping criterion.

Table 10 summarizes the results obtained in calibration, test and validation data sets for the determination of the presence/absence of the 13 metals, where PP stands for the samples that contain the corresponding metal and the network hits, NN is used for the samples that do not contain the corresponding metal and the network hits, PN encompasses the samples that contain the metal ion but the network fails in its classification, and NP is for the samples than do not contain the metal but the network recognizes its presence.

In Table 10, the first column shows the analyzed metal, column 2 describes the threshold τ used for experimental calibration and columns 3-6, 7-10, 11-14 are the calibration, test and validation results, respectively.

Table 10. Summary of single metal ion detection in samples. Column 2: cut-off value (Molar concentration) to distinguish between presence or absence of metal concentration; Columns 3-14: % of samples in calibration, test and validation data containing metal that are correctly classified (PP), % of samples containing metal that are not correctly classified (PN), % of samples with no metal that are correctly classified (NN), % of samples with no metal that are not correctly classified (NP); Column 15: Average success in detection of positive and negative samples.

Metal	τ	Calibration				Test				Validation				Mean
		PP	PN	NP	NN	PP	PN	NP	NN	PP	PN	NP	NN	Success
		(%)	(%)	(%)	(%)	(%)	(%)	(%)	(%)	(%)	(%)	(%)	(%)	(%)
Zn(II)	10^{-5}	100	0	100	0	100	0	100	0	100	0	100	0	100
Cu(II)	10^{-5}	100	0	100	0	100	0	100	0	100	0	100	0	100
Ni(II)	10^{-5}	100	0	100	0	100	0	100	0	100	0	100	0	100
Fe(III)	10^{-5}	100	0	100	0	100	0	100	0	100	0	100	0	100
Pb(II)	10^{-5}	85.7	14.3	100	0	66.7	33.3	100	0	33.3	66.7	98.5	1.5	98.7
	10^{-4}	100	0	99.7	0.3	100	0	100	0	0	100	98.5	1.5	99.1
	10^{-3}	100	0	99.4	0.6	100	0	100	0	100	0	98.5	1.5	99.3
Cd(II)	10^{-5}	100	0	100	0	100	0	100	0	100	0	97	3	99.6
Cr(III)	10^{-5}	76.9	23.1	100	0	100	0	100	0	80	20	100	0	99.1
	10^{-4}	100	0	100	0	100	0	100	0	100	0	100	0	100
Hg(II)	10^{-5}	100	0	100	0	100	0	100	0	100	0	100	0	100
Al(III)	10^{-5}	100	0	100	0	100	0	100	0	100	0	100	0	100
Fe(II)	10^{-5}	100	0	100	0	100	0	100	0	100	0	98.5	1.5	99.8
Co(II)	10^{-5}	100	0	100	0	100	0	100	0	100	0	100	0	100
Mn(II)	10^{-5}	91.7	8.3	100	0	75	25	100	0	25	75	98.4	1.6	98.7
	10^{-4}	100	0	100	0	100	0	100	0	100	0	100	0	100
Sb(III)	10^{-5}	100	0	100	0	100	0	100	0	100	0	100	0	100

Finally, column 15 summarizes the hits of metal discrimination for the given threshold τ. According to Table 10, we obtained an average success in the classification of samples containing a metal of over 99.3 %. We also included the experiments for threshold calculation for those metals with τ over 10^{-5} M. In summary, 10 of the 13 metal ions can be determined with no error. We also note that all errors are false negatives for those metals that cannot be distinguished completely,

i.e. samples that do not contain any metal concentration but the system detects the presence of metal ions.

Feasibility of detection and quantification of metal concentration in mixtures (stage 2)

Once we showed the feasibility of detecting 13 metals with our approach, we went a step further and tested our proposal in samples containing mixtures of different metals.

We selected mixtures of up to 5 metals for this experimentation as a proof of concept (Zn(II), Cu(II), Ni(II), Cd(II), and Co(II)). More specifically, we did the experimentation with 8 different combinations of 2-metal samples, 9 of 3-metal samples, 5 of 4-metal samples and 1 of 5-metal samples, in all cases at 10^{-5} M, to perform experiments that show the feasibility of detecting the metals in mixtures and discover whether the concentration value of each one can be determined.

The result was a data set containing 115 mixture samples, including replicates, plus the data from samples containing different concentrations of a single metal used in the previous section. The data set was split into calibration (70%), test (15%) and validation (15%) data. A classification MLP neural network with 7 inputs (coming from the color hue parameter from each sensor in the array) and 1 output for the detection of each metal in the sample was trained separately using the methodology previously described. These neural networks are in charge of classifying the presence/absence of metal ions in samples, according to Stage 1 in Figure 1. Table 11 describes the results for metal ion detection in mixtures, and the notation of this table is the same as the one provided for Table 5.

Table 11 shows that 3 of 5 metals may be completely distinguished in mixture samples regardless of the number of metals in the solution. Zn(II) and Cd(II) cannot be fully determined, but the hit success exceeds 90% in all calibration, test and

validation data sets obtaining a classification success percentage of 98.4% and 98.1%, respectively.

Table 11. Summary of metal ion detection in mixtures: Columns 2-13: % of samples in calibration, test and validation data containing metal that are correctly classified (PP), % of samples containing metal that are not correctly classified (PN), % of samples with no metal that are correctly classified (NN), % of samples with no metal that are not correctly classified (NP); Column 14: Average success in detection of positive and negative samples.

Metal	Calibration				Test				Validation				Mean
	PP (%)	PN (%)	NP (%)	NN (%)	PP (%)	PN (%)	NP (%)	NN (%)	PP (%)	PN (%)	NP (%)	NN (%)	Success (%)
Zn(II)	98.4	1.6	99.4	0.6	100	0	93.5	6.5	100	0	97.1	2.9	98.4
Cu(II)	100	0	100	0	100	0	100	0	100	0	100	0	100
Ni(II)	100	0	100	0	100	0	100	0	100	0	100	0	100
Cd(II)	97.1	2.9	100	0	91.7	8.3	100	0	92.9	7.1	93.9	6.1	98.1
Co(II)	100	0	100	0	100	0	100	0	100	0	100	0	100

After the determination of the presence/absence of metal ions, the next step was to calculate the concentration value of the detected metals in a sample, according to Stage 2 in Figure 1. Non-linear regression MLP neural networks were trained with this purpose, one for each metal. Each network had 13 input values (h_1, h_2, …, h_7, m_{Zn}, m_{Cu}, m_{Ni}, m_{Cd}, m_{Co}): 7 H parameters and the presence (value 1) or absence (value 0) of each metal i in the solution, m_i calculated in Stage1. Each network was matched with a metal and had a single output value, which is an estimation of the concentration of its corresponding metal in a sample. The same data set proposed for the detection of the presence/absence of metals was used for calibration (70% of data), test (15%) and validation (15%). The training procedure for these non-linear regression MLP neural networks had the same experimental settings as that for classification MLP and cross-validation was also applied 100 times. Table 12 describes the results obtained for the concentration estimation of Zn(II), Cu(II),

Ni(II), Cd(II) and Co(II), assuming that Stage 1 is able to detect the metals in the solutions without fail.

Table 12. Summary for estimation of heavy metal concentration in mixture samples. Columns 2-10: Mean error (M.E.), standard deviation of error (S.D.), and maximum error found in a sample (Max. E.), in log (molar concentration), for calibration, test and validation data.

Metal	Calibration			Test			Validation		
	M.E. (log C_M)	S.D. (log C_M)	Max.E. (log C_M)	M.E. (log C_M)	S.D. (log C_M)	Max.E. (log C_M)	M.E. (log C_M)	S.D. (log C_M)	Max.E. (log C_M)
Zn(II)	0.010	0.025	0.181	0.020	0.078	0.510	0.021	0.072	0.359
Cu(II)	0.004	0.010	0.078	0.004	0.010	0.058	0.002	0.005	0.023
Ni(II)	0.005	0.019	0.181	0.018	0.064	0.293	0.010	0.038	0.241
Cd(II)	0.022	0.069	0.506	0.019	0.057	0.337	0.020	0.056	0.259
Co(II)	0.001	0.002	0.020	0.013	0.056	0.353	0.090	0.545	3.732

According to Table 12, the proposed model is able to provide an estimation of metal concentration with an average precision lower than a decimal unit with respect to the real molar concentration. Thus, if a sample contains a metal concentration of $1.0 \cdot 10^{-4}$ M, then the system error is $1.0 \cdot 10^{-5}$ M on average. More specifically, the average error for Zn(II) is 0.02±0.07 log(M), for Cu(II) is 0.004±0.01 log(M), for Ni(II) is 0.02±0.06 log(M), for Cd(II) is 0.02±0.06 log(M) and for Co(II) is 0.01±0.54 log(M). The maximum mean error occurs with Zn(II) and Cd(II), and the lowest with Cu(II). It is also important to note the maximum error for Co(II) in validation. In this sample, the system generated a predicted concentration value for a sample that did not contain any concentration of Co(II), so that the prediction error is high. To avoid this situation, the integration of Stages 1 and 2 in our approach helps to determine the absence of this metal in the sample in Stage 1, so that the whole system does not produce this type of error for the concentration determination in Stage 2. The following section discusses the results obtained using both stages.

Discussion of the application of stage 1 and stage 2 simultaneously

This section presents the results of the system performance when both Stages 1 and 2 were applied simultaneously to provide metal ion detection and concentration estimation in samples. In the first stage, classification information on the presence/absence of metal ions is provided. According to Table 11, all the metals but Zn(II) and Cd(II) can be determined with 100% success. For Zn(II), we obtained an average success of 98.4%, and 98.1% success for Cd(II).

Thus, for the remaining 1.6% and 1.9% of cases in which the metal presence is not suitably detected, this error is translated to the second stage for the estimation of error concentration. The estimation of metal concentration is limited to the discrimination of the presence of suitable metals in Stage 1. Figure 6 helps to support this conclusion, where a high error rate is observed for those solutions that were not correctly classified, and high accuracy for the ones where the metals were identified successfully.

This is also the reason for the standard deviation increases in the prediction accuracy. It is easy to distinguish false positives and false negatives in this figure, for the cases of Zn(II) and Cd(II), due to an unsuitable discrimination in Stage 1.

In addition, the errors occurring in the estimation stage may be self-corrected by our approach using the information of the presence/absence of metals in Stage 1. This is the case with the maximum validation error for Co(II), which was drastically reduced after the combination of both stages in the approach.

Table 13 supports the data shown in Figure 1 and describes the error provided by our system when both stages are used simultaneously. The table shows the errors in samples containing 1 to 5 metals, as a support for the experiments carried out in the previous sections and support for Tables 10 and 11.

According to our previous reasoning, mean and maximum error increases in Zn(II) and Cd(II) due to false positives/negatives and they are reduced in Co(II).

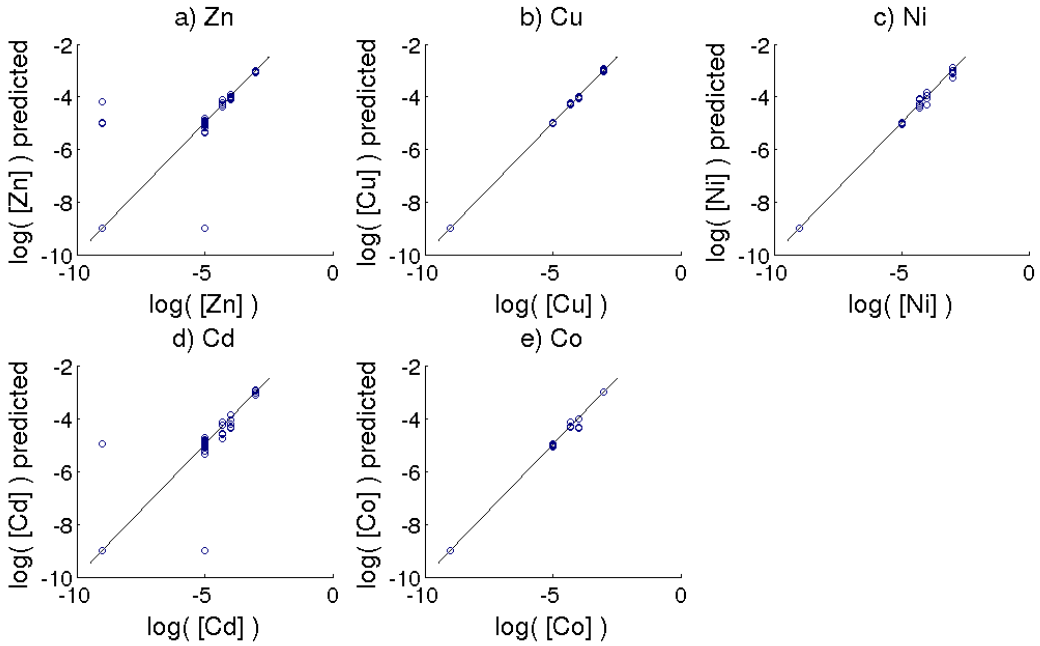

Figure 6. Outliers in Zn(II) and Cd(II) classification and regression line for the concentration estimation of mixture samples: a) Zn(II); b) Cu(II); c) Ni(II); d) Cd(II); e) Co(II).

To validate our conclusions, we applied statistical tests to verify the correlation of reference and predicted metal concentration values for those cases with no classification error in Stage 1. Thus, we obtained a determination coefficient R^2=0.99 for Zn(II) data, R^2=1 for Cu(II), R^2=0.99 for Ni(II), R^2=0.99 for Cd(II), and R^2=0.99 for Co(II). In addition, we checked the bias coefficient and slope of the regression line [X]'=A*[X]+B, where [X]' stands for the predicted concentration values and [X] for the reference ones, to test whether the system experiences systematic errors.

Table 13. Summary of approach performance for determination of presence/absence of metal ions in mixtures and estimation of detected metal concentrations: Column 1: number of metals in sample; Column 2: % success in detecting metal ion concentration in samples, mean error of estimation error for detected metal concentration (M.E.), standard deviation of estimation error (S.D.), and maximum error found in a sample estimation (Max. E.); Columns 3-7: results for each metal analyzed.

Metals in sample	Results	Zn(II)	Cu(II)	Ni(II)	Cd(II)	Co(II)
1	% Detection	99	100	100	98.5	100
	M.E. (log C_M)	0.053	0.003	0.009	0.058	0.005
	S.D.(log C_M)	0.442	0.011	0.041	0.403	0.036
	Max. E. (log C_M)	0.053	0.003	0.009	0.058	0.005
2	% Detection	100	100	100	97.5	100
	M.E. (log C_M)	0.018	0.006	0	0.118	0.001
	S.D.(log C_M)	0.036	0.008	0.001	0.638	0.001
	Max. E. (log C_M)	0.018	0.006	0	0.118	0.001
3	% Detection	93.3	100	100	97.8	100
	M.E. (log C_M)	0.282	0.005	0.003	0.107	0.004
	S.D.(log C_M)	1.007	0.007	0.006	0.594	0.011
	Max. E. (log C_M)	0.282	0.005	0.003	0.107	0.004
4	% Detection	100	100	100	96	100
	M.E. (log C_M)	0.014	0.005	0.011	0.185	0.005
	S.D.(log C_M)	0.013	0.006	0.011	0.796	0.009
	Max. E. (log C_M)	0.014	0.005	0.011	0.185	0.005
5	% Detection	100	100	100	100	100
	M.E. (log C_M)	0.038	0.007	0.02	0.026	0.001
	S.D.(log C_M)	0.03	0.015	0.02	0.009	0.001
	Max. E. (log C_M)	0.038	0.007	0.02	0.026	0.001
Average results	% Detection	98.4	100	100	98.1	100
	M.E. (log C_M)	0.047	0.002	0.004	0.051	0.002
	S.D.(log C_M)	0.381	0.007	0.023	0.37	0.021
	Max. E. (log C_M)	0.047	0.002	0.004	0.051	0.002

For this analysis, we obtained the parameters [Zn(II)]'= 0.99 ·[Zn(II)]-0.0003; [Cu(II)]'= 1.0006 ·[Cu(II)]+0.006; [Ni(II)]'= 0.99 ·[Ni(II)]-0.009, [Cd(II)]'= 0.99 ·[Cd (II)]-0.02; and [Co(II)]'= 0.99 ·[Co(II)]-0.03.

In all cases, we verified that the slope of the regression line is close to value 1 and the bias value is close to 0. Therefore, we can state that the calibrated approach does not suffer from systematic errors and is able to provide an accurate prediction of the metal ion concentration in the mixture samples.

CONCLUSIONS

A simple, convenient and rapid color-based sensor array for the identification and determination of metal ions is presented. The method is based on a disposable 31 mm x 19 mm nylon membrane with 35 sensing areas with 7 commercial chromogenic reagents prepared by inkjet printing. The change in color after reaction during 10 min with a sample of water and measurement with a photographic camera is evaluated by the tonal color coordinate H of the HSV color space. The high reproducibility in the fabrication of the sensing array (average precision error 0.81%) makes is possible to identify up to 13 metal ions in aqueous solutions.

A two-stage approach based on neural networks was designed to both detect the presence of metal ions in a mixture and estimate the existing metal concentration. In the first stage, the approach determines which metals are in the sample with a minimum success of 98.1%. This hit percentage is limited to a precision cut-off concentration value of 10^{-5} M for the existing metals. In the second stage, the hue parameters and the results of the determination step are used to estimate the concentration of each metal in the solution, with the average precision lower than a decimal unit with respect to the real molar concentration. Statistical tests were applied to validate the model over real data and a high correlation was obtained

between the reference and predicted heavy metal concentrations. Ongoing work suggests that further development will lead to a truly portable functional handheld device that will be reported in a future study.

REFERENCES

1. Duffus, J. H. Heavy metals- A meaningless term?Pure Appl. Chem.2002,74 (5), 793-807.

2. EPA Clean Water Act;Code of Federal Regulations at 40 CFR 401.15; 72.

3. Vlasov, Y.; Legin, A.; Rudnitskaya, A.; Di Natale, C.; D'Amico, A. Nonspecific sensor arrays (electronic tongue) for chemical analysis of liquids: (IUPAC technical report). Pure Appl. Chem.2005,77 (11), 1965-1983.

4. Ciosek, P.; Wroblewski, W. Sensor arrays for liquid sensing - electronic tongue systems. Analyst2007,132 (10), 963-978.

5. Erenas, M. M.; Piñeiro, O.; Pegalajar, M. C.; Cuellar, M. P.; de Orbe Paya, I.; Capitan-Vallvey, L. F. A surface fit approach with a disposable optical tongue for alkaline ion analysis. Anal. Chim. Acta2011,694 (1-2), 128-135.

6. Bourgeois, W.; Romain, A. C.; Nicolas, J.; Stuetz, R. M. The use of sensor arrays for environmental monitoring: interests and limitations. J. Environ. Monit.2003,5 (6), 852-860.

7. Feng, L.; Zhang, Y.; Wen, L.; Chen, L.; Shen, Z.; Guan, Y. Discrimination of Trace Heavy-Metal Ions by Filtration on Sol-Gel Membrane Arrays. Chem. --Eur. J.2011,17 (4), 1101-1104, S1101-1.

8. Mayr, T.; Liebsch, G.; Klimant, I.; Wolfbeis, O. S. Multi-ion imaging using fluorescent sensors in a microtiterplate array format. Analyst2002,127 (2), 201-203.

9. Mayr, T.; Igel, C.; Liebsch, G.; Klimant, I.; Wolfbeis, O. S. Cross-Reactive Metal Ion Sensor Array in a Micro Titer Plate Format. Anal. Chem.2003,75 (17), 4389-4396.

10. Niu, L. Y.; Li, H.; Feng, L.; Guan, Y. S.; Chen, Y. Z.; Duan, C. F.; Wu, L. Z.; Guan, Y. F.; Tung, C. H.; Yang, Q. Z. BODIPY-based fluorometric sensor array for the highly sensitive identification of heavy-metal ions. Anal. Chim. Acta2013,775, 93-99.

11. Palacios, M. A.; Wang, Z.; Montes, V. A.; Zyryanov, G. V.; Anzenbacher, P. Rational Design of a Minimal Size Sensor Array for Metal Ion Detection. J. Am. Chem. Soc.2008,130 (31), 10307-10314.

12. Wang, Z.; Palacios, M. A.; Anzenbacher, P. Fluorescence Sensor Array for Metal Ion Detection Based on Various Coordination Chemistries: General Performance and Potential Application. Anal. Chem.2008,80 (19), 7451-7459.

13. Palacios, M. A.; Wang, Z.; Montes, V. A.; Zyryanov, G. V.; Hausch, B. J.; Jursikova, K.; Anzenbacher, J. Hydroxyquinolines with extended fluorophores: arrays for turn-on and ratiometric sensing of cations. Chem. Comm.2007,36, 3708-3710.

14. Hossain, S. M. Z.; Brennan, J. D. b-Galactosidase-Based Colorimetric Paper Sensor for Determination of Heavy Metals. Anal. Chem.2011,83 (22), 8772-8778.

15. Feng, L.; Li, X.; Li, H.; Yang, W.; Chen, L.; Guan, Y. Enhancement of sensitivity of paper-based sensor array for the identification of heavy-metal ions. Anal. Chim. Acta2013,780, 74-80.

16. Feng, L.; Li, H.; Niu, L. Y.; Guan, Y. S.; Duan, C. F.; Guan, Y. F.; Tung, C. H.; Yang, Q. Z. A fluorometric paper-based sensor array for the discrimination of heavy-metal ions. Talanta2013,108, 103-108.

17. Cantrell, K.; Erenas, M. M.; Orbe-Paya, I.; Capitán-Vallvey, L. F. Use of the Hue Parameter of the Hue, Saturation, Value Color Space as a Quantitative Analytical Parameter for Bitonal Optical Sensors. Anal. Chem.2010,82 (2), 531-542.

18. Rezaei, B.; Hadadzadeh, H.; Azimi, A. Nickel(II) Selective PVC-Based Membrane Sensor Using a Schiff Base. Intern. J. Spec.2011,2011 (Article ID 746372), 7 pages.

19. Haykin, S. Neural Networks: A comprehensive foundation; Prentice Hall: Upper Saddle River, NJ, USA, 1999.

20. Cuellar, M. P.; Capel-Cuevas, S.; Pegalajar, M. C.; de Orbe-Paya, I.; Capitán-Vallvey, L. F. Minimization of sensing elements for full-range optical pH device formulation. New J. Chem.2011,35 (5), 1042-1053.

21. Erenas, M. M.; Pegalajar, M. C.; Cuellar, M. P.; de Orbe Paya, I.; Capitan-Vallvey, L. F. Disposable optical tongue for alkaline ion analysis. Sens. Actuators B2011,156 (2), 976-982.

22. Cuellar, M. P.; Delgado, M.; Pegalajar, M. C. An application of non-linear programming to train recurrent neural networks in time series prediction problems. Proc.International Conference on Enterprise and Information Systems: Miami, FL, USA, 2005; pp 35-42.

23. Lapresta-Fernandez, A.; Huertas, R.; Melgosa, M.; Capitán-Vallvey, L. F. Multianalyte imaging in one-shot format sensors for natural waters. Anal. Chim. Acta2009,636 (2), 210-217.

24. Ariza-Avidad, M.; Cuellar, M. P.; Salinas-Castillo, A.; Pegalajar, M. C.; Vukovic, J.; Capitan-Vallvey, L. F. Feasibility of the use of disposable optical tongue based on neural networks for heavy metal identification and determination. Anal. Chim. Acta2013,783 (0), 56-64.

25. Capel-Cuevas, S.; Cuellar, M. P.; De Orbé Payá, I.; Pegalajar, M. C.; Capitán-Vallvey, L. F. Full-range optical pH sensor based on imaging techniques. Anal. Chim. Acta2010,681 (1-2), 71-81.

26. Lapresta-Fernandez, A.; Capitán-Vallvey, L. F. Multi-ion detection by one-shot optical sensors using a color digital photographic camera. Analyst2011,136 (19), 3917-3926.

27. Lopez Ruiz, N.; Ariza-Avidad, M.; Martinez-Olmos, A.; Vukovic, J.; Palma, A. J.; Capitan-Vallvey, L. F. Handheld colorimeter for determination of heavy metal concentrations. J. Phys. : Conf. Ser.2011,307, 012037-1-012037/6.

28. Ando, B. Inkjet Printing: A Real Opportunity for the Next Generation of Low-Cost Sensors. IEEE Instrumentation & Measurement Magazine2013,16 (3), 44-48.

29. Derby, B. Inkjet printing of functional and structural materials: fluid property requirements, feature stability, and resolution. Annu. Rev. Mater. Res.2010,40, 395-414.

INKJET-PRINTED DISPOSABLE METAL COMPLEXING INDICATOR-DISPLACEMENT ASSAY FOR SULFIDE DETERMINATION IN WATER

ABSTRACT

A sulfide selective colorimetric metal complexing indicator–displacement assay has been developed utilizing an immobilized Cu (II) complex of the azo dye 1-(2-pyridylazo)-2-naphthol printed on Nylon support. The change in color measured from the image of the disposable membrane acquired by a digital camera using the H coordinate of the HSV color space as the analytical parameter, is able to sense sulfide in aqueous solution at pH 7.4 with detection limit of 0.10 μM and a precision between 2 to 11 %.

INTRODUCTION

Hydrogen sulfide is essential for life as cardioprotector, neuroprotector and neuromodulator and at the same time toxic at a higher concentration level.[1] The determination of gas or aqueous sulfide species is of great interest for a wide range of application areas by using different methods including titrimetric, optical, electrochemical, separative as chromatography or electrophoresis and sensors.[2-7]

Different approximations have been used for both gaseous and aqueous sulfide sensing, being more difficult to recognize anions in aqueous media because of their strong hydration and pH dependence.[8] Circumscribing to the case of sulfide in aqueous media, and organizing according to different strategies used for optical anion sensing, very few examples of binding site-signaling subunit approach have been described.[9] In that type of sensors binding site and signaling units are covalently linked, as is the case of fluorescein mercury acetate immobilized into ethyl cellulose membrane which suffers fluorescence quenching upon mercury coordination by sulfide.[10,11] Another example is the self-assembled monolayer protected gold

nanocluster of calixarene dithiocarbamate ligand proposed for colorimetric sulfide determination based on the recognition of sulfide by intermolecular hydrogen bond through NH groups that triggers gold particle aggregation (detection limit 10 nM).[12]

More amply used is the displacement approach, in which both subunits are not covalently attached but form a molecular ensemble of some type. The reaction of target anion, sulfide in this case, with ensemble triggers a displacement reaction which modulates an optical signal based that could be based on several mechanisms.[13] The major requirements for this assay are reversibility in the interaction between binding and signaling units and that their interaction constant has to be lower than between binding site and target anion and different enough than potential interfering species.[9]

Among displacement approach the metal complexing indicator–displacement assays is the most usual, mainly for high reactivity anions, as is the case for sulfide. In this assay a metal, typically Zn(II) or Cu(II), is complexed with a receptor and with an indicator, although the receptor could play the role of indicator, and the addition of target anion causes the displacement of the indicator (or receptor) and concomitant optical changes.

As an example of colorimetric assay can be mentioned the Cu(II) complex of 1-(2-pyridylazo)-2-naphthol (PAN) that produce in hydroalcoholic media a remarkable change of color upon reaction with sulfide that form CuS and release PAN.[14] A similar concept underlay in the use of the orange Cu(II) complex of a boron-dipyrromethene (Bodipy) that turn to pink after reaction with sulfide.[15] The use of a fluorescent indicator that is displaced from a receptor upon the introduction of an analyte can potentially reduce the detection limit with respect to the tests based on color. It could be cited the use of the Cu(II) complex of a quinoline derivatized thiosemicarbazone in hydroorganic media that produce a significant color and fluorescence changes with sulfide (detection limit 0.44 μM).[16,17] Similarly, a

hydroorganic solution of the Zn(II) mixed ligand complex containing tris(pyrazolyl)borate and 7-mercapto-4-methylcoumarin shows a remarkable reduction in fluorescence upon substitution of coumarin derivative by sulfide.[18] A slightly different strategy is used by Choi et al. proposing an assay in which the fluorescence of a fluorescein derivative having a dipicolylamine binding site is quenched efficiently by Cu(II) complexation in aqueous solution being recovered in the presence of sulfide (detection limit 0.42 μM).[19] Also can be cited the microtiter plate assay array of similar type for the colorimetric identification of ten anions including sulfide in water or the similar assay array for three biothiols in biological samples.[20,21]

The chemodosimeter approach has also been used for sulfide sensing by using different types of irreversible reactions some of them based on their reducer and nucleophilic character. Chen et al. reference some of the reactions proposed mainly for sulfide in biological systems.[21] As an example one can cite the reduction by sulfide of some azido derivatives to the amine moiety of fluorogenic dyes: rhodamine-based dyes with a pendant azide, azidocoumarin or naphthalimide azide. [22-24] The reaction of pyrylium salts with sulfide in hydroorganic media produce a ring opening and cyclization to give the parent thiopyrilium derivatives have been proposed by Jimenez et al. for colorimetric sulfide determination.[25] Chemodosimeters based on double nucleophilic character of sulfide have been revised by Zhao et al. that suggest the use of a tricyanoethylene derivative for colorimetric sulfide sensing in hydroalcoholic media.[26] A very different approach is used by Hatamie et al. that use Cu nanoparticles to sense sulfide in aqueous solution based on the decrease of plasmonic band upon interaction with sulfide that form colloidal CuS (limit of detection 8.1 μM).[27]

The most of the assays for sulfide above referenced are accomplished in hydroorganic or aqueous media reagents included, but the integration of processes in

a solid-phase spectrometric assay is a way to ease the procedure, make cheaper the analysis and facilitate the use and lifetime of reagents.[28] The presented combination of piezoelectric inkjet technology to increase the reproducibility of the preparation of sulfide responsive membranes, based on PAN-Cu complex, along with the use of membrane color as analytical parameter, namely the H coordinate of HSV color space, obtained by a digital camera results in a simple an accurate assay for sulfide.[29]

EXPERIMENTAL

Materials

Sulfide solutions were prepared daily from $Na_2S \cdot 9H_2O$ (Panreac, Barcelona, Spain) in water and standardized by iodimetric titration.[30] Working standard solutions of Cu(II) (100 μg mL^{-1}) were prepared by appropriate dilution of the standard stock solution (1,000 μg mL^{-1}) (Sigma-Aldrich) acidified with conc. HNO_3. A buffer phosphate solution containing 0.5 M phosphate (Na_2HPO_4) adjusted to the necessary pH by adding NaOH or HCl of appropriate concentrations was prepared. The rest of reagents used were: 1-(2-pyridylazo)-2-naphthol (PAN), $CuCl_2 \cdot 2H_2O$, ethylene glycol (EG), isopropanol, ethanol, and low viscosity carboxymethylcellulose sodium salt (CMC), all purchased from Sigma (Sigma-Aldrich Química S.A., Madrid, Spain). All reagents were of analytical-reagent grade and were used without any further purification, and reverse osmosis type quality water (Milli-RO 12 plus Milli-Q station (Millipore, Bedford, MA, USA), conductivity 18.2 mS) was used throughout. As support for membrane printing was used nylon transfer membranes Biodyne A purchased from Pall (Pall Life Sciences, Ann Arbor, MI, USA).

Synthesis of PAN-Cu complex

The PAN-Cu complex was prepared according to the procedure described by Zhang et all.[14] To a solution of 0.5 mmol of PAN in 75 mL of ethanol a solution of 0.5 mmol of $CuCl_2 \cdot 2H_2O$ in 3 mL of water was added. After stirring for 2 hours, the dark-red complex formed was filtered, rinsed 3 times with 95% ethanol and then dried under vacuum.

Preparation of inkjet-printed disposable sensor

The sulfide disposable sensors were printed using a Fujifilm Dimatix DMP-2831 printer (Fujifilm Dimatix, Inc., Santa Clara, CA, USA) with cartridges consisting of 16 nozzles with a nominal droplet size of 10 pL. Sensing membranes were printed on Nylon membrane Biodyne A (pore size 0.45 μ m) as an array of 4 identical membranes in column. After printing the disposable sensors were stored in a closed container at room temperature to enables low solvent evaporation and then kept in a dark place until use to avoid photodegradation. Inks used for printing were prepared from hydroalcoholic solution of PAN-Cu complex and PAN, respectively, with rheological characteristics adjusted to printer requirements (10-12 cPs viscosity; 28-33 dynes cm-1 surface tension; <100 ºC boiling point; >1 g cm-3 density; <0.2 μm particle size; 4-9 pH) with appropriate reagents (Table 1). Viscometer Visco Basic Plus (Fungilab, Barcelona, Spain) and surface tensiometer Theta Lite Attension (Biolin Scientific AB, Stockholm, Sweden) were used to characterize inks. Prepared inks were degassed after using by means an ultrasonic bath to avoid dissolved gas, which inhibits jetting.

The inks were filtered through 0.2 μm filter before filling the cartridge, and then maintained in vacuum almost two hours after use for optimal jetting.

Table 1. Composition and characteristics of sulfide sensing ink.

Chromogenic reagent	Membrane polymer	Humectant	Solvent % w/w			Viscosity	Surface tension	Density
PAN-Cu, % w/w	CMC, % w/w	EG, % w/w	Isopropanol	Ethanol	H_2O	cPs, 33°C	dynes cm^{-1}	g cm^{-3}
0.12	0.59	33.10	7.81	18.62	39.75	12.7	32.88	1.015

Image capture and processing

The change in colour from violet to yellow of the PAN-Cu membrane, when reacting with sulphide in aqueous solution, was measured with a digital camera Canon PowerShot G12 (Canon Inc., Tokio, Japan). The optimized setting conditions used to photograph the sensor were: macro, ISO 100, shutter speed 1/500s, aperture value f/4 and focal length of 6.1 mm. To keep all the image-gathering conditions the same, a Cube Light Box was used (Figure 1).

The camera was placed in the front of a homemade white wooden box with two LED 6500 K lamps placed at 45º with respect to the digital camera, with the array in a fixed position inside the box to be isolated from external radiation, a position that was maintained constant for all the experiments. For the image acquisitions and digitalization, a Canon PowerShot G12 camera (Canon Inc., Tokio, Japan) was used.

To evaluate the colour change of the printed sensor both before and after reacting with analyte, a photograph was taken in JPEG format. Then, the images were treated with Adobe Photoshop CS5 software to remove the areas containing no relevant information, using a negative image of the printed sensor, which plays the role of a mask. The average R G B values for the pixels were determined for each image. The H coordinate, or hue of the HSV (Hue, Saturation, and Value) colour space was used to monitor the reaction. The RGB values of the selected pixels in each image were processed with a set of scripts and functions developed in Matlab r2010b (The MathWorks121 Inc, Natick, MA, USA) to determine the H coordinate.[29] This coordinate has a circular nature and it can be defined as an angle that varies between 0 and 360º. The colorimetric change between the PAN-Cu and PAN reported in this study ranges from 300 to 41º crossing 0º; thus, to have a continuous change in processing data we add 360º to all the values ranging between 0 and 41º. In this way all H values ranges between 300º and 401º.

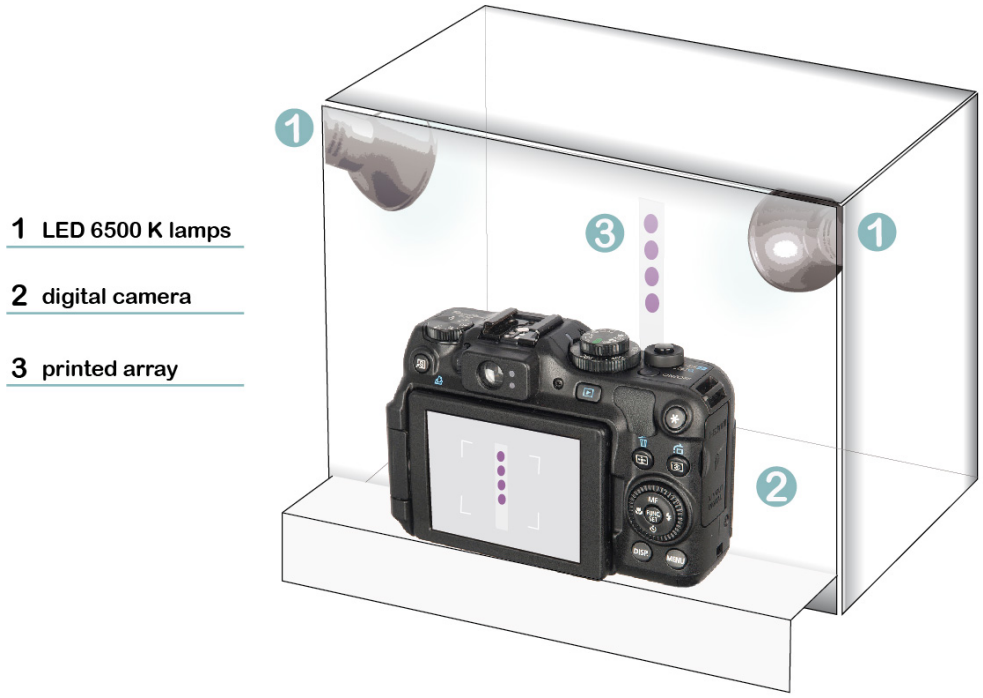

Fig. 1. Cube light box for sulphide sensing membrane image acquisition.

Sensor response evaluation

The response of the four membrane printed array to sulphide was evaluated from different standards solutions of sulphide from $5 \cdot 10^{-8}$ to $1.45 \cdot 10^{-4}$ M by adding needed volume of each standard, to a 10 mL polyethylene plastic tube with pH adjusted to 7.4 with 2 mL of 0.5 M buffer phosphate solution. The disposable array was then introduced for 5 min into the tube without shaking and then placed in their position in the Cube Light Box where the images were acquired by the camera. The sensing arrays were not conditioned before use. A recovery study with mineral water samples without pre-treatment doped at three different concentrations levels, $1.45 \cdot 10^{-6}$, $5.8 \cdot 10^{-6}$ and $1.45 \cdot 10^{-5}$ M was carried out.

Safety cautions

Special caution was taken in the preparation and handling of all hydrogen sulphide and cyanide solutions. Nitrile gloves, protective clothing and safety glasses were worn all the time. Preparation of sulphide and cyanide stock solutions was carried out under an appropriate extractor hood. Also, special care was taken to avoid the release of chemicals to the environment. Thus, hazardous wastes were collected, stored in appropriate glass containers, labelled and sent to waste management services of the University of Granada.

RESULTS AND DISCUSSION

2-Pyridylazo compounds conform a group of reagents amply used in chemical analysis for a variety of purposes mainly as chromogenic agent and extractant,[31,32] highlighting 1-(2-pyridylazo)-2-naphthol (PAN) a rapid-reacting ligand [33] that can act as bidentate or terdentate chelating ligand [34] well known as metallochromic indicator and colorimetric reagent for many metal ions. A 1:1 stoichiometry is usually observed when PAN is used as chromogenic reagent for different metals in ion-exchange materials,[35-38] lipophilic salts [39] and adsorbents.[40-42] With Cu(II) in the presence of chloride form a neutral mixed ligand 1:1 complex [43] through the formation of a close to square coplanar chelate with two five-membered ring and the fourth equatorial coordination position occupied by chloride resulting in a van der Waals dimer when is isolated as a solid.[44]

The interaction between metal complexes and anions through coordination effects is a usual way for anion sensing due to the small influence of protic solvents.[15] The use of ligands which exhibit signalling units such as chromophore is an advantageous strategy through a judicious selection of metal ion and ligand for a given anion taking into account stability constants involved and colour change. The

magenta coloured 1:1 PAN-Cu complex in hydroalcoholic solution (λmax 562 nm) react reversibly with sulphide under neutral or basic conditions turning the solution to yellow colour (λmax 468 nm). This is the basis of procedure proposed by Zhang and Jin for spectrophotometric determination of sulphide in solution.[14] We are interested in the printing of stable and reproducible sensing membranes for sulphide analysis based in colour measurement with highly distributed imaging devices as could be digital cameras.

Chemical ink preparation

Water-based printing is an interesting technology for industry and consumers who care about the environment and their impact, presenting advantages such as it does not require additional dry and/or curing process, reducing in this way costs of manufacture. To prepare two water-based chemical inks containing PAN and the previously synthesized chromogenic reagent PAN-Cu complex it is needed to control their rheological properties at jetting temperature, such as viscosity, surface tension and density. To maintain a high proportion of water (40%) with suitable surface tension for appropriate inkjet printing and also to solubilise the PAN and PAN-Cu complex, ethanol and isopropanol were included. To achieve the required ink viscosity ethylene glycol was included in the formulation, which also provides a high boiling point, avoiding precipitation of complex in the nozzles. CMC was incorporated to raise the viscosity to printer technical specifications and to improve the adherence of the ink to the support. The use CMC, a viscosity-increasing water-miscible agent, gives stability to the mixture facilitating the incorporation of chromogenic reagent to sensing membrane, although a low proportion (<1%) it is used in order to avoid the obstruction of nozzles. Additionally, its dispersing properties stabilize the ink composition preventing particles aggregation processes, which can obstruct the nozzles (Table 1). The substrate selected in this study for

printing purposes was Biodyne A, an amphoteric Nylon 6.6 membrane, resistant to the ink solvents used and highly versatile due to contains both negatively and positively charged groups, enabling to bind both metallic complex and free reagent without leaching in contact with the aqueous sulphide.

Design of the disposable assay

The size and shape of printed sensing membrane must fulfil conditions of allows to colorimetric changes can be easily distinguished by the naked eye and be able to frame and focus the membrane array with the camera. A set of circular geometric shapes were tested selecting membranes of 3 mm diameter for their good perceptibility; additionally, in order to maintain a balance between colour information required and low data storage a resolution of 3,648 x 2,736 pixels was used to image capture. Considering the diameter of the membrane, this means 10,550 pixels of colour information. Once optimized, 4 replicates of PAN-Cu sensing membrane were printed in a column. To optimize both the chemical ink and the substrate used, 72 arrays of 4 replicates each were printed on a nylon sheet of 20 x 20 cm. A study of the reproducibility of inkjet-printing sensor fabrication process respect to colour homogeneity shows an H variability of the 0.8%.

Sensing mechanism

Sensing mechanism is based upon interaction between sulphide and PAN-Cu complex changing colour from magenta to yellow, which is perceptible to the naked human eye. To describe the sensing mechanism, we study both the reactions between PAN containing printed membrane and Cu(II) and PAN-Cu membrane and sulphide at pH 7.4 using as dependent variable the colour coordinate H. Assuming a 1:1 stoichiometry the complexation can be described with eq. 1:

$$Cu^{2+} + \overline{HL} + X^{-} \leftrightarrow \overline{CuLX} + H^{+} \quad \text{(Eq. 1)}$$

which is characterized by a constant Ke that includes a complex stability constant, acidity constant, distribution constant between aqueous and membrane phases of different species, and dissociation constant. The activity of the Cu ion in the aqueous phase is related to the equilibrium constant Ke through a sigmoidal response function (eq. 2) that includes the experimental degree of uncomplexed chromogenic reagent α (eq. 3). The α value was obtained from the H coordinate of membrane equilibrated with buffer (H_{PAN}) and 10^{-3} M Cu(II) ($H_{PAN\text{-}Cu}$), respectively.

$$K_e = \frac{(1-\alpha)\cdot a_{H^+}}{\alpha \cdot a_{Cu^{2+}} \cdot a_{X^-}} \quad \text{(Eq. 2)}$$

$$\alpha = \frac{H - H_{PANCu}}{H_{PAN} - H_{PANCu}} \quad \text{(Eq. 3)}$$

The good fit of experimental data to eq. 2 (R^2 = 0.9986) supports the 1:1 stoichiometry, with a Ke of $8.23 \cdot 10^6$.

The recognition process of sulphide by PAN-Cu membrane is coupled –through an electroneutrality condition- to the coextraction of a proton from solution, which is complexed by a PAN molecule released from PAN-Cu complex by CuS precipitation (eq. 4). The colour change from magenta PAN-Cu complex to yellow PAN acts as a transducer of the recognition process. The low solubility of CuS (Ks $1.27 \cdot 10^{-36}$) [45] compared to stability constant of PAN complex (Ke_1 $3.55 \cdot 10^4$; Ke_2 $4.27 \cdot 10^{12}$ in aqueous solution) [46] boost the recognition and the high selectivity of membrane towards sulphide.

$$\overline{PANCuCl} + S^{2-} + H^{+} \leftrightarrow \overline{PAN^{-} \cdot H^{+}} + CuS\downarrow + Cl^{-} \quad \text{(Eq. 4)}$$

The ion activities of sulphide and proton in aqueous phase are related to the equilibrium constant Ke' and α through eq. 5.

$$K'_e = \frac{C_{PANCuCl} \cdot \alpha \cdot a_{Cl^-}}{C_{PANCuCl} \cdot (1-\alpha) \cdot a_{S^{2-}} \cdot a_{H^+}} \qquad \text{(Eq. 5)}$$

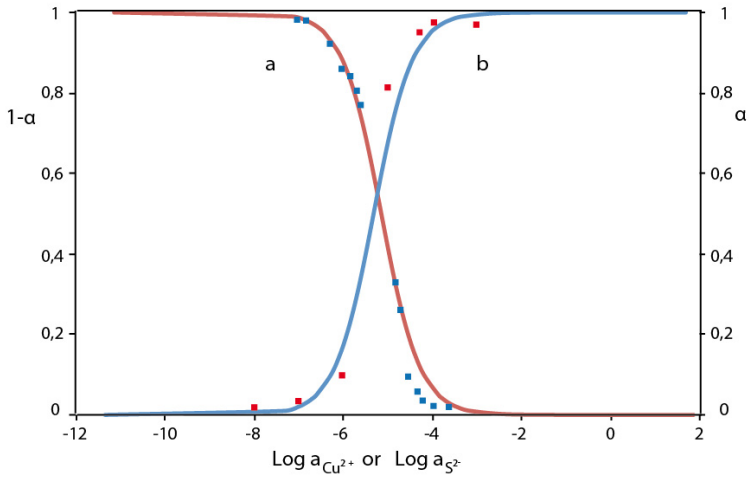

Fig. 2 Response curves. a) α as a function of sulphide activity for PAN-Cu membrane; b) 1-α as a function of Cu activity for PAN membrane. Solid lines are theoretical curves. Although through the paper only appears the term sulphide, the existing species at the working pH is hydrogen sulphide.

The equilibrium constant Ke' includes, in addition to constants above indicated the solubility product constant and the acidity constants for H_2S. The experimental value α, the degree of unreacted complex, is obtained from the H coordinate of membrane equilibrated with buffer (H_{PAN-Cu}) and 10^{-3} M sulphide (H_{PAN}), respectively. Figure 2 shows the fit of experimental data to eq. 5 (R^2 = 0.9903) with a Ke' of $3.5 \cdot 10^7$.

Optimization of experimental conditions

The study of the influence of pH between 6.0 and 9.0 for a constant sulphide concentration ($6 \cdot 10^{-6}$ M) show small dependence, selecting pH 7.4 phosphate buffer 0.05 M as reaction medium. The effect of the ionic strength studied varying the NaCl concentration from 100 to 5,000 mM, higher than levels generally found in mineral water, for the same sulphide concentration is unnoticeable. The reaction time was studied at low sulphide concentration being apparent the progress of the reaction with time up to 10 min, the time selected for the assay. No leaching was observed for the reaction time selected.

Analytical characterization

To characterize the assay for sulphide using a digital camera, a set of 16 standard solutions was prepared at pH 7.4 and containing between $5 \cdot 10^{-8}$ and $2 \cdot 10^{-4}$ M sulphide. For each standard solution 4 replicates were analyzed each time. The colour of PAN-Cu sensing membrane change from magenta to yellow that suppose a gradual increase of the H parameter from 301 to 401. As there is no direct linear relationship between analytical parameter H and sulphide concentration we proposed three different data processing for calibration purposes.

First is based on sigmoidal relationship, usual with this type of sensors, between H and the logarithm of the sulphide concentration; thus, a Boltzmann fit (eq. 6) was tested as calibration function with excellent adjustment (R^2: 0.9952), where a0 to a3 are adjusting coefficients (a_0: -5.672; standard deviation (SD): 0.0218; a_1: 404.3; SD: 1.381; a_2: 306.4; SD: 1.855; a_3: 0.2305; SD: 0.0239) (see Figure 3a).

$$H = a_2 + \frac{a_1 - a_2}{1 + \exp\left(\frac{a_0 - \log[S^{2-}]}{a_3}\right)} \qquad \text{(Eq. 6)}$$

The detection limit (LOD) was established as a function of the standard deviation of the background noise obtained with buffer.[47,48] The intersection of the response function and the highest value of the background noise band define the LOD, reported as a logarithm. The average H value coming from 12 different membranes, adding their standard deviation three times, was used as the detection limit of the assay, resulting 0.44 μM or 14.10 μg L^{-1}. For the upper limit, we considered 14 μM or 473 μ g L^{-1}. A second type of calibration data processing used was the linear relationship in the middle of the sigmoidal response function defined by means of a lack-of-fit test and as the detection limit the intersection of this linear calibration function and a linear function adjusted in the minimal slope zone of lower sulphide concentration.[49] Two series of standards was prepared one in the minimum slope zone of lower concentration (4 standards, 4 replicates each one), between 10^{-8} and 10^{-7} M and another in the maximum slope (5 standards, 4 replicates each one), between 6 μM and 1 μM. After check the linearity of both series by applying the lack-of-fit test, the intercept of both functions give a detection limit of 0.63 μM or 20 μg L-1. From the intercept of the linear calibration function with the abscissa at the H value for PAN-Cu, a value of 7.68 μM or 246 μg L^{-1} was obtained for the upper limit of the measuring range. This type of calibration offers a better precision and sensitivity although a shorter dynamic range.

A third calibration type was applied in order to expand the short range of previous calibration maintaining the advantages of the linear calibration. Thus, a decimal logistic transformation [49] was applied (eq. 7) to the sigmoidal calibration curve obtaining a wide linear calibration function curve increasing in this way the linear dynamic range.[50]

$$\log \frac{1-\alpha}{\alpha} = K + A \cdot \log[S^{2-}] \qquad \text{(Eq. 7)}$$

The adjusting parameters obtained were K= 7.07 and A = 1.211 with R2 = 0.9606 (Figure 2) that suppose an analytical range from 0.10 μM to 145 μM or 4,640 μg L^{-1} that suppose an increase in the obtained linear dynamic range. A possible drawback of this logit linearization is the fact that precision of measurements decreases with parabolic profile towards the edge of linear dynamic range, although these values are acceptable for disposable-type assays.

The precision was studied in the middle of the linear range at three concentration levels obtaining relative standard deviations between 11 and 2 % (1.5 μ M, SD: 10.7%; 2.4 μ M, SD: 5.1%; 13 μ M, SD: 2.1%). The analytical characteristics of the assay improve the proposed by Zhang et al. based on the same chemistry but in aqueous solution that works between 2 and 500 μM.[14]

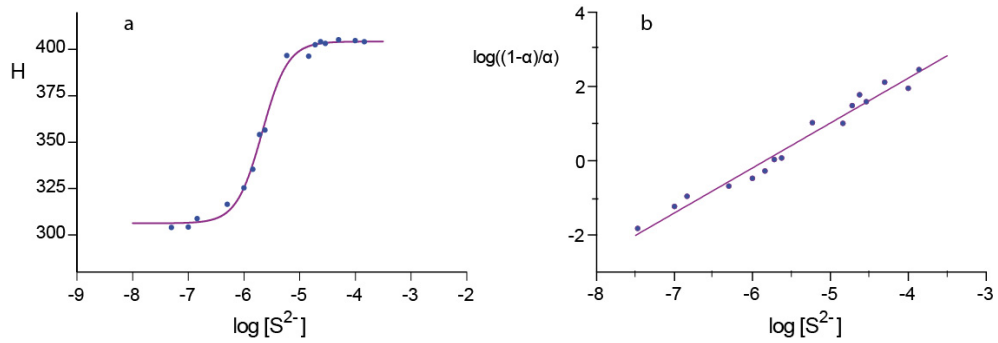

Figure 3. a. Calibration data fit with Boltzman equation. b. Linear calibration data processed by non linear fitting.

Selectivity

The colorimetric assay for sulphide was extensively tested for interfering anions in order to evaluate their selectivity. Thus, we measure the H change of sensing membrane after reaction with eleven relevant anions selected because of their high environmental interest : $PO_3^{3-}, Cl^-, CN^-, CH_3COO^-, F^-, CO_3^{2-}, Br^-, NO_3^-, SO_4^{2-}, SO_3^{2-}$, S^{2-}.

Only in the case of sulphide and cyanide there is a significant change in the H value of the membrane, due in the last case, to formation of stable cyanide complexes of Cu(I) ($\beta_4 Cu(CN)_4^{3-}$) (28.93) that release PAN changing the colour of membrane.[51]

Interfering anions study

An interference study was also carried out to observe the possible effect on the response of the sulphide sensing membrane when other anions besides the analyte were present. The variation of H parameter was evaluated after reaction of membrane at pH 7.4 with a solution $5 \cdot 10^{-5}$ M in sulphide and $7 \cdot 10^{-5}$ M in potential interfering coexisting anions.

As it was expected by the previous study, there is only one interfering species, the cyanide ion that changed the H parameter value from 301 to 375. The rest of the anions did not change the original value of the sensor tone with sulphide significantly, with a maximum standard deviation of 3.61. The tolerance, defined as the amount of foreign species that produced an error equal to ±5% in the determination of the analyte, was studied for cyanide in the determination of 5 μM sulphide, finding a value of 20 μM. The results of both, the selectivity and the interfering ions study are presented in Figure 4.

Shelf-life evaluation

The stability of sensing membranes is a very important issue for any real application. The long-term stability of sulphide membranes was studied at 180 days before inkjet printed membrane, maintained in darkness at room temperature, and measuring the colour periodically. There was a no significant difference between H values along the period of time studied (maximum variability 3.5%).

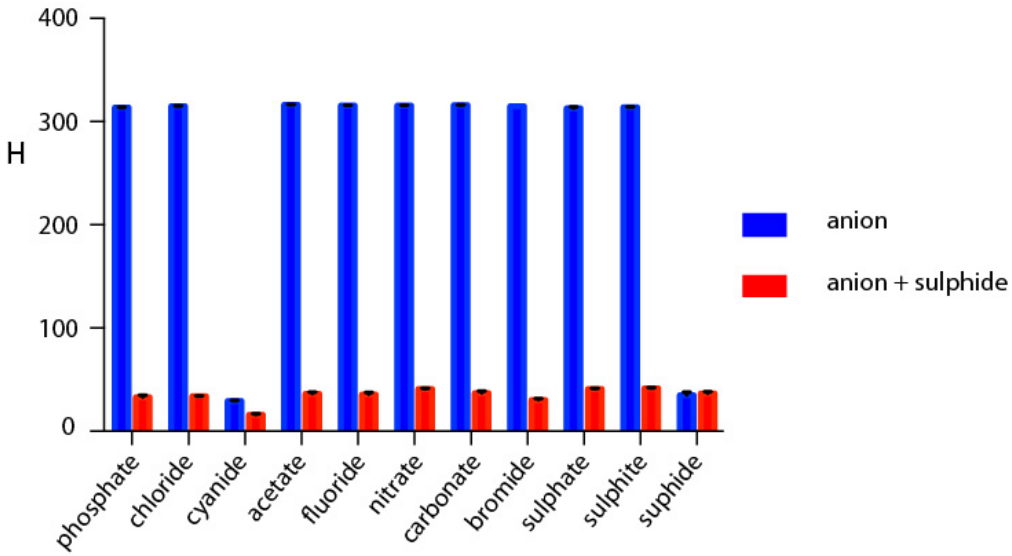

Figure 4. Variation of H parameter of the PAN-Cu sensing membrane in the presence of eleven anions (blue) and sulphide and different anions (red).

Real sample testing

The proposed assay was applied to the determination of free sulphide in seven different mineral water samples.

Since no sulphide was detected in those water samples, they were spiked at different concentrations level of analyte prior to reaction with sensing membrane. The samples were analyzed following the general procedure, and the obtained recovery results are shown in Table 2 demonstrating the high potential of the novel optical assay for the analysis of trace levels of sulphide in real samples.

Table 2. Recoveries for several sulphide-spiked mineral waters samples using the proposed colorimetric assay.

Mineral water	Spiked sulphide (μM)	Recovery (%)
Aro	1.45	98,3 ± 0,691
	5.8	97.3±0.665
	14.5	99,2±0,686
Eden	1.45	97±1,056
	5.8	96,6±0,427
	14.5	98,4±0,447
Fuensanta	1.45	98,6±0,536
	5.8	96±1,088
	14.5	98,2±0,627
Aguabona	1.45	99,2±0,707
	5.8	95±1,239
	14.5	95±1,103
Lanjarón	1.45	99,49±0,786
	5.8	96,5±0,232
	14.5	96,1±0,873
Villadrau	1.45	99,5±0,563
	5.8	96±1,008
	14.5	97±1,537
Aqua Nevada	1.45	98±1,154
	5.8	96,0±0,715
	14.5	98±1,368

CONCLUSIONS

We have successfully designed a selective colorimetric metal complexing indicator–displacement assay for sulphide in aqueous media and physiological pH based on colorimetric on a chemosensing ensemble approach. The solid phase assay

is prepared by inkjet printing of Cu(II) complex of the azo dye 1-(2-pyridylazo)-2-naphthol on Nylon support, resulting in a cheap and very stable membrane for sulphide determination based on a fast displacement reaction which takes place in minutes. The reaction of both PAN and PAN-Cu membranes against Cu(II) and sulphide, respectively, were modelled calculating their equilibrium constants. In order to simplify the assay, the change in colour from magenta to yellow in the presence of sulphide, the colour of membrane was used as analytical parameter, measured with the hue (H) coordinate of the HSV colour space. The colour was obtained by using a digital camera, which opens the door to the use of this assay with other amply distributed imaging devices as could be smartphones. The assay present a good sensitivity for sulphide with detection limit of 0.1 μM and analytical range extended up to three order of magnitude.

REFERENCES

1. J.W. Elrod, J.W. Calvert, J. Morrison, J.E. Doeller, D.W. Kraus, L. Tao, X. Jiao, R. Scalia, L. Kiss, C. Szabo, H. Kimura, C.W. Chow and D.J. Lefer, PNAS 2007, 104, 15560-15565.

2. P. Nagy, Z. Palinkas, A. Nagy, B. Budai, I. Toth and A. Vasas, Biochim.Biophys.Acta, Gen.Subj. 2014, 1840, 876-891.

3. D. Haydt, R. Hornberger, Proc.Int.Sch.Hydrocarbon Meas. 2011, 86th, a23-1-a23/8.

4. S.K. Pandey, K.H. Kim and K.T. Tang, TrAC, Trends Anal.Chem. 2012, 32, 87-99.

5. B. Farmer, S. Trimble, Proc.Annu.ISA Anal.Div.Symp. 2009, 54th, 31-1-31/20.

6. L. Ferrer, M. Miro, J.M. Estela and V. Cerda, TrAC, Trends Anal.Chem. 2007, 26, 413-422.

7. N.S. Lawrence, J. Davis and R.G. Compton, Talanta 2000, 52, 771-784.

8. P.D. Beer, P.A. Gale, Angew.Chem.Int.Ed. 2001, 40, 486-516.

9. R. Martinez-Mañez, F. Sancenon, Chem Rev. 2003, 103, 4419-4476.

10. M.M.F. Choi, P. Hawkins, Anal.Chim.Acta 1997, 344, 105-110.

11. M.M.F. Choi, Analyst 1998, 123, 1631-1634.

12. A. Pandya, K.V. Joshi, N.R. Modi and S.K. Menon, Sens.Actuators B 2012, 168, 54-61.

13. B.T. Nguyen, E.V. Anslyn, Coord.Chem.Rev. 2006, 250, 3118-3127.

14. D. Zhang, W. Jin, Spectrochim.Acta A 2012, 90, 35-39.

15. Z.h. Chen, Y. Lu, Y.b. He and X.h. Huang, Sens.Actuators B 2010, 149, 407-412.

16. L. Tang, P. Zhou, Z. Huang, J. Zhao and M. Cai, Bull.Korean Chem.Soc. 2013, 34, 2905-2908.

17. L. Tang, P. Zhou, Q. Zhang, Z. Huang, J. Zhao and M. Cai, Inorg.Chem.Commun. 2013, 36, 100-104.

18. E. Galardon, A. Tomas, P. Roussel and I. Artaud, Dalton Trans. 2009, 9126-9130.

19. M.G. Choi, S. Cha, H. Lee, H.L. Jeon and S.K. Chang, Chem.Commun. 2009, 7390-7392.

20. L. Feng, H. Li, X. Li, L. Chen, Z. Shen and Y. Guan, Anal.Chim.Acta 2012, 743, 1-8.

21. S. Qian, H. Lin, Anal.Bioanal.Chem. 2014, 406, 1903-1908.

22. B. Chen, W. Li, C. Lv, M. Zhao, H. Jin, H. Jin, J. Du, L. Zhang and X. Tang, Analyst 2013, 138, 946-951.

23. A.R. Lippert, E.J. New and C.J. Chang, J.Am.Chem.Soc. 2011, 133, 10078-10080.

24. L.A. Montoya, M.D. Pluth, Chem.Comm. 2012, 48, 4767-4769.

25. D. Jimenez, R. Martinez-Mañez, F. Sancenon, J.V. Ros-Lis, A. Benito and J. Soto, J.Am.Chem.Soc. 2003, 125, 9000-9001.

26. Y. Zhao, X. Zhu, H. Kan, W. Wang, B. Zhu, B. Du and X. Zhang, Analyst 2012, 137, 5576-5580.

27. A. Hatamie, B. Zargar and A. Jalali, Talanta 2014, 121, 234-238.

28. L.F. Capitán-Vallvey, M.D. Fernandez-Ramos in Integrated Analytical Systems, Alegret, S., Ed. ed. , Elsevier Science B.V, Amsterdam, 2003, 81-159.

29. K. Cantrell, M.M. Erenas, I. Orbe-Paya and L.F. Capitán-Vallvey, Anal.Chem. 2010, 82, 531-542.

30. A.E. Greenbery, J.J. Connors D. Jenkins in Standard Methods for the Examination of Water and Wastewater, 15th edn. ed., American Publich Health Association, Washington, DC, 1980.

31. H. Seiler, A. Sigel H. Sigel in Handbook on Metals in Clinical and Analytical Chemistry, CRC Press, 1994.

32. S. Shibata in , Flaschka, H. A.; Barnard, A. J., Eds. ed. , Marcel Decker, New York, 1972.

33. C.D. Hubbard, A. Pacheco, J.Inorg.Nucl.Chem. 1977, 39, 1373-1375.

34. S. Ooi, D.E. Carter and Q. Fernando, Chem.Comm. 1967, 1301-1302.

35. S.D. Kolev, T.J. Cardwell, R.W. Cattrall and L.d. Coo, Talanta 2010, 82, 1156-1163.

36. F. Lazaro, M.D.L. de Castro and M. Valcarcel, Anal.Chim.Acta 1988, 214, 217-227.

37. J.E. Madden, T.J. Cardwell, R.W. Cattrall and L.W. Deady, Anal.Chim.Acta 1996, 319, 129-134.

38. S.B. Savvin, L.M. Trutneva, O.P. Shvoeva, V.K. Belyaeva and I.N. Marov, Zh.Neorg.Khim. 1991, 36, 393-399.

39. N. Alizadeh, A. Moemeni and M. Shamsipur, Anal.Chim.Acta 2003, 464, 187-196.

40. I.M. Maksimova, E.I. Morosanova, A.A. Kukhto, N.M. Kuz'min and Y. Zolotov, Zh.Anal.Khim. 1994, 49, 1210-1214.

41. E. Morosanova, A. Velikorodnyi and Yu. Zolotov, Fresenius J.Anal.Chem. 1998, 361, 305-308.

42. S.A. Morozko, V.M. Ivanov, J.Anal.Chem. 1995, 50, 572-578.

43. J.A. Szabo, V. Nikolasev, Acta Phys.Chem. 1969, 15, 59-61.

44. H. Adams, R.M. Bucknall, D.E. Fenton, M. Garcia and J. Oakes, Polyhedron 1998, 17, 4169-4177.

45. W.M. Haynes in CRC Handbook of Chemistry and Physics, 94th Edition, CRC Press, Boca Raton, Florida, 2013.

46. L.d. Coo, T.J. Cardwell, R.W. Cattrall and S.D. Kolev, Dokl.Bulg.Akad.Nauk. 2001, 54, 53-56.

47. M. Lerchi, E. Bakker, B. Rusterholz and W. Simon, Anal.Chem. 1992, 64, 1534-1540.

48. M.D. Fernandez-Ramos, L. Cuadros-Rodriguez, E. Arroyo-Guerrero and L.F. Capitán-Vallvey, Anal.Bioanal.Chem. 2011, 401, 2881-2889.

49. E. Bakker, P. Bühlmann and E. Pretsch, Chem Rev. 1997, 97, 3083-3132.

50. L.F. Capitán-Vallvey, E. Arroyo-Guerrero, M.D. Fernandez-Ramos and L. Cuadros-Rodriguez, Anal.Chim.Acta 2006, 561, 156-163.

51. M.T. Beck, Pure Appl.Chem. 1987, 59, 1703-1720.

CONCLUSIONS

In this chapter we intend to improve the reproducibility of the optical sensing membranes prepared in Chapter I. Various printing techniques were tested, however, the ink-jetting technique offered better results and was used to prepare arrays of chromogenic reagents to be used for develop an optical tongue for metal ions and anion discrimination.

The main conclusions we can draw from the study conducted are the following:

1. We have prepared and tested different sensing membranes for metal ions based on eleven different conventional chromogenic reagents containing different types and amounts of polymers, plasticizers, lipophilic salts, dispersing agents and humectants. After a study of their characteristics and response against 13 target metal ions, seven membranes were selected.
2. A sensing array was prepared by an ink-jet printing technique after adjusting the compositional and rheological properties of seven chemical inks containing chromogenic reagents previously selected. A study of the fabrication reproducibility, either inter- or intraday, has shown a high precision compared to previous printing techniques (average precision error 0.81%).
3. The array was optimized in size, using a number of membranes, replicates and printed layers resulting in a design that consisted of seven different sensing membranes printed in rows, with two printed layers each, with five replicates printed in adjacent columns, producing a 35 membrane matrix, which allowed printing of a 28 array matrix on the same 20 x 20 cm nylon sheet.

4. A simple stage with a conventional photographic camera and a standard illumination system in a white wooden box is enough for image acquisition of the array after reaction with metals in a target solution. This opens the door to the use of more a simple system that could be used with smartphone-based procedures.
5. The color change of each sensing membrane that comprise the array, evaluated by the tonal coordinate H of the HSV color space, was used in this work as the analytical parameter to evaluate the color change of all the sensing membranes after they react with the metal solutions.
6. Through a two-stage approach based on artificial neural networks we have demonstrated the detection of metal ions present in water samples and also demonstrated the ability to measure metal ion concentration. In the first stage, with a success rate of 98.1 %, we are able to achieve the classification of 13 metals in the sample with a detection limit of 10^{-5} M. In this stage 10 of the 13 metal ions can be determined without error. In the second stage, the estimation of the concentration of each metal in the solution was studied. We selected mixtures of up to 5 metals as a proof of concept (Zn(II), Cu(II), Ni(II), Cd(II), and Co(II)) and demonstrated both high precision and accuracy in the determination of these metals.
7. A selective colorimetric metal complex indicator–displacement assay for sulphide determination in aqueous media and physiological pH has been proposed
8. The assay is based on a membrane prepared by the ink-jet printing of a Cu(II) complex of the azo dye 1-(2-pyridylazo)-2-naphthol on a nylon support, resulting in a cheap and very stable membrane for sulphide determination with a fast displacement reaction, which takes place in minutes.

9. We have modelled the reaction of both PAN and PAN-Cu membranes against Cu(II) and sulphide, respectively, and their equilibrium constants were calculated.
10. The change in colour of the membrane, from magenta to yellow, in the presence of sulphide, was used as an analytical parameter. The H coordinate of the HSV color space was obtained with only a digital camera, which opens the door to the use of this assay with other widely distributed imaging devices and could even be used with highly popular smartphones.
11. The assay presented a good sensitivity for sulphide with a detection limit of 0.10 μM and an analytical range of over three orders of magnitude.

Section II

Nanomaterials and sensors

NANOSCIENCE AND NANOTECHNOLOGY

What is nanotechnology? This is not an easy question to answer since this term includes a wide range of meanings. Indeed, the prefix 'nano' comes from the Greek word 'nanos' meaning 'a dwarf'. Hence, 'nanotechnology' might mean the use of a technology to perform really 'tiny' things. The term 'nano' has also used as a useful prefix in science field to mean 1 billionth (using billion in its American sense of a one followed by nine zeros). Nanotechnology is related to a greatly multidisciplinary field of applied science whose main goal is the fabrication of something having less size than 100 nm (1 nm is a billionth of a meter) on an atomic and molecular scale (Definition of nanoscale term collected by International Standardization Organization (ISO) [1].

Nanoscience primarily deals with synthesis, characterization, exploration, and exploitation of nanostructured materials. These materials are characterized by at least one dimension in the nanometer range [2].

As for its meaning, nanotechnology is expected to be associated with the technologies that are operating at the nanoscale and, in fact, is the general sense in which the term is used today. At this point, it would be important to differentiate between 'nanoscience', which is the study of phenomena at the very small scale, and 'nanotechnology', which implies the goal to achieve an end that is somehow useful. In 1994, the Royal Society adopted the following definitions: [3] In one hand Nanoscience was defined as the study of phenomena and manipulation of materials at atomic, molecular and macromolecular scales, where properties differ significantly from those at larger scale and on the other hand Nanotechnology involve the design, characterization, production and application of structures, devices and systems through the control of the shape and size at nanometer level.

The physicist Richard P. Feynman, was the first to introduce the concept of nanotechnology in a talk titled "There´s plenty of room at the bottom" at an American Physical Society meeting at Caltech in 1959[4]. Feynman suggested the possibility that one can manipulate individual atoms and molecules, by using one set of accurate tools to build and operate another proportionally smaller set. In this scenario surface tension and Van der Waals attraction would become much more important than gravity. At the nanoscale, some physical and chemical material properties can differ significantly from those of the bulk structured materials of the same composition; for example, crystals in the nanometer scale have a low melting point and reduced lattice constants, since the number of surface atoms or ions becomes a significant fraction of the total number of atoms or ions and the surface energy plays a significant role in the thermal stability. Therefore, many material properties must now be revisited in light of the fact that a considerable increase in the surface-to-volume ratio is associated with the reduction in material size to the nanoscale, often having a prominent effect on material performance.

Afterwards the term "nanotechnology" was firstly defined by Prof. Norio Taniguchi from Tokyo Science University in 1974 [5]: "nanotechnology mainly consists of the processing, separation, consolidation and deformation of materials by one atom or by one molecule".

One of the main goals of analytical chemistry is the development of new analysis methods either to improve existing methods or to meet the demands of new social or economic problems that require chemical information to be acquired. Thus analytical chemistry can play a major role in nanoscience and nanotechnology: first, analytical chemistry can obtain information on the chemical composition and characterization of nanomaterials generated, while on the other hand, nanotechnological products can be used in the development of new tools and new analytical chemical analysis procedures with superior performance to those currently

existing [6]. Such analysis tools are able to characterize the physicochemical properties of nanomaterials that may arise from many different areas of scientific disciplines.

Furthermore, the development of analytical methods based on nanotechnologies can contribute to simplification and/or improvement of analytical processes or the development of new methods analysis. That is, the need of Nanoscience and Nanotechnology Chemical Analytics for proper characterization of nanomaterials and at the same time, these nanomaterials can offer a promising and innovative way in analytical chemistry, summarized in Figure 1, where two key facets of the relationship are distinguished between Nanoscience, Nanotechnology and Analytical Chemistry. As can be seen, nanomaterials can be considered as useful tools for optimization and innovation of all stages of the analytical process, or may be the means of analysis (e.g. their physico-chemical characterization).

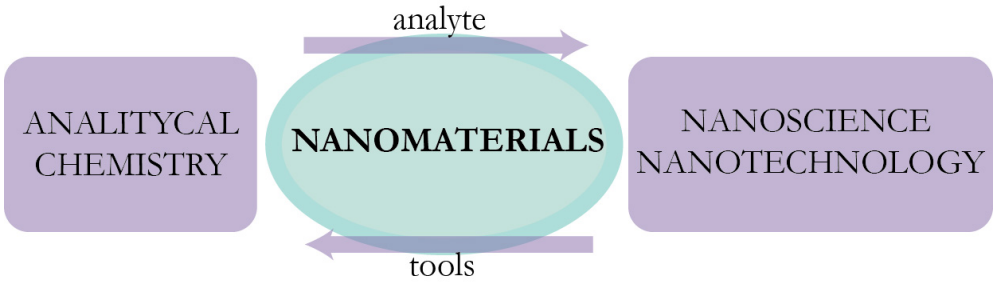

Figure 1. Relationship between nanotechnology and analytical science

Indeed, nanomaterials may participate differently in each of the stages of the analytical process for their outstanding properties (e.g. improving concentration and purification steps, allowing preparation of new stationary phases based on nanomaterials and improving the detection) [6]. In summary, Nanoscience and Nanotechnology are doubly integrated into Analytical Chemistry, leading to a new field called Analytical Nanoscience and Nanotechnology.

Nanomaterials

Synthesis and characterization of nanomaterials are currently attracting high attention as a crucial aspect of nanotechnology research. Nanomaterials are characterized by their use in specific fields, such as field emission, gas sensing, medical diagnostics, field-effect transistors, photovoltaics, and catalysis. It becomes a real challenge to explore different ways to control and manipulate the desired physical and chemical properties of materials as well as the material's potential applications. Thus, nanomaterials are significantly determined by two important nanoscale geometrical parameters: size and shape [7]. Key attributes include: grain size on the order of 1–100 nm, extremely large specific surface area, stronger, more ductile materials and chemically very active materials [8].

In the literature one can find many definitions of the term nanomaterial, although a number of different definitions are currently available, a practicable and unambiguous definition of a nanomaterial is yet to arise [9]. The definition recommended by the European Commission is based on a reference report by the European Commission Joint Research Centre (JRC) [10] and a scientific opinion by the SCENIHR [11]. Inevitably, the final wording and especially the thresholds will comprise political compromises. In this regard, the European Commission states in its Recommendation [12] that nanomaterial is by definition a natural, incidental or manufactured material containing particles, in an unbound state or as an aggregate or as an agglomerate and where, for 50% or more of the nanomaterial, one or more external dimensions is in the size range 1 nm–100 nm. Only in specific cases and where warranted by concerns for the environment, health, safety or competitiveness the number 50 % may be replaced by a threshold between 1 % and 50 %.

Only quantum mechanics can correctly describe most behavior of nanoscale materials [13]. As materials are reduced to the nanoscale, they can suddenly show

significant different properties compared to what they may exhibit on a macroscale, allowing unique applications [14]. The concept of size effect refers to the strong influence of the nanocrystal on the physical properties produced by the size of the nanocrystal [15-17].

The term morphology is used to describe the study of form comprising shape, size and structure. Unlike bulk materials, the functional characteristics of nanomaterials or nanodevices are strongly associated with their shape [18]. It has been reported that most of distinct shape effects are observed in the density of energy states, and where the band-gap of nanomaterials is also affected by shape [19].

General classification of nanomaterials

The materials sintered by means of the controlled manipulation of their microstructure on the atomic level may be classified into three groups [2]. The first category comprises materials with reduced dimensions and/or dimensionality in the form of isolated, substrate-supported or embedded nanometer-sized particles, thin wires or thin films. This is the case of materials which properties depend on the microstructure as catalysts or semiconductors utilizing single or multilayer quantum well structures.

The second category comprises materials in which the nanometer sized microstructure is limited to a thin (nanometer-sized) surface region of a bulk material. For example, surfaces with enhanced corrosion resistance, hardness, or protective coatings.

The third category comprises bulk solids with a nanometer-scale microstructure. Those are solids in which the chemical composition, the atomic arrangement and/or the size of the building blocks forming the solid varies on a length scale of a few nanometers throughout the bulk.

One of the basic results of materials science is the insight that most properties of solids depend on the microstructure. A reduction in the spatial dimension, or confinement of particles or quasi-particles in a particular crystallographic direction within a structure generally leads to changes in physical properties of the system in that direction.

Materials at the nanoscale level are known to have physical and chemical properties that can be markedly different from those of their bulk counterparts. Conventionally, crystalline materials having morphological features smaller than 100 nm, in at least one dimension, are said to be nanomaterials. However, if the size, in at least one dimension, is smaller than the exciton Bohr radius for a given material, the nanomaterial is quantum confined. Although there are different properties to classify nanomaterials (e.g., morphology, dimensionality, and composition), it is useful to classify them according to the number of dimensions of confinement, or the number of dimensions which lie within the nanometer range (Figure 2):

a) 0D-zero-dimensional structures, those are materials confined in all three dimensions, e.g. nano-pores and nano-particles as quantum dots, carbon dots.

b) 1D nanomaterials with two dimensions at the nm scale and no confinement along one dimension of the material; e.g. filamentary structures where the length is substantially greater than the cross-sectional dimensions such as nanotubes, nanowires or quantum wires.

c) 2D nanomaterials with one dimension at the nm scale and no confinement along two dimensions of the material; e.g. layered or laminate structures, as thin films, layered films or quantum wells.

d) 3D nano-structured materials, systems confined in three dimensions, e.g. structures typically composed of consolidated equiaxed crystallites.

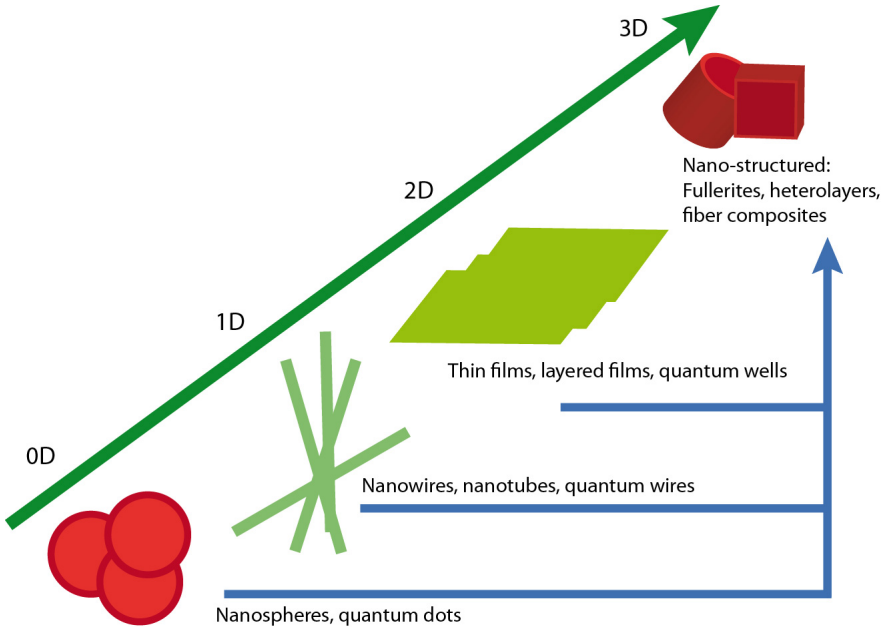

Figure 2 Dimensionality classification of nanostructures[20].

Synthesis of nanomaterials

There are two general approaches to the synthesis of nanomaterials and the fabrication of nanostructures: one is the bottom-up approach, which is the miniaturization of the components, and the other is the top-down approach where manipulation of nanostructured materials is accomplished by physical manipulation with external tools.

Bottom-up approaches to nanofabrication use chemical or physical forces operating at the nanoscale to assemble basic units into larger structures. Bottom-up approaches seek to have smaller components arrange themselves into more complex assemblies, while top-down approaches seek to create nanoscale devices by using larger, externally-controlled ones to direct their assembly. Top-down methods

include high-energy milling, ion implantation, lithography, laser ablation, sputtering, vapor condensation, etc.

Bottom-up approaches to nanomaterials use synthesis and molecular organization at the molecular scale to manifest properties at the nanoscale. It requires a deep understanding of the individual molecular structure of nanomaterials, their assemblies and dynamic behaviors, and it also requires a broad multidisciplinary approach. Bottom-up methods include sol-gel, precipitation, electron deposition, cluster assembly/consolidation, self-assembly, self-alignment, chemical vapor deposition, atomic layer deposition, anodization, etc. (See Figure 3). [2]

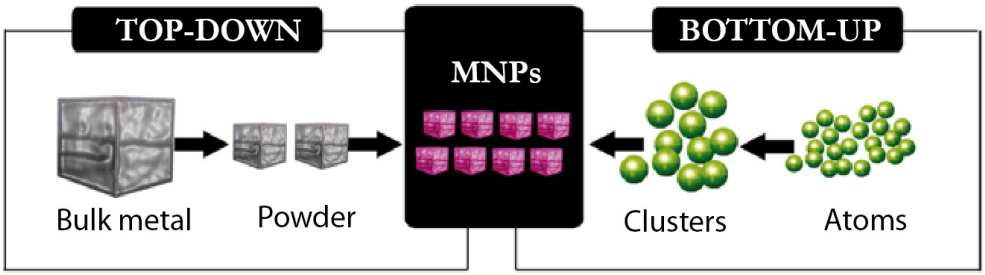

Figure 3. Bottom-up and top-down approaches for synthesis of nanomaterials

Photonic crystals

The photonic structures appeared in nature several hundred millions years ago. In the living world, color is used for communication and this important function strongly impacts the individual chances of survival as well as the chances to reproduce. This has a statistical influence on species populations. Therefore, because they are involved in evolution, natural color-generating structures are – from some point of view – highly optimized. Natural photonic crystal-type structures, which affect light-wave propagation, occur in insects, spiders, birds, fishes and other marine animals, or in plants. Animals such as certain butterflies and beetles use them for mimicry and survival techniques, for example, to distract predators (Figure 4) [21].

Figure 4. The flower beetle *Chrysina resplendens* displays a permanent metallic gold appearance.

Photonic crystals can be considered as periodic arrangements of regularly shaped materials (often a multiplicity of layers or spheres in a host polymer) with different dielectric constants. Periodicity can vary from single-dimensional (1D) to three-dimensional (3D) (Figure 5).

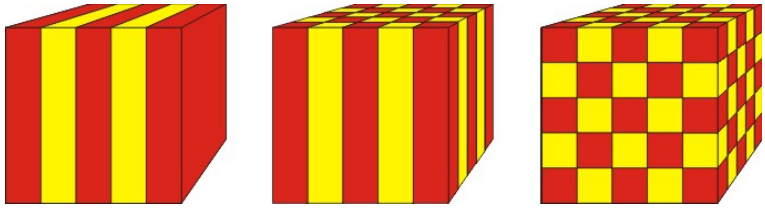

Figure 5. Schematic representation of the three types of photonic crystals. The different colors represent materials with different dielectric constants. 1) Periodic in one dimension; 2) Periodic in two dimensions; 3) Periodic in three dimensions.

Photonic crystals have distinct wavelengths of reflection that are governed by the distance between the layers or spheres, and this causes their specific color. From a physical point of view, the photonic crystals can be described as nanoarchitectures

composed by a periodic arrangement of regularly shaped, mostly transparent materials with different dielectric constants. The material is engineered such that only light of a certain wavelength can propagate through the lattice of this arrangement [22].

One-dimensional photonic crystals are the simplest one in which the periodicity exists in only one dimension. These are also known as Bragg reflectors or Bragg stacks, which reflect one specific wavelength. They are typically produced by techniques such as layer-by-layer deposition, multiple spin coating, or photolithography.

Two-dimensional photonic crystals are characterized by their periodicity in two spatial directions. They are produced by complex top-down methods such as photolithography and etching techniques and the nanostructures can be varied in form, order, size, and defects to manipulate their properties.

Three-dimensional photonic crystals display periodicity in three dimensions. Examples in nature of common 3D structures are opals and inverse opals. Although there are several different top-down approaches to produce 3D photonic crystals, chemical bottom-up methods are now simpler and cheaper.

A photonic crystal array can be considered as dielectric spheres within a dielectric medium such as air or solvent. An important property of photonic crystals is that they reflect certain wavelengths similarly to X-ray diffraction regularly arranged atoms in a structure. The Bragg's law of diffraction describes the constructive interference according to eq. 1

$$2d\cos\theta = m\lambda \qquad \text{(eq. 1)}$$

where d is the distance between atomic planes, θ is the angle of incident light, m is the order of diffraction, and λ is the wavelength of incident light. Combining the Bragg's law with Snell's law of refraction results eq. 2

$$2d\left(n_{eff}^2 - \sin^2\theta\right)^{1/2} = m\lambda \qquad \text{(eq. 2)}$$

where n_{eff} is the mean effective refractive index, defined according to eq. 3

$$n_{eff}^2 = n_p^2 V_p + n_m^2 V_m \quad \text{(eq. 3)}$$

where n_p and n_m are the refractive indices of the particles and surrounding medium, respectively, and V_p and V_m are the respective volume fractions.

The reflected wavelength can be calculated using the center-to-center distance D between the particles according to eq. 4.

$$\sqrt{\frac{8}{3}} D\left(n_{eff}^2 - \sin^2\theta\right)^{1/2} = m\lambda \quad \text{(eq. 4)}$$

The use of photonic crystals in chemical sensing is based on the modification of the reflected wavelength by a chemical that modifies either the distance or refractive index. The types of photonic crystal sensors can be classified into three major types [23]: a) on-chip nanoscale resonators or waveguides; b) Bragg stacks made of mesoporous photonic crystals, and c) colloidally templated 3D photonic crystals [23].

The first type based on either on-chip nanoscale resonators or waveguides are generally actuated by either changes in the local refractive index surrounding the cavities, or by adsorption of proteins [24]. Many advantages can be cited: a) the small mode volume and sensor footprint allow that relatively small molecules, such as single proteins, to induce measurable changes in the cavity resonance, and also enable many sensors to be integrated into a single, CMOS-compatible chip; b) As the photonic crystal cavities have much smaller line widths, that is, higher quality factors than typical Bragg reflection peaks, very small perturbations can be detected enhancing the sensitivity of the sensors; c) Large-scale fabrication is often compatible with the CMOS technique, thereby potentially allowing easy integration of this type of sensor into consumer electronics. The main drawback of this kind of sensor includes the cost, power, and complexity of the readout as well as precise nanofabrication, for which a limited for high quality factors.

The second type of sensors based on photonic crystals uses Bragg stacks made of materials such as mesoporous silicon/silica/titania and are based on the adsorption of analyte in the pores. They show the advantage of the small size of the pores, which enables such sensors to gain specificity and sensitivity compared to simple refractive index sensors. This is achieved through a couple of mechanisms: a) for larger molecules, the size of the pores can actually be tuned to filter for specific analytes [25]; b) for smaller molecules, mesoporous materials can have sufficiently small pores and high porosity so that single-layer adsorption creates a large change in the effective refractive index. This allows the use of selective adsorption, rather than only differences in the refractive index of the adsorbing material [26]. Among their disadvantages can be cited a limited choice of available materials compared to colloidal PhCs, but greater than that for integrated resonators, and colorimetric readout methods have been developed albeit with a trade-off in sensitivity, since broad peaks are typically being actuated and large shifts (30–50 nm) are required for visible color change [27]. Additionally, because of the spectroscopic readouts used, they can be made at a lower cost than for integrated resonators with high Q factors [26].

The third type of sensors are the colloidally templated 3D photonic crystals (e.g. opals or inverse opals) [28;29]. They possess the advantages of enabling many types of materials to be incorporated into the structure, and many different sensing mechanisms can be used, which include changes in the refractive index resulting from pore filling, polymer/hydrogel swelling by liquids, and changes induced by physical stimuli such as strain, electric fields, magnetic fields. As a drawback, colorimetric detection requires large resonance shifts and thus limits the sensitivity of many of the sensing mechanisms.

Porous silicon

A type of interesting material for use as a photonic crystal type is porous silicon. Nanoporous silica results from the electrochemical anodization of single crystalline silicon wafers with hydrofluoric acid. Pore morphology and pore size can be modified by controlling the current density, the type and concentration of dopant, orientation of the crystalline Si, and the electrolyte concentration in order to form macro-, meso-, and micropores [30].

The electrochemically driven reaction consists of a boron doped single crystalline silicon working electrode in a HF electrolyte that upon application of current, causes a reaction whereby Si is attacked by a fluoride ion that replaces the reactive hydrides on the Si surface releasing hydrogen.

Pore formation ranging from ~1-20 nm occurs as the Si atoms are displaced in the form of SiF_4 and SiF_6^{2-} species (Scheme 1).

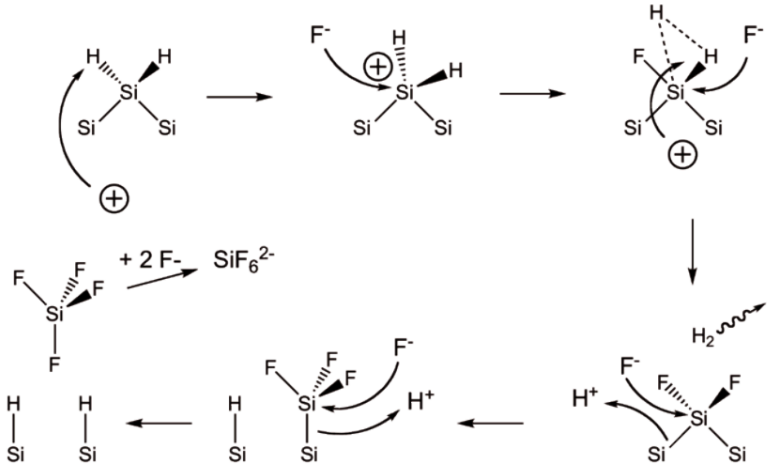

Scheme 1. Porous silicon formation.

Depending on the etching conditions by either application of a constant current pulse or by the sinusoidal modulation of current one can obtain a tunable signal in the reflectivity spectrum of the material.

Upon illumination of the films with white light at an angle incident to the film, an interference pattern can be observed with the aid of a CCD spectrometer.

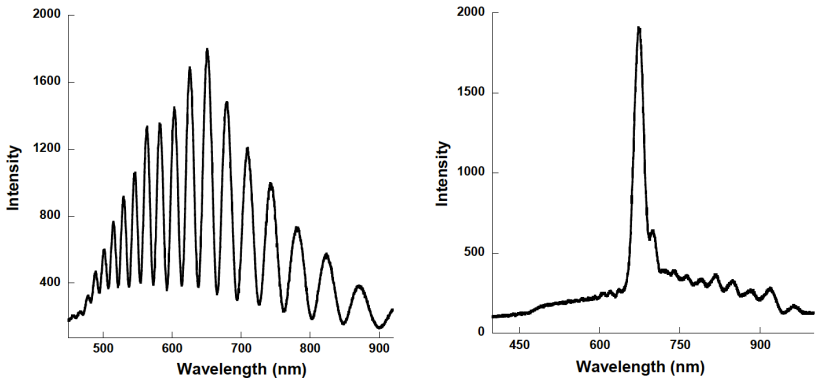

Figure 6. a) Reflectance spectrum of a Fabry-Pérot film; b) Reflectance spectrum of a rugate film.

Depending on the electrochemical etching conditions; various nanostructures can be fabricated within the film including a rugate filter or Fabry-Pérot film (Figure 6a). For Fabry-Pérot interference, the peak maxima and minima represent constructive and destructive interference, respectively, from the porous silicon/air and porous silicon/crystalline silicon interfaces. The interference patterns can also be tuned to resonate as a single reflectance signal known as a rugate (Figure 6b) that can be fabricated by applying a sinusoidal variation of current during the etching process, and this type of spectral peak can be conveniently tuned to resonate at many different wavelengths in the visible spectrum. The observable changes in the Fabry-Pérot interference patterns upon incorporation of analyte into the film allow one to monitor the infusion or diffusion of analyte from the porous matrix. The observable changes obey the Fabry-Pérot interference relationship (eq. 2).

In addition to the use of porous silicon as sensing material for different types of sensors and biosensors [23;25;26;31-39], another interesting use of this material is drug

delivery. Drug delivery is an expanding field in medicine that seeks to improve the efficacy of the drug by either extending the time at which the drug is considered therapeutically relevant or localizing the drug directly to the diseased site. Controlling the rate at which drug is delivered to the patient through a sophisticated delivery device would eliminate the need for multiple administrations and increase the efficacy of the therapy. The most highly used materials for drug delivery are polymers, for their chemical and physical properties, mainly biodegradablity, biocompatibility, mechanical strength, and elasticity. The release rate of the drug incorporated into the polymeric matrix is typically dependent on the degradation properties of the polymer.

Other materials investigated for controlled drug delivery are porous materials and reservoir devices, which use a void volume to house therapeutics and release them either constitutively from the reservoirs or upon application of an external stimulus. One of these materials is the biocompatible silica, an extensively studied type of porous material. Porous silicon is a good candidate for controlled and localized release of therapeutics within the body due to the ease of processing, tunable pore sizes and volumes, high surface area within the material, and convenient routes to chemical modification.

An interesting property of porous Si is the ability to easily tune the pore sizes and volumes during electrochemical etching [40]. Other porous materials require some advanced design protocols to control pore size. Control over the porosity and pore size is obtained by adjusting the current settings during the electrochemical processing of porous silicon. Typically, greater current density used in fabrication produces larger pores. Large pores are desirable when incorporating sizable molecules or drugs within the pores. Not only is pore size and porosity important regarding the range of molecules to be incorporated within the pores, but it also determines degradation rates of the porous Si [41]. Smaller pores provide more surface

area and expose more sites upon which aqueous media can attack. With smaller porous filaments within the film, greater dissolution rates of porous Si are attained. This provides a convenient means to control degradation rates of porous Si. The current density used in the electrochemical etch determines the pore size, shape, and porosity of the films and in turn determines the dissolution rate of the porous Si. One important feature of porous Si is the ability to tune the degradation rates of the material as the porosity and type of Si determines the lifetime of the material *in vivo*.

Other characteristics of porous silicon as material to release drugs, is their ability to "self-report" drug delivery. The incorporation of analyte into the porous Si film causes the interference patterns to shift to higher wavelengths which are dependent on the composition/refractive index of the guest molecule. On the other hand, when drug diffuses from the porous matrix, the interference patterns shift to lower wavelengths yielding information on the release of drug from the porous matrix [38;42;43] (see Figure 7 and 8).

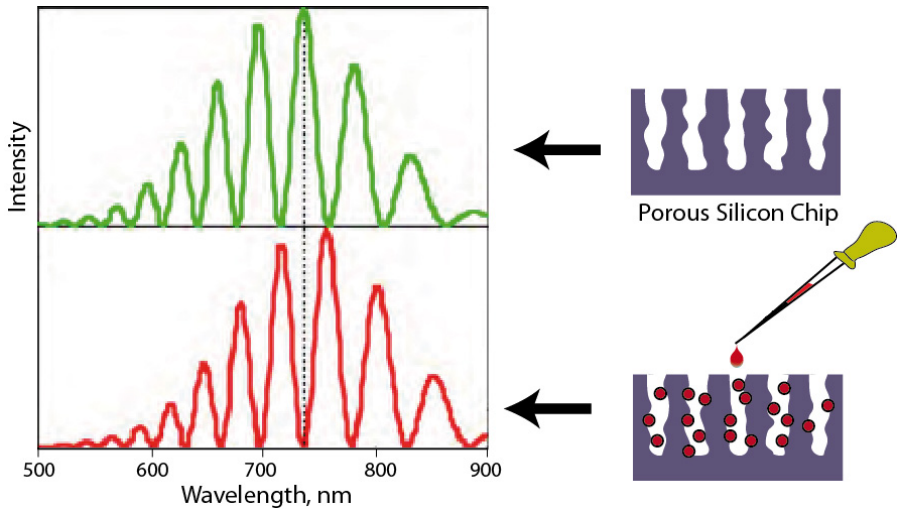

Figure 7. Schematic showing the change (red shift) in a Fabry-Pérot reflectance spectrum upon addition of analyte (drug molecules) into the porous matrix [44].

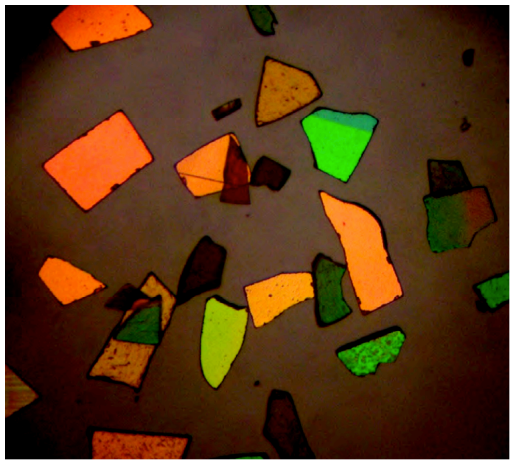

Figure 8. Light microscope image of porous Si particles [44].

REFERENCES

1. ISO. ISO/TS 12805:2011 Nanotechnologies - Materials specifications - Guidance on specifying nano-objects. Internet . 2011.

2. V. Pokropivny, R. Lohmus, I. Hussainova, A. Pokropivny S. Vlassov in *Introduction to nanomaterials and nanotechnology,* Tartu, 2007.

3. The Royal Society and Royal Academy of Engineering, Nanoscience and Nanotechnologies: Opportunities and Uncertainties,2014.

4. R.P. Feynman, *Eng.Sci.* 1960, 23, 22-36.

5. Taniguchi, N. *Proceeding of International Conference on Production Engineering* , 1974 18-23.

6. M. Valcarcel, B.M. Simonet, *Anal.Bioanal.Chem.* 2011, 399, 1-2.

7. Y.w. Jun, J.s. Choi and J. Cheon, *Angew.Chem.Int.Ed.* 2006, 45, 3414-3439.

8. M.G. Lines, *J.Alloy Compd.;* 2008, 449, 242-245.

9. W.G. Kreyling, M. Semmler-Behnke and Q. Chaudhry, *Nano Today* 2010, 5, 165-168.

10. Rauscher, Hubert, Roebben, Gert, Sokull-Kluettgen, Birgit, Gibson, Peter, Putaud, Jean-Philippe, and Stamm, Hermann, Considerations on a Definition of Nanomaterial for Regulatory Purposes,2010.

11. SCENIHR, SCENIHR's Opinion on: Scientific Basis for the Definition of the Term "nanomaterial",2010.

12. EU Commission, *OJEU* 2011, 275, 38-40.

13. B. Gao, J. Jiang, K. Liu, Z. Wu, W. Lu and Y. Luo, *J.Comput.Chem.* 2008, 29, 434-444.

14. H. Zeng, J. Li, J.P. Liu, Z.L. Wang and S. Sun, *Nature* 2002, 420, 395-398.

15. A.P. Alivisatos, *Science* 1996, 271, 933-937.

16. R. Jin, Y. Cao, C.A. Mirkin, K.L. Kelly, G.C. Schatz and J.G. Zheng, *Science* 2001, 294, 1901-1903.

17. G. Ouyang, C.X. Wang and G.W. Yang, *Chem Rev.* 2009, 109, 4221-4247.

18. M.K. Sanyal, A. Datta and S. Hazra, *Pure Appl.Chem.* 2002, 74, 1553-1570.

19. Y.w. Jun, J.s. Choi and J. Cheon, *Angew.Chem.Int.Ed.* 2006, 45, 3414-3439.

20. J.A. Garcia-Calzon, M.E. Diaz-Garcia, *TrAC, Trends Anal.Chem.* 2012, 35, 27-38.

21. J.P. Vigneron, P. Simonis, *Physica B Condens.Matter* 2012, 407, 4032-4036.

22. J.D. Joannopoulos, S.G. Johnson, J.N. Winn R.D. Meade in *Photonic Crystals: Molding the Flow of Light,* 2nd ed. ed., University Press Princeton, Princeton, 2008.

23. C. Fenzl, T. Hirsch and O.S. Wolfbeis, *Angew.Chem.Int.Ed.* 2014, 53, 3318-3335.

24. S. Mandal, X. Serey and D. Erickson, *Nano Lett.* 2009, 10, 99-104.

25. M.M. Orosco, C. Pacholski and M.J. Sailor, *Nat Nano* 2009, 4, 255-258.

26. L.D. Bonifacio, D.P. Puzzo, S. Breslav, B.M. Willey, A. McGeer and G.A. Ozin, *Adv.Mater.* 2010, 22, 1351-1354.

27. H. Xu, P. Wu, C. Zhu, A. Elbaz and Z.Z. Gu, *J.Mater.Chem.C* 2013, 1, 6087-6098.

28. X. Xu, A.V. Goponenko and S.A. Asher, *J.Am.Chem.Soc.* 2008, 130, 3113-3119.

29. C. Fenzl, S. Wilhelm, T. Hirsch and O.S. Wolfbeis, *ACS Appl.Mater.Interfaces* 2012, 5, 173-178.

30. L. Canham in *Properties of Porous Silicon,* Short Run Press Ltd, London, 1997.

31. R.R. Chandler-Henderson, B. Sweryda-Krawiec and J.L. Coffer, *J.Phys.Chem.* 1995, 99, 8851-8855.

32. K. P. Dancil, PhD Thesis, University of California, 1999.

33. T.L. Kelly, S. Garcia and M.J. Sailor, *Nano Lett.* 2011, 11, 3169-3173.

34. S.E. Letant, M.J. Sailor, *Adv.Mater.* 2000, 12, 355-359.

35. R.J. Martin-Palma, M.J. Sailor, *J.Mater.Res.* 2013, 28, 151.

36. C. Pacholski, M. Sartor, M.J. Sailor, F. Cunin and G.M. Miskelly, *J.Am.Chem.Soc.* 2005, 127, 11636-11645.

37. A.M. Ruminski, M.M. Moore and M.J. Sailor, *Adv.Funct.Mater.* 2008, 18, 3418-3426.

38. B. Sciacca, E. Secret, S. Pace, P. Gonzalez, F. Geobaldo, F. Quignard and F. Cunin, *J.Mater.Chem.* 2011, 21, 2294-2302.

39. C.K. Tsang, T.L. Kelly, M.J. Sailor and Y.Y. Li, *ACS Nano* 2012, 6, 10546-10554.

40. G. Zhang in *Modern Aspects of Electrochemistry*, Vayenas, C. G.; White, R.Gamboa-Adelco, M., Eds. ed. , 39 ed., Springer US, 2006, 65-133.

41. S.H.C. Anderson, H. Elliott, D.J. Wallis, L.T. Canham and J.J. Powell, *Phys.Stat.Sol.(a)* 2003, 197, 331-335.

42. S.M. Haidary, E.P. Corcoles and N.K. Ali, *J.Nanomater.* 2012, 830503, 15.

43. E.C. Wu, J.S. Andrew, L. Cheng, W.R. Freeman, L. Pearson and M.J. Sailor, *Biomaterials* 2011, 32, 1957-1966.

44. M.J. Sailor in *Porous Silicon in Practice: Preparation, Characterization and Applications,* Wiley-VCH Verlag GmbH & Co. KGaA, 2012.

Chapter III

Synthesis and properties of carbon nanoparticles

CHAPTER III: SYNTHESIS AND PROPERTIES OF CARBON NANOPARTICLES

OBJECTIVES

The main goal of this chapter is to explore the analytical possibilities of the carbon nanoparticles, nanodots or carbon dots (Cdots). These particles are typically 10 - 45 nm with a specific surface area of 30 - 50 m^2 g^{-1} and have interesting analytical possibilities that vary with the structure of the particles and synthetic methodology used for particles preparation. The overall objective of the work presented in this chapter is the preparation of carbon dots, evaluation of their luminescent properties and their use as a sensing material for optical sensors.

The specific objectives to achieve in this chapter are:

- Use of different synthetic routes for Cdots preparation and to study the different factors influencing the synthesis.
- Characterization of the Cdots prepared.
- Evaluation of their absorption and luminescence properties, as well as the evaluation of their ability for recognizing various molecular species, mainly metallic ions.
- Study of the cytotoxicity and cell permeability of Cdots and investigation of the ability of Cdtos to sense metallic ions in biological systems.

CARBON DOTS FOR COPPER DETECTION WITH DOWN AND UPCONVERSION FLUORESCENT PROPERTIES AS EXCITATION SOURCE

ABSTRACT

Carbon dots were synthesized by a simple and "green" strategy for selective and sensitive detection of Cu(II) ions detection using both down- and up-conversion fluorescence. These fluorescent nanosensors demonstrated low cytotoxicity and were applied for the intracellular sensing and imaging of Cu(II) in biological systems.

INTRODUCTION

It is well known that copper Cu(II) detection in cells is crucial due to Cu(II) plays essential structural roles in many proteins and enzymes; however, high intracellular Cu(II) concentrations may be toxic for the organism. Accordingly, Cu(II) is a key trace element for many biological mechanisms and otherwise is listed as priority pollutant by the Environmental Protection Agency (EPA). For this reason, currently, there is a great interest to develop new nanomaterials and novel green and low cost synthetic designs for heavy metals detection.[1]

Fluorescent nanoparticles (NPs) including quantum dots, dye-doped NPs and rare earth-based NPs have been a major focus of research and development during the past decade for being used in sensing and bioimaging. To date, large amounts of "classic" photoluminescent NPs have been developed from novel materials but, in contrast, also they have raised new concerns over their potential toxicity and environmental harm.[2] On the other hand, they show several drawbacks, such as the involvement of a high number of extra processes to modify the particle surface which at the end it is time-consuming. So far, a great effort has been made to develop green methodologies that allow synthesizing new nanomaterials in order to

replace the toxic compounds, organic solvents, current costs and time-consuming processes.

Recently, new NPs called Carbon dots (Cdots) have emerged and attracted growing interest in analytical and bioanalytical chemistry. Cdots exhibit excellent fluorescent properties with high photostability, high quantum yield, water solubility and favourable biocompatibility. They have simple and cost-effective synthesis and possess an environmentally friendly method at large scale. Although these Cdots-based materials hold great promise in nanotechnology and nanomedicine, much work is still necessary to explore the full potential of these nanomaterials in the development of advanced smart sensors. Additionally, Cdots show size dependent photoluminescence and upconversion luminescence properties due to multiphoton process that lead to anti Stokes type emission.[3]

Thus, we can expect that Cdots may possess interesting luminescent properties such as visible and upconversion fluorescent simultaneously, which are extremely important for fundamental and practical applications. In particular, the up-conversion fluorescent materials can convert a longer wavelength radiation (e.g., near infrared light (NIR)) into shorter wavelength fluorescence (e.g., visible light). In comparison with downconversion fluorescent materials, upconversion materials have many advantages for future biological applications, such as to be non-invasive, improved tissue penetration depth at NIR radiation and show absence of autofluorescence in biological tissues.[4]

Most of the upconversion fluorescence materials reported so far are inorganic crystals doped with rare-earth elements, encapsulated organic dyes or quantum dots in silica shell. Until now, there are only few materials which can display both, down and upconversion fluorescence implemented in optical sensors.[5] However, to our knowledge, no fluorescent nanosensors for Cu(II) detection based on upconverting fluorescent of Cdots have been reported yet.

In the present work, the synthesis of optical sensors for Cu(II) detection through UV and NIR as excitation source has been performed. These nanosensors are expected to be used for selective and sensitive Cu(II) detection in environment and biological systems.

EXPERIMENTAL SECTION

Synthesis of cdots

The water soluble Cdots were synthesized by rapid and one-step procedure with a microwave by pyrolyzing citric acid in presence of polyethylenimine (PEI). Briefly, 1 g citric acid and 0.5 g PEI were dissolved in 20 mL of hot water. Then, it was placed in a microwave and heated at 180 ºC for 5 min at maximum potential (850W). When cooled down to room temperature, the yellow color solution was purified by ultrafiltration.

Instrumentation

Microwave Milestone MicroSYNTH was use for synthesis. XRD were carried out at the Centre of Scientific Instrumentation (University of Granada) on a Fisons-Carlo Erba analyser model EA 1108. The IR spectra on powdered samples were recorded with a ThermoNicolet IR200FTIR by using KBr pellets.

Fluorescence data were collected using a Varian Cary Eclipse luminescence spectrometer (Varian Ibérica, Madrid, Spain). A Confocal microscope LSM 510 Meta (ZEISS, Jena, Germany) equipped with ZEN 2009 software and a UV laser (405 nm) and Enterprise II (Coherent Inc., Santa Clara, CA, USA) was used. Fluorescence decay traces were recorded in the Time Correlated Single Photon Counting (TCSPC) mode using the Fluo-Time 200 fluorometer (PicoQuant, GmbH, Germany). Briefly, the samples were excited through a 405 nm pulsed laser (EPL 405, Edinburgh

Instruments) with a 10 MHz repetition rate. The full width at half maximum of the laser pulse was 90 ps. The fluorescence was collected after crossing through a polarizer set at the magic angle and a 2 nm bandwidth monochromator. Fluorescence decay histograms of Cdots were collected using a TimeHarp 200 board, with a time increment per channel of 36 ps, at the emission wavelengths of 435 nm. The histograms of the instrument response function (IRF) were determined using LUDOX scatterer, and sample decays were recorded until they reached 6 x 10^4 counts in the peak channel. Such a large number of counts were collected because it is well known that complex decays can be well described by the simplest exponential models if the fitting is carried out from experimental data with a low number of counts per channel.

Nihydrin colorimetric assay

We added 0.5 mL of cyanide-acetate buffer (0.0002 M NaCN in acetate buffer 3.8 M pH 5.3-5.4) and 0.5 mL of 3% ninhydrin solution in 2-methoxyethanol to 1 mL sample containing amino groups. The samples were heated for 15 min in a water bath kept at 100 ºC. Maximal color was developed after 10-12 min. immediately after removing it from the water bath, we added rapidly 5 mL of isopropyl alcohol-water (1:1) diluent. Then, we shook it vigorously and allowed it to cool to room temperature [17].

Methods of analysis time resolved fluorescence decay time

Time resolved fluorescence decay traces were deconvoluted from the signal and fitted using the FluoFit 4.4 package (Picoquant). The experimental decay traces were fitted to triexponential functions via a Levenberg–Marquardt algorithm based on nonlinear least-squares error minimization deconvolution method. Usually, up to

three different exponential terms were used to fit the experimental decay traces. The quality of the fits was judged by the reduced chi-squared method, χ^2, the weighted residuals and the correlation functions. The latter two were checked for random distributions. To compare the photoluminescence lifetime of the free Cdots and Cdots in presence of Cu(II) at different concentrations, it was necessary to determine their average lifetime using eq. 1:

$$\tau_{ave} = \sum a_i \tau_i^2 / \sum a_i \tau_i \quad \text{(Eq. 1)}$$

where a_i are the pre-exponential factors and τ_i are the lifetimes obtained in the triexponential fitting of the decay curves of Cdots emission.

Cell culture

For culturing NIH-3T3, cells were grown in DMEM high glucose including 10% fetal calf serum at 37°C and 5 % CO_2. Incubation with Cdots was performed under culturing conditions. Cdots were then diluted 10^4-fold in culturing medium. For live cell imaging cells were mounted in coverslips in Leibovitz L-15 medium including 10 % fetal calf serum.

Live cell imaging

Cells were imaged on a LSM 510 Meta (ZEISS, Jena, Germany) equipped with ZEN 2009 software, using a heating Insert P (PeCon, Erbach, Germany) to keep the temperature at 37°C. Cdots were excited with a 405 nm laser, resulting fluorescence was collected from 450 to 750 nm for spectroscopy and from 450 to 550 nm for imaging. The scanner and detector were mounted on an inverted microscope (X) equipped with an oil immersion X-numerical aperture 60x objective (Zeiss). In order to stain membranes, cells were pre-stained in protein free media with 0.005 % ($w.v^{-1}$)

Evans blue. Evans blue was excited with a 514 nm laser line; its fluorescence was recorded using a 585 nm long pass filter.

Dynamic Light Scattering (DLS) demonstrated that they are well dispersed with an average size of 12 nm (0.212 PDI) (see Figure 1).

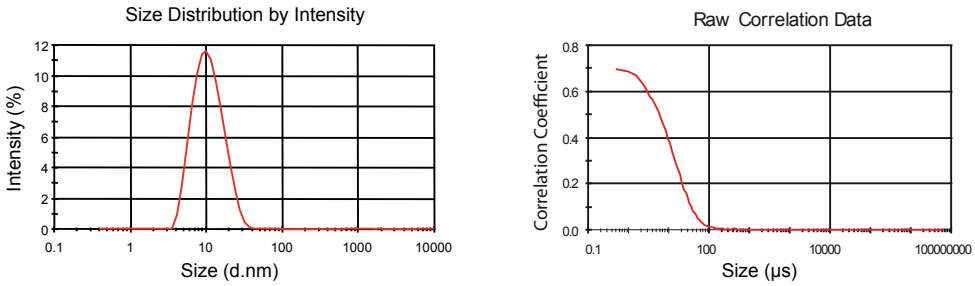

Figure 1. DLS showed some dispersion of Cdots at pH = 4. (a) size distribution intensity and (b) raw correlation data.

The infrared spectrum of Cdots given in Figure 2shows typical bands of PEI.

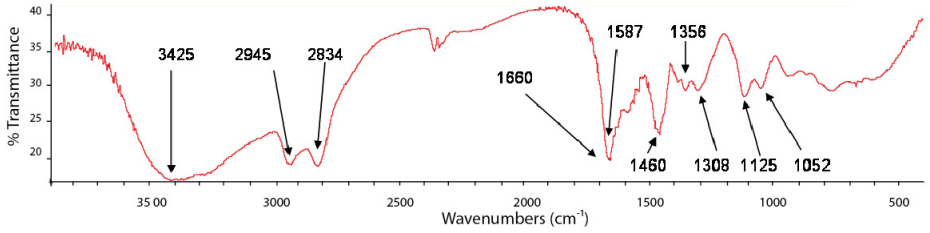

Figure 2. FTIR spectrum of Cdots.

The zeta potential at pH 4 was +21 mV and the ninhydrin colorimetric assay confirms the presence of primary and secondary amines on the nanoparticle surface (Figure 3).

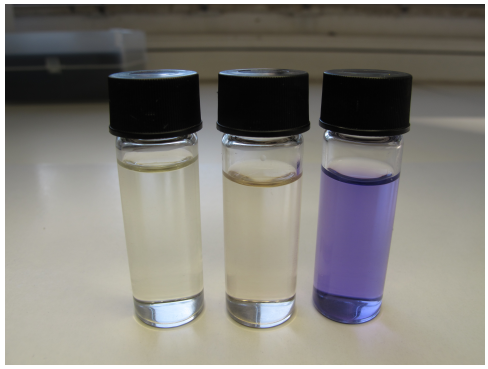

Figure 3. Photographs of solutions under nihydrin colorimetric assay. (a) Water, (b) Cdots without PEI and (c) Cdots with PEI.

X-ray diffraction (XRD) pattern display a broad diffraction peak at 2Φ=18.5º (Figure 4), suggesting an amorphous material.

As shown in Figure 5, the Cdots exhibit excellent water solubility and blue luminescence under UV excitation light (365 nm).

To further explore the optical properties of Cdots, a detailed fluorescence study was performed using different excitation wavelengths (see Figure 6).

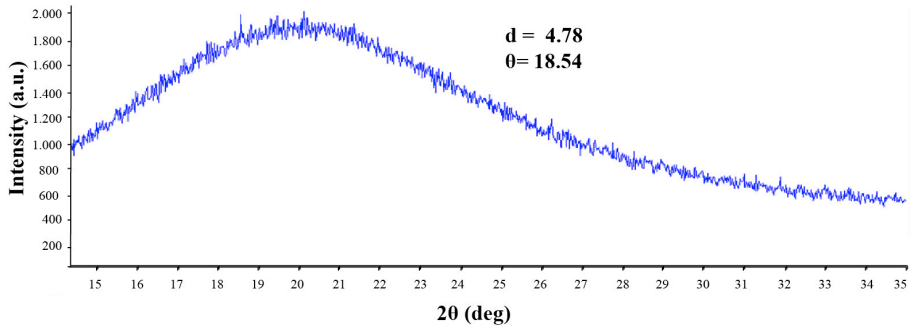

Figure 4. XRD spectrum of Cdots.

Using quinine sulphate as standard, the fluorescence quantum yield was found to be 30%.

Figure 5. Photographs of Cdots solutions under visible light (right) and UV beam of 365 nm (left) in comparation with only water.

Remarkably, these Cdots NPs also exhibit good upconversion fluorescent properties besides their strong emission luminescence in 450-650 nm range. Figure 6 shows the fluorescent spectra of Cdots excited by long wavelength light (maximum intensity with 850 nm excitation) with the upconversion emissions located in the range of 380-550 nm. Therefore, this result suggests that Cdots may be used as a powerful reagent and label in biological applications as well as for an appropriate sensor design for environmental applications.

The influence of pH on these Cdots in the range 2-11 was studied. The results showed that the maximum fluorescence activity of the Cdots was observed at pH = 4 (see Figure 7 in the ESI†), which may be attributed to the protonation of amino

groups. The good fluorescence presented by the Cdots over a wide range (pH = 2-8), makes them of a valuable use for biological applications.

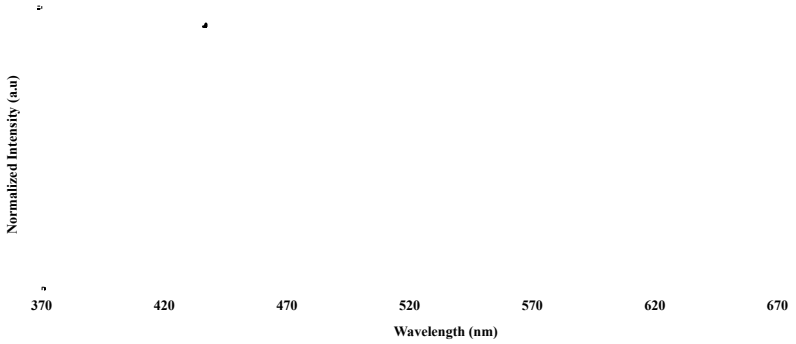

Figure 6. Fluorescent emission by UV excitation 350 nm (gray line) and NIR excitation 850 nm (black line).

After characterizing the Cdots, it was checked whether the amine groups in Cdots kept the properties for Cu(II) and other metals recognition. For such purpose, the quenching behaviour of Cu(II) ions in the luminescence properties of the Cdots was investigated in pH 4 buffer.

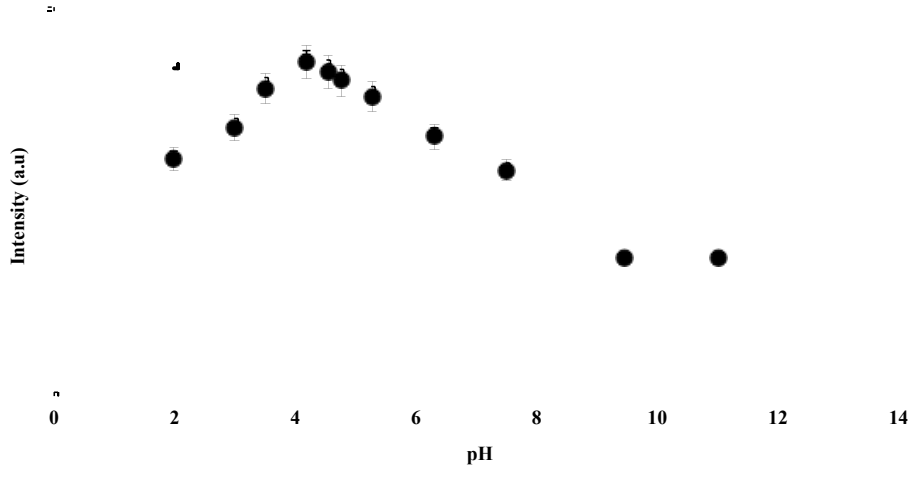

Figure 7. Effect of pH on the fluorescence intensity of Cdots.

In recent published works, this quenching effect is described and assumed that results from the inner filter effect.[6] The quenching efficiency of the fluorescence by Cu(II) was nearly fitted to the Stern-Volmer equation ($I_0/I = K_{SV}[Q]+1$), which correlates the fluorescence intensity, I, at different concentrations of the quencher, [Q], (being I_0 the fluorescence intensity at [Q] = 0, and K_{SV} the Stern-Volmer constant). However, in this case, the plot I_0/I versus [Q] shows a degree of non-linearity what indicates the presence of both static and dynamic quenching of the fluorescence in the mechanism of interaction (Figure 8).

This result was confirmed by the measurement of fluorescence lifetime. The decay curves of Cdots showed tri-exponential behaviour, in agreement with previous reports.[3] The fluorescence decay curves were also Cu(II) sensitive.

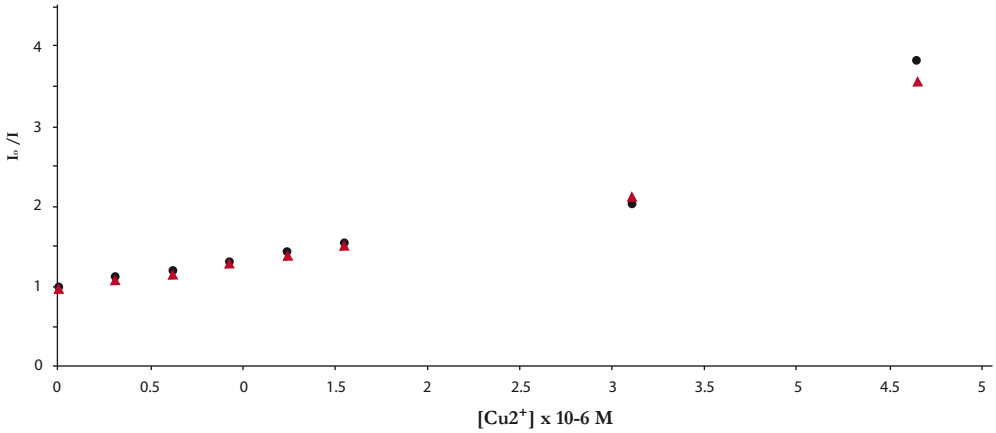

Figure 8. Intensity based (I_0/I) Stern-Volmer plot deviation. Black for 370 nm excitation and red for 870 nm excitation.

Prior to the addition of Cu(II), the longest decay time of Cdots was 11.55 ± 0.22 ns, the intermediate component was 3.07 ± 0.19 ns and the shortest decay time was 0.54 ± 0.06 ns. Interestingly, we found that when we added 1.55 μM Cu(II), the lifetime components decreased to 10.62 ± 0.23, 2.79 ± 0.22 and 0.52 ± 0.07 ns,

respectively. The subsequent analysis of the tri-exponential behaviour of the Cdots fluorescence decays[7] showed that the intensity-weighted average lifetime of Cdots presented a dependence on the Cu(II) value, that was decreasing from 7.94 ± 0.10 ns to 4.19 ± 0.10 ns in presence of 4 μM Cu(II). The average lifetime was linear in range 0 to 1.55 μM Cu(II), what indicates that Cdots lifetime might be used in the future for Cu(II) quantification.

The following modified Stern–Volmer plot should then be used when static and dynamic quenching occur simultaneously $I_0/I = 1 + (K_{SV} + K_{eq})[Q] + K_{SV}K_{eq}[Q]^2$. This modified Eq. was used in our experiments and a better fit of the experimental data was obtained using both fluorescence intensities (see Figure 9).

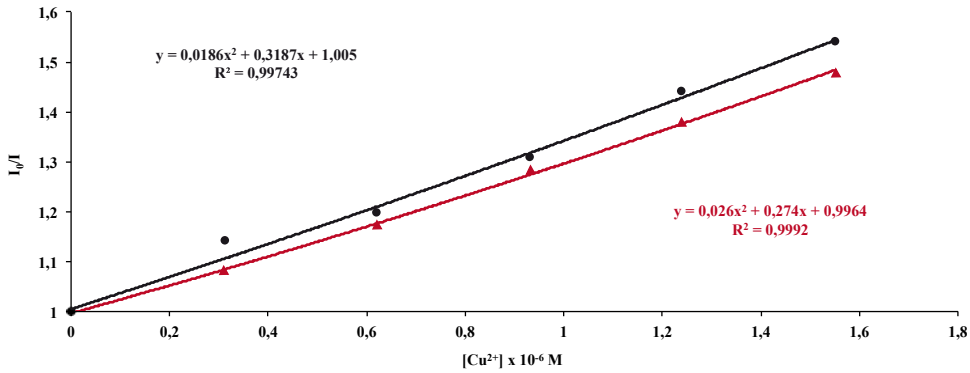

Figure 9. Intensity based (I0/I) Stern-Volmer plot. Black for 370 nm excitation and red for 870 nm excitation.

To evaluate the selectivity of the Cdots for Cu(II) recognition, we measured the fluorescence changes of Cdots in the presence of different ionic species such as 1 μM of Cu(II), Fe(III), Hg(II), Mn(II), Zn(II), Cr(III), Co(II), Pb(II), Ni(II), Al(III), Cd(II), K(I), Na(I). The results of this study are presented in Figure 10 (a). Additionally, the possible interferences of coexisting cations in Cu(II) detection was also tested (see Figure 10(b)) and we found that the response of the Cdots to Cu(II)

was almost unchanged before and after addition of other interfering ions. Taken together, all these results demonstrate that our Cdots are highly selective for Cu(II) detection.

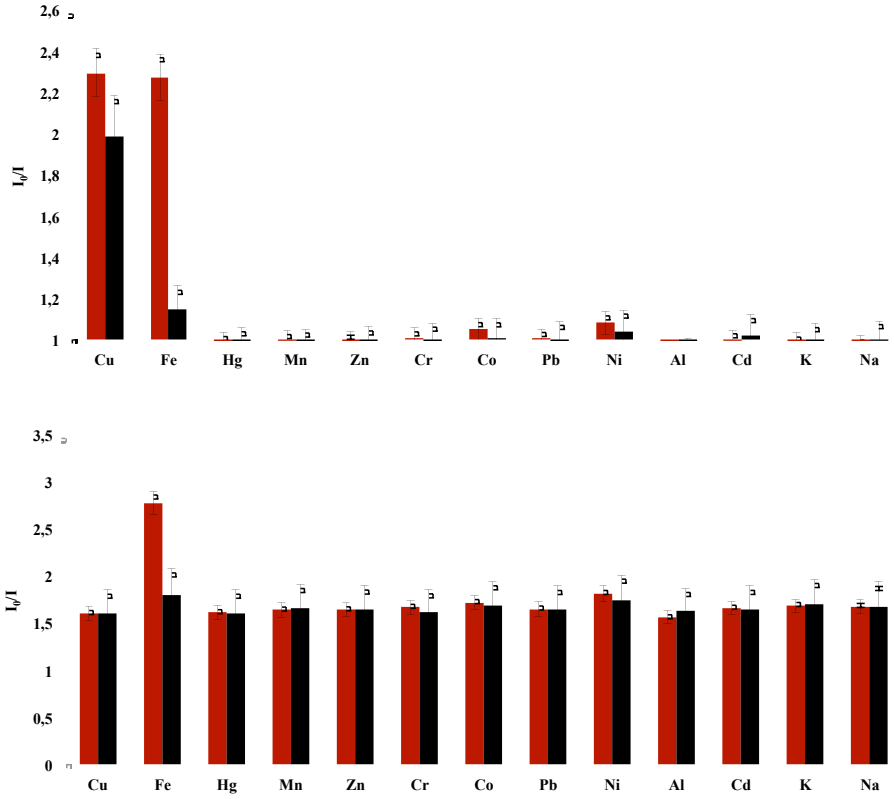

Figure 10 (a) Selectivity of the Cdots for Cu(II) over other ionic species. (b) Response profiles of Cdots by Cu(II) in presence of different ionic species. UV excitation 350 nm (red), NIR excitation 850 nm (black).

Only the presence of Fe^{3+} ions resulted in a dramatic decrease of fluorescence of Cdots at the excitation wavelength of 350 nm. The quenching effect produced by Fe^{3+} was attributed to an inner filter caused by its strong absorption at the mentioned excitation wavelength (also confirmed by the unaltered lifetime of Cdots, data not shown).[8] This interference could be eliminated when the excitation is 850 nm,

because then, the Fe(III) does not suffer inner filter at this excitation wavelength. That is a useful advantage of this upconverting nanoparticle.

Calibration graphs were obtained from the triplicate fluorescence signals of buffered solutions by increasing Cu(II) concentration at two excitation wavelengths (350 and 850 nm) following the general procedure. The reproducibility of the proposed method, evaluated with the standard deviation of five replicates of a sample containing 1 μM Cu(II), showed a relative error of 6 % when exciting with UV and 12% when exciting with NIR. The limit of the detection (LD), calculated as the concentration of Cu(II) which produces an analytical signal that is three fold the standard deviation of the blank signal (IUPAC criterion), was 0.09 and 0.12 μ M Cu(II) for UV and NIR excitation wavelength, respectively. Table 1 summarized the LD and linear dynamic range of previous methods for Cu(II) determination.

Table 1. Carbon dots, quantum dots and upcorverting NPs fluorescent based assays for Cu(II) determination.

	Linear Dinamic Range (μM)	Limit of Detection (μM)
CdS-Peptide [9]	0.5-10	0.5
CdS-Thioglycerol [10]	0.3-20	0.1
ZnS [11]	1-100	7.1
CdS-Cysteine [12]	0.05-2	0.05
$NaYF_4:Yb^{3+}/Er^{3+}$ [13]	1-10	1
CDots-TEPA [14]	1-100	0.01
Cdots [15]	0.01-0.1	0.001
Cdots-PEI	0.3-1.6	0.09[a] 0.12[b]

[a] UV excitation wavelength

[b] NIR excitation wavelength

For further biological applications, 3-(4,5-dimethylthiazol-2-yl)-2,5-diphenyltetrazolium bromide) (MTT) assays were carried out to determine the cytotoxicity of the Cdots in HEK293 cells. Exposure of HEK293 cells to low concentrations of Cdots (< 2 mg mL^{-1}) did not produce any cell toxicity (see Figure 11).

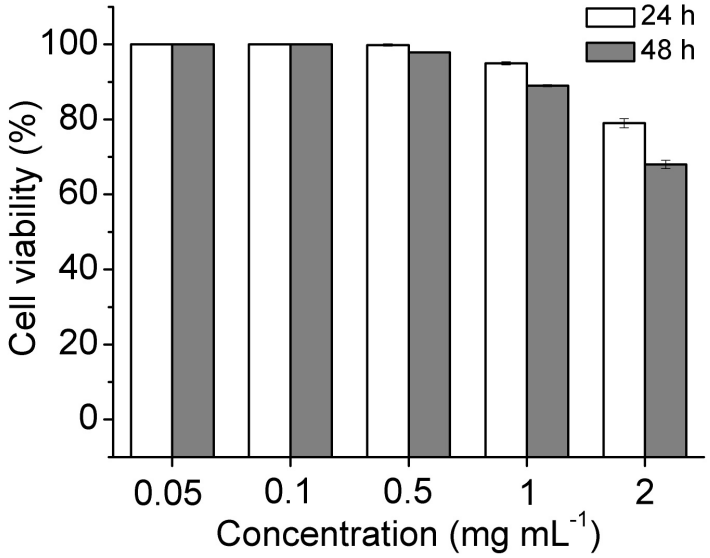

Figure 11. Cell viability values (%) estimated by MTT proliferation tests versus incubation with increasing concentrations of Cdots (0.05, 0.1, 0.5, 1, 2 mg mL^{-1}) at 37°C 5 % CO_2 for 24 h. Data are presented as mean ± S.E.M.

However, as expected, upon addition of the fluorescent Cdots at up to 2 mg mL^{-1} the viability of the HEK293 cells declined by ~ 10 % after 24 h preincubation and ~ 30 % after 48 h. Thus, the prepared Cdots can be considered to be non toxic and biocompatible for detection of Cu(II) ions in living cells.

On the other hand, NIH-3T3 cells were treated with Cdots in 10^4 fold dilution under culturing conditions for 24 h. Treated cells showed dot shaped localizations of Cdots throughout cell bodies and did not reveal any impact of the Cdots on the

cellular morphology. In order to confirm Cdots localization within the cells, membranes were stained using the Evans blue. Confocal stacking of Evans blue stained cells revealed that the Cdots were internalized into the cells (see Figure12).

The sensitivity of Cdots towards Cu(II) was further probed by setting the Cu(II) concentration to 5 x 10^{-4} M $CuCl_2$ solution (in Tween 20 in 0.05; $v.v^{-1}$, for 5 min) to Cdots treated cells.

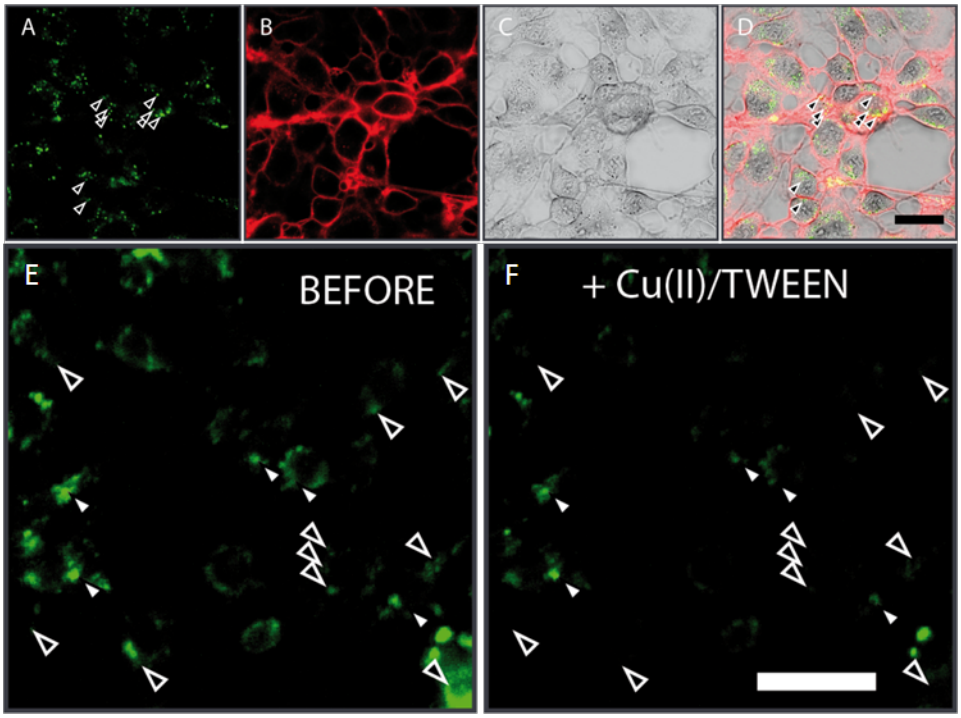

Figure 12. Confocal fluorescence images of Cdots-treated NIH-3T3 cells. (A) Fluorescence detection of Cdots in NIH-3T3 cells; Cdots exhibit dot shaped localizations, exemplified by arrowheads. (B) Cellular membrane staining with Evans blue. (C) bright field image of NIH-3T3 cells. (D) Overlay of bright field, Evans blue staining and Cdots fluorescence. (E) Cdot fluorescence in NIH-3T3 cells before Cu(II) treatment. Arrowheads with black core demonstrate Cdots agglomerations outside the cells. Arrowheads with white cores exemplify Cdots inside the cells. (F) Cdots fluorescence instantly after addition of Cu(II) solution; Fluorescence from Cdots outstide and inside the cells vanished (see arrowheads with black cores) and now point to dark spots. Scale bars = 20 μm.

Interestingly, the blue and green fluorescence of Cdot agglomerations outside the cells instantly vanished (indicated by arrowheads with black cores in Figure 12 E and F,) and fluorescence from intracellular Cdots agglomerations decreased slightly (arrowheads with white cores in Figure 12 E and F). As seen in Figure 13, Cdots fluorescence signals showed a significant decrease after Cu(II) exposure within the time either at extracellular or intracellular level. The results gained by live cell imaging demonstrate that Cdots can be internalized in cells under culturing conditions. Based on morphology and cellular division rate no major toxic effects were observed. Despite being dissolved in a complex mixture of organic compounds like cell culture media Cdots still retained their sensitivity towards Cu(II) ions (see Fig. 12 E, F and Figure 13).

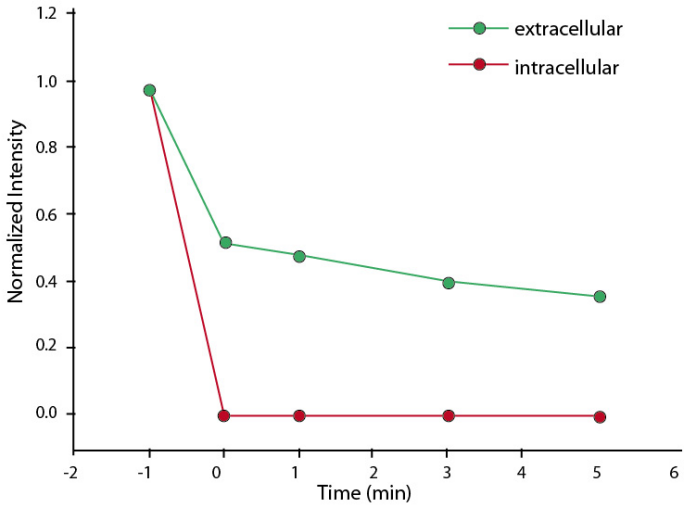

Figure 13. Quantification of the Cdots fluorescence signal after Cu(II) exposure in NIH-3T3 cells.

CONCLUSIONS

In conclusion, we have synthesized Cdots with down and upconversion luminescence properties for selective and sensitive detection of Cu(II). In addition,

these fluorescent nanosensors show low cytotoxicity and good cell permeability, thus they can be successfully used for sensing and imaging of Cu(II) in biological systems.

ACKNOWLEDGEMENTS

This work was supported by Projects CTQ2009-14428-C02-01 from the *Ministerio de Economia y Competitividad* (Spain). European Community 6th Framework program, NanoEar project, grant number: NMP4-CT-2006-026556). Med El-Medical Electronics (Austria) and we thanks to "*Reincorporacion de Doctores UGR*" programs and Greib start-up projects for young researchers.

REFERENCES

1 (*a*) US EPA, Federal Register 44:69464 ed., EPA, 1979; (*b*) R. Uauy, M. Olivares and M. Gonzalez, *Am. J. Clin. Nutr.*, 1998, 67, 952S; (c) K. J. Barnham, C. L. Masters and A. I. Bush, *Nat. Rev. Drug Discovery*, 2004, 3, 205.

2 (*a*) D. Mhamma, W. Ramadan, A. Rana, C. Rode, B. Hannuyer and S. Orgale, *Green Chem.*, 2011, 13, 1990. (*b*) J. Ming, R. Liu, G. Liang, Y. Yu and F. Zhao, *J. Mater. Chem.*, 2011, 21, 10929.

3 (*a*) S. N. Baker and G. A. Baker, *Angew. Chem. Int. Ed.,* 2010, 49, 2. (*b*) J. C. G. Estevez da Silva and H. M. R. Gonçalves, *Trends Anal. Chem.*, 2011, 30, 1327. *(c)* X. Jia, J. Li and E. Wang, *Nanoscale*, 2012, 4, 5572. *(d)* S. Sahu, B. Behera, T. K. Maiti and S. Mohapatra, *Chem. Commun.*, 2012, 48, 8835.

4 (*a*) H. Hu, L. Q. Xiong, J. Zhou, F. Y. Li, T. Y. Cao and C. H. Huang, *Chem.–Eur. J.*, 2009, 15, 3577; (*b*) R. Kumar, M. Nyk, T. Y. Ohulchanskyy, C. A. Flask and P. N. Prasad, *Adv. Funct. Mater.,* 2009, 19, 1; (*c*) W. Denk, J. H. Strickler and W. W. Webb, *Science*, 1990, 248, 73; (*d*) Z. Q. Li and Y. Zhang, Nanotechnology, 2008, 19, 345606.

5 (*a*) L. N. Sun, H. S. Peng, M. I. J. Stich, D. Achatz and O. S. Wolfbeis, *Chem. Commun.*, 2009, 5000; (*b*) J. Zhang, B. Li, L. Zhang and H. Jiang, *Chem. Commun.*, 2012, 48, 4860. (*c*) D. E. Achatz, R. J. Meier, L. H. Fischer and O. S. Wolfbeis, *Angew. Chem., Int. Ed.*, 2011, 50, 260; (*d*) J. Zhang, B. Li, L. Zhang and H. Jiang, *Nanoscale*, 2012, advanced article.

6 Y. Dong, R. Wang, G. Li, C. Chen, Y. Chi and G. Chen, *Anal. Chem.*, 2012, 84, 6220.

7 M.J. Ruedas-Rama, A. Orte, E. A. H. Hall, J. M. Alvarez-Pez and A.M. Talavera, Chem. Commun., 2011, 47, 2898.

8 M.T. Fernandez-Arguelles, W. J. Jin, J.M. Costa-Fernández, R. Pereiro and A. Sanz-Medel, Anal. Chim. Acta, 2005, 549, 20.

9 K. M. Gattas-Asfura and R. M. Leblanc, Chem. Commun., 2003, 2684.

10 K. M. Gattas-Asfura and R. M. Leblanc, Chem. Commun., 2003, 2684.

11 Y. Chen and Z. Rosenzweig, Anal. Chem., 2002, 74, 5132.

12 M. Koneswarana and R. Narayanaswamy, Sens. Actuators B, 2009, 139, 104.

13 J. L. Chen, A. F. Zheng, Y. C. Gao, C. Y. He, G. H. Wu, Y. C. Chen, X. M. Kai and C. Q. Zhu, Spectrochimica Acta Part A, 2008, 69, 1044

14 J. Zhang, B. Li, L. Zhang and H. Jiang, Chem. Commun., 2012, 48, 4860.

15 Q. Qu, A. Zhu, X. Shao, G. Shi and Y. Tian, Chem. Commun., 2012, 48, 5473.

16 S. Liu, J. Tian, L. Wang, Y. Zhang, X. Qin, Y. Luo, A. M. Asiri, A. O. Al-Youbi and X. Sun, Adv. Mater., 2012, 2037.

17 Rosen, H. Arch. Biochem. Biophys. 1957, 67, 10-15.

ChemComm RSC Publishing

COMMUNICATION View Article Online
View Journal | View Issue

Carbon dots for copper detection with down and upconversion fluorescent properties as excitation sources†

Cite this: Chem. Commun., 2013, 49, 1103

Received 4th September 2012,
Accepted 14th December 2012

DOI: 10.1039/c2cc36450f

www.rsc.org/chemcomm

Alfonso Salinas-Castillo,*[a] Maria Ariza-Avidad,[a] Christian Pritz,[b] Maria Camprubí-Robles,[c] Belen Fernández,[d] Maria J. Ruedas-Rama,[e] Alicia Megia-Fernández,[f] Alejandro Lapresta-Fernández,[a] Francisco Santoyo-Gonzalez,[f] Annelies Schrott-Fischer[b] and Luis F. Capitan-Vallvey[a]

Carbon dots were synthesized by a simple and green strategy for selective and sensitive Cu^{2+} ion detection using both down and upconversion fluorescence. These fluorescent nanosensors show low cytotoxicity and are applied for intracellular sensing and imaging of Cu^{2+} in biological systems.

It is well known that copper (Cu^{2+}) detection in cells is crucial as it plays essential structural roles in many proteins and enzymes; however, high intracellular Cu^{2+} concentrations may be toxic to organisms. Accordingly, Cu^{2+} is a key trace element for many biological mechanisms and otherwise is listed as a priority pollutant by the Environmental Protection Agency (EPA). For this reason, currently, there is great interest in developing new nanomaterials and novel green and low cost synthetic designs for heavy metal detection.[1]

Fluorescent nanoparticles (NPs) including quantum dots, dye-doped NPs and rare earth-based NPs have been a major focus of research and development during the past decade for use in sensing and bioimaging. To date, large amounts of "classic" photoluminescent NPs have been developed from novel materials but, in contrast, they have also raised new concern over their potential toxicity and environmental hazards.[2] On the other hand, they have several drawbacks, such as the involvement of a large number of extra processes to modify the particle surface which at the end is time-consuming. So far, great effort has been made to develop green methodologies that allow synthesizing new nanomaterials in order to replace the toxic compounds, organic solvents, current cost and time-consuming processes.

Recently, new NPs called Carbon dots (Cdots) have emerged and attracted growing interest in analytical and bioanalytical chemistry. Cdots exhibit excellent fluorescent properties with high photostability, high quantum yield, water solubility and favourable biocompatibility. They can be synthesised using a simple and cost-effective method and using an environmentally friendly method at large scale. Although these Cdot-based materials hold great promise in nanotechnology and nanomedicine, much work is still necessary to explore the full potential of these nanomaterials in the development of advanced smart sensors. Additionally, Cdots show size dependent photoluminescence and upconversion luminescence properties due to a multi-photon process, which lead to anti Stokes type emission.[3]

Thus, we can expect that Cdots may possess interesting luminescent properties such as visible and upconversion fluorescence simultaneously, which are extremely important for fundamental and practical applications. In particular, the up-conversion fluorescent materials can convert a longer wavelength radiation (*e.g.* near infrared light (NIR)) into shorter wavelength fluorescence (*e.g.* visible light). In comparison with downconversion fluorescent materials, upconversion materials have many advantages for future biological applications, such as non-invasiveness, improved tissue penetration depth under NIR radiation and absence of autofluorescence in biological tissues.[4]

Most of the upconversion fluorescence materials reported so far are inorganic crystals doped with rare-earth elements, encapsulated organic dyes or quantum dots in silica shells. Until now, there are only a few materials which can display both down and upconversion fluorescence implemented in optical sensors.[5] However, to our knowledge, no fluorescent nanosensors for Cu^{2+} detection based on upconvertion fluorescence of Cdots have been reported yet.

In the present work, the synthesis of optical sensors for Cu^{2+} detection using UV and NIR as excitation sources has been performed. These nanosensors are expected to be used for

[a] RChem, Department of Analytical Chemistry, Faculty of Sciences, University of Granada, E-18071 Granada, Spain. E-mail: alfonsos@ugr.es; Fax: +34 958 243 328; Tel: +34 958 248 436
[b] Department of Otolaryngology, Medical University of Innsbruck, Anichstr. 35, A-6020 Innsbruck, Austria
[c] Institute of Molecular and Cellular Biology, Miguel Hernández University, 03202, Elche, Spain
[d] The Institute of Parasitology and Biomedicine 'López-Neyra', Spanish National Research Council, 18100, Armilla, Spain
[e] Department of Physical Chemistry, Faculty of Pharmacy, University of Granada, E-18071 Granada, Spain
[f] Department of Organic Chemistry, Faculty of Sciences, University of Granada, E-18071 Granada, Spain

† Electronic supplementary information (ESI) available: Experimental details. See DOI: 10.1039/c2cc36450f

This journal is © The Royal Society of Chemistry 2013

DOI: 10.1039/c2cc36450f

ANNEX 1

MICROSYSTEM-ASSISTED SYNTHESIS OF CARBON DOTS WITH FLUORESCENT AND COLORIMETRIC PROPERTIES FOR PH DETECTION

ABSTRACT

The present paper describes the use of a microfluidic system to synthesize carbon dots (Cdots) and their use as optical pH sensors. The synthesis is based on the thermal decomposition of ascorbic acid in dimethyl sulfoxide. The proposed microsystem is composed of a fluidic and a thermal platform, which enable a proper control of the synthetic variables. Uniform and monodispersed 3.3 nm-sized Cdots have been synthesized, the optical characterization of which showed up their down/upconversion luminescence and colorimetric properties. The obtained Cdots have been used for pH detection with down and upconverison fluorescent properties as excitation sources. Naked eye or photograph digital camera has been also implemented as detection systems with Hue parameter, showing a linear pH range form 3.5 to 10.2. On the other hand, cytotoxicity and permeability of the Cdots on human embryonic kidney cells experiments revealed their adsorption on cell without causing any impact on the cellular morphology.

INTRODUCTION

The recent application of fluorescent nanoparticles (NPs) such as quantum dots, dye-doped NPs and rare earth-based NPs in biomedical sensing and imaging has become a major issue of research during the last years. Although a wide range of diverse photoluminescent NPs have been developed from new materials, an increased concern about their potential environmental and human health toxicity

exists.[1] Moreover, some NPs-associated drawbacks like the modification of their surface for a particular function imply highly time-consuming processes.

At the moment, one of the most attractive NPs are Carbon dots (Cdots), which have recently had a major relevance in analytical and bioanalytical chemistry mainly due to their excellent luminescent properties and elevated biocompatibility as well as their low cost synthesis.[2] However, although these Cdots are very promising NPs in nanotechnology and nanobiomedicine, more research needs to be done either to investigate their potential for sensor development or to identify novel synthesis approaches. In addition, Cdots show size dependent photoluminiscence and upconversion luminiscence properties leading to anti Stokes type emission.[3]

Many different approaches have been presented until the date to synthesize Cdots. They are based on two routes, top-down and bottom-up methods. The top-down methods prepared from larger carbon materials (graphite, carbon nanotubes, carbon soots, activate carbon), using arc discharge, laser ablation or electrochemical oxidation.[4] The bottom-up routes synthesizes Cdots from molecular precursors combustion, thermal decomposition, acid dehydration, ultrasonic or microwave pyrolysis.[5] However, most of these synthetic approaches present poor reproducibility, which leads to obtain Cdots with different optical and electronic properties in the diverse batches performed.

In this sense, microfluidic systems can offer some advantages when synthesizing nanoparticles. They permit a proper control of some critic synthetic variables such as the mass and temperature transference due to the small dimensions of the fluidic channels, which are on the contrary, difficult to manage in conventional methods. Moreover, the addition of reagents can be computer-controlled, which permits varying as desired flow rates or injection volumes to obtain products of reactions of different characteristics as well as confers safety to the operator. On the other hand, the easy and fast modification of the hydrodynamic parameters permits performing

many different reactions in a short time, which considerably simplifies the optimization process for the synthesis of nanomaterials. All this leads to obtain uniform and well dispersed colloids in a reproducible way, namely with the same electronic, optical and chemical properties, what is of great importance for the application of nanomaterials in the (bio)analytical field. Proof of all the advantages enumerated is the large number of papers devoted to that in the literature.[6]

Ceramic microfluidic systems have shown great potential in the synthesis of nanoparticles.[7] This material and its associated technology (Low-Temperature Co-fired Ceramics technology (LTCC)) allow the integration of diverse electronic or fluidic components in a simple, low cost and rapid way. Its multilayer approach enables the easy construction of three-dimensional structures, and its compatibility with screen-printing techniques permits the integration of many electronic components, such as detection or heating systems.[8-9]

Herein, we synthesize Cdots in a microfluidic system composed of two modules, one for microfluidics and another for heating and temperature control. A proper optimization of the chemical and hydrodynamic parameters has been performed in order to obtain stable and well-dispersed Cdots. As far as we are concerned, no microfluidic approach has still been reported for synthesizing Cdots.

The optical properties of the obtained Cdots have been used for the development of a fluorescent sensor for pH detection using UV and NIR excitation sources. Additionally, due to color changes of Cdots by using a photograph digital camera and Hue (H) parameter, the visual detection of pH was possible.

Finally, the cytotoxicity and permeability of the NP in human embryonic kidney cells have been also studied to demonstrate their suitableness as sensors or labels in biomedical applications by bioimaging.

EXPERIMENTAL

Microsystem materials and components

DuPont 951 green tapes (DupontTM, Germany) were used to fabricate both the microfluidic and the heating modules. DuPont 5742 gold cofirable conductor paste was required in order to perform the screen-printing step for the construction of the heating platform, since the gold paste acts as the resistor. DuPont 6141 paste was used to fill the vias of the heating platform. For the control of the temperature, a class A PT100 temperature sensor was preferred (Innovative Sensor Technology, Switzerland). The sensor was glued in the bottom of the heating module by means of epoxy (EPO-TEK® H20E, Billerica, MA, USA), and a PIC18F4431 microcontroller (Microchip Inc., Arizona, USA) was used to accomplish the digital PID control system, which controls the temperature as desired.

Involving the flow system, a 10 mL syringe (Hamilton series GASTIGHT 1000 TLL, Bonaduz, GR, Switzerland) was required, where reagents were placed for their injection in the microfluidic system by means of a syringe pump (540 060 TSE systems, Bad Homburg, Germany). To complete the fluidic system, PTFE tubes (i.d. 0.9 mm) were used between the syringe and the microfluidic platform; and o-rings and conic PTFE cones were used for their connection.

Instrumentation

Optical properties of the nanoparticles were obtained by means of a Varian Cary Eclipse (Varian Ibérica, Madrid, Spain) and Fluorolog1 Modular (Horiba Jobin Yvon, France) spectrofluorometers. Zeta-potential measurement was carried out on a Zetasizer Nano ZS90 (Malvern, Worcestershire, U.K.). XRD were performed at the Centre of Scientific Instrumentation (University of Granada, Spain) on a Fisons-Carlo Erba analyser model EA 1108. The FTIR spectra on powdered samples were

recorded with a ThermoNicolet IR200FTIR (Thermo Fisher Scientific Inc., Madrid, Spain) by using KBr pellets.

The shape and dimensions of the core of the particles were measured by a high resolution transmission electron microscope (HRTEM), JEOL 2011 (Tokyo, Japan). The samples were prepared by dipping a copper grid, which was coated with a thin carbon film, in the carbon dots suspension.

Crison pH meter (Crison Instruments, Barcelona, Spain, model Basic 20) was used for pH measurements.

pH measurement procedure

The pH of 2 mL of Cdots solutions was regulated by adding different volumes of required concentrations of HCl or NaOH and measuring it with a pH meter. The fluorescence spectra and the image capture with a digital camera were recorded at different pH values.

Image acquisition and treatment for colorimetric pH determination

For the image acquisitions and digitalization a Canon PowerShot G12 (Madrid, Spain) was used. To keep all the image-gathering under the same conditions a Cube Light Box was developed. The vials with 2 mL of Cdots are located inside the box, so they are exempt from external light. The only light source is formed by a LED (Light-Emitting Diode) system with direct current. All parameters of the camera were set and optimized. The vial position was fixed for all experiments.

The obtained images were stored in TIFF (True Image File Format) file format to prevent any loss of information since it does not compress the image. To extract the hue parameter from each sensing element in the scanned image, software developed by the research group in Matlab was used. H coordinate was calculated from the R, G and B coordinates of each pixel using eq. 1. The H value, determined for each

sensing element, was the mode of the hues calculated for all the pixels in the solution, since this parameter provides a low error during the image processing.

$$H = \frac{\left(\frac{G-B}{max_{channel}-min_{channel}}+0\right)}{6} \qquad \text{If max= R*}$$

$$\mathrm{H} = \frac{\left(\frac{\mathrm{B-R}}{\mathrm{max_{channel}-min_{channel}}}+2\right)}{6} \qquad \text{If max= G} \qquad \text{(Eq. 1)}$$

$$\mathrm{H} = \frac{\left(\frac{\mathrm{R-G}}{\mathrm{max_{channel}-min_{channel}}}+4\right)}{6} \qquad \text{If max= B}$$

*if H is less than 0 then add 1 to H

Cell culture

Human embryonic kidney HEK293 cells were cultured in Dulbecco's modified Eagle's medium (DMEM) supplemented with 10 % fetal bovine serum, 2 mM L-glutamine and 1 % penicillin–streptomycin solution at 37 °C with 5 % humidified CO_2. Cells were plated at 20000 cells/well onto glass bottom petri dishes previously coated with 10 g mL^{-1} poly-L-lysine. After 24 h in culture, cells were incubated for 24 or 48 h at 37 °C with different concentrations of Cdots (0.1, 0.2, 0.4, 0.6, 0.8, 1 mg mL^{-1}) dispersed in complete culture medium.

Cytotoxicity assay

In vitro proliferation assay compared the growth rate of HEK293 cells by 3-(4,5-dimethyl-1,3-thiazol-2-yl)-2,5-diphenyl-2H-tetrazol-3-ium bromide (MTT) after

plating $2x10^4$ cells/well on a 96-well flat-bottom plate for 24 and 48 h at 37 °C in 5 % CO_2. MTT (5 mg mL^{-1}) reagent was added to each well and incubated for 4 h at 37 °C. Thereafter, 150 mL/well of 100 % DMSO were added, mixed thoroughly to dissolve the dark blue crystals and plates were subsequently read on an ELISA reader at a wavelength of 570 nm.

Fluorescence microscopy

Fluorescence measurements were performed with a Zeiss (Oberkochen, Germany) Axiovert200 inverted microscope fitted with an ORCA-ER CCD camera (Hamamatsu, Bridgewater, NJ) through a 20x air objective. Nanoparticles were excited at 360/380 nm using a computer-controlled Lambda10-2 filter wheel (Sutter Instruments, Novato, CA), and emitted fluorescence was filtered with a 440/535 nm long-pass filter. Images were processed with Image J software.

RESULTS AND DISCUSSION

Design and fabrication of the microsystem

The microsystem for the synthesis of Cdots was based in two separate modules: a microfluidic platform and a heating module with temperature control. The general fabrication procedure of ceramic microsystems is detailed elsewhere.[10] Since the LTCC technology is a multilayer approach, the final design of the device has to be divided in different layers in order to create the partial design by means of computer-assisted design (CAD) software. In this step, it has to be taken into account the ~15 % shrinkage on each axis of Dupont 951 green tapes during the sintering process. Once the design is done, laser machine (LPKF Protolaser 200, Garbsen, Germany) transferees the diverse patterns to different layers. Next step in the construction of the device involves the screen-printing of those layers that require conductive pastes.

In this case, this step was necessary in the layers which composed the heating platform (resistor and vias to connect the tracks). The heater was conceived in base of a gold paste screen-printed resistor, which was deposited in a radial configuration. Then, the slabs are aligned in aluminum plates using fiducial holes and laminated by a thermo-compression process at 100 ºC and 3000 psi. The LTCC layers are finally sintered in a programmable box furnace (Carbolite CBCWF11/23P16, Afora, Barcelona, Spain) by applying a temperature profile.

As explained before, two different modules were preferred to carry out the synthesis of carbon dots, which were mechanically, attached taking care of obtaining the best contact between them. In this way, if one of the modules has to be modified, it can be replaced without changing the other one. Both modules were designed and constructed based on a previous microsystem.[9]

The fluidic platform had one inlet for the entrance of reagents followed by a simple Z shape channel to increase the residence time of reagents inside the microsystem and allow their thermal conditioning, and one outlet from where the Cdots formed leave the system. The Z shape fluidic structure was constructed in a circular shape in order to make it coincide with the resistance of the heating module. Moreover, the channel for reagents was constructed in only one layer of ceramic substrate, since deeper channels could generate no uniform thermal patterns thought the solution. All this contributes to obtain a well controlled heat transfer from the thermal platform to the liquid flowing in the microfluidic platform, which ensures the optimal and uniform formation of carbon dots thought the microsystem.[11] As it can be observed in Fig.1, the whole module consisted on 7 ceramic layers, which once sintered formed a block of 6.0 mm diameter and 1.4 mm thick. An image of the different layers that compose both the fluidic and the heating platforms is depicted in Fig. 1.

To make feasible a proper control of the temperature, a class A PT100 sensor was attached by means of epoxy in the reverse of the bottom layer, taking care of positioning the sensor in a central zone of the resistance.

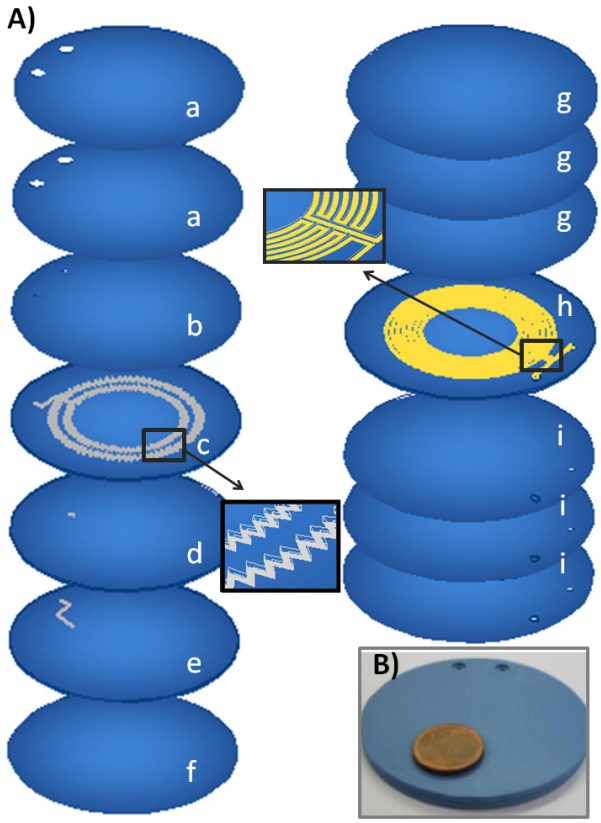

Figure 1. A) Scheme of the different layers that compose the microfluidic system for the synthesis of carbon dots. Layers a-f correspond to the microfluidic platform: a) top layers, where o-rings are placed; b) entrance and exit for reagents and the product; c) inlet of reagents and bidimensional micromixer; d) intermediate layer for the connexion of the fluidic structure; e) outlet for the synthesized carbon dots; f) bottom layer. Layers g-i composes the thermal platform: g) top layers; h) embedded screen-printed heater; i) bottom layers with vias to connect the tracks of the resistance. **B)** Picture of both the microfluidic and the heating platforms mechanically attached.

Electronics for temperature control is detailed elsewhere.[9] Briefly, a temperature controller with a digital PID topology was implemented on a PIC18F4431 microcontroller computer controlled. An electronic circuit maintained a constant intensity in order to avoid interferences with temperature measurements due to self-heating, and amplified the control signal generated by the PID controller. The system estimated the error from the PT100 sensor thought the obtained feedback signal and corrected it by specific differential equations programmed in the digital PID control system implemented in the microcontroller code. Then, the signal was amplified and applied to the gold resistor. The system was programmed to work from 150 to 250 ºC.

Heat transfer in the thermal platform exhibited a radial distribution, and it was found to provide the temperature desired in the fluidic system, since the sensor is located at an equally distance than the microfluidic structure.[11]

Synthesis of cdots

For the synthesis of Cdots, ascorbic acid (Panreac, 99 %) was chosen as a simple and low cost source of carbon, and dimethyl sulfoxide (DMSO) (Baker Chemical, 0.3 % water) was preferred as solvent due to the high temperatures that this compound can bear.

In order to obtain controllable and reproducible carbon dots, an optimization of certain parameters of the microsystem is required. The optimized values were determined as a function of the maximum fluorescence intensity recorded with a spectrofluorometer, since the synthesized Cdots are pretended to be used for sensing and bioimaging applications.

As in many other nanoparticle syntheses that involve the decomposition of reagents, temperature plays an important role. Thus, the first parameter to study was the reaction temperature. Since ascorbic acid has a melting point of 188 ºC, six

different temperatures around this value (180, 190, 195, 200, 210 and 240 ºC) were chosen. The concentration of ascorbic acid and the flow rate were fixed to 0.1 mg mL^{-1} and 20 μL min^{-1} respectively. As it can be observed in Fig. 2, only weak fluorescence intensity was observed from the Cdots synthesized at 180º C, which indicates the poor formation of the nanoparticles under the ascorbic acid melting point. A clear improvement is observed when performing the reaction in the same conditions but increasing the temperature over this threshold. On the other hand, from 190º C until 240 ºC the fluorescence intensity remained practically constant. The small decrease observed is probably due to the decomposition of the solvent (boiling point of 189 ºC), which generates gaseous species such as SO_2.[12] Thus, 190 ºC was preferred as the optimized value for temperature to perform the synthesis. All the fluorescence emission spectra of recorded Cdots exhibit the same maximum peak, located over 420 nm.

The concentration of ascorbic acid was also studied. Four different concentrations were evaluated (0.1, 0.2, 0.3 and 0.4 mg mL^{-1}), while temperature was fixed to 190 ºC and flow rate to 20 μL min^{-1}. As shown in Fig. 2, the concentration that provided higher intensity of fluorescence in these conditions was 0.2 mg mL^{-1}, and thus, this value was selected for further optimization.

Finally, the flow rate of reagents in the microfluidic system was evaluated, while the rest of parameters were fixed at the optimized conditions (a temperature of 190 ºC and an ascorbic acid concentration of 0.2 mg mL^{-1}). The tested values included 5, 10, 20, 40, 60 and 80 μL min^{-1}.

As presented in Fig. 2, the more slowly the liquid flowed in the system, the higher fluorescence was achieved. This was in concordance with the fact that the time that reagents spend in the microfluidic system determines the reaction time for the formation of the colloids.

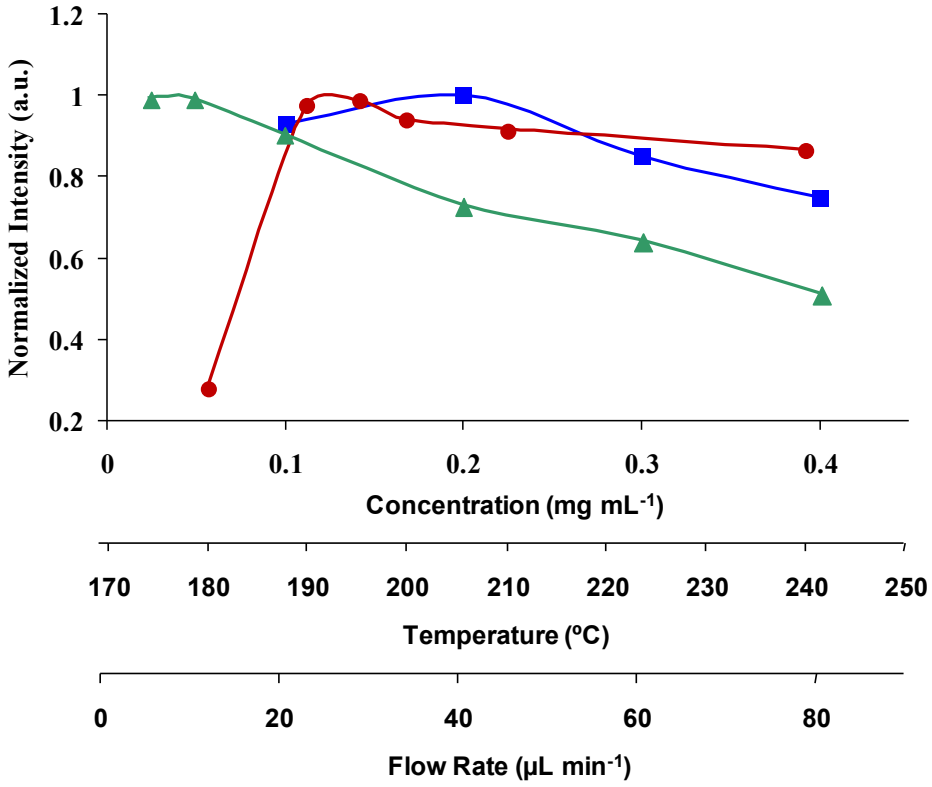

Figure 2. Optimization of the chemical and hydrodynamic parameters for the synthesis of Cdots in the ceramic microfluidic system (λ_{exc}= 325 nm, λ_{em}= 420 nm). Red circles: temperature (ºC), Blue squares: Concentration (µg mL^{-1}), Green triangles: Flow rate (µL min^{-1}).

This is a critical variable,[13] and, in this work, a 10 µL min^{-1} (instead of 5 µL min^{-1}) was selected as a compromise between the intensity of fluorescence and the final amount of obtained colloidal in a reasonable synthesis time.

Characterization of cdots

Cdots synthesized in the microsystem were dialyzed against Milli-Q water using spectra/pro dialysis membrane with cut-off of 1 KDa for their purification and characterized by several techniques.

The core and shape of the nanoparticles were defined by Transmission Electron Microscopy (TEM).

Fig. 3A shows a TEM image, where monodispersed spherical carbon dots can be observed. The average size found was of 3.3 ± 0.3 nm from the counting of more than 250 particles, which demonstrates the synthesis reproducibility of the microsystem.

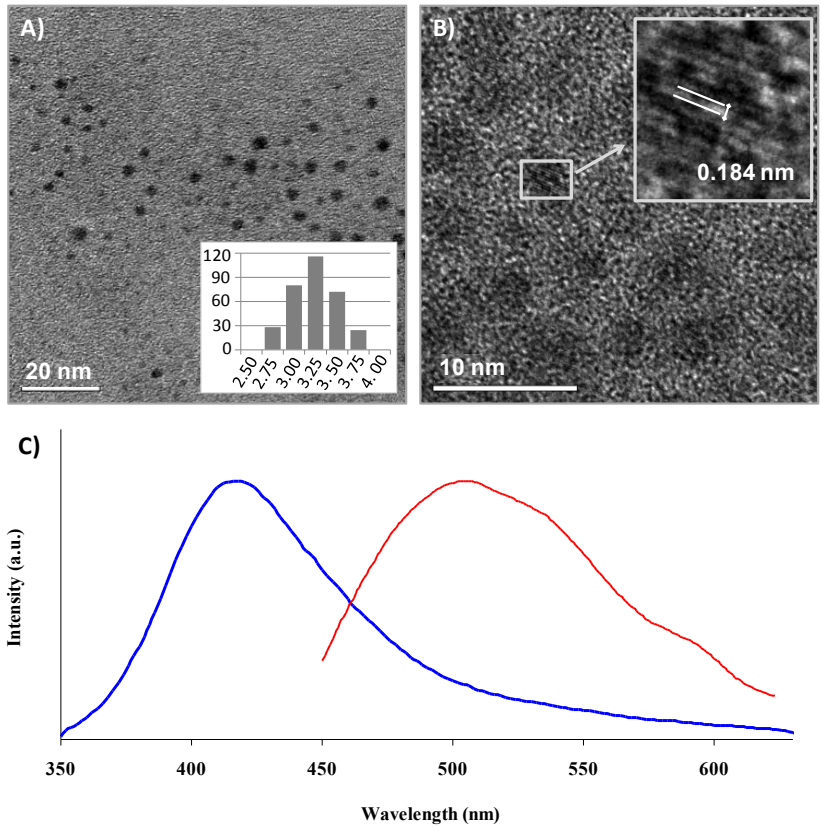

Figure 3. Characterization of the synthesized Cdots in the microfluidic system. A) TEM image with the size-histogram and the calculated average size. B) HRTEM image and an amplification with the lattice fringes highlighted. C) Fluorescence emission spectrum by UV excitation at 325 nm (in blue) and by NIR excitation at 850 nm (in red).

HRTEM (High-Resolution Transmission Electron Microscopy) images (Fig. 3B) revealed crystalline nanoparticles, as was also probed by the clear ring structure of the selected area electron diffraction (SAED) pattern image. Lattice planes with 0.18 nm spacing were found in the crystalline images from the colloidal, which is consistent with the (102) diffraction planes of sp^2 graphitic carbon.[14] The bright rings observed in the SAED pattern can be attributed to (100) and (102) lattice planes of graphite (inset Fig. 3B).

FTIR spectrum of Cdots showed the typical bands of stretching vibrations of O-H at 3400 cm^{-1}, ester group at 1780 cm^{-1} and C=O at 1622 cm^{-1}. X-ray diffraction (XRD) pattern displayed a broad diffraction peak at $2\Phi = 20.5^{o}$. Different Zeta potential values were obtained for the synthesized Cdots, varying from acid pH (8 mV) to basic pH (-14 mV), which confirms the presence of carboxyl groups on the surface of the nanoparticles.

Cdots exhibited excellent water solubility and blue luminescence under UV excitation light (365 nm). Using quinine sulphate as standard, the fluorescence quantum yield was found to be 2.6 %, which is comparable to previous reports.

To further explore the optical properties of Cdots, a detailed fluorescence study was performed using different excitation wavelengths (Fig. 3C). It is remarkable that these Cdots also exhibit good upconversion fluorescent properties besides their strong luminescence in visible under NIR excitation sources. Fig. 3C shows the fluorescent spectra of Cdots excited at 325 nm with emission in the range of 360-500 nm (see Fig. 3C blue), and excited by longer wavelength light (maximum intensity with 850 nm excitation, see Fig. 3C red) with the up-conversion emissions located in the range of 450-600 nm. Therefore, these results suggest that Cdots may be used as a powerful component in biological applications as well as an appropriate sensor design for environmental applications.

Sensing applications

It is already known that Cdots are pH sensitive. Indeed, diverse works can be found in the literature, which describes the sensitivity of Cdots to pH depending on their external composition (carbonyls, amines, hydroxyls, esters, etc.). In particular, a previous study showed that Cdots synthesized from ascorbic acid pyrolysis were capable to detect small pH changes by colorimetry or fluorimetry.[5c] Namely, the intensity of fluorescence change with protonation and deprotonation of the carboxyl groups of the surface Cdots cause electrostatic doping/charging to Cdots and shift the Fermi level. Similarly, the color of the Cdots solutions change with pH cause electronic changes of π-π^* and n-π^* by refilling or depleting their valence bands.[15]

Since the obtained Cdots have the same matrix, it is expected to find the same behavior and therefore, one can take advantage to go forward on their application as pH sensors.

Fluorescent sensor for pH. The influence of pH on the synthesized Cdots in the range pH 2-11 was studied. The results showed that the maximum fluorescence emission (420 nm) of the Cdots at 325 nm excitation decreased linearly as the pH increase from 4.5-11.5 (Fig. 4A), and same results were obtained by excitation at 850 nm and emission at 505 nm (Fig 4B).

The good emission fluorescence presented at 400 or 505 nm by the Cdots over a wide range of pH (4.5-11.5) makes them of a valuable use for future biological applications.

In order to test the reversibility of the proposed nanosensor, the pH of Cdots was changed from 5 to 10 and back to 5 four times, and the fluorescence by down and upconverting excitation emission values in all cases. The results confirmed the good reversibility of the nanosensor (see Fig. 4C). The relative standard deviations were less than 5 % for the five measurements.

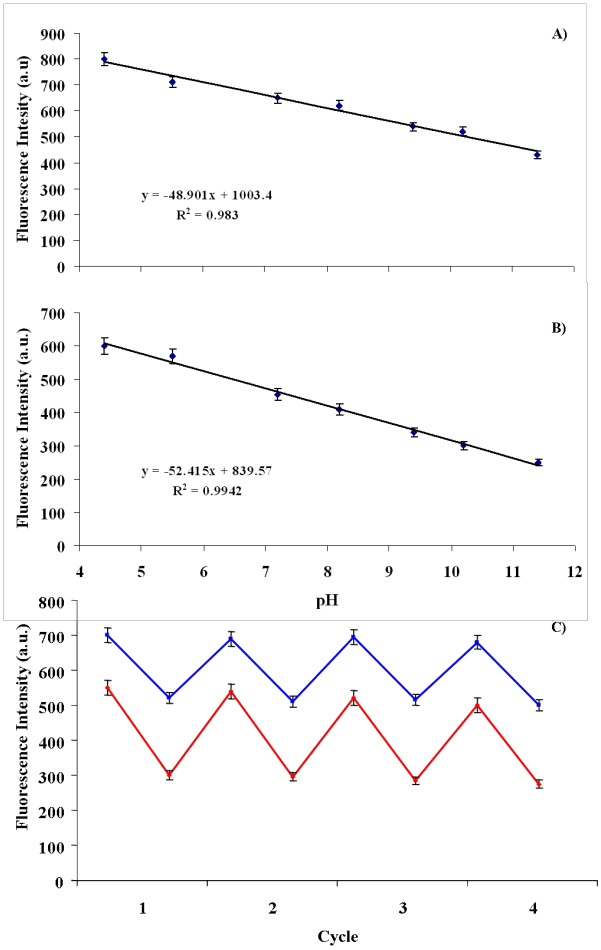

Figure 4. Linear calibration plots for pH detection are shown in **A)** for fluorescence (λ_{exc} = 325 nm, λ_{ems} = 420 nm) and **B)** for up-conversion fluorescence (λ_{exc} = 850nm, λ_{ems} = 505 nm). **C)** Plots of the fluorescence intensity as a function of ph cycles ($\lambda_{exc/ems}$ = 325/420 nm blue, ($\lambda_{exc\ /ems}$ = 850/505 nm red).

Colorimetric sensor for pH. Once observed the change in the intensity color of Cdots with pH, it is reasonable to use these properties to determine pH by measurement of color from captured images by camera. By far, the most commonly used color space is RGB, the coordinates of which are used for processing with multivariate techniques. However, we used the HSV color space in this work, whose

main characteristic is that it represents useful information about the color in one single parameter, the H coordinate. Previous studies from the research group have shown that the use of H value is stable, simple to calculate, and easy obtained from commercial devices, maintaining a superior precision with variations at reagents colorimetric concentration, detector spectral response and illumination.[16]

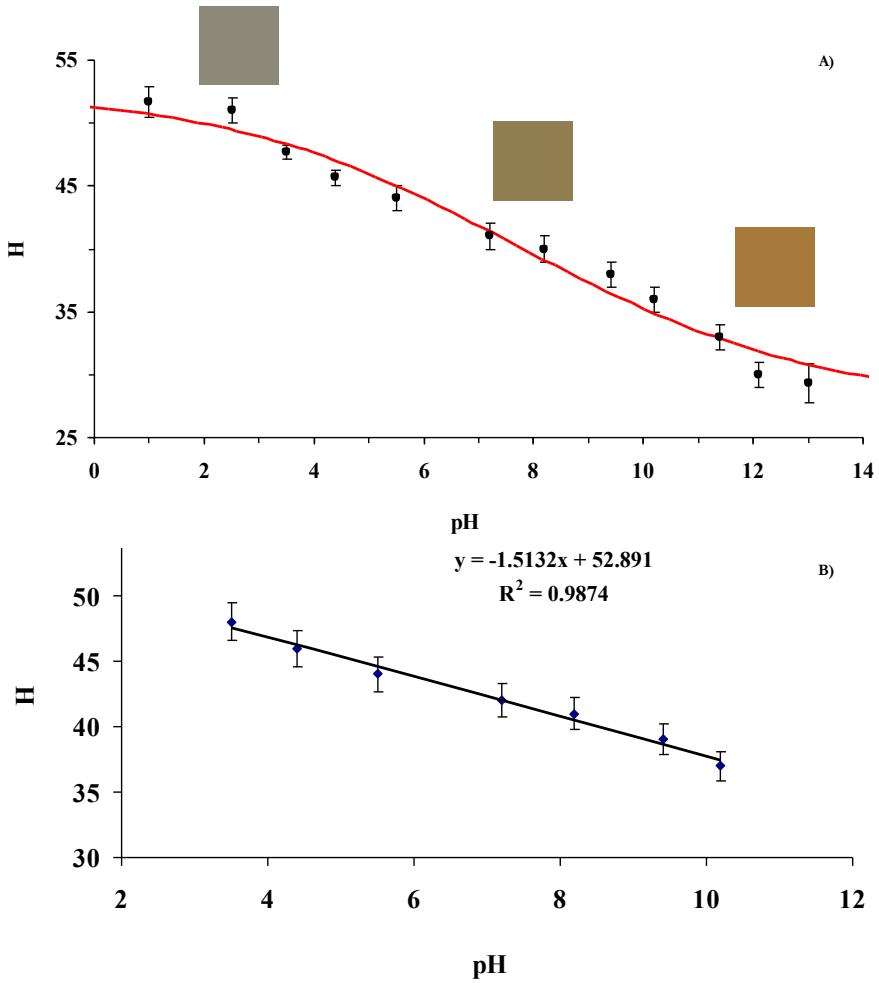

Figure 5. A) Colorimetric response of Cdots in the pH ranges from 1.5-13. **B)** Linear range for pH colorimetric detection.

As seen in Fig. 5A, the effect of pH on Cdots color is reflected by a shift from grey colors corresponding to acid pH values, yellow-orange color associated with medium pH values, and to brown color related to more basic pH values, which can be also easily observed by eye.

The relationship between the analytical parameter H and pH was adjusted to a sigmoidal fit using a Boltzmann type equation, giving an apparent pKa value of 6.7, which is in concordance with the acidic groups present in the surface of Cdots.[17] As it can be seen from both approaches, a wide linear range can be obtained from pH 3.5 to 10.2 (Fig. 5B).

Bioimaging and cytotoxicity.

Fluorescence microscopy allowed us to examine the cellular localization of Cdots in HEK293 cells.

Interestingly, we found that fluorescent Cdots were adsorbed on the cell membrane of HEK293 cells after a short incubation (24 h) (right panel in Fig. 6a). Cells showed dot shaped localizations of Cdots (red arrow, Fig. 6A) throughout cell bodies and did not reveal any impact of the Cdots on the cellular morphology. No evidence of fluorescence was observed in the control sample of untreated cells (data not shown). As shown in Fig. 6B, cell viability was not affected in presence of these concentrations of Cdots, demonstrating that these non-toxic nanoparticles can act as suitable biosensors or bioimaging in living organisms.

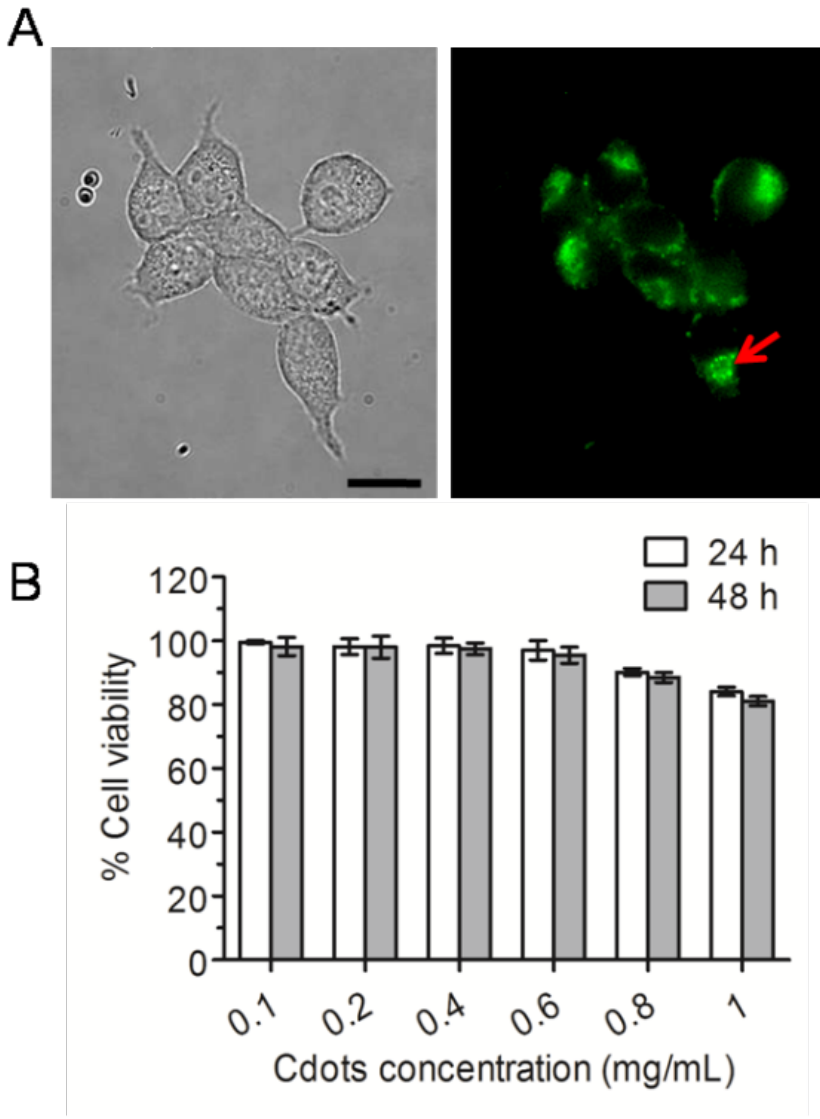

Figure 6. Biological characterization of Cdots in HEK293 cells. **A)** Transmitted light brightfield image of HEK293 cells (left panel) and fluorescence image showing in green the Cdots in the membrane edges and localized in small dots (red arrow). Scale bar = 10 μM. **B)** MTT assay revealed no change in cell viability of HEK293 cells following a treatment with increasing concentrations of Cdots for 24 and 48 h at 37°C.

CONCLUSIONS

A microfluidic system has been proposed for the automatic synthesis of carbon dots. The system is composed of two separate platforms to increase its versatility, one for heating and control of the temperature, and other for microfluidics. The radial configuration of the heater as well as of the microfluidic pattern, which perfectly matches with the screen-printed resistor, permits a controlled mass and temperature transference. Once the hydrodynamic parameters of the microsystem were optimized, Cdots with proper optical properties were obtained. The narrow size distribution observed in the characterization of the synthesized Cdots demonstrates the reproducibility of the microsystem. Further characterization of the synthesized Cdots showed optical properties as well as their pH dependence, which were used for the development of a pH fluorescent sensor using both UV and NIR excitation sources. Naked eye and photography digital camera detection systems for colorimetric pH detection were implemented using H parameter, obtaining a linear response in a wide range of pH values. Cytotoxicity and permeability studies on cells did not reveal any impact on the cellular morphology. Viability of cells was not affected in presence of diverse concentrations of Cdots, demonstrating their suitability for biosensing or bioimaging applications in the biomedical field.

REFERENCES

1 *(a)* D. Mhamma, W. Ramadan, A. Rana, C. Rode, B. Hannuyer and S. Orgale, *Green Chem.*, 2011, 13, 1990. *(b)* J. Ming, R. Liu, G. Liang, Y. Yu and F. Zhao, *J. Mater. Chem.*, 2011, 21, 10929.

2 *(a)* K. Qu, J. Wang, J. Ren and Xi. Qu, *Chem. Eur. J.*, 2013, 19(22), 7243. (*b*) L. Zhou, Y. Lin, Z. Huang, J. Ren and X. Qu, *Chem.. Comm.,* 2012, 48(8), 1147.

3 *(a)* S. N. Baker and G. A. Baker, *Angew. Chem. Int. Ed.,*2010, 49, 2. *(b)* J. C. G. Estevez da Silva and H. M. R. Gonçalves, *Trends Anal. Chem.*, 2011, 30, 1327.*(c)* S. K. Bhunia, A. Saha, A. R. Maity, S. C. Ray and N. R. Jana, *Scientic reports*, 2013, 3, 1473. *(e*) H. Li, Z. Kang, Y. Liu and S. T. Lee, *J. Mater. Chem.*, 2012, 22, 24230.

4 *(a)* H. Ming, Z. Ma, Y. Liu, K. Pan, H. Yu, F. Wang and Z. Kang, *Dalton Trans.*, 2012, 41, 9526. *(b)* L. Zheng, Y. Chi, Y. Dong, J. Lin and B. Wang, *J. Am. Chem. Soc.*, 2009, 131, 4564.

5 *(a)* X. Zhai, P. Zhang, C. Liu, J. Bai, W. Li and L. Dai, W. Liu, *Chem. Commun.*,2012, 48, 7955. *(b)* A. Salinas-Castillo, M. Ariza-Avidad, C. Pritz, M. Camprubí-Robles, B. Fernández, M. J. Ruedas-Rama, A. Megía-Fernández, A. Lapresta-Fernández, F. Santoyo-Gonzalez, A. Schrott-Fischer and L. F. Capitan-Vallvey, *Chem. Commun.*, 2013, 49, 1103. *(c)* X. Jia, J. Li and E. Wang, *Nanoscale*, 2012, 4, 5572.

6 *(a)* A. M. Nightingale, S. H. Krishnadasan, D. Berhanu, X. Niu, C. Drury, R. McIntyre, E. Valsami-Jones and J. C. deMello, *Lab Chip,* 2011, 11, 1221. *(b)* H. Wang, X. Li, M. Uehara, Y. Yamaguchi, H. Nakamura, M. Miyazaki, H. Shimizu and H. Maeda, *Chem. Commun.,* 2004, 48. *(c)* E. M. Chan, A. P. Alivisatos and R. A. Mathies, *J. Am. Chem. Soc.,* 2005, 127, 13854.

7 *(a)* S. Gomez-de Pedro, M. Puyol, D. Izquierdo, I. Salinas, J.M. de la Fuente and J. Alonso-Chamarro, *Nanoscale*, 2012, 4(4), 1328. *(b)* S. Gomez de Pedro, M. Puyol and J. Alonso, *Nanotechnol.*, 2010, 21(41), 415603.

8 *(a)* C. S. Martinez-Cisneros, Z. daRocha, M. Ferreira, F. Valdes, A. Seabra, M. Gongora-Rubio and J. Alonso-Chamarro, *Anal. Chem.,* 2009, 81, 7448. *(b)* G. Fercher, A. Haller, W. Smetana and M. J. Vellekoop, *Analyst,* 2010, 135, 965.

9 S. Gómez-de Pedro, C. S. Martínez-Cisneros, M. Puyol and J. Alonso-Chamarro, *Lab Chip*, 2012, 12, 1979.

10 N. Ibáñez-García, C. S. Martínez-Cisneros, F. Valdés and J. Alonso, *TrAC, Trends Anal. Chem.*, 2008, 27, 24.

11 C. S. Martínez-Cisneros, S. Gómez-de Pedro, J. García-García, M. Puyol and J. Alonso-Chamarro, *Chem. Eng. J.,* 2012, 211-212, 432.

12 F. C. Thyrion and G. Debecker, *Int. J. Chem. Kinet.,* 1973, 5, 583.

13 B. K. H. Yen, N. E. Stott, K. F. Jensen and M. G. Bawendi*, Adv. Mater.,* 2003, 15, 1858.

14 L. Tian, D. Ghosh, W. Chen, S. Pradhan, X. Chang and S. Chen, *Chem. Mater.,*2009, 21, 2803.

*15 (a)*J .L Chen and X. P. Yan*, Chem. Commun.,* 2011, 47, 3135. *(b)* W. kong, H. Wu, Z. Ye, R. Li, T. Xu and B. Zhang, *J. Lumin.,* 2014, 148, 238.

16 *(a)* K. Cantrell, M. M. Erenas, I. De Orbe-Payá and L. F. Capitán-Vallvey, *Anal. Chem.*, 2010, 82, 531. *(b)* M. Ariza-Avidad, M. P. Cuellar, A. Salinas-Castillo, M. C. Pegalajar, J. Vukovic and L. F. Capitán-Vallvey, *Anal. Chim. Acta*, 2013, 783, 56.

17 A. Lapresta-Fernández and L. F. Capitán-Vallvey, *Anal. Chim. Acta*, 2011, 706, 328.

View Article Online
DOI: 10.1039/C4NR00573B

Journal Name

RSCPublishing

ARTICLE

Microsystem-assisted synthesis of carbon dots with fluorescent and colorimetric properties for pH detection

Cite this: DOI: 10.1039/x0xx00000x

Received 00th January 2013,
Accepted 00th January 2013

DOI: 10.1039/x0xx00000x

www.rsc.org/

S. Gómez-de Pedro,[a] A. Salinas-Castillo,*[b] M. Ariza-Avidad,[b] A. Lapresta-Fernández,[b] C. Sánchez-González,[c] C. S. Martínez-Cisneros,[a] M.Puyol,[a] L. F. Capitan-Vallvey[b] and J. Alonso-Chamarro[a]

The present paper describes the use of a microfluidic system to synthesize carbon dots (Cdots) and their use as optical pH sensors. The synthesis is based on the thermal decomposition of ascorbic acid in dimethyl sulfoxide. The proposed microsystem is composed of a fluidic and a thermal platform, which enable a proper control of the synthetic variables. Uniform and monodispersed 3.3 nm-sized Cdots have been synthesized, the optical characterization of which showed up their down/upconversion luminescence and colorimetric properties. The obtained Cdots have been used for pH detection with down and upconverison fluorescent properties as excitation sources. Naked eye or photograph digital camera has been also implemented as detection systems with Hue parameter, showing a linear pH range form 3.5 to 10.2. On the other hand, cytotoxicity and permeability of the Cdots on human embryonic kidney cells experiments revealed their adsorption on cell without causing any impact on the cellular morphology.

1. Introduction

The recent application of fluorescent nanoparticles (NPs) such as quantum dots, dye-doped NPs and rare earth-based NPs in biomedical sensing and imaging has become a major issue of research during the last years. Although a wide range of diverse photoluminescent NPs have been developed from new materials, an increased concern about their potential environmental and human health toxicity exists.[1] Moreover, some NPs-associated drawbacks like the modification of their surface for a particular function imply highly time-consuming processes.

At the moment, one of the most attractive NPs are Carbon dots (Cdots), which have recently had a major relevance in analytical and bioanalytical chemistry mainly due to their excellent luminescent properties and elevated biocompatibility as well as their low cost synthesis.[2] However, although these Cdots are very promising NPs in nanotechnology and nanobiomedicine, more research needs to be done either to investigate their potential for sensor development or to identify novel synthesis approaches. In addition, Cdots show size dependent photoluminiscence and upconversion luminiscence properties leading to anti Stokes type emission.[3]

Many different approaches have been presented until the date to synthesize Cdots. They are based on two routes, top-down and bottom-up methods. The top-down methods prepared from larger carbon materials (graphite, carbon nanotubes, carbon soots, activate carbon), using arc discharge, laser ablation or electrochemical oxidation.[4] The bottom-up routes synthesizes Cdots from molecular precursors combustion, thermal decomposition, acid dehydration, ultrasonic or microwave pyrolysis.[5] However, most of these synthetic approaches present poor reproducibility, which leads to obtain Cdots with different optical and electronic properties in the diverse batches performed.

In this sense, microfluidic systems can offer some advantages when synthesizing nanoparticles. They permit a proper control of some critic synthetic variables such as the mass and temperature transference due to the small dimensions of the fluidic channels, which are on the contrary, difficult to manage in conventional methods. Moreover, the addition of reagents can be computer-controlled, which permits varying as desired flow rates or injection volumes to obtain products of reactions of different characteristics as well as confers safety to the operator. On the other hand, the easy and fast modification of the hydrodynamic parameters permits performing many different reactions in a short time, which considerably simplifies the optimization process for the synthesis of nanomaterials. All this leads to obtain uniform and well dispersed colloids in a reproducible way, namely with the same

This journal is © The Royal Society of Chemistry 2013

DOI: 10.1039/x0xx00000x

CONCLUSIONS

The purpose of this chapter has been the synthesis and characterization of carbon nanoparticles as well as the evaluation of their potential as a sensing material for biological applications.

A summary of the main conclusions obtained in this work are mentioned below:

- The microwave-assisted pyrolysis of citric acid in the presence of polyethylenimine permit the synthesis of carbon dots with an average size of 12 nm, where the dots are positively charged due to the presence of primary and secondary amines on the nanoparticle surface.
- Synthesized Cdots exhibit remarkable fluorescence in the 450-650 nm range over a wide pH range (pH = 2-8), with decay curves showing tri-exponential behaviour. Additionally, these Cdots also exhibit up-conversion fluorescence in the range of 380-550 nm when excited at 850 nm.
- A study of the influence of 14 metal ions on the fluorescence of Cdots shows an intense quenching from Cu(II) and Fe(III), where the quenching from Cu(II) is due to the presence of both static and dynamic quenching and in the case of Fe(III) is due to inner filter mechanism and can be avoided by up-conversion exciting at 850 nm.
- A procedure for Cu(II) determination is established based on fluorescence quenching both by down-conversion and up-conversion with detection limits of 0.09 and 0.12 μM, respectively.
- Non cytotoxicity and permeability of the Cdots nanoparticles in human embryonic kidney cells is demonstrated, being used for sensing and imaging of Cu(II) in biological systems.

- A new procedure for Cdots synthesis is presented based on thermal decomposition of ascorbic acid, a source of carbon, in dimethyl sulfoxide in a microsystem composed of a fluidic and a thermal platform, which enable a proper control of the synthetic variables. The average size of Cdots is 3.3 nm where carboxylic groups are present on the surface of the nanoparticles.
- The Cdots show changes in fluorescence with protonation and deprotonation of the carboxyl groups of the surface causing electrostatic doping/charging to Cdots and shifting the Fermi level. Similarly, the color of Cdots solutions change with pH causing electronic transitions of π-π* and n-π* orbitals.
- The synthesized Cdots are used to detect small pH changes by both colorimetry, using a digital camera, or fluorimetry in a wide linear range (pH 3.5 to 10.2).
- Fluorescent Cdots were absorbed on the surface of HEK293 cells, and did not affect the cellular morphology suggesting their use as suitable pH sensors for bioimaging in living organisms.

Chapter IV

Color properties of porous silicon

CHAPTER IV: COLOR PROPERTIES OF THE POROUS SILICON

OBJECTIVES

The goal of chapter IV is to explore the use of digital cameras to monitor the degradation of porous silicon. This photonic crystal nanomaterial suffers degradation in the presence of water which causes a change in the color that typically is monitored by their reflectance spectra. The monitoring of degradation by imaging devices would allow the facile monitoring of porous silicon for use in drug delivery or molecular sensors, two of the most important applications for the material.

As specific objectives to achieve in this chapter we can mention:

- Synthesis and characterization of nanostructured porous silicon.
- Monitoring the porous silicon degradation in aqueous solution simultaneously by digital imaging with a digital camera and spectrophotometric measurements.
- Comparison of results with the previously used methodology.
- Evaluation of RGB and HSV color spaces to monitor the degradation of porous silicon nanostructures.

MONITORING OF DEGRADATION OF POROUS SILICON PHOTONIC CRYSTALS USING DIGITAL PHOTOGRAPHY

ABSTRACT

We report the monitoring of porous silicon (pSi) degradation in aqueous solutions using a consumer-grade digital camera. To facilitate optical monitoring, the pSi samples were prepared as one-dimensional photonic crystals (rugate filters) by electrochemical etching of highly doped p-type Si wafers using a periodic etch waveform. Four pSi formulations, representing chemistries relevant for self-reporting drug delivery applications, were tested: (1) freshly etched pSi (fpSi), (2) fpSi subjected to partial thermal oxidation to generate porous silica (pSi-o), (3) pSi-o silanized with methoxy(dimethyl)octylsilane to give (pSi-oC_8), and (4) fpSi coated with the biodegradable polymer chitosan (pSi-ch). Accelerated degradation of the samples in ethanol-containing aqueous basic buffers (pH 10 or 12) was monitored *in situ* by digital imaging with a consumer-grade digital camera with simultaneous optical reflectance spectrophotometric point measurements. As the nanostructured porous silicon matrix dissolved, a hypochromic shift in the wavelength of the rugate reflectance peak resulted in visible color changes from red to green. While the H coordinate in the HSV color space calculated using the acquired photographs was a good monitor of degradation at short times ($t<100$ min), it was not a useful monitor of sample degradation at longer times since it was influenced by reflections of the broad spectral output of the lamp as well as from the narrow rugate reflectance band. However, with a processing of the raw RGB data, a good correlation with the EOT data was observed. This suggests the RGB data itself could be a possible method for the monitoring of processes where color shifts can be used as an analytical method. A monotonic relationship was observed between the wavelength of the rugate reflectance peak and the H parameter value in the HSV color space of photographs

taken during the first part of the degradation process, calculated from the average RGB values of each image by first independently normalizing each channel (R, G and B) using their maximum and minimum value over the time course of the degradation process. The spectrophotometric measurements and digital image analyses were in agreement and reported relative stabilities of the samples, where pSi-oC_8 > pSi-o > pSi > pSi-ch.

BACKGROUND

The position of the maximum wavelength of the reflectance peak of a porous silicon-based photonic crystal can be an effective reporter of degradation due to oxidation and dissolution of the silicon matrix in aqueous media. The temporal evolution of the visible reflectance spectrum of porous silicon (pSi) or the oxidized porous silica (pSi-o) has been used to monitor the dissolution process and the release of drugs trapped in the porous matrix [1,2]. Porous silicon has potential uses for drug delivery because pSi is biocompatible and biodegradable. In addition, peaks in its reflectance spectrum can be tuned to fall within the near infrared region of the electromagnetic spectrum, allowing direct monitoring through tissue [3-5]. In this work, we aimed to use a consumer-grade digital camera to monitor the degradation of freshly etched and modified pSi photonic crystals (rugate filters) rather than using a spectrophotometer. While this constrains the reflectance measurements to lie within the visible spectrum, measurement of the spectral changes of pSi by digital photography can enable monitoring of pSi degradation and drug delivery in non-laboratory settings. The use of digital photography for monitoring the degradation of pSi in aqueous media was validated by simultaneous spectrophotometric measurements of the pSi reflectance spectrum.

METHODS

Preparation of freshly etched porous silicon chips (fpSi):

Porous silicon was prepared by anodic electrochemical etching of highly doped 0.95 mΩ·cm p^{++}-type (100)-oriented silicon wafer (Virginia Semiconductor, Fredericksburg, Virginia, USA) in a 3:1 (v/v) mixture of aqueous hydrofluoric acid (49%) and ethanol.

The fpSi samples were prepared in a Teflon etch cell that exposed 1.2 cm^2 of the polished face of the Si wafer, where the bottom of the wafer was bound to aluminum foil. A platinum spiral was used as a counter-electrode. A rugate filter was generated using a current density modulated with 100 cycles of a sinusoidal waveform oscillating between 15 and 108 mA cm^{-2}, with periods on the order of 6 s depending on the desired wavelength of maximum reflectivity. After etching, the fpSi samples were rinsed with ethanol and dried in a stream of nitrogen.

Preparation of porous silicon coated with chitosan (pSi-ch):

A 1% chitosan solution was prepared by dissolving 10 mg chitosan from crab shells, 85% deacetylated from Sigma Aldrich, in 1 mL of 15% v/v aqueous acetic acid and stirred overnight. The fpSi sample was coated with this polymer solution by spin coating (Laurell WS-400B-6NPP-Lite, Laurell Technologies, North Wales, PA) using 150 μL of chitosan at a final speed of 100 rpm for 10 min and then drying at room temperature under nitrogen. The sample was then placed under vacuum to evaporate the remaining solvent. After the deposition, the pSi-ch samples were heated at 70ºC on a hot plate for 10 min to allow a small amount of polymer infiltration into the pores. This resulted in a slight red shift in the rugate reflectance peak position.

Preparation of oxidized porous silicon (pSi-o):

Starting with fpSi, the samples were partially thermally oxidized in air by heating from room temperature to 600 ºC at a rate of 10 °C min^{-1} and then holding the temperature at 600 °C for 1h in a muffle furnace (Thermo Fisher Scientific, Pittsburg, PA, USA). The samples were then slowly cooled to room temperature.

Preparation of porous silicon with a modified surface (pSi-oC_8):

Silanized oxidized porous silicon samples were prepared as follows: pSi-o samples were treated with 4% (v/v) aqueous hydrochloric acid (HCl 37 wt%; Sigma-Aldrich) for 1 h at room temperature and washed with deionized water. The resulting hydroxyl-terminated pSi-o samples were transferred to a Schlenk flask and degassed for 4 h under vacuum, then 4 mL of anhydrous toluene was added, followed by 415 µL of methoxy(dimethyl)octylsilane. The flask was heated at 120 °C in an oil bath under a nitrogen atmosphere overnight. The pSi-oC_8 samples were then washed with toluene (Sigma-Aldrich), dimethylformamide (Sigma-Aldrich), ethanol (Fisher-Scientific) and ether (Sigma-Aldrich), three times each, dried at room temperature and stored under vacuum in a desiccator.

Instrumental procedures

The porosity and thickness of the porous silicon layers were estimated by the Spectroscopic Liquid Infiltration Method (SLIM), based on the measurement of the thin film interference components of the reflectance spectra of the samples before and after infiltration of a liquid (ethanol) with known refractive index [6] by using an Ocean Optics USB-2000 spectrometer configured for specular reflectance, working in back-reflection configuration in the range 400-1000 nm. The reflectance spectra were recorded at 5 spots distributed across each sample in order to evaluate the

homogeneity of each porous silicon sample. The values of the porosity and the thickness were determined by means of the two component Bruggeman effective medium approximation [7]. The extent of chitosan infiltration into the porous silicon sample was also evaluated from the reflectance spectrum.

The freshly prepared (fpSi) and modified (pSi-o, pSi-ch, and pSi-oC_8) porous silicon samples were characterized using a Fourier transform infrared (ATR-FTIR) spectra that were recorded using a Thermo Scientific Nicolet 6700 FTIR with a Smart iTR diamond ATR fixture. The morphology of the porous silicon was measured by Scanning Electron Microscopy (SEM) using FEI XL30 SEM operating in secondary electron imaging mode. To avoid sample charging anomalies, the porous Si samples were metalized with a thin layer of gold prior to the SEM analysis. The pore size and the porosity oscillations of the rugate filter structure were evaluated with this analysis.

Measurement of porous silicon degradation

The pSi degradation was studied using a custom designed transparent flow cell system with a total volume of 4.5 mL (including connections). The solution was applied to the bottom of the sample using a peristaltic pump at a rate of 10 μL min^{-1} and room temperature (20±1ºC). The solutions were either 1:1 (v/v) ethanol: 0.5 M carbonate/borate buffer (pH 10) for the non-oxidised pSi samples (fpSi and pSi-ch) or 20:80 (v/v) ethanol: 0.04 M phosphate buffer (pH 12) for the oxidized and silanized pSi samples (pSi-o and pSi-oC_8). Ethanol was included in the buffers to improve the permeation of solutions into the pores and reduce the formation of bubbles that could affect the subsequent image analysis. The freshly etched and chitosan-coated samples (fpSi and pSi-ch) were monitored until complete degradation at 300 min whereas the hydrolytically more resistant oxidized and

modified samples (pSi-o and pSi-oC_8) were monitored for 3000 min, enough time to complete degradation.

The degradation of the fpSi, pSi-o, pSi-ch and pSi-oC_8 samples were monitored by obtaining reflectance spectra (spectrophotometer) and photographs (digital camera) every 5 min through the front cover of the flow cell until after complete degradation had occurred (300 min and 3000 min). To obtain both measurements simultaneously, the optical paths for the reflectance probe and the camera were located in front of the flow cell normal to the sample surface as is shown in Figure 1.

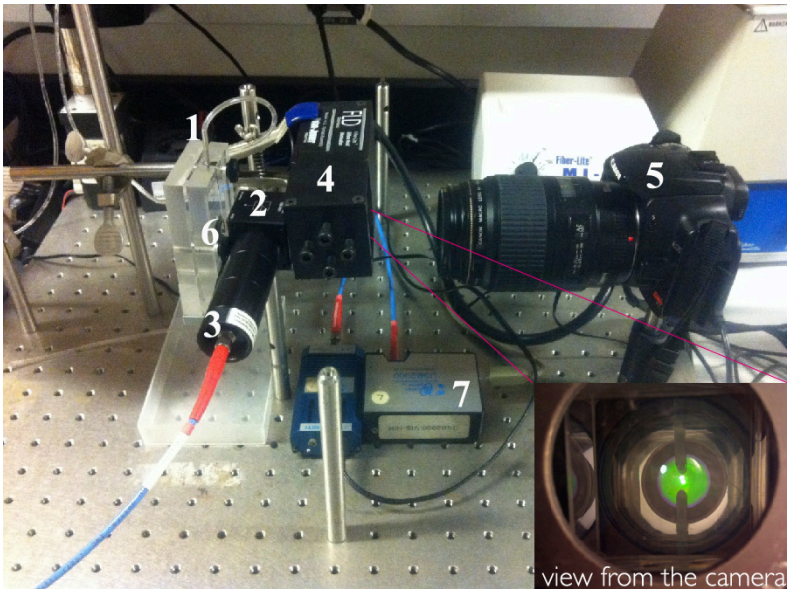

Figure 1. Photograph of equipment for the simultaneous acquisition of photographs and reflectance spectra: 1. Flow cell containing pSi sample, 2. Beam splitter, 3. Reflectance probe connected to fiber-optic spectrophotometer, 4. Diffuse axial illuminator with tungsten light source, 5. Digital camera, 6. pSi sample, 7. Spectrophotometer. Inset: image of the pSi sample as captured by the digital camera.

The sample was illuminated by means of a diffuse axial illuminator coupled to a Fiber-lite MI-150 (Dolan Jenner) light source with an approximate color temperature

of 3000 K mounted between the flow cell and the camera. A beam splitter (Thorlabs CM1-BS2 Cube-Mounted Non-Polarizing Beamsplitter 50:50 0.7-1.1 μm) between the diffuse axial illuminator and the flow cell allowed simultaneous measurement of the reflectance spectrum over 400-1000 nm with the reflectance probe of a fiber optic spectrophotometer (Ocean Optics USB-2000-VIS-NIR). The reflectance probe was rigidly fixed to the beamsplitter via lens tubes containing a focusing lens.

The reflectance spectrum acquisition was controlled by Spectrasuite software (Ocean Optics, Inc.). The position of the rugate reflectance peak and the FFT of the portion the reflectivity spectrum that displayed Fabry-Perot interference fringes in each reflectivity spectrum were calculated using custom routines in Igor (Wavemetrics, Inc.). The shifts in the position of the peaks in the FFT spectra indicate a change in effective optical thickness (EOT or 2nL where n is the effective refractive index and L is the thickness of the layer) of the porous silicon samples.

Digital images were acquired with a Canon EOS 500D (Digital Rebel Xti) digital camera with an EF-S 60 mm f/2.8 macro lens. In order to use the camera as a colorimeter, the geometry of the imaging equipment was rigidly fixed and the flow cell was exposed to constant lighting. The camera settings were fixed at ISO 400, aperture value *f*/ 4.5, shutter speed 1/2 s, and white balance set for a tungsten light source. Canon EOS Utility software was used to remotely operate the camera from a computer and to transfer the JPG images from the camera to the computer.

Image analysis

The JPG images were pre-processed using Photoshop CS5 (Adobe Systems). First, a color curve balance correction for each image was made selecting as a reference point a portion of the silicon wafer that was not in contact with the buffer solution. Next, the portion of each image containing the pixels corresponding to the degrading porous silicon sample (ca. 1.2 x 10^5 pixels) was defined using a mask,

Figure 2. This mask was applied to remove the areas obscured by the flow cell inlet and outlet.

Figure 2. Images showing the change in color of the pSi sample during degradation and the mask used to select pixels for image analysis.

The average R G B values for these pixels were determined for each image. The H coordinate [8] of the HSV (Hue, Saturation, and Value) color space, was used to monitor the porous Si degradation since it represents the dominant color in one single parameter. The RGB values of the selected pixels in each image were processed with a set of scripts and functions developed in Matlab r2010b (The MathWorks121 Inc, Natick, MA, USA) to determine the H coordinate in the HSV color space, which is defined as in eq 1.

$$\begin{cases} \left(\dfrac{G-B}{\max_{min}-\min_{channel}}+0\right)\cdot 60\,; & \text{if } \max = R^{*} \\ \left(\dfrac{B-R}{\max_{min}-\min_{channel}}+2\right)\cdot 60\,; & \text{if } \max = G \\ \left(\dfrac{R-G}{\max_{min}-\min_{channel}}+4\right)\cdot 60\,; & \text{if } \max = B \end{cases} \qquad \text{(eq. 1)}$$

* if H less than 0, then add 360 to H

The H values reported in this paper are the modes (the most repeated values) of the H coordinates calculated for all the pixels of a sample in a given image converted to a 0-360° scale, since the mode proved to be a robust parameter during the image processing. The H coordinate has a circular nature and so can be defined as an angle that varies between 0 and 360° [9]. However, because of the wavelength of the rugate band maxima and the lighting conditions used in our experiments, the H values for the images varied monotonically over a more limited range (20°-70°).

In this work, due to the processing we have used prior to our H calculation we report the values on a 0-1 scale. H values calculated by applying the above equations to the as-acquired images were not monotonic with time. A monotonic function was obtained in the following manner: The average RGB values for each image were normalized, with each channel being normalized independently using the maximum and minimum value for that channel observed during the degradation process. The H value of these processed values was then calculated.

RESULTS AND DISCUSSION

Characterization of porous Si:

The different porous Si rugate samples had thicknesses in the range 20-25 μm and average porosities of 53-62%, and displayed a single narrow band between 581 and 603 nm in their visible reflectance spectra.

The freshly etched porous Si samples had a maximum reflectance peak centered at 593 nm (standard deviation 3.73 nm; n=5). The thickness and porosity of fpSi were 22.8 μm (1.2 μm) and 53.4% (1.6%), respectively, both measured by SLIM. The average diameter of the pores was 20 nm as calculated from the top surface SEM images (Figure 3a) and a channel-like mesoporous structure was observed in cross-sectional SEM images (Figure 3b). The ATR-FTIR spectrum of fpSi (Figure 4a)

shows a band at 2100 cm^{-1} due to the presence of Si-H_x groups (x: 1-3) [10]; a 905 cm^{-1} band assigned to the SiH_2 scissor mode [11]; and a 667 cm^{-1} band due to SiH wagging mode. The small band at 1050 cm^{-1} due to Si-O stretching modes suggests a small amount of oxidation has occurred after etching [12].

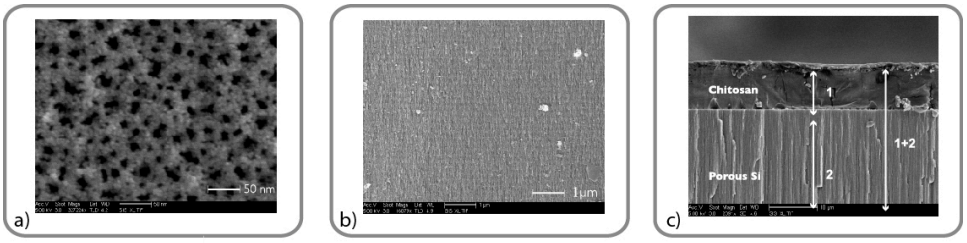

Figure 3. SEM images of the porous silicon a) top view showing the pore openings in fpSi, b) partial cross-section showing the rugate modulations in porosity in fpSi, c) cross section of chitosan coated porous silicon (pSi-ch).

Chitosan, a positively charged natural polysaccharide which is both biodegradable and biocompatible, was investigated as a protecting coating for pSi due to its reported potential use in drug delivery studies [13]. A film of chitosan was deposited on the porous Si surface by a spin coater. In order to evaluate the infiltration of the chitosan into the pores of the fpSi sample, cross-sectional SEM and reflectance spectra were compared before and after chitosan coating. The range of thickness achieved by spin coating was 8 - 12 µm according to SEM results, with the two well defined separate layers suggesting little infiltration of chitosan into the pores (Figure 3c). More precise information about the extent of chitosan infiltration into pSi was obtained from reflectance spectra of the hybrid. The reflectance spectra of the fpSi samples coated with chitosan showed a red shift of 8 nm in the maximum of the rugate peak. However, analysis of the thin-film interference fringes, which are also

present in the reflectance spectrum, allowed more detailed investigation of the changes to the pore filling.

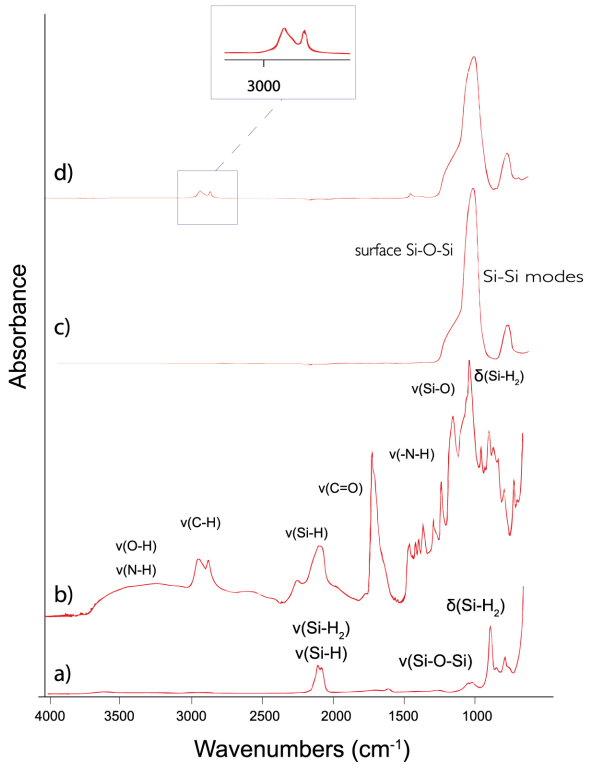

Figure 4. ATR-FTIR spectra of a) freshly etched pSi (fpSi), b) freshly etched pSi with a layer of chitosan (pSi-ch), c) pSi samples after oxidation (pSi-o), d) pSi samples after oxidation and silylation with methoxy(dimethyl)octylsilane (pSi-oC_8).

When chitosan is spin-coated onto the pSi surface and then warmed slightly, the chitosan forms an optically-smooth film on top of the pSi layer, which leads to an additional Fabry–Pérot optical interference layer. Therefore, the FFT of the

reflectance spectrum displays two major peaks (Figure 5). The position of the peak at an effective optical thickness (EOT) of 60.2 μm ($EOT_2 = 2n_2L_2$, where n_2 is the effective refractive index of the layer and L_2 is its thickness) is slightly larger than the position of the corresponding peak observed in the FFT spectrum of the unmodified fpSi (59.7 μm). This peak is assigned to the pSi layer initially, and also to the pSi layer which included a small amount of incorporated chitosan after modification. The second major peak in the FFT spectrum appears at an EOT of 77.4 μm ($EOT_3=2n_3L_3$). This peak comes from interference between the top surface of the chitosan (the air/chitosan interface) and the bottom of the porous Si film (the bulk Si/porous Si interface). A third peak with $EOT_1 = 2n_1L_1$ that is expected for the chitosan layer at 17.2 μm, according to the relationship: $EOT_1 + EOT_2 = EOT_3$, is not observable due to the small difference between chitosan and pSi refractive indexes [14]. This data indicates that chitosan does not significantly infiltrate the porous Si layer and is in agreement with the SEM images and the results from Pastor et al. who concluded that chitosan penetration into the inner structure of partially-oxidised pSi is hindered [15]. Thus, the structure of pSi-ch samples consists of an array of porous reservoirs capped with a chitosan layer.

Upon loading of chitosan onto the fpSi, new bands appear in the FTIR spectrum (Figure 4b). The broad band at 3350 cm^{-1} is assigned to both O–H and N-H stretching, the bands at 2915 and 2857 cm^{-1} are due to C-H stretching vibration modes, while the aliphatic CH_2 bending appears at 1453 cm^{-1} and the C=O stretching vibration mode appears at 1710 cm^{-1}. The intense band at 1043 cm^{-1} has contributions from the C–O stretching mode in addition to Si–O stretching modes [1].

Partial thermal oxidation of fpSi resulted in a hypsochromic shift of the rugate band maximum by 65 nm. The IR spectrum of pSi-o shows significant oxidation of the porous silicon has occurred (Figure 4c). The broad band at 1050 cm^{-1} is due to

Si-O-Si vibrations, which while very small in the FTIR spectra of fpSi, is now the major band. At the same time, the Si-H_x stretching modes disappear completely, although there is a band at 900 cm^{-1} that has been attributed to Si-Si modes [11].

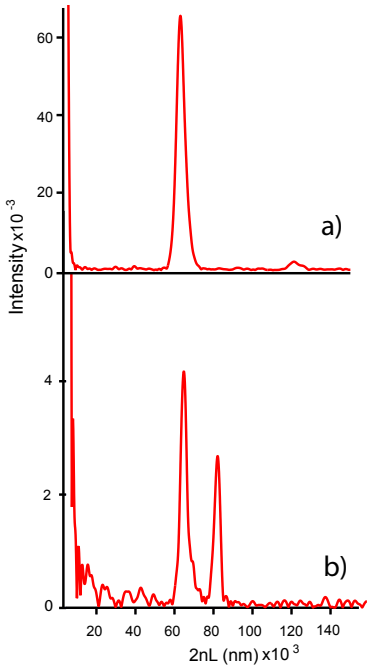

Figure 5. FFT of the visible reflectance spectrum obtained from pSi with (a) and without (b) a coating of chitosan.

Finally, some of the oxidized pSi samples were chemically modified using silane chemistry (pSi-oC_8). This resulted in the position of the maximum of the rugate reflectance band being shifted hypsochromically about 65 nm from that in freshly etched pSi, showing that the silanisation step has not greatly altered the porosity or refractive index of the sample. The IR spectrum supports the successful silanization since it contains C-H stretching bands at 2950 and 2920 cm^{-1} (Figure 4d).[11]

Monitoring of porous silicon degradation

Hydride-terminated porous silicon undergoes degradation when immersed in aqueous solutions, with release of gaseous or soluble species, due to two processes: 1) oxidation of the silicon matrix to silica by water or various reactive oxygen species; and 2) hydrolysis to soluble orthosilicic species [16]. This degradation hinders its use in some applications although controlled degradation is useful for applications such as drug delivery. Different strategies have been applied to improve the stability of porous silicon [17], such as oxidation of the surface under controlled conditions [18], derivatization forming Si-C bonds on the surface via different organic reactions [19,20] or covering the porous structure with protective polymeric films [1].

The degradation of porous silicon in aqueous solution depends on several factors, with pH being a key factor. In acidic or neutral aqueous media the degradation proceeds slowly but in basic solutions hydroxide reacts with both Si-H and Si-O surface species [21]. Buffer solutions with pH values that would lead to moderately rapid degradation of the porous Si samples (time for degradation ca. 300 – 3000 min) were selected for this study. Due to the differing stabilities of the samples, a pH 10 buffer was used for the freshly etched and chitosan-coated samples (fpSi and pSi-ch) while a pH 12 buffer was used for the hydrolytically more resistant oxidized and modified samples (pSi-o and pSi-oC_8). In both cases, ethanol was added to the buffers to ensure wetting of the porous silicon layer and to reduce the formation of adherent gas bubbles on the samples.

Porous Si rugate filters show characteristic reflectance spectra due to the periodic oscillations of porosity in the direction normal to the surface. Changes in the average refractive index of the porous silicon film due to infiltration of compounds into the pores or alteration of the porous silicon matrix modify the wavelength of maximum reflectance providing an useful method for sensing [22]. The oxidation of the porous

silicon matrix to silica decreases the effective refractive index, which causes a hypsochromic shift in the position of the maximum reflectance peak in the spectrum, and the dissolution of the porous layer can both decrease the thickness of the layer and increase the porosity, both processes leading to a reduction in the effective optical thickness. Therefore, the shifts in the Fabry-Perot interference fringe pattern observed in the visible reflectance spectra and the wavelength of the rugate peak maximum can be used to measure and compare the stability of different porous Si samples. The effective optical thickness of porous silicon samples can be obtained in real time using a Fast Fourier Transform of the reflectance spectra [21,23]. One strategy to then compare the degradation of different porous Si surface samples in aqueous media involves calculating the relative change in effective optical thickness defined as

$$\frac{\Delta \mathrm{EOT}}{\mathrm{EOT_0}}\% = \frac{\mathrm{EOT}-\mathrm{EOT_0}}{\mathrm{EOT_0}} \cdot 100\% \qquad \text{(eq. 2)}$$

where EOT_0 is the value of EOT (eq. 2) measured when the porous Si surface is initially exposed to flowing buffer. The degradation of the pSi surface is then monitored by this relative decrease in optical thickness [24]. The degradation of the four porous Si sample types in the present study as measured by EOT changes over the first 80 min of the degradation is shown Figure 6. The data indicate that the stability of these samples decreases in the following order: oxidized pSi with silanization > oxidized pSi > freshly etched porous Si > chitosan coated pSi, since the initial rates of relative EOT change during the degradation are 0.0059; 0.011; 0.217; and 0.37 %/min respectively even though the former two samples are immersed in a solution at higher pH (12 vs 10). The degradation rate is higher for porous silicon coated by chitosan than for fresh pSi for the first 25 minutes, but there is a subsequent decrease in the degradation rate of the chitosan-coated sample

so that at later times it degrades more slowly than fresh porous silicon, with relative EOT changes of 0.066 and 0.108 %/min, respectively. The increased rate of degradation for the chitosan-coated porous silicon sample is in apparent contrast to the previously reported studies of chitosan-coated porous silicon, however those studies used hydrosilylated porous silicon or oxidized porous silicon [1,14,15]. The increased degradation of pSi-ch compared even to freshly etched porous silicon may be due to the amines present in chitosan, since amines can increase the rate of porous silicon hydrolysis [25,26]. It also suggests that the chitosan layer contains cracks or fissures such that the aqueous solution readily infiltrates the underlying fpSi layer.

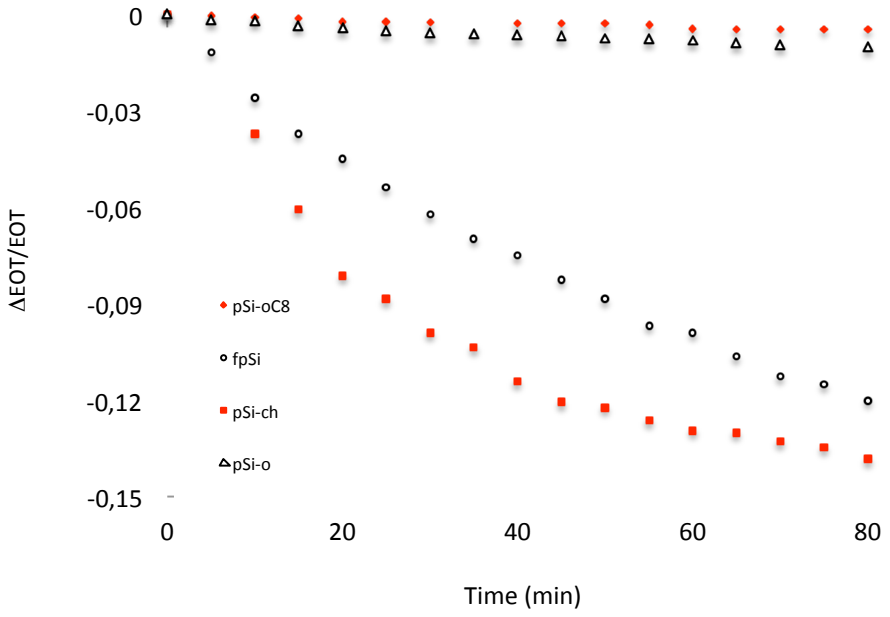

Figure 6. Plots of the relative change in the effective optical thickness (EOT) of the pSi samples as a function of time exposed to buffer solutions at 20 ± 1 °C. fpSi and pSi-ch were exposed to 1:1 (v/v) 0.5 M carbonate/borate buffer (pH 10): ethanol while the oxidized and silanized samples pSi-o and pSi-oC_8 were exposed to 80:20 (v/v) 0.04 M phosphate buffer (pH 12): ethanol.

The degradation of porous Si, typically monitored by reflection or transmission measurements using a spectrophotometer, can also be monitored using digital photography if the degradation results in a color change. Colors, which are qualities representing visual experiences [27,28], can be quantified by a number of methods or color spaces. Color spaces can be classified into four groups related by different types of transformations: linear-light tri-stimulus, xy chromaticity, perceptually uniform and hue oriented [28]. All of the color spaces can be derived from the RGB information supplied by devices such as cameras and scanners. The HSV color space used in this work represents the cognitive color information associated with a change in dominant wavelength of the observed signal in a single parameter, the hue component H. Previous studies have shown that the use of the H coordinate to monitor the output of bitonal sensors that produce a change in color allows all color information to be condensed into a single parameter [8,29]. The H coordinate is simple to calculate, and easily obtained from commercial imaging devices, and shows little dependence on variations in color intensity or variations in brightness of illumination. Here we investigate using this H coordinate to monitor a narrow reflectance band that shifts in wavelength over time. We initially investigated calculating the H coordinate for the as-acquired images. There was some variability of the H coordinate across the porous silicon samples during the degradation process, so that the H parameter we have used in the following analysis is the mode of the H coordinates from all the pixels corresponding to the porous silicon.

Changes in the ΔEOT/EOT and in the H parameter over the complete time of the degradation experiment are shown in Figure 7 and Figure 8, respectively.

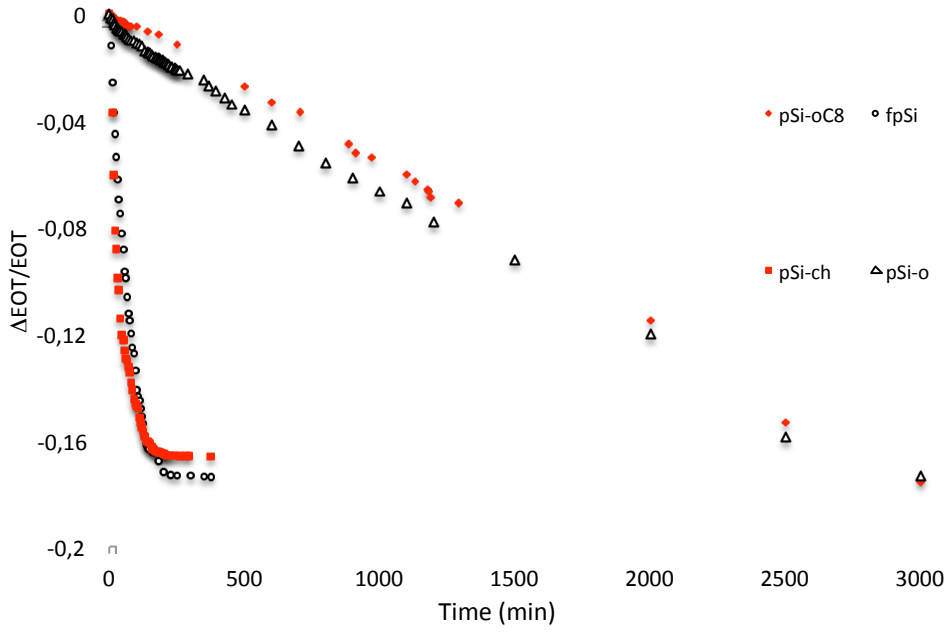

Figure 7. Changes in the ΔEOT/EOT over the complete time of the degradation experiment.

As the porous silicon degradation process occurs the H parameter begins to increase from ca. 0.033 to a maximum value of 0.18. This parameter increases during the degradation process from ca. 12 and reaches a maximum value of 66 degrees (using the 0-360º range).

These changes in the parameter values are manifested in a visible color change from red to green and a decrease and increase in the red and green channels of the images respectively (Figure 9a). Once all the pSi had dissolved, the mirror-like silicon wafer substrate was exposed. Reflection of the tungsten light source from this bare silicon surface was yellow as captured by the camera. This reflection from the substrate resulted in a *reduction* in the magnitude of the H parameter from ca. 0.18 to

0.11 degrees at very long times (at time >100 min for fpSi and pSi-ch, >500 min for pSi-o and >1000 min for pSi-oC_8) (Figure 8).

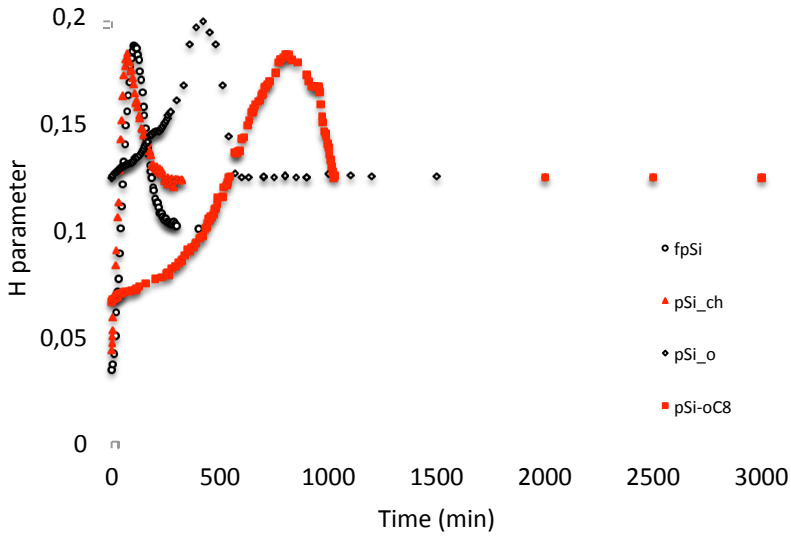

Figure 8. Changes in the H parameter over the complete time of the degradation experiment.

Because of this non-monotonic behavior of hue we investigated other functions of the red, green and blue channels that might provide a measure of degradation over the whole time of the reaction. We found that pre-processing the data by taking the average red channel value for each image and normalizing it using the minimum and maximum observed average red values during the degradation process, and doing the same for the other two channels and then applying eq 1 to these normalized channels gave a suitable monotonic function, Figure 9b. Since the value obtained does not correspond directly to the perceived color we refer to it as the scaled H parameter. The relative change in this H parameter was very similar to that for hue over the first 100 min of the degradation reaction, but at longer times the scaled H parameter continued to increase in a monotonic manner in contrast to the behavior of the hue.

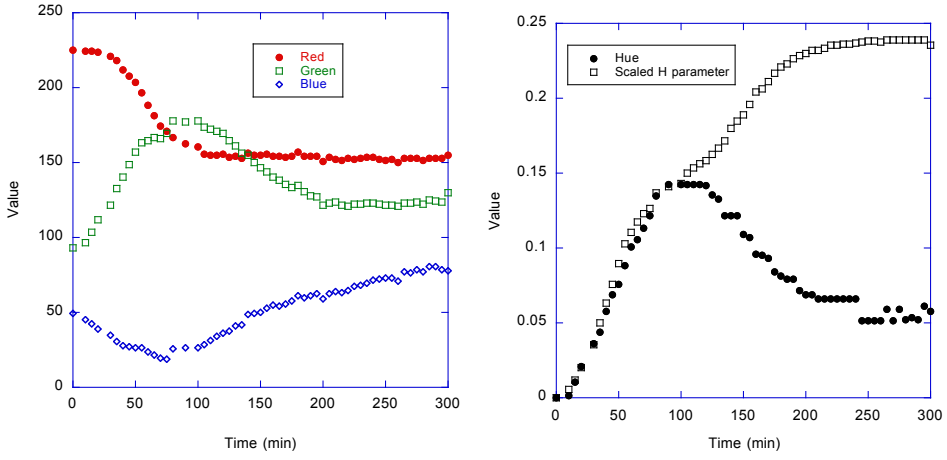

Figure 9. a) Plot showing the change in average RGB values from images of fp-Si as it degrades. b) Plot showing the hue derived from the as-acquired images and the scaled H-parameter derived from RGB values pre-processed as described in the text.

Measurement of the color evolution using the scaled H parameter confirmed the previously observed trend regarding the stability of the porous silicon samples towards degradation. We then used this scaled H parameter to compare the degradation of the four porous silicon samples. Thus, Figure 10 shows a comparison of the normalized value $((H-H_{initial})/(H_{max}-H_{initial}))$ with the normalized change in effective optical thickness for the fpSi sample. The stability of the different silicon surfaces can be ranked by their initial rate of degradation, with the stabilities being in the order: oxidized pSi with silanization > oxidized pSi > freshly etched porous Si > chitosan coated pSi, with corresponding rates of the normalized H parameter being 0.00060; 0.0012; 0.0093; and 0.017 min^{-1}, respectively.

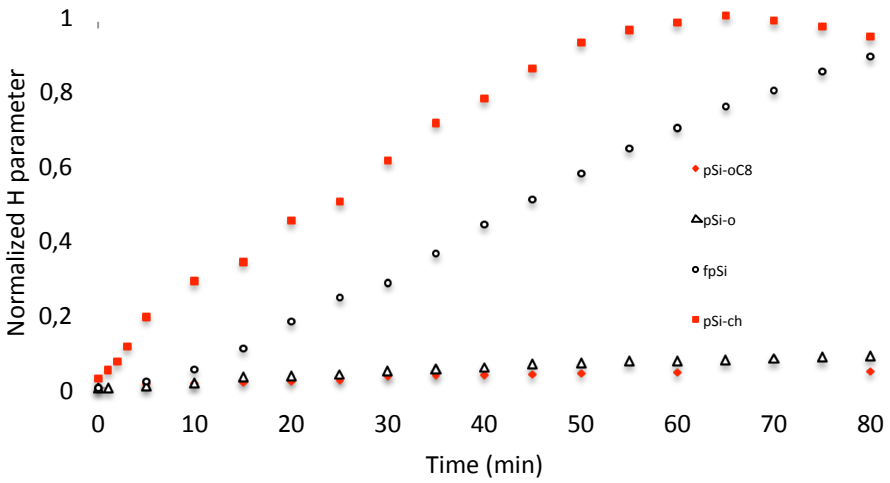

Figure 10. Evolution of the normalized H parameter during the first 300 min for all the samples, fpSi, pSi-ch, pSi-o and pSi-oC$_8$. The experimental conditions are as given for Figure 6.

By comparing the degradation kinetics of the porous silicon samples using normalized reflectance values (either rugate position or EOT) and normalized H values (Figure 11) we conclude that it is possible to obtain semiquantitative information about porous silicon stability using H parameter only up to the first point of degradation.

In Figure 12 is represented both H parameter normalized and rugate position (nm) versus time during the first 100 min.

Using hue to monitor complete degradation is limited due to the interfering effect of the reflection of the broad light source spectrum from the porous silicon, silicon substrate and other surfaces within the light path. However the use of a different light source with increased intensity in the blue-green regions of the spectrum compared to the lamp used may reduce this problem. The behavior of the hue parameter for porous rugate samples with the reflectance bands is also very dependent on the white balance value used during the image pre-processing step.

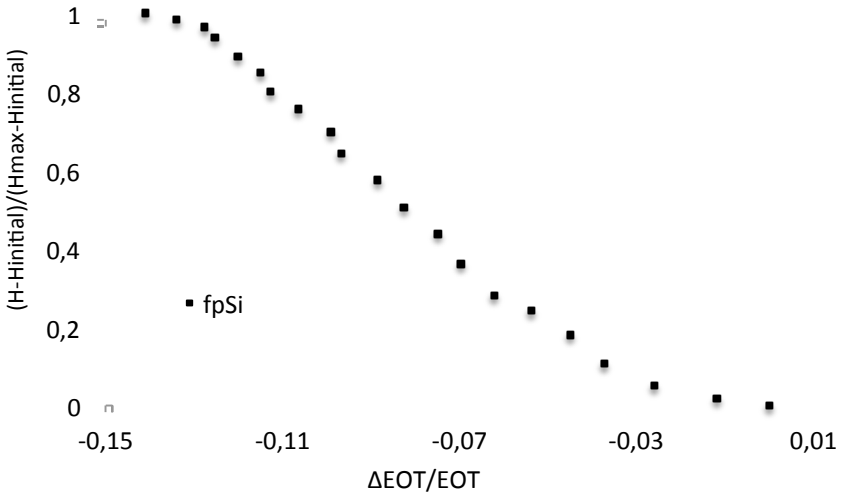

Figure 11. Normalized value $((H-H_{initial})/(H_{max}-H_{initial}))$ compare to the normalized change in effective optical thickness for the fpSi sample.

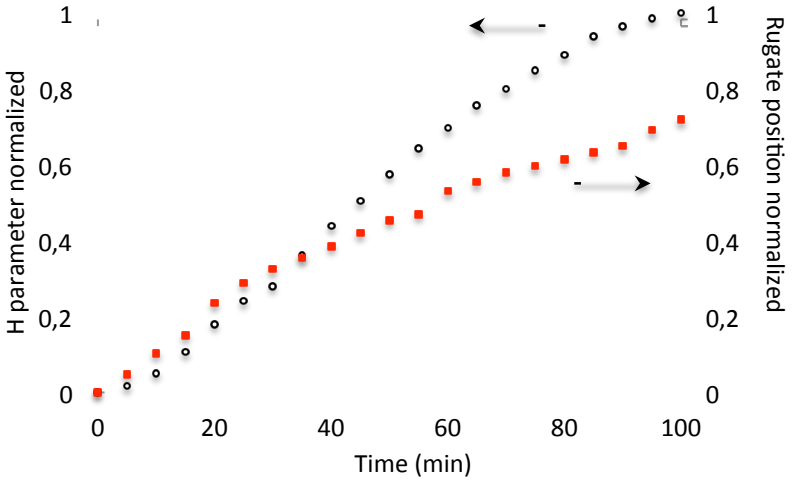

Figure 12. H parameter normalized and rugate position (nm) during the first 100 min (moment from which it is no longer possible to relate directly the H parameter to the silicon degradation process due to the illumination source).

The advantage of the proposed procedure to monitor the early times of porous Si degradation using the H parameter, and with 2b/(r+g) parameter for later times of this process derived from digital photographs is due to instrumental simplicity, where one only needs a digital camera, easy signal processing, and a color coordinate calculation from the region of interest in the image. The digital imaging approach enables use of less sophisticated, inexpensive instrumentation (such as a cell phone camera), advantageous for applications such as remote sensing or medical diagnostics.

The analysis of the H parameter reveals a two-phase process whereby first there is an initial increase in the amount of the green channel, and subsequently a decrease. In contrast, blue initially decreases and then increases (See Figure 9a).

The method of analysis was implemented with other data analysis by first considering the following points:

1. The two phase nature of the process in both the freshly prepared (fpSi) and (pSi-ch) samples.
2. The fact that there is an obvious shift in color from the initial to final states of the degradation process.
3. The raw RGB data presents itself an opportunity for analysis and is the best method to monitor hue.
4. Any increase in one channel must be compensated by a corresponding decrease in a separate channel to maintain normality in any color shift.

Therefore, using these four points the method is as follows. First, the raw pixel values for the red, green, and blue channels were taken. The red, green, and blue channels were normalized to 1 by dividing by each channel by the initial value. The average value of the RGB signal is thus (1+1+1)/3, or 1.

If there is a change in color, then the final color will be different from this initial value of 1. This final value was used as the color representation to which the

degradation process will be normalized. Therefore, at each time point the R, G, and B channels were followed and each channels deviation from its initial value of 1 were monitored, for example if red had an initial value of 211, 211/211 would be the initial value. Next, at a 20 min time point the pixel value was 205, the R-value in the analysis presented would thus be 0.96. This would imply that the red channel had shifted, and there was a corresponding increase in one of the G or B channels to compensate for the shift in the red channel.

Using this same type of analysis for the G and B channels at the 20 min time point where the G and B channels gave values of 1.35 and 0.5. These values were averaged in order to get a new average value that deviates from 1, in this case, a new value of 0.94; therefore the deviation of the average color from the initial color will allow one to follow the path of the color shift using only raw RGB data. The final state of the color will then guide this analysis of the degradation process. This final state of the color will serve as the point to which the average color shift is progressing towards. We will determine this final state of the color shift by observing the point at which the channels show no more shift, or when the R G and B channels flatline.

After processing the data, an exponential decay line affords very good correlation with EOT data thus confirming the validity of the method (See Figure 13).

The possibility for the deviation from the EOT data could arise from a variety of factors, namely the R G B data, light, systematic error, or the requirement for a more exhaustive work to see if the H parameter has potential. All of these factors could be investigated in future works.

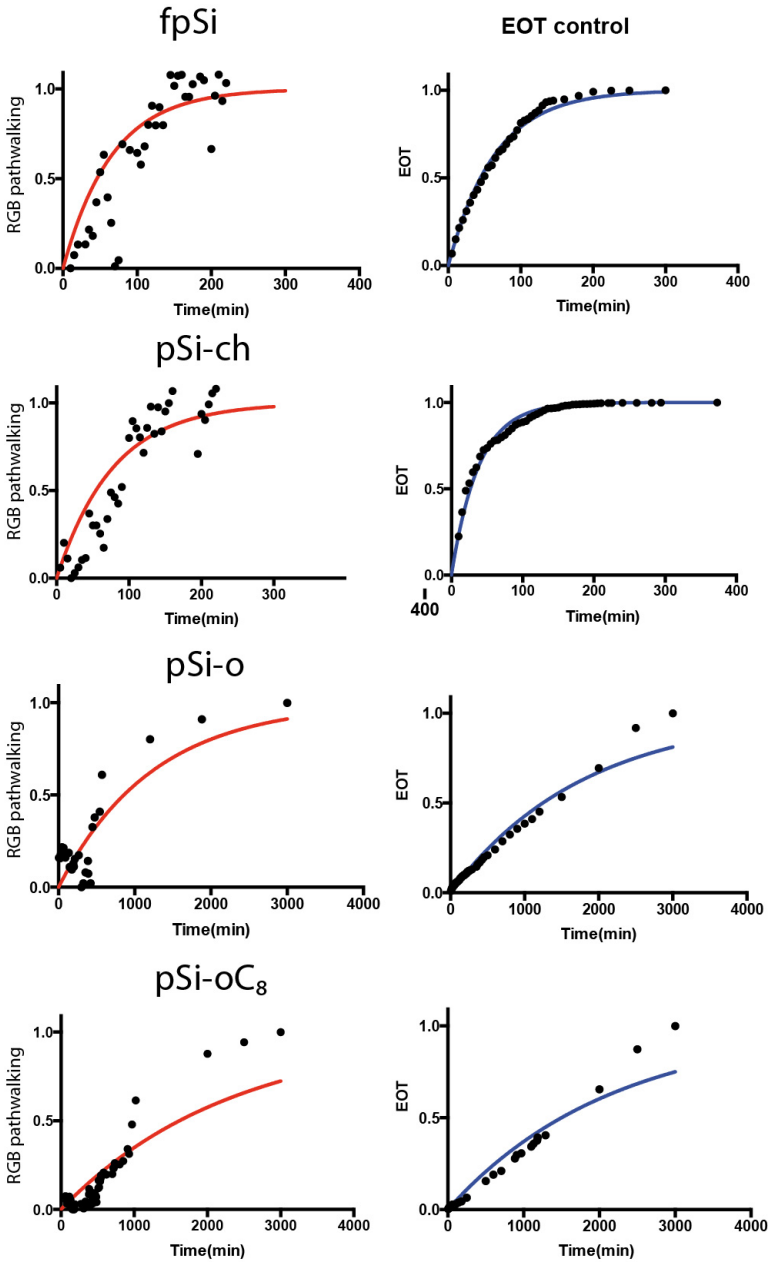

Figure 13. Correlation between the "RGB pathwalking" and the EOT control method.

CONCLUSIONS

We have demonstrated that the degradation of porous silicon in basic aqueous buffers can be monitored in situ by digital imaging with a consumer-grade digital camera and have validated this approach with simultaneous spectrophotometric measurement of the optical reflectance spectra. An approximately linear correlation between the wavelength of the maximum of the rugate reflectance band and the H parameter of HSV color space was observed during the early time points of the degradation process. Importantly, inclusion of a normalization parameter 2b/(r+g) (scaled H parmeter) allows for visualization of the entire degradation process despite the deviation from linearity by using only the H parameter. A similar relationship was also noted between the H parameter and the effective optical thickness of the samples. These results indicate that the samples were degrading via dissolution of the pore walls, rather than just dissolution from the top of the porous silicon layer downwards.

The relative stabilities of the four porous silicon types obtained by the four measurement methods were consistent (EOT, H parameter, RGB normalized and RGB path walking), indicating that all methods could be used to monitor relative sample degradation. However, whereas measurement of the rugate peak wavelength and effective optical thickness requires a spectrophotometer, the determination of RGB and HSV values was obtained using a consumer-grade digital camera and standard software. Indeed, the H-parameter approach could be applied using a low-cost camera or the camera within a mobile phone or mobile computing device. This would then allow such measurements to be made outside the laboratory and at comparatively low cost.

While this work reports results from monitoring degradation of intact porous silicon films attached to a crystalline silicon substrate, a similar approach should be

possible to monitor particles of porous silicon. The potential use of color measurements to monitor both degradation and drug delivery from porous silicon micro-particles would require only simple cameras and illuminants and could even be coupled to use with smartphones.

REFERENCES

1. Sciacca, B; Secret, E; Pace, S; Gonzalez, P; Geobaldo, F; Quignard, F; Cunin, F : Chitosan-functionalized porous silicon optical transducer for the detection of carboxylic acid-containing drugs in water. *J. Mater. Chem. 2011*, *21*: 2294.

2. Janshoff, A; Dancil, K P; Steinem, C; Greiner, D P; Lin, V S Y; Gurtner, C; Motesharei, K; Sailor, M J; Ghadiri, M R : Macroporous p-Type Silicon Fabry-Perot Layers. Fabrication, Characterization, and Applications in Biosensing. *J. Am. Chem. Soc. 1998*, *120*: 12108.

3. Cunin, F; Schmedake, T A; Link, J R; Li, Y Y; Koh, J; Bhatia, S N; Sailor, M J : Biomolecular screening with encoded porous-silicon photonic crystals. *Nat. Mater. 2002*, *1*: 39.

4. Li, Y Y; Cunin, F; Link, J R; Gao, T; Betts, R E; Reiver, S H; Chin, V; Bhatia, S N; Sailor, M J : Polymer Replicas of Photonic Porous Silicon for Sensing and Drug Delivery Applications. *Science 2003*, *299*: 2045.

5. Kilian, K A; Lai, L M H; Magenau, A; Cartland, S; Bocking, T; Di Girolamo, N; Gal, M; Gaus, K; Gooding, J J : Smart Tissue Culture: in Situ Monitoring of the Activity of Protease Enzymes Secreted from Live Cells Using Nanostructured Photonic Crystals. *Nano Lett. 2009*, *9*: 2021.

6. Pacholski, C; Sartor, M; Sailor, M J; Cunin, F; Miskelly, G M : Biosensing Using Porous Silicon Double-Layer Interferometers: Reflective Interferometric Fourier Transform Spectroscopy. *J. Am. Chem. Soc. 2005*, *127*: 11636.

7. Rouquerol, F.; Rouquerol, J.; Sing, K. *Adsorption by powders and porous solids;* 11 ed.; Academic Press: San Diego, 1999, Vol. 3, 191.

8. Cantrell, K; Erenas, M M; Orbe-Paya, I; Capitán-Vallvey, L F : Use of the Hue Parameter of the Hue, Saturation, Value Color Space as a Quantitative Analytical Parameter for Bitonal Optical Sensors. *Anal. Chem. 2010*, *82*: 531.

9. Smith, A R : Color gamut transform pairs. *Proceedings of the 5th Annual Conference on Computer Graphics and Interactive Techniques 1978*, 12.

10. Bisi, O; Ossicini, S; Pavesi, L : Porous silicon: a quantum sponge structure for silicon based optoelectronics. *Surf. Sci. Rep. 2000*, *38*: 1.

11. Mawhinney, D B; Glass, J A, Jr.; Yates, J T : FTIR Study of the Oxidation of Porous Silicon. *J. Phys. Chem. B 1997*, *101*: 1202.

12. Amato, G.; Delerue, C.; Von Bardeleben, H. J. *Structural and Optical Properties of Porous Silicon Nanostructures;* Gordon and Breach Science Publishers: 1998, 54.

13. Wu, E C; Andrew, J S; Cheng, L; Freeman, W R; Pearson, L; Sailor, M J : Real-time monitoring of sustained drug release using the optical properties of porous silicon photonic crystal particles. *Biomaterials 2011*, *32*: 1957.

14. Wu, J; Sailor, M J : Chitosan Hydrogel-Capped Porous SiO2 as a pH Responsive Nano-Valve for Triggered Release of Insulin. *Advances Func. Mat. 2009*, *19*: 733.

15. Pastor, E; Matveeva, E; Valle-Gallego, A; Goycoolea, F M; Garcia-Fuentes, M : Protein delivery based on uncoated and chitosan-coated mesoporous silicon microparticles. *Colloids Surf. , B 2011*, *88*: 601.

16. Wu, E C; Park, J H; Park, J; Segal, E; Cunin, F; Sailor, M J : Oxidation-Triggered Release of Fluorescent Molecules or Drugs from Mesoporous Si Microparticles. *ACS Nano 2008*, *2*: 2401.

17. Lees, I N; Lin, H; Canaria, C A; Gurtner, C; Sailor, M J; Miskelly, G M : Chemical Stability of Porous Silicon Surfaces Electrochemically Modified with Functional Alkyl Species. *Langmuir 2003*, *19*: 9812.

18. Zangooie, S; Bjorklund, R; Arwin, H : Protein adsorption in thermally oxidized porous silicon layers. *Thin Sol. Films 1998*, *313-314*: 825.

19. Buriak, J M : Organometallic Chemistry on Silicon and Germanium Surfaces. *Chem. Rev. 2002*, *102*: 1271.

20. Song, J H; Sailor, M J : Reaction of Photoluminescent Porous Silicon Surfaces with Lithium Reagents To Form Silicon-Carbon Bound Surface Species. *Inorg. Chem. 1999*, *38*: 1498.

21. Sailor, M. J. *Porous Silicon in Practice;* Wiley-VCH Verlag GmbH: Weinheim, Germany, 2012.

22. Fenzl, C; Hirsch, T; Wolfbeis, O S : Photonic Crystals for Chemical Sensing and Biosensing. *Angew. Chem. Int. Ed. 2014*, *53*: 3318.

23. Letant, S E; Sailor, M J : Detection of HF gas with a porous silicon interferometer. *Adv. Mater. 2000*, *12*: 355.

24. Tsang, C K; Kelly, T L; Sailor, M J; Li, Y Y : Highly Stable Porous Silicon-Carbon Composites as Label-Free Optical Biosensors. *ACS Nano 2012*, *6*: 10546.

25. Chandler-Henderson, R R; Sweryda-Krawiec, B; Coffer, J L : Steric Considerations in the Amine-Induced Quenching of Luminescent Porous Silicon. *J. Phys. Chem. 1995*, *99*: 8851.

26. Sweryda-Krawiec, B; Chandler-Henderson, R R; Coffer, J L; Rho, Y G; Pinizzotto, R F : A Comparison of Porous Silicon and Silicon Nanocrystallite Photoluminescence Quenching with Amines. *J. Phys. Chem. 1996*, *100*: 13776.

27. Maund, B. Color. 2006. Metaphysics Research Lab, CSLI, Stanford University. Stanford Encyclopedie of Philosophy.

28. Wyszecki, G.; Stiles, W. S. *Color Science: Concepts and Methods, Quantitative Data and Formulae;* Wiley Classics Library: Denver, USA, 2000.

29. Ariza-Avidad, M; Cuellar, M P; Salinas-Castillo, A; Pegalajar, M C; Vukovic, J; Capitan-Vallvey, L F : Feasibility of the use of disposable optical tongue based on

neural networks for heavy metal identification and determination. *Anal. Chim. Acta 2013*, *783*: 56.

CONCLUSIONS

In the final chapter we aim to present the possibility of monitoring porous silicon sample degradation with a conventional camera.

The following are the main conclusions of the chapter IV:

- Different procedures have been used to increase the stability of porous silicon samples.
- A system was developed in order to measure porous silicon degradation through spectrophotometric and color measurements simultaneously.
- The most common technique used to evaluate the porous silicon samples degradation has been the measure of the thickness changes. This technique was used as a validation method to evaluate the colorimetric measurements with the camera. Data processes with two color spaces; HSV and RGB were carried on in order to monitor the porous silicon degradation.
- An acceptable correlation was found between both measures.
- This study offers an alternative of sensor phases monitoring through systems out of the laboratory with biomedical applications.

CONCLUSIONES GENERALES

1. Se ha llevado a cabo el diseño, preparación y caracterización de sensores para incorporar en lenguas ópticas. Se han preparado membranas para iones metálicos basadas en reactivos cromogénicos convencionales (PAN, PAR, zincon, difenilcarbacida, cadión, ditizona, entre otros). Se ha caracterizado y modelado el comportamiento de dichas membranas frente a iones metálicos mediante espectrofotometría así como medida de color usando diversos sistemas de imagen como escáneres y cámaras fotográficas digitales. En el caso de color se ha usado como parámetro analítico los espacios de color RGB y HSV, comprobando que la coordenada tonal del espacio HSV es la que muestra mejores prestaciones. Se ha comprobado la validez de las membranas con propósitos analíticos para la resolución de mezclas de Zn(II), Cu(II), Ni(II), Fe(II) y Fe(III) en control de calidad de productos farmacéuticos utilizando regresión lineal multicomponente con recuperaciones próximas al 100%. Por otra parte, se ha utilizado un enfoque en dos etapas basado en redes neuronales que en una primera clasifica y en la segunda determina las concentraciones con errores aceptables.
2. Se ha desarrollado un prototipo de instrumento portátil para determinar mezclas de iones metálicos usando una matriz de 8 sensores basada en dos reactivos cromogénicos diferentes. Para la captura de imágenes utiliza una μ-cámara CCD a color programable que opera con la luz ambiente y utiliza una pantalla táctil para la presentación de las imágenes y la selección manual de la zona de la imagen a analizar. El propio instrumento es el que realiza el procesamiento de la imagen presentando la concentración en la pantalla LCD del mismo. En resumen se consigue un instrumento portátil con diseño electrónico simple y un número reducido de componentes electrónicos que realiza el análisis con membranas de un uso, siendo necesario solo el ajuste de pH de la muestra.

3. Se han preparado membranas y matrices de membranas mediante la técnica de impresión por chorro de tinta. Para ello, se han modificado las formulaciones de las tintas de manera que cumplan con los requerimientos de la impresora. Tras ensayar diversos tipos de soportes y condiciones para la impresión por chorro de tinta se han preparado matrices 7 membranas diferentes con 5 réplicas de cada una para evaluar la presencia de 13 iones metálicos. Un estudio de la reproducibilidad de la fabricación de las matrices de sensores ha mostrado una alta precisión en comparación con las técnicas de impresión anteriores (precisión 0,81%).
4. La adquisición de imágenes de la matriz antes y después de la reacción de las membranas con las disoluciones conteniendo iones metálicos se realizó con una cámara fotográfica convencional y un sistema de iluminación estándar utilizando una caja de luz. Para evaluar el cambio de color de las membranas, esta lengua óptica utilizó como parámetro analítico la coordenada H del espacio de color HSV. Se utilizaron diversos procedimientos multivariados de clasificación y cuantificación de iones metálicos, basados en redes neuronales artificiales. La etapa de la clasificación para 13 metales, alcanzó un éxito mínimo del 98,1%, con un umbral mínimo de 10^{-5} M. En esta etapa 10 de los 13 iones metálicos se identifican prácticamente sin error, siendo los errores observados para el resto de metales que no se pueden distinguir completamente, siempre falsos negativos. En la segunda etapa, se determina la concentración de cada metal en la disolución. Se seleccionaron las mezclas de hasta 5 metales (Zn (II), Cu (II), Ni (II), Cd (II) y Co (II)), siendo la precisión media encontrada en todos los casos inferior a una unidad decimal respecto a la concentración molar presente. Los resultados encontrados abren la puerta al empleo de smartphones en conjunción con la lengua óptica desarrollada.

5. Se ha propuesto un ensayo de desplazamiento de tipo indicador complejante-metal para la determinación selectiva de sulfuro en medio acuoso a pH fisiológico. El ensayo utiliza una membrana impresa por la técnica de inyección por chorro conteniendo el complejo de Cu (II) del colorante azoico 1-(2-piridilazo)-2-naftol en soporte de nylon. Se ha modelado las reacciones tanto de PAN inmovilizado en nylon con Cu(II) como de PAN-Cu también inmovilizado con sulfuro y calculado sus constantes de equilibrio. Las imágenes de las membranas después de reaccionar fueron recogidas con una cámara fotográfica convencional y como parámetro analítico se utilizó la coordenada H. Se han utilizado diversas aproximaciones para establecer las funciones de calibrado: ajuste de Boltzmann para la relacion sigmoidal observada entre H y el logaritmo de la concentracion de sulfuro, aproximación lineal en la zona de máxima pendiente del sigmoide y linealización completa utilizando una transformación logistica decimal. El mejor límite de detección encontrado ha sido de 0,11 μM con una precisión que oscila entre el 2 y el 11 %. El procedimiento desarrollado es muy barato siendo la membrana estable con un tiempo de respuesta no superior a 10 minutos.
6. Se han sintetizado nanopartículas de tipo carbón dots mediante pirolisis asistida por microondas de ácido cítrico en presencia de polietilenimina obteniéndose nanopartículas con un tamaño medio de 12 nm con carga positiva debido a la presencia de grupos aminas primaria y secundaria en la superficie de las nanopartículas. Este material presentan fluorescencia en un amplio rango de pH (pH = 2-8) así como emisión up-conversion entre 380-550 nm cuando se excita a 850 nm. Estudiada la influencia de 14 iones metálicos sobre la emisión fluorescente de las nanopartículas sintetizadas se observó una intensa atenuación de fluorescencia en presencia de Cu (II) y Fe

(III). En el caso de Cu (II) la atenuación es tanto estática como dinámica como se desprende del estudio de los tiempos de vida y en el caso de Fe (III) es debido a un mecanismo de filtro interno, por lo que no se observa trabajando por up-conversion excitando a 850 nm. Se ha establecido un procedimiento selectivo para la determinación de Cu (II) midiendo la atenuación de fluorescencia tanto por down-conversion como por up-conversion con límites de detección de 0,09 y 0,12 M, respectivamente. Tras demostrar la ausencia de citotoxicidad así como la permeabilidad de las nanopartículas en células del riñón de embriones humanos, se propuso el procedimiento para la detección de Cu(II) por técnicas de imagen en sistemas biológicos.

7. Se ha presentado un nuevo procedimiento para la síntesis de carbon dots por descomposición térmica de ácido ascórbico utilizado como fuente de carbono, en dimetilsulfóxido utilizando un sistema microfluídico que incluye tanto una plataforma fluídica y otra térmica que permiten el control de todas las variables de síntesis. El tamaño medio de las nanopartículas obtenidas fue de 3,3 nm con grupos carboxílicos en la superficie. Por ello se observa un cambio de fluorescencia en dichas partículas con el cambio de pH del medio debido a la protonación/desprotonación de los grupos carboxilo superficiales lo que causa el dopaje electrostático de las nanopartículas y un cambio en el nivel de Fermi. Del mismo modo, el color de las disoluciones de cdots cambia con el pH provocando cambios electrónicos Π-Π^* y n-Π^* por llenado o vaciado de sus bandas de valencia. Con estos carbon dots se pueden detectar pequeños cambios de pH tanto por fluorimetría como por colorimetría, utilizando una cámara digital, con un amplio rango lineal (pH 3.5 a 10.2). Se comprobó que este nanomaterial permea membranas celulares

no afectando a la morfología celular, por lo que pueden ser usados como sensores de pH para bioimaging de pH en organismos vivos.

8. Se ha sintetizado y caracterizado silicio poroso nanoestructurado y se ha procedido a estudiar su degradación en medio acuoso por procesos hidrolíticos y oxidativos. Se ha tratado de monitorizar dicha degradación a través de los cambios de color que ocurren en ese material fotónico. Se han utilizado diferentes procedimientos para incrementar la estabilidad de las muestras de silicio poroso fresco, tales como el recubrimiento de la superficie del material poroso con una capa de polímero (chitosan), su oxidación parcial pirolítica y su oxidación y posterior funcionalización superficial con metoxidimetiloctilsilano. Para estudiar la degradación del silicio poroso en las muestras, se pusieron en contacto con un flujo continuo de disolución acuosa tamponada. Se midió simultáneamente con un espectrofotómetro para obtener el espectro interferencial, utilizado como sistema de referencia, y la medida de color recogiendo imágenes con una cámara fotográfica. La técnica más comúnmente usada para evaluar las muestras de silicio poroso han sido la medida de cambios de espesor. El procesado de la señal se llevó a cabo con dos espacios de color, RGB y HSV. Se ha demostrado que existe una buena correlación entre las medidas de color y las espectrofotométricas, demostrando ser esta una posible alternativa para la monitorización de fases sensoras basadas en silicio poroso fuera del laboratorio con aplicaciones biomédicas.

ACKNOWLEDGMENT FINANCIATION

This doctoral dissertation has been supported from the We acknowledge financial support from the Ministerio de Economía y Competitividad, Secretaría del Estado de Investigación, desarrollo e innovación, Gobierno de España, grant with reference BES-2010-030103. Dirección General de Investigación y Gestión del Plan Nacional de I+D+i (Spain) (Projects CTQ2009-14428-C02-01 and CTQ2009-14428-C02-02; and Junta de Andalucía (Proyectos de Excelencia P07-FQM-1467, P08-FQM-3535 and P10-FQM-5974). These projects were partially supported by European Regional Development Funds (ERDF). European Community 6th Framework program, NanoEar project, grant number: NMP4-CT-2006-026556). Med El-Medical Electronics (Austria) and we thanks to "Reincorporacion de Doctores UGR" programs and Greib start-up projects for young researchers and the U.S. National Science Foundation under Grant No. DMR-1210417.